Identification, Quantification, and Characterization of Per- and Polyfluoroalkyl Substances (PFAS) in Soil and Groundwater by High-Resolution Mass Spectrometry and Oxidative Transformation

Dissertation

der Mathematisch-Naturwissenschaftlichen Fakultät

der Eberhard Karls Universität Tübingen

zur Erlangung des Grades eines

Doktors der Naturwissenschaften

(Dr. rer. nat.)

vorgelegt von

M. Sc. Catharina Capitain

aus Lörrach

Tübingen

2026

Gedruckt mit Genehmigung der Mathematisch-Naturwissenschaftlichen Fakultät der Eberhard Karls Universität Tübingen.

Tag der mündlichen Qualifikation:	09.03.2026
Dekan:	Prof. Dr. Thilo Stehle
1. Berichterstatter:	Prof. Dr. Christian Zwiener
2. Berichterstatter:	Prof. Dr. Peter Grathwohl

Declaration

I hereby declare that this dissertation is my own work and has been prepared independently. Any sources and assistance have been properly acknowledged.

I confirm that generative AI tools were used for language editing (grammar, sentence structure, and phrasing) and to support background research, literature clarification, and coding assistance. In addition, AI tools were used to assist in the initial phrasing and drafting of certain text passages. All scientific content, data interpretation, research conclusions, and critical assessments were developed independently by the author.

I further declare that this dissertation complies with the regulations of good scientific practice of the University of Tübingen and contains no plagiarism.

Signed,

Catharina Capitain

Abstract

The uncontrolled release of aqueous film-forming foam (AFFF) during a major fire in Reilingen, Germany, in 2008 resulted in significant contamination of soil and groundwater with per- and polyfluoroalkyl substances (PFAS). Due to the proprietary nature of AFFF formulations, the identity and environmental behavior of these fluorochemical surfactants remain largely obscured, highlighting the need for comprehensive site-specific characterization. This dissertation presents a systematic, multi-faceted analytical approach to elucidate the composition, abundance, and transformation of PFAS at this contaminated site.

Using an optimized extraction protocol combined with liquid chromatography high-resolution quadrupole time-of-flight mass spectrometry (HPLC-QTOF-MS), a total of 124 PFAS from 42 subclasses were identified, spanning anionic, cationic, and zwitterionic compounds with perfluoroalkyl chains ranging from 3 to 14 carbon atoms. Notably, one previously unreported PFAS subclass was discovered, and nine additional PFAS subclasses were detected in soil for the first time. These findings highlight the complexity of AFFF contamination and the presence of both primary and secondary precursors, including numerous by-products and intermediates formed under environmental conditions.

To overcome limitations associated with the lack of analytical standards, a novel semiquantification approach for non-target screening (NTS) was developed, combining matrix-matched calibration and ionization class-specific average calibration curves. This method enabled the (semi)quantification of 96 tentatively identified PFAS in addition to 28 target compounds, revealing that semiquantified PFAS concentrations exceeded those of conventional target analytes. Validation against extractable organofluorine (EOF) demonstrated a closed mass balance (102%), confirming the robustness and applicability of the approach for complex environmental matrices.

Furthermore, the PhotoTOP assay was applied for the first time to both AFFF standards and contaminated soil, facilitating photocatalytic oxidation of PFAS precursors into quantifiable perfluoroalkyl carboxylic acids. Target and non-target analyses identified numerous novel intermediates of the PhotoTOP, including perfluoroalkyl sulfonamide- and fluorotelomer sulfonamide-based compounds, dimers, fluorotelomer betaines, and unsaturated perfluoroalkyl sulfonic acids. Semiquantitative mass balance analysis indicated near-complete conversion of precursors, while kinetic investigations provided insight into transformation rates and

persistence, giving information on potential environmental fate and long-term PFAS release from soils.

Overall, this dissertation demonstrates the power of combining non-target screening, semiquantification, and oxidative conversion approaches to provide a detailed, validated characterization of the AFFF-related PFAS contamination. The findings have broad implications for environmental monitoring, remediation planning, regulatory compliance, and risk assessment, while also establishing a methodological approach that can be adapted to other complex matrices such as wastewater, sediments, and consumer products.

Zusammenfassung

Die unkontrollierte Freisetzung von wasserfilmbildenden Löschschäumen (aqueous film-forming foams, AFFF) während eines Großbrandes in Reilingen, Deutschland, im Jahr 2008 führte zu einer erheblichen Kontamination von Boden und Grundwasser mit per- und polyfluorierten Alkylsubstanzen (PFAS). Aufgrund der proprietären Zusammensetzung von AFFFs bleiben die Identität und das Umweltverhalten dieser fluorierten Tenside weitgehend unbekannt, was zeigt, wie wichtig eine umfassende, standortspezifische Charakterisierung ist. Diese Dissertation zeigt einen systematischen, multifaktoriellen analytischen Ansatz, um Zusammensetzung, Konzentration und Transformation von PFAS an diesem kontaminierten Standort zu untersuchen.

Mittels eines optimierten Extraktionsprotokolls kombiniert mit Hochleistungsflüssigkeits-chromatographie gekoppelt an hochauflösende Quadrupol-Time-of-Flight-Massenspektrometrie (HPLC-QTOF-MS) konnten insgesamt 124 PFAS aus 42 Subklassen identifiziert werden. Dazu zählen anionische, kationische und zwitterionische Verbindungen mit Perfluoralkylketten von 3 bis 14 Kohlenstoffatomen. Es wurde eine zuvor unbekannte PFAS-Subklasse entdeckt, und neun weitere PFAS-Subklassen wurden erstmals im Boden nachgewiesen. Diese Ergebnisse verdeutlichen die Komplexität der AFFF-Kontamination und die Präsenz sowohl primärer als auch sekundärer Vorläufersubstanzen, einschließlich zahlreicher Neben- und Zwischenprodukte, die unter Umweltbedingungen gebildet werden.

Um die Probleme durch fehlende analytische Standards zu umgehen, wurde ein neuer semiquantitativer Ansatz für das Non-Target Screening (NTS) entwickelt, der matrixangepasste Kalibrierung und Ionisierungsklassen-spezifische Durchschnittskalibrierkurven kombiniert. Mit dieser Methode konnten 96 vorläufig identifizierte PFAS zusätzlich zu 28 Target-Verbindungen (semi)quantifiziert werden, wobei die semiquantifizierten Konzentrationen die der herkömmlichen Target-Analyten überstiegen. Die Validierung anhand des extrahierbaren organischen Fluors (EOF) zeigte eine geschlossene Massenbilanz (102 %) und bestätigte die Robustheit und Anwendbarkeit des Ansatzes in komplexen Umweltmatrices.

Darüber hinaus wurde erstmals der PhotoTOP-Assay sowohl auf AFFF-Standards als auch auf kontaminierte Bodenproben angewendet, um die photokatalytische Oxidation von PFAS-Vorläufern zu quantifizierbaren Perfluorcarbonsäuren zu ermöglichen. Target- und Non-Target-Analysen identifizierten zahlreiche neue Zwischenprodukte, darunter Perfluoralkyl- und Fluortelomer-Sulfonamid-Verbindungen, Dimere, Fluortelomer-Betaine und ungesättigte

perfluorierte Sulfonsäuren. Die semiquantitative Massenbilanz zeigte eine nahezu vollständige Umsetzung der Vorläufer, während die Untersuchung der Kinetik Einblicke in Transformationsraten und Persistenz gab und so mögliches Umweltverhalten und langfristige PFAS-Freisetzung aus Böden beleuchten.

Insgesamt zeigt diese Dissertation die Leistungsfähigkeit der Kombination von Non-Target Screening, Semiquantifizierung und oxidativer Konversion, um eine detaillierte und validierte Charakterisierung der AFFF-bedingten PFAS-Kontamination zu ermöglichen. Die Ergebnisse haben weitreichende Implikationen für Umweltüberwachung, Sanierungsplanung, regulatorische Einhaltung und Risikobewertung und bieten methodische Grundlagen, die auch auf andere komplexe Matrizes wie Abwasser, Sedimente und Konsumgüter übertragbar sind.

Acknowledgements

First, I would like to sincerely thank Prof. Dr. Christian Zwiener for giving me the opportunity to conduct my research in his working group. I greatly appreciate the scientific knowledge I have gained during this time, the many helpful discussions, and his support and flexibility throughout my work.

I also thank Prof. Dr. Peter Grathwohl for serving as the second supervisor of my thesis.

I would also like to thank all the members of the Environmental Analytical Chemistry Group: Dr. Jonathan Zweigle, Dr. Boris Bugsel, Melanie Schüßler, Miriam Haußecker, Dr. Bernat Oró-Nolla, and Stephanie Nowak. Thank you for sharing your expertise in analytical and instrumental techniques, creating a pleasant working atmosphere, engaging in discussions, and providing assistance with laboratory issues. But especially for fixing the instruments hundreds of times, for the funny conversations in our office, and for Steffi's delicious treats that kept us going.

I am deeply grateful to my partner, Benjamin Boyn, for his emotional support throughout the duration of my thesis. My daughter, Malia Tiana Capitain, has been a constant source of motivation, bringing joy and positive distraction from my work, for which I am truly thankful.

I also thank my family and friends for their support and encouragement.

Finally, I acknowledge the Federal Ministry of Research, Technology, and Space (BMFTR) for funding the project PFClean (02WGW1665C).

List of Publications

Publication 1:

Schüßler M, Capitain C, Bugsel B, Zweigle J, Zwiener C (2024). Non-target screening reveals 124 PFAS at an AFFF-impacted field site in Germany specified by novel systematic terminology. *Analytical and Bioanalytical Chemistry*, 417 (27), 6049-6064. DOI: 10.1007/s00216-024-05611-3

Author contributions: MS and CC contributed equally to this work and share first authorship. MS: conceptualization, writing of original draft (focus on soil sampling and processing, instrumental analysis, NTS workflow, data evaluation, PFAS identification, distributions, AFFF manufacturer). CC: conceptualization, writing of original draft (focus on extraction method, terminology, confidence level, PFAS identification). JZ and BB contributed to PFAS identification and reviewed the manuscript. CZ supervised the study, supported data interpretation, and reviewed and revised the manuscript.

Publication 2:

Capitain C, Schüßler M, Bugsel B, Zweigle J, Vogel C, Leube P, Zwiener C (2025). Implementation of Matrix-Matched Semiquantification of PFAS in AFFF-Contaminated Soil. *Environmental Science & Technology*, 59 (14), 7338-7347. DOI: 10.1021/acs.est.4c14255

Author contributions: CC and MS contributed equally to this work and share first authorship. CC and MS: conceptualization, writing of original draft. BB and JZ: reviewing. CV and PL: performance of EOF measurements. CZ: supervision of the study, supporting data interpretation, reviewing and revising the manuscript.

Publication 3:

Capitain C, Zwiener C (2025). Characterization of per- and polyfluoroalkyl substances (PFAS) in AFFF-contaminated soil by photocatalytic oxidation (PhotoTOP). *Analytical and Bioanalytical Chemistry*. DOI: 10.1007/s00216-025-06208-0

Author contributions: CC: conceptualization, writing of the original draft. CZ: supervision of the study, supporting data interpretation, reviewing and revising the manuscript.

Oral and Poster presentations

- Capitain C, Schüßler M, Zwiener C (2024). Characterization of per- and polyfluoroalkyl substances (PFAS) in AFFF-contaminated soil by photocatalytic oxidation (PhotoTOP). Poster presentation at *Wasser 2024* in Limburg an der Lahn.

- Capitain C, Schüßler M, Bugsel B, Zweigle J, Vogel C, Leube P, Zwiener C (2025). Implementation of matrix matched semiquantification of PFAS in AFFF contaminated soil. Poster presentation at *Wasser 2025* in Münster.

- Capitain C, Schüßler M, Bugsel B, Zweigle J, Vogel C, Leube P, Zwiener C (2025). Herausforderung Löschschaum-Kontamination – Neue Ansätze mit quantitativem Nontarget Screening. Oral presentation at *PFAS – Analytik, Bewertung, Sanierung, Seminar des Fortbildungsverbunds Boden und Altlasten Baden-Württemberg 2025* in Rastatt.

Contents

List of Abbreviations

^{19}F-NMR	Fluorine-19 nuclear magnetic resonance spectroscopy
AAQ	Absolute accuracy quotient
ACC	Average calibration curves
AFFF	Aqueous film-forming foam
AI	Artificial intelligence
APCI	Atmospheric pressure chemical ionization
APPI	Atmospheric pressure photoionization
CIC	Combustion ion chromatography
ddMS^2	Data-dependent MS^2
ECF	Electrochemical fluorination
ECHA	European Chemicals Agency
EOF	Extractable organofluorine
ESI	Electrospray ionization
EU	European Union
FAIR	Findable, accessible, interoperable, and reusable
FTB	Fluorotelomer betaine
FT-ICR	Fourier transform ion cyclotron resonance
FTSA	Fluorotelomer sulfonic acid
FTSAm	Fluorotelomer sulfonamide
FTSAm-Pr-B	Fluorotelomer sulfonamide propyl betaine
GC	Gas chromatography
HF	Hydrogen fluoride
HFPO-DA	Hexafluoropropylene oxide dimer acid
HILIC	Hydrophilic interaction liquid chromatography
HPLC	High performance liquid chromatography
HRMS	High-resolution mass spectrometry
IC	Ion chromatography
IUPAC	International Union of Pure and Applied Chemistry
LC	Liquid chromatography
m/C	Mass-to-carbon ratio
MB	Mass balance
ME	Matrix effect
ML	Machine learning
MS/MS	Tandem mass spectrometry
n	Number of carbon atoms
NIST	National Institute of Standards and Technology
NTS	Non-targeted screening
OECD	Organisation for Economic Co-operation and Development
PFAA	Perfluoroalkyl acid
PFAI	Perfluoroalkyl iodide
PFAS	Per- and polyfluoroalkyl substances
PFASAm-Pr-DiMeAm	Perfluoroalkyl sulfonamide propyl dimethylamine

PFCA	Perfluoroalkyl carboxylic acid
PFEI	Pentafluoroethyl iodide
PFHxS	Perfluorohexane sulfonic acid
PFNA	Perfluorononanoic acid
PFOA	Perfluorooctanoic acid
PFOS	Perfluorooctane sulfonic acid
PFSA	Perfluoroalkyl sulfonic acid
ppq	Part per quadrillion
QC	Quality control
QqQ	Triple quadrupole
QTOF	quadrupole time-of-flight
REACH	Registration, Evaluation, Authorisation and Restriction of Chemicals
RF	Response factor
RP	Reversed-phase
RT	Retention time
SFC	Supercritical fluid chromatography
SPE	Solid-phase extraction
TF	Total fluorine
TFA	Trifluoroacetic acid
TFE	Tetrafluoroethylene
TiO_2	Titanium dioxide
TOP	Total oxidizable precursor
TP	Transformation product
UV	Ultraviolet

1. Introduction

1.1. Per- and Polyfluoroalkyl Substances (PFAS)

Per- and polyfluoroalkyl substances (PFAS) represent a large class of anthropogenic chemicals. Originally, PFAS were defined by Buck et al. (2011) [1] as compounds containing perfluoroalkyl moieties (C_nF_{2n+1}), where *n* denotes the number of carbon atoms. This definition encompassed over 4,700 substances. However, in 2021, the Organisation for Economic Co-operation and Development (OECD) introduced a broader definition, classifying all substances containing a CF_2 or CF_3 group (excluding CF_2H and CF_2-halogen groups) as PFAS. Under this expanded criterion, more than 7 million individual substances now fall within the PFAS category [2-4]. Some individuals and organizations may seek for a redefinition of PFAS, endorsed by the International Union of Pure and Applied Chemistry (IUPAC), to exclude certain fluorinated chemical subgroups from the current broad classification [5,6].

Most PFAS consist of fluorinated carbon chains, and the strength of the carbon-fluorine bond makes them extremely resistant. This results in extraordinary properties, including exceptional chemical and thermal stability, high fire resistance, water and grease repellency, nonstick behavior, and the ability to reduce surface tension in aqueous systems [7]. Due to their unique properties, PFAS have been used in a wide range of applications since the 1950s [8]. The first commercially available compounds were perfluoroalkyl sulfonic acids (PFSAs), such as perfluorooctane sulfonic acid (PFOS), and perfluoroalkyl carboxylic acids (PFCAs), such as perfluorooctanoic acid (PFOA) [7]. Since then, the global demand for PFAS has grown exponentially and is now estimated to encompass several thousand substances [5].

Initially, PFAS were synthesized using electrochemical fluorination (ECF). In this process, an organic precursor undergoes electrolysis in anhydrous hydrogen fluoride (HF), leading to the replacement of all hydrogen atoms with fluorine atoms. Due to the involvement of free radicals, the carbon chains may break, rearrange, or form cleaved, branched, and cyclic structures. This results in a mixture of linear and branched perfluoroalkyl chains of a given chain length [1,9,10]. Today, PFAS are primarily synthesized via telomerization. In the initial step, perfluoroalkyl iodides (PFAIs), most commonly pentafluoroethyl iodide (PFEI), react with tetrafluoroethylene (TFE), producing a mixture of longer, even-numbered perfluoroalkyl iodides [11]. In a subsequent step, ethylene is typically inserted. Fluorotelomerization yields linear, even-numbered perfluoroalkyl chains featuring a C_2H_2 spacer followed by a functional

group [1]. Most PFAS consist of two structural components, namely a fluorinated segment that is both hydrophobic and lipophobic and a hydrophilic functional group. In polyfluoroalkyl substances, these two parts are connected by the additional hydrocarbon linker [7].

Due to their favorable properties, PFAS are used in a wide range of applications, including firefighting foams, paints and inks, cookware and food-contact materials, sportswear and military uniforms, medical equipment, motor oil additives, and many others [7]. They are widely used and, in some cases, difficult to substitute, particularly in applications such as protective workwear for firefighters, where stringent safety requirements must be met [12].

The entry of PFAS into the environment involve various pathways through which these substances enter different environmental compartments. These include industrial emissions that release PFAS directly into air, water, and soil, as well as wastewater from treatment plants that introduce these substances into water bodies and soils. Atmospheric deposition through rain or snow also transports PFAS into soils and water. Another pathway is the disposal of PFAS-containing waste in landfills, which can lead to contamination. In agriculture, PFAS enter the soil and food chain through the use of contaminated products like pesticides and fertilizers. Additionally, air acts as a long-term transport medium, contributing to the global spread of PFAS. The use of products such as carpets, clothing, and food packaging also leads to a direct entry of PFAS into the environment [13]. Once released into the environment, PFAS remain unaltered or are transformed into transformation products (TPs) like PFAAs (perfluoroalkyl acids), which do not break down further, either abiotically or biotically. This persistence in the environment is why they are often referred to as "forever chemicals" [1,7,12,14].

The massive production, extensive use, and extreme stability of PFAS have resulted in their widespread presence. They are found globally in surface soil, surface water, modern groundwater, precipitation, recent ice, the troposphere, the biosphere, and the built environment [15-19]. PFAS contamination can occur as widespread background levels or as concentrated hotspots near specific sources. At contaminated sites, PFAS concentrations are generally orders of magnitude higher than background levels [20-24].

Not only the longevity and the widespread occurrence are problematic, but also the bioaccumulation, biomagnification, and toxic effects of various precursors, by-products, and transformation products [25,26]. PFAS exposure has been associated with numerous human diseases and malignancies, such as reproductive toxicity [27], immunotoxicity [28], increased cholesterol levels [29], neurodevelopmental abnormalities [30,31], cancer [32], and more.

Therefore, concerns have grown in the last decades, leading to new regulations, phase out, and production shift to alternative substances. Short-chain analogues, defined as PFCAs with < 7 perfluorinated carbons and PFSAs with < 6 perfluorinated carbons [33], have been shown to be less bioaccumulative and potentially toxic than long-chain PFAS [34]. Therefore, the commercial production of PFAS has shifted towards short chain alternatives as well as new fluorinated moieties like per- and polyfluorinated ethers, and generally towards polyfluorinated substances to obtain a better degradability [1,33]. Several PFAS have already been banned or are strictly regulated, including PFOS, PFOA, PFHxS, C9 to C14 PFCAs, and GenX (hexafluoropropylene oxide dimer acid, HFPO-DA) [35-37]. Instead of banning individual PFAS, which has repeatedly led to the substitution of one compound by another with similar toxicological properties, a new restriction proposal has been drafted under the European Union (EU) REACH (Registration, Evaluation, Authorisation and Restriction of Chemicals) regulation process. If enacted, it would result in a comprehensive ban on all PFAS, with only a few exceptions [38].

Additionally, the EU Drinking Water Directive (EU 2020/2184) introduced two key limits: a maximum of 0.10 µg/L for the sum of 20 specific PFAS (*PFAS-20*) and 0.50 µg/L for total PFAS, encompassing all measurable compounds. These thresholds must be implemented by January 12, 2026 [39,40]. In line with this, Germany revised its national Drinking Water Ordinance in June 2023, aligning with EU requirements. Furthermore, Germany introduces a stricter limit of 20 ng/L for four high-risk PFAS (*PFAS-4*: PFOA, perfluorononanoic acid (PFNA), perfluorohexane sulfonic acid (PFHxS), and PFOS), effective from January 2028, to further enhance public health protection [41-43].

The introduction of new regulations and growing awareness of the PFAS problem have motivated method validation and standardization, including interlaboratory comparison studies [44], significant improvements in analytical techniques enabling quantification at the part-per-quadrillion (ppq) level [45], the expansion of target analytes (e.g. using parameters such as extractable organofluorine, EOF) [46], the investigation of various environmental matrices, the implementation of monitoring programs [47,48], testing of removal technologies in water treatment [49], and the development of assessment tools and risk models [25].

1.2. Aqueous Film-Forming Foam (AFFF) Contaminated Soil and Groundwater

A major application of PFAS is in fluorosurfactant-based firefighting foams, particularly AFFFs, which are employed to extinguish Class B fires involving flammable liquids, such as oil, jet fuel, other non-water-soluble hydrocarbons, alcohols, and acetone [50]. PFAS are crucial for maintaining foam stability and promoting the formation of a water film that separates the burning material from the foam, preventing reignition [51].

Various manufacturers produce AFFF products, leading to different chemical formulations [52,53]. Historically, 3M was the sole producer of AFFF formulations containing PFCAs, PFSAs, and their derivatives, most notably through its Light Water brand in which PFOS was a key ingredient until its phase-out in the early 2000s [52,54-57]. While 3M's early AFFF formulations were based on ECF-derived PFAS, other manufacturers began to develop alternatives. Starting in the 1970s and lasting until around the 2010s, a broader array of legacy fluorotelomer AFFFs made by companies such as Ansul, National Foam, Chemguard, and Chemours entered the market [54,57]. These relied on long-chain fluorotelomer precursors. In more recent years, the industry has shifted to modern C_6 fluorotelomer AFFFs, which use short-chain PFAS as surfactants and are marketed as less harmful, even though they remain highly persistent in the environment [58]. PFAS in AFFFs are often cationic or zwitterionic, and some of the widely used examples include perfluoroalkyl sulfonamide propyl dimethylamines (PFASAm-Pr-DiMeAms), fluorotelomer sulfonamide propyl betaines (FTSAm-Pr-Bs), and n:1:2 fluorotelomer betaines (n:1:2 FTBs), among others [57,59,60]. However, because manufacturers are not required to disclose the exact formulations of their AFFF products, a large portion of the PFAS present in these foams remains unreported [59].

As AFFF is directly discharged into the environment during firefighting operations, training exercises, or accidental releases, areas surrounding these activities often exhibit high diversity and elevated levels of PFAS contamination [60-63]. Soils near fire training sites, airports, military bases, and industrial facilities can accumulate high concentrations of PFAS, while surface water and groundwater may become contaminated through runoff, infiltration, or leaching [64,65]. Once released, these PFAS undergo transformation processes. Studies have shown that various PFAS in AFFF formulations can degrade into legacy PFAS such as PFAAs, fluorotelomer sulfonic acids (FTSAs), and fluorotelomer sulfonamides (FTSAms) via processes like photochemical oxidation or biodegradation [66-70]. These TPs, such as PFAAs, are highly persistent in the environment. Short-chain TPs are more mobile, allowing them to

migrate into groundwater, whereas long-chain TPs are predominantly retained in the upper soil layers, as well as zwitterionic and cationic precursors, which tend to bind with negatively charged soil particles due to electrostatic interactions [61,71]. The widespread persistence and environmental mobility of precursors or TPs make AFFF-associated contamination a major concern for both environmental and public health.

In June 2023, the European Chemicals Agency (ECHA) adopted its final opinion supporting a gradual ban on the use of PFAS in firefighting foams to reduce environmental emissions [72]. Following this, the Commission Regulation (EU) 2025/1988 of October 2, 2025, formally amended REACH Annex XVII to prohibit PFAS in firefighting foams above 1 mg/L, with the ban taking effect on October 23, 2030 and sector-specific transition periods allowing a phased phase-out [73]. Replacing PFAS-containing foam with alternative fluorine-free foams remains challenging due to variations in their performance across different Class B fire scenarios. Although fluorine-free foams demonstrate greater biodegradability and reduced environmental persistence, some formulations exhibit similar environmental impacts and equal or even higher toxicity. Further research is needed to address existing knowledge gaps in areas such as fire suppression performance, environmental fate, transport, bioaccumulation, and toxicity [58,74,75].

One notable example of AFFF contamination occurred in Reilingen, southwest Germany, following a major fire at a mattress storehouse in 2008. During the incident, several fire departments responded and deployed large quantities of AFFF to suppress the blaze. The foam runoff entered an drainage ditch and subsequently spread into surrounding agricultural land, causing widespread environmental contamination [76].

1.3. PFAS Analysis in Environmental Samples

Reliable analysis of PFAS in environmental samples, such as soil and groundwater, is critical to assess contamination, understand their fate and transport, and support effective regulation and remediation. However, PFAS analysis remains highly challenging. Thousands of PFAS are currently in use, yet only a limited number of analytical reference standards are commercially available, restricting the scope of targeted analyses [77-79]. In addition, the structural diversity and physicochemical properties of PFAS lead to variable extraction recoveries [60], inconsistent ionization efficiencies [80,81], and difficulties in chromatographic retention [82-84]. Analytical sensitivity is further complicated by the often low concentrations of PFAS in real-world samples, which demand highly selective and sensitive methods [85-87]. Together,

these challenges highlight the urgent need for continued advances in PFAS detection and quantification methodologies.

First of all, soil and groundwater samples must be collected with strict contamination prevention measures to avoid introducing background PFAS from equipment or materials. Homogenization and proper storage are essential to maintain sample quality until analysis [88].

Extraction of PFAS from environmental samples is highly matrix-dependent, with water and soil requiring different approaches to achieve reliable recoveries. Inconsistent extraction efficiencies across methods contribute to variability in measured PFAS concentrations, which can arise from differences in solvent selection, extraction technique, and clean-up procedures. For aqueous samples, solid-phase extraction (SPE) is the most commonly applied method, providing efficient concentration and clean-up of PFAS prior to instrumental analysis [87,89]. In contrast, soil samples typically require more intensive extraction procedures, such as the use of organic solvents, sonication-assisted extraction, and subsequent clean-up steps. Soil extraction is further complicated by the complex composition of the matrix. High organic matter content, clay, and other particulates can strongly bind PFAS, especially long-chain and cationic or zwitterionic compounds, due to electrostatic interactions with negatively charged soil components, reducing extraction efficiency [90]. Short-chain PFAS are generally more mobile and easier to recover [91]. Several studies have highlighted these challenges and evaluated different extraction approaches [60,78,92]. For example, Nickerson et al. (2020) [60] developed a method involving sequential basic and acidic methanol extractions to recover anionic, cationic, and zwitterionic PFAS from field-collected, AFFF-impacted soils, while Munoz et al. (2018) [92] demonstrated that traditional extraction methods for anionic PFAS may underperform for cationic and zwitterionic compounds, and that sequential methanol-based extractions with ammonium acetate or hydrochloric acid provide improved recoveries from diverse soil matrices.

Following extraction, PFAS in environmental samples are typically analyzed using advanced analytical workflows that combine chromatographic separation, ionization, and mass spectrometric detection. Separation of PFAS prior to detection is necessary to prevent signal overlap and matrix interference, ensuring accurate and sensitive mass-spectrometric detection. High performance liquid chromatography (HPLC) under reversed-phase (RP) conditions is the most commonly used technique for polar, ionic, and semi-volatile PFAS, whereas gas chromatography (GC) is occasionally applied for more volatile PFAS [7]. Ionization is a key determinant of analytical sensitivity. Electrospray ionization (ESI) is the most widely used

method for PFAS, capable of operating in negative mode for anionic or zwitterionic compounds and positive mode for cationic or zwitterionic compounds. Alternative techniques, such as atmospheric pressure chemical ionization (APCI) and atmospheric pressure photoionization (APPI) are rarely applied [7,64,87]. Ionization efficiency depends on PFAS physicochemical properties, such as polarity, acid-base properties, and molecular volume, the properties of the eluent, and the geometry of the ionization source [93,94], as well as on the sample matrix [95], with matrix effects (MEs) potentially causing signal suppression or enhancement [96]. These effects are mitigated using isotopically labeled internal standards or matrix-matched calibration [96]. Detection and quantification of PFAS are performed using either tandem mass spectrometry (MS/MS) or high-resolution mass spectrometry (HRMS). MS/MS, typically implemented on triple quadrupole (QqQ) instruments, is highly sensitive and selective, ideal targeted screening and quantification of known PFAS using analytical reference standards [87]. Limited availability of standards, however, restricts the number of PFAS that can be reliably measured [77-79]. In contrast, HRMS instruments, including quadrupole time-of-flight (QTOF), Orbitrap, or Fourier transform ion cyclotron resonance (FT-ICR), provide very high mass accuracy and resolving power, enabling non-targeted screening (NTS) of unknown or emerging PFAS [87]. Due to the large datasets generated, data reduction and prioritization strategies are employed, often based on retention time and mass-to-carbon ratio. Prioritized features are evaluated based on exact mass, mass defect, isotopic pattern, MS/MS fragmentation spectra, peak shape, and the presence of homologous series [97]. Software tools such as PFΔScreen [98], Compound Discoverer [99], and FluoroMatch [100] facilitate systematic prioritization and identification.

Because traditional targeted analysis focuses on a predefined set of known PFAS, numerous unidentified or emerging compounds in environmental samples may remain undetected and unquantified. To address this limitation, semiquantitative non-targeted screening (qNTS) approaches are essential, which enable approximate quantification of a broader spectrum of PFAS [94]. This provides a more comprehensive assessment of contamination, particularly in complex matrices such as AFFF-impacted soils. A common strategy for semiquantification relies on using a structurally similar compound as a surrogate for the analyte of interest. The molar response factor (RF) of the surrogate, calculated as the ratio of the measured signal to its known concentration, is then applied to estimate the concentration of the suspect PFAS [101-103]. While conceptually straightforward, this approach depends on the availability of suitable surrogates, can be time-consuming, and often lacks accuracy when the analyte differs structurally. Alternative strategies have been proposed to improve semiquantification. For

example, average calibration curves (ACCs) were developed by Cao et al. (2023) [104], bootstrap-sampled surrogate calibrations were employed by Pu et al. (2024) [105], and machine learning approaches have been applied to predict ionization efficiencies in ESI, as demonstrated by Lauria et al. (2024) [106].

In addition to targeted and non-targeted approaches, sum parameter methods provide an alternative or complementary approach to assess total PFAS contamination. These approaches aim to capture the overall PFAS burden in a sample, including both known and unknown compounds, and can be particularly useful when the chemical diversity is high or analytical reference standards are unavailable. Common sum parameter techniques include total fluorine (TF), EOF, and the total oxidizable precursor (TOP) or PhotoTOP assay [107]. TF measures the overall concentration of all fluorine species, both organic and inorganic, present in a sample, providing a broad estimate of total fluorine content but potentially overestimating PFAS due to the inclusion of non-PFAS fluorine sources [108]. By contrast, EOF focuses only on the organic, extractable fraction, which is more representative of total PFAS but may still include non-PFAS organofluorines. EOF analysis typically involves solvent extraction of organofluorine compounds followed by combustion of the extract and quantification of the released fluoride ions [78,109-114]. The TOP assay is used to assess PFAS precursors that are difficult to detect directly but can be converted into stable, measurable end products through oxidation. In this method, PFAS precursors are exposed to strong oxidizing agents that transform them into stable end products such as PFCAs, which can then be quantified using conventional targeted analysis. Compared to TF and EOF, TOP partially preserves the original perfluorinated chain lengths, offering more meaningful information about the composition of PFAS precursors [115-119]. The PhotoTOP assay serves as an alternative to the conventional TOP assay, differing mainly in the oxidation process. The method employs ultraviolet (UV) light in combination with titanium dioxide (TiO_2) as a catalyst to drive photochemical oxidation of PFAS precursors. Compared to TOP, PhotoTOP avoids high salt concentrations, allows for direct sample injection, better preserves perfluoroalkyl chain lengths due to milder oxidation conditions, and enables monitoring of the reaction by sampling at multiple time points, thereby improving both accuracy and reliability [120,121].

2. Aims of the thesis

This dissertation aims to provide a comprehensive assessment of PFAS contamination at a site impacted by AFFF, using Reilingen in southwest Germany as a representative case study. Reilingen was selected because a major fire incident in 2008 led to the large-scale deployment of firefighting foam. Runoff from the foam entered an drainage ditch and spread into adjacent agricultural land, creating a well-documented example of PFAS contamination in both soil and groundwater.

PFAS present in AFFF formulations represent a chemically diverse group that extends far beyond the commonly studied PFAAs. Many of these compounds, especially cationic and zwitterionic species, lack commercially available reference standards, which hampers both detection and quantitative assessment. Furthermore, AFFF formulations have changed over time, and the identity and proportions of PFAS present in more recent foams remain only partially understood. These knowledge gaps call for innovative analytical approaches capable of capturing the full spectrum of PFAS, including unknown precursors and TPs.

The first objective of this work was therefore to develop and apply an extraction protocol optimized for soil matrices in order to recover a broad range of AFFF PFAS. The second objective was to perform target and non-target screening to characterize the contamination profile in soil and groundwater, enabling the identification of both known compounds and previously unreported PFAS. The third objective was to establish a matrix-matched semiquantification strategy using ionization class-specific average calibration curves (AACs) to enable quantification beyond the available target PFAS, complemented by a fluorine mass balance based on EOF to validate this novel approach. Lastly, the aim was to investigate the environmental fate and transformation behavior of AFFF PFAS using the PhotoTOP assay. This method not only provides a sum parameter for overall transformation potential but also provides insights into degradation pathways, the formation of intermediate products, the stability of precursor compounds, and the transformation kinetics.

By integrating the results of the three underlying studies (Appendix 1-3), including target and non-target screening, semiquantification, and the PhotoTOP assay, this dissertation provides a holistic understanding of PFAS occurrence, distribution, transformation pathways, and environmental persistence at the Reilingen site and contributes broadly to the characterization of PFAS contamination from AFFF use. Throughout the thesis, the consistent novel terminology introduced in Appendix 1 was applied.

3. Methods

3.1. Sampling and Processing of Soil and Water Samples

Soil and groundwater samples were collected in May 2023 at the *Nachtwaidgraben* field site in Reilingen. Four spatially distributed drill cores were taken to a maximum depth of 3 m. Each core was sectioned into six 0.5 m intervals, and composite samples were prepared for each depth interval, yielding six soil samples. The composites were dried, ground, and sieved. Groundwater was sampled from a roadside monitoring well and centrifuged prior to analysis. Details on the sampling site and processing are provided in Appendix 1.

3.2. PFAS Extraction from Soil

To identify an effective extraction procedure for PFAS in soil, several methods were initially evaluated, including methanol (MeOH) alone, MeOH with additives (0.1 M NH_4OH or 0.4 M NH_4Ac), and the combined acid/base approach described by Nickerson et al. (2020) [60]. Based on recovery efficiency, sequential triple extraction with MeOH containing 0.4 M NH_4Ac was selected as the final method. Detailed information on chemicals and extraction procedures is provided in Appendix 1.

3.3. Analysis of PFAS

3.3.1. Instrumental Analysis

Soil extracts and groundwater samples were analyzed using HPLC coupled to a QTOF with ESI. Separation was performed on a C18 RP column using a gradient of water and MeOH with 2 mM NH_4Ac. The ESI source was operated in both positive and negative ionization modes, and iterative data-dependent MS^2 (dd MS^2) acquisition was applied to maximize MS^2 coverage. Detailed instrumental parameters and quality control (QC) procedures are provided in Appendices 1 and 2.

3.3.2. Target and Non-Target Screening

Target screening (confidence level 1) was performed using 51 PFAS analytical reference standards by matching accurate mass, retention time (RT), and MS^2 spectra. Details on the available standards are provided in Appendix 1.

The first step in the NTS workflow was feature reduction and prioritization, performed using the Python-based software tool PFΔScreen [98]. Detected features were filtered and ranked

based on blank correction, their mass-to-carbon ratio (m/C), and RT to identify potential PFAS. Features with m/C > 23 and RT > 4 min were retained, reflecting the typical m/C range of PFAS (30-60) and the chromatographic behavior, where highly polar compounds elute in the first 4 min, while moderately polar to non-polar substances such as PFAS of interest elute later [122]. Further correlation of features allowed grouping of fragments and adducts with their molecular ions.

After feature reduction and prioritization, suspect screening was performed using PFΔScreen [98] with a suspect list from the National Institute of Standards and Technology (NIST) [123] combined with an in-house prepared suspect list. In addition, measured data were manually screened against relevant AFFF-related PFAS reported in the literature, which allowed inclusion of low-abundance features that were not detected by the feature-finding algorithm of PFΔScreen. Prioritized features, both with and without a suspect hit, as well as manually identified features from the literature, were subjected to structural confirmation or identification. Identification began by checking all possible molecular ions in both negative and positive ESI modes to determine the ionic character (anionic, cationic, or zwitterionic). The presence of homologues was checked by examining CF_2 and C_2F_4 repeating units using the Raw Data Visualization tool in PFΔScreen, indicating ECF-based or fluorotelomer-derived structures, respectively [124]. Peak shapes were also examined, as non-baseline-separated split peaks often suggest differently branched and/or linear isomers typical of ECF-based compounds. For suspect hits, isotopic patterns were compared with the proposed formulas. In cases without a proposed structure, isotopic patterns and exact masses were used to suggest molecular formulas via MSTools [125] and ChemCalc [126].

When available, MS^2 spectra were manually inspected for fragments consistent with the proposed structure. Features without suspect hits were analyzed for typical PFAS fragments and characteristic fragment differences. The software MetFrag [127] was additionally used to support structural verification.

To classify the identified substances, a confidence level scheme adapted from Charbonnet et al. (2022) [128] was applied. As PFAS are rarely represented in MS^2 libraries, the library-matching criterion was omitted, and the mass-to-carbon ratio (m/C > 25) was included as an additional criterion. Where available, MS^2 data from peer-reviewed literature were also considered to support the assigned confidence levels, following the general approach of Schymanski et al. (2014) [129]. Detailed information on the NTS workflow, including software settings,

parameters, feature prioritization, identification, and confidence level assignment, is provided in Appendix 1.

3.3.3. Quantification and Semiquantification

Matrix effects can significantly influence ionization efficiency and, consequently, the quantification of PFAS. Due to the limited availability of isotopically labeled internal standards, quantification and semiquantification were performed using a standard addition approach (matrix-matched calibration) to account for MEs. For identified PFAS (confidence level 1) in the topsoil, standard addition was carried out using the respective analytical reference standards.

Semiquantification was performed using an average calibration curve approach similar to that described by Cao et al. (2023) [104]. ACCs were derived from the matrix-matched calibration curves of available PFAS reference standards via log-log transformation of molar concentration and signal intensity. The calibration curves were established using the topsoil extract to account for MEs representative of the sample matrices. To enhance accuracy, separate ACCs were constructed for four major PFAS ionization classes: carboxylic acids, sulfonic acids, sulfonamides, and cationic/zwitterionic PFAS. Absolute accuracy quotients (AAQs) were calculated to identify outliers for exclusion from the ACCs and to assess the overall accuracy of the semiquantification approach. The resulting class-specific calibration models were applied to estimate concentrations of tentatively identified PFAS (confidence level 2 and 3) in the topsoil.

As the matrix-matched ACCs were established based on the topsoil extract, their applicability to deeper soil layers was evaluated by determining MEs for each depth using isotopically labeled internal standards. The calibration curves of individual PFAS standards for quantification, as well as the constructed ACCs for semiquantification, were subsequently applied to the respective soil layers.

Extractable organofluorine was determined for the topsoil extract by combustion ion chromatography (CIC) to assess the extractable fluorine mass balance (MB). Details on quantification and semiquantification workflows, EOF analysis, and calculations are provided in Appendix 2.

3.4. PhotoTOP Assay

Photocatalytic oxidation experiments were conducted using the previously developed PhotoTOP protocol [120] to investigate the transformation of AFFF-related PFAS. The protocol was applied to selected AFFF PFAS reference standards, the collected topsoil sample, and a

methanolic extract of the soil sample. For the experiments, TiO_2 was used as a photocatalyst and mixed with the respective matrices (standards, soil, or extract). After solvent evaporation and resuspension in water, samples were irradiated in a UV photoreactor. During irradiation, aliquots were periodically collected and prepared for subsequent PFAS analysis.

Target PFAS were quantified using HPLC coupled to a QqQ with ESI. Separation was performed on a C18 RP column using a gradient of water and MeOH with 2 mM NH_4Ac. Electrospray ionization was operated in both positive and negative mode. Suspect and non-target PFAS were analyzed using the HPLC-QTOF setup described in section 3.3.1.

To evaluate the kinetics and stability of the different PFAS during the PhotoTOP experiments, the transformation and formation profiles were fitted using four model types, depending on the shape of the curves: logistic formation, exponential decay, a combination of logistic formation and exponential decay, and a two-step exponential formation and decay. Detailed information on the PhotoTOP workflow, instrumental parameters, and kinetic modeling is provided in Appendix 3.

4. Results and Discussion

4.1. Combined Target and Non-target Screening for Comprehensive PFAS Identification in Soil and Groundwater

NTS Workflow

Both target and non-target screening approaches were applied to comprehensively identify PFAS in soil and groundwater. While target screening allows confident identification of known PFAS, NTS produces large and complex datasets that require systematic data reduction to focus on relevant features. Therefore, feature reduction and prioritization were implemented as the first step of the NTS workflow.

The upper horizon of soil sample (0-0.5 m) was analyzed by LC-HRMS in both positive and negative ESI modes, and data evaluation was performed using PFΔScreen. The raw output contained 2262 and 1921 non-target features in ESI^- and ESI^+, respectively, after isotope cluster componentization. Prioritization was achieved by retaining only features with m/C > 23 and RT > 4 min, separating highly fluorinated PFAS from hydrocarbon-dominated matrix compounds and early-eluting polar substances. This step reduced total peak areas by 79% (ESI^-) and 82% (ESI^+), corresponding to a 95% reduction in the number of features. From the prioritized features, 92-94% of the peak areas could be identified as PFAS (confidence levels 1-3), while an additional 3-6% were classified as potential PFAS (confidence levels 4-5, Figure 1 a). This confirms that the m/C- and RT-based prioritization efficiently reduced the dataset while retaining the vast majority of PFAS, thereby effectively minimizing data complexity and providing a solid basis for subsequent structural identification and semiquantification.

Overall, 124 features of 42 subclasses were identified as PFAS in soil (confidence levels 1-3). Among these, 10 subclasses were confirmed using analytical reference standards at confidence level 1, 28 were assigned to confidence level 2, and 4 to confidence level 3. These three confidence levels accounted for 52.7%, 41.7%, and 0.3% of the identified peak area, respectively. A subset of 12 subclasses, comprising 25 individual compounds, was also detected in the groundwater. An additional 114 features were assigned to confidence levels 4 and 5, including 17 homologous series, together representing 5.2% of the identified peak area (Figure 1 b). The large proportion of tentatively identified substances (confidence levels 2-5) indicates

that the extent of PFAS contamination far exceeds the subset of known target compounds, highlighting the importance of qNTS for comprehensive assessment in such contaminated sites.

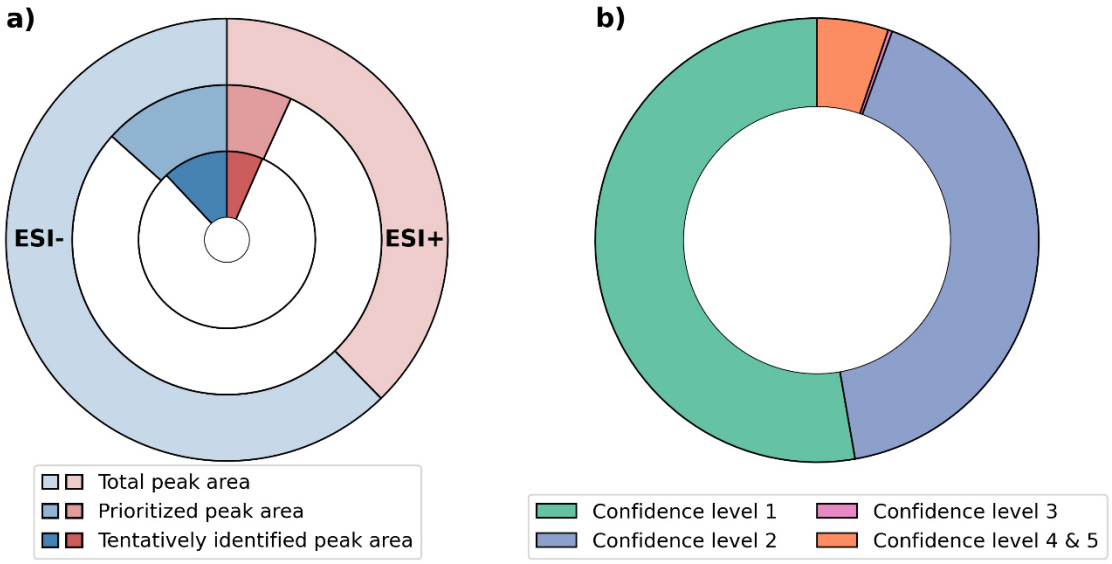

Figure 1: a) Cumulative peak areas of all detected features in the topsoil sample based on the PFΔScreen output (outer section), peak areas of prioritized features (middle section), and peak areas of features tentatively identified as PFAS (inner section) in negative and positive ESI modes. Peak areas of in-source fragments and adducts were combined with the corresponding parent ions. b) Distribution of peak areas of tentatively identified PFAS across the assigned confidence levels in the topsoil.

Identified PFAS in Soil and Groundwater

Only PFAS subclasses identified with confidence levels 1-3 are discussed in the following sections, and all substances are referred to by their respective acronyms (Appendices 1 and 2). A total of 42 subclasses were identified in soil and 12 in groundwater. These classes, along with their detected chain lengths, are summarized in Table 1.

The previously unreported PFAS subclass n:2/m:2 FTSAm dimer was identified in the soil sample (highlighted in red in Table 1), comprising two homologues, 6:2/6:2 and 6:2/8:2 FTSAm dimers. The corresponding m/z values have previously been reported as unknown features [130,131], but were structurally elucidated for the first time in this study. MS^2 spectra strongly support these structures, showing multiple diagnostic fragments, including the characteristic $[SO_2NH_2]^-$ fragment indicating a sulfonamide group, as well as multiple neutral losses of HF typical for fluorotelomer-based PFAS. Chromatographic separation from corresponding monomeric n:2 FTSAm analogues rules out dimer formation as an ionization artifact.

To the best of our knowledge, nine additional PFAS subclasses were detected in soil for the first time (highlighted in purple in Table 1). These include two FTSA derivatives (K-n:2 FTSA and

U-n:2 FTSA), three fluorotelomer betaines (n:1:3, n:2, and n:4 FTB), three fluorotelomer sulfonamides (n:2-U-Pr-DiMeAm, n:2 FTSAm-PrA, and n:2 FTSAm-*N*-Me-*N*-PrA), and one fluorotelomer sulfone (n:2 FTSy-(2′)OHPr-TriMeAm).

The K-n:2 FTSA and U-n:2 FTSA subclasses were identified based on MS^2 fragments of the unsaturated fluorinated carbon chain and the diagnostic $[SO_3H]^-$ fragment, characteristic of the sulfonic acid moiety. These MS^2 patterns are consistent with previous observations by Fang et al. (2024) [132], who detected K-6:2 FTSA and U-6:2 FTSA as biotransformation products of 6:2 FTSA in aerobic sludge. Chromatographic separation confirms that the U-n:2 FTSAs are not artifacts of in-source fragmentation from K-n:2 FTSAs.

The n:2 FTB, n:1:3 FTB, and n:4 FTB subclasses were identified based on diagnostic fragments $[C_4H_{10}NO_2]^+$, $[C_5H_{12}NO_2]^+$, and $[C_4H_8NO_2]^+$, indicative of the betaine moiety, with at least one fragment detected for at least one homologue of each class. MS^2 spectra of FTBs are generally sparse due to the fixed positive charge on the quaternary ammonium group, making accurate mass and isotopic patterns essential for confident identification. These subclasses were previously reported in Ansulite AFFF at low abundance [53].

The three FTSAm-based subclasses n:2 FTSAm-U-Pr-DiMeAm, n:2 FTSAm-PrA, and n:2 FTSAm-*N*-Me-*N*-PrA were identified based on diagnostic MS^2 fragments. For 6:2 FTSAm-U-Pr-DiMeAm, fragments including $[C_{10}H_9F_{13}NO_2S]^+$ (from loss of the terminal C_3H_7N group) and quaternary ammonium fragments supported the proposed structure and matched literature data [132]. 6:2 FTSAm-PrA showed fragments corresponding to the fluorinated carbon moiety and functional groups ($[NSO_2]^-$, $[FSO_2]^-$, $[C_3H_6NO_4S]^-$) including HF losses. For 6:2 FTSAm-*N*-Me-*N*-PrA, fragments such as $[SO_2NH_2]^-$ and $[C_4H_8NO_4S]^-$ support the fluorotelomer structure and indicate the functional groups and non-fluorinated moiety, in agreement with Fang et al. (2024) [132]. The n = 6 homologues of all three subclasses have been previously detected as biotransformation products of 6:2 FTSAm-Pr-DiMeNO in aerobic sludge [132], and 6:2 FTSAm-PrA was observed as an intermediate in the aerobic biodegradation of 6:2 FTSAm-Pr-DiMeAm [133].

The MS^2 spectra of the n:2 FTSy-(2′)OHPr-TriMeAm subclass revealed fragments consistent with the proposed structure, including losses of terminal moieties (C_3H_9N and further C_3H_4O) from the molecular ion and fragments from the terminal end of the molecule ($[C_6H_{16}NO_3S]^+$, $[C_3H_7O_3S]^+$, $[C_5H_{12}NO]^+$). This subclass has previously been reported in various AFFF formulations [53,59,134,135].

For the remaining 32 PFAS subclasses detected in soil and groundwater, identification was based on the workflow described above. A detailed account of the identification process, including supporting MS^2 spectra and fragment assignment for each level 2 and 3 substance, is provided in Appendix 1.

Table 1: Summary of PFAS identified in topsoil (S1) and groundwater (GW). The table includes all previously detected subclasses in soil for which at least one homologue was assigned confidence levels 1-3. Newly identified PFAS are highlighted in red, and PFAS newly identified in soil are highlighted in purple. Identified homologues are shown in brackets; some homologues may have lower confidence levels. For simplicity, only one positional isomer is depicted when the exact position is uncertain. K-PFSA/U-E-PFSA are shown in brackets to indicate that both structural assignments are possible.

Row	Common base structure	Subclass defining moiety (R)			
1	**PFAAs & FTAAs** 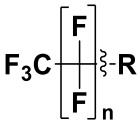	**PFCA** (S1: C_4-C_{12}, GW: C_3-C_7) 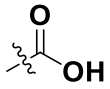	**PFSA** (S1: C_3-C_{13}, GW: C_4-C_8) 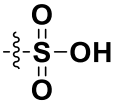	**n:3 FTCA** (S1: n = 3-9) 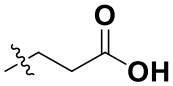	**n:2 FTSA** (S1: n = 6-14, GW: n = 6) 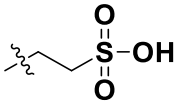
2	**PFSA derivatives** 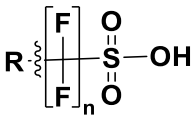	**Cl-PFSA** (S1:C_6, C_8) 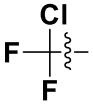	**K-PFSA** (S1: C_6-C_{14}) 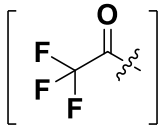	**SF_5 -PFSA** (S1:C_7-C_{10}) 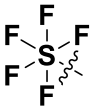	**H-PFSA** (S1:C_8, C_{10}) 
3	**U-PFSA derivatives** 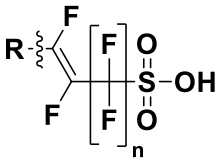	**U-PFSA** (S1: C_6-C_{15}) 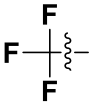	**U-E-PFSA** (S1: C_7-C_{15}) 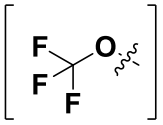	**SF_5-U-PFSA** (S1: C_8-C_{10}) 	
4	**FTSA derivatives** 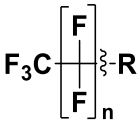	**OH-n:2 FTSA** (S1: n = 6, 8) 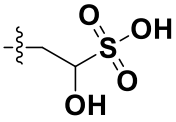	**K-n:2 FTSA** (S1: n = 6-10, GW: n = 6) 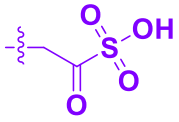	**U-n:2 FTSA** (S1: n = 6, 8) 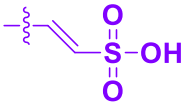	
5	**PFASAm and derivatives** 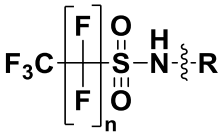	**PFASAm** (S1: C_3-C_8, GW: C_3-C_6) 	**PFASAm-Me** (S1: C_4, C_6, C_8, GW: C_8) 	**PFASAm-EtA** (S1: C_6, C_8, GW: C_8) 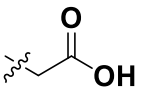	

6	**PFASAm-Pr-based AFFF PFAS** 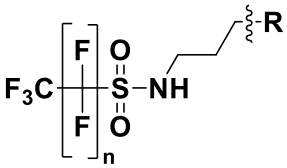	**PFASAm-Pr-DiMeAm** (S1: C_6, C_8) 	**PFASAm-Pr-TriMeAm** (S1: C_6, C_8) 	**PFASAm-Pr-B** (S1: C_4-C_6, C_8) 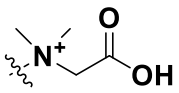	**PFASAm-PrSA** (S1: C_4-C_6) 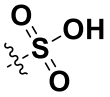
7	**FTBs** 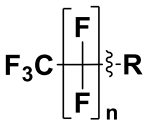	**n:1:2 FTB** (S1: n = 5-15, GW: n = 5, 7) 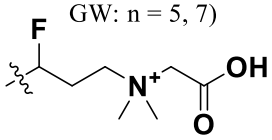	**n:1:3 FTB** (S1: n = 5-9) 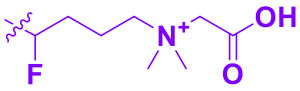		
		n:2 FTB (S1: n = 6-12) 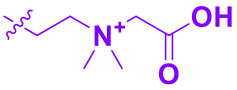	**n:3 FTB** (S1: n = 5-13, GW: n = 5, 7) 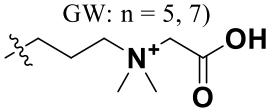	**n:4 FTB** (S1: n = 4-10) 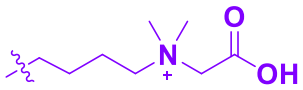	
8	**FTSAm and derivatives** 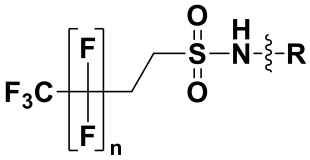	**n:2 FTSAm** (S1: n = 6-10, GW: n = 6) 	**n:2/m:2 FTSAm dimer** (S1: n = 6/m = 6, 8) 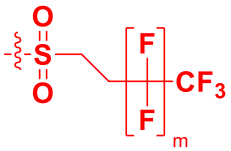	**n:2 FTSAm-Pr-MeAm** (S1: n = 6) 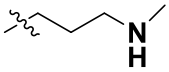	
		n:2 FTSAm-Pr-DiMeAm (S1: n = 6, 8) 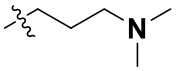	**n:2 FTSAm-U-Pr-DiMeAm** (S1: n = 6) 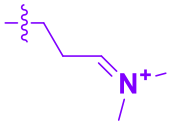	**n:2 FTSAm-Pr-DiMeNO** (S1: n = 6, 8) 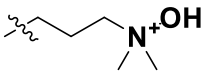	
		n:2 FTSAm-Pr-B (S1: n = 4-12, GW = 6) 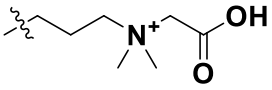	**n:2 FTSAm-PrA** (S1: n = 6) 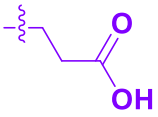	**n:2 FTSAm-*N*-Me-*N*-PrA** (S1: n = 6) 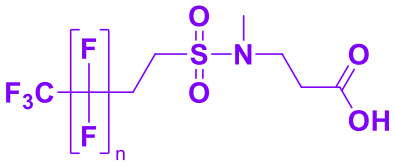	
9	**FTSy derivatives** 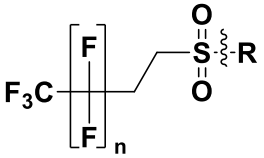	**n:2 FTSy-PrA** (S1: n = 4-8) 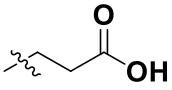	**n:2 FTSy-(2′)OHPr-TriMeAm** (S1: n = 4-8) 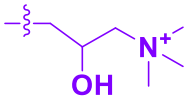	**n:2 FTSy-Pr-Ad-(5′,5′)DiMeEtSA** (S1: n = 6-12) 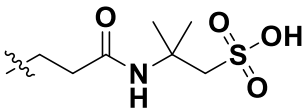	
10	**FTSO derivatives** 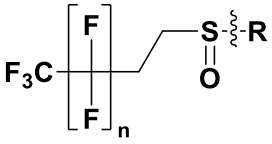	**n:2 FTSO-(2′)OHPr-TriMeAm** (S1: n = 4-8) 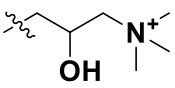	**n:2 FTSO-Pr-Ad-(5′,5′)DiMeEtSA** (S1: n = 6) 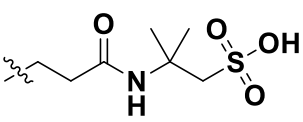		

11	Others	PFASyA (S1: C_8)	PFASAm-*N*-PrSA-*N*-Pr-DiMeAm (S1: C_4-C_6)	n:2 FTTh-(2′)OHPr-TriMeAm (S1: n = 4-10, GW: n = 4)
	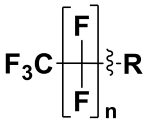	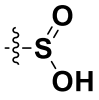	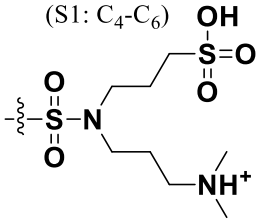	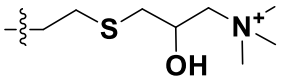

Occurrence of identified PFAS in AFFF formulations

A broad spectrum of PFAS identified in the Reilingen soil has previously been reported in AFFF formulations, reflecting the use of both ECF- and FT-based production technologies. PFAAs, including PFCA and PFSA, constituted major active ingredients in various AFFF formulations historically produced by 3M and Angus [55,59,64]. In addition, fluorotelomer-based acids such as n:2 FTSA are known constituents of several commercial foams, and n:3 FTCA have likewise been detected in such products, though at low concentrations [65,135,136]. PFSA derivatives, such as Cl-, H-, K-, SF_5-, U-PFSA, as well as the FTSA derivative OH-n:2 FTSA, have been identified in AFFF formulations [65,131]. Perfluoroalkane sulfonamides and related derivatives also occur in AFFF formulations. Among them, PFASAm-Pr-DiMeAm is one of the most predominant AFFF ingredients, while other PFASAm-based substances such as PFASAm, PFASAm-Pr-TriMeAm, PFASAm-Pr-B, and PFASAm-PrSA have also been reported in commercial foams [53,65,136]. In addition, an isomer of PFASAm-*N*-PrSA-*N*-Pr-DiMeAm has been reported in AFFF [65]. FTBs form another important class of AFFF-related PFAS. Particularly, n:1:2 FTBs and n:3 FTBs have been frequently detected in commercial foams [52,53,59,64,134], whereas n:2, n:1:3, and n:4 FTBs occur in lower abundance [53,65]. Several n:2 FTSAm-based PFAS have likewise been identified in AFFF, including n:2 FTSAm-MeAm, n:2 FTSAm-Pr-DiMeAm, n:2 FTSAm-Pr-DiMeNO, n:2 FTSAm-Pr-B, and the m/z corresponding to the n:2/m:2 FTSAm dimer [53,55,59,63-65,131,134-136]. Both n:2 FTSy-(2′)OHPr-TriMeAm and n:2 FTSO-(2′)OHPr-TriMeAm have previously been reported in AFFF formulations [53,59,131,134,135,137]. Among these, the sulfoxide analogue 6:2 FTSO-(2′)OHPr-TriMeAm is known to be one of the most abundant PFAS in contemporary AFFF products [135], whereas its sulfonyl precursor 6:2 FTSy-(2′)OHPr-TriMeAm typically occurs only at low levels, likely as an impurity [59,134]. The related thio compound n:2 FTTh-(2′)OHPr-TriMeAm is also a well-established AFFF ingredient and has been detected in several formulations from different manufacturers [52,53,59,64,134,135]. In addition, 6:2 FTSy-Pr-Ad-(5′,5′)DiMeEtSA, 6:2 FTSO-Pr-Ad-(5′,5′)DiMeEtSA, and 6:2 FTTh-Pr-Ad-

(5′,5′)DiMeEtSA are widely used AFFF compounds and have been repeatedly reported in AFFF formulations [52,53,59,64,131,134-136]. Overall, the presence of both FT-based and ECF-based precursor structures in the Reilingen soil strongly indicates that AFFF formulations from multiple manufacturers and from different production eras were used at the site. This suggests the application of both historical and more contemporary AFFF products during firefighting activities.

Implications from NTS

Even more than 15 years after AFFF application, contaminated sites still exhibit a complex mixture of PFAS and their TPs, confirming their long-term role as sources of PFAAs through ongoing precursor degradation. Comprehensive characterization of these mixtures is therefore essential for effective remediation planning and risk assessment. NTS proved to be a powerful approach for identifying a broad range of AFFF-related PFAS beyond the scope of targeted analyses, particularly in the absence of analytical standards for many cationic and emerging compounds. To complement structural elucidation, semiquantitative evaluation provides an important step toward assessing environmental relevance and relative abundance of detected PFAS. The following section focuses on the applied semiquantification approach and its role in estimating PFAS concentrations in the investigated soil samples.

4.2. Quantitative and Semiquantitative Assessment of PFAS in Soil

Semiquantification Method Validation

To enable quantitative assessment of the AFFF-derived PFAS contamination, including the numerous tentatively identified PFAS, a matrix-matched semiquantification approach was developed and validated. A total of 39 analytical PFAS standards were grouped into four ionization-based classes (carboxylic acids, sulfonic acids, sulfonamides, and cationic/zwitterionic PFAS) and used to construct class-specific ACCs. This approach was selected to account for MEs through standard addition and improve accuracy compared to a single, non-class-specific ACC by accounting for class-dependent ionization behavior.

Separate ACCs were generated for each PFAS ionization class and evaluated by re-estimating the concentrations of all 39 standards across seven calibration levels and four matrix dilutions, yielding up to 28 data points per standard (Figure 2 a). The resulting AAQs demonstrated class-dependent accuracy. Median AAQs were 1.78× for cationic/zwitterionic compounds, 1.70× for carboxylic acids, 1.32× for sulfonic acids, and 2.27× for sulfonamides (Figure 2 b). These

values fall within the typical error range reported for semiquantification approaches [94,104-106] and highlight the benefit of separating ionization classes: combining all anionic PFAS into a single ACC increased both the median AAQ (2.15×) and its variability. The broader AAQ distribution observed for sulfonamides reflects the large structural diversity covered by only six standards.

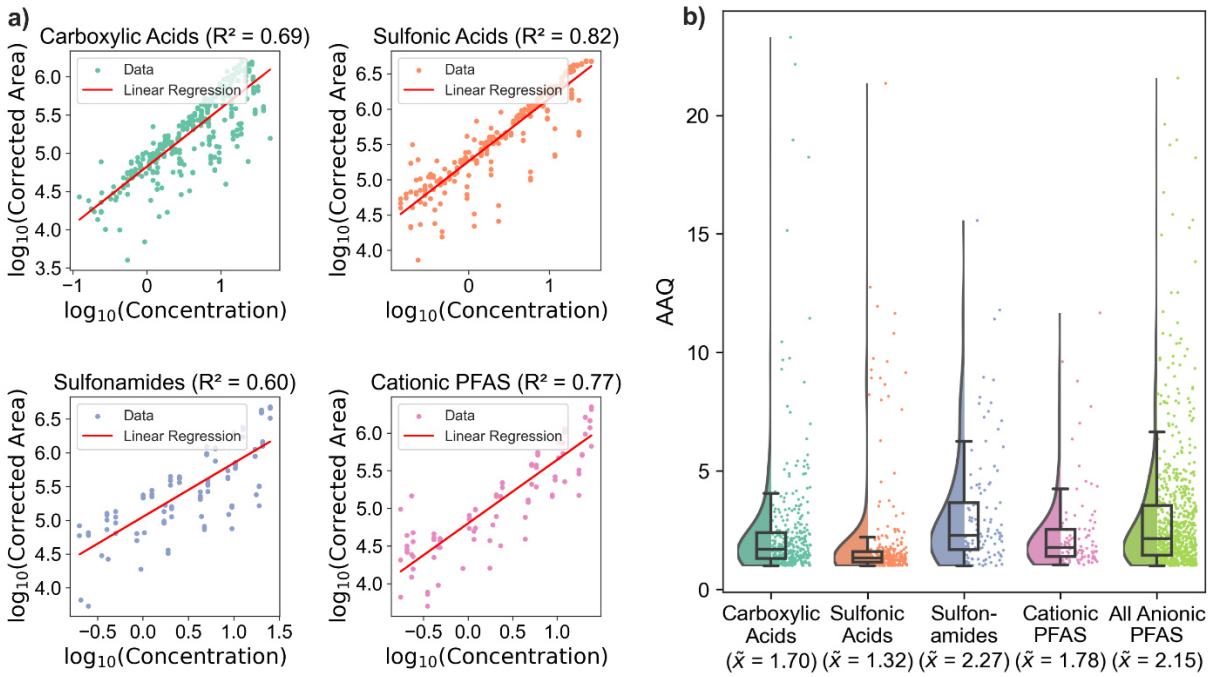

Figure 2: a) Matrix-matched average calibration curves (ACCs) for four ionization classes based on 39 authentic standards at 7 concentration levels and 4 matrix dilutions (dots represent measured data, lines represent linear regression). b) Absolute accuracy quotients (AAQ) of the semiquantification of standards for the four ionization classes and all anionic PFAS (box plots with median, 25 and 75 percentile and violin plots). Reprinted with permission from Capitain C, Schüßler M, Bugsel B, Zweigle J, Vogel C, Leube P, Zwiener C (2025). Implementation of Matrix-Matched Semiquantification of PFAS in AFFF-Contaminated Soil. *Environmental Science & Technology*, 59 (14), 7338-7347. DOI: 10.1021/acs.est.4c14255. Copyright 2025 American Chemical Society.

To verify the transferability of the ACCs to deeper soil layers, MEs across all depth intervals were evaluated using isotopically labeled internal standards. Most compounds showed moderate enhancement in deeper soils, whereas short-chain PFCAs exhibited signal suppression. For the majority of labeled standards, MEs ranged between -40% and +35%, which is acceptable for semiquantification (Appendix 2). Exceptions were PFOS and PFNA, whose MEs were influenced by coelution with highly concentrated PFOS in the topsoil. Such compounds were excluded from ACC construction. Given the overall moderate variability and the fact that ACCs were also based on diluted matrices exhibiting lower MEs, the topsoil-

derived ACCs were considered suitable for semiquantifying PFAS in all soil depths, with minor deviations (<40%) remaining within the expected uncertainty range of semiquantitative analysis.

PFAS Concentrations in Topsoil

PFAS concentrations in the topsoil were semiquantified using the four matrix-matched ACCs developed for the distinct ionization classes. In total, 96 tentatively identified AFFF-related PFAS were semiquantified, yielding a combined concentration of 7.86 µg/g. Cationic/zwitterionic PFAS constituted by far the dominant fraction, accounting with 6.83 µg/g for 87% of the semiquantified mass. Sulfonamide-based PFAS contributed an additional 0.69 µg/g, while carboxylates and sulfonates were present only at comparatively low concentrations (0.14 µg/g and 0.21 µg/g, respectively). Quantification based on authentic standards was possible for 28 PFAS, resulting in a summed concentration of 7.33 µg/g, again dominated with approximately 60% by cationic/zwitterionic AFFFs. The combined dataset of quantified and semiquantified PFAS resulted in a total PFAS burden of 15.19 µg/g.

The highest concentrations were observed for several positive ionized PFAS, including 6:2 FTSAm-Pr (zwitterionic), 6:2 FTSO-(2′)OHPr-TriMeAm, 6:2 FTSy-(2′)OHPr-TriMeAm, and various FTBs, but also for legacy compounds such as PFOS and fluorotelomer-derived substances including 6:2 FTSAm and various FTSAs (Figure 3).

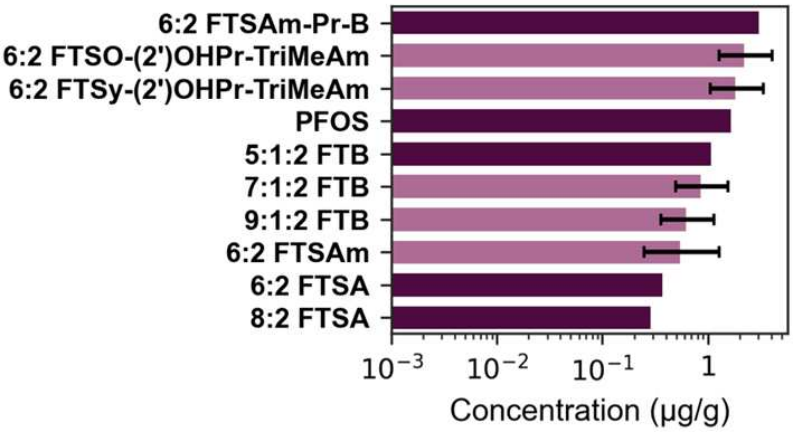

Figure 3: Concentrations of quantified (dark purple) and semiquantified (light purple) PFAS in the extract of topsoil in µg/g displayed with a logarithmic scale. Only the ten compounds with the highest concentrations are shown (all compounds in Appendix 2). Error bars for semiquantified PFAS represent the median AAQ of the corresponding ionization class. Modified with permission from Capitain C, Schüßler M, Bugsel B, Zweigle J, Vogel C, Leube P, Zwiener C (2025). Implementation of Matrix-Matched Semiquantification of PFAS in AFFF-Contaminated Soil. *Environmental Science & Technology*, 59 (14), 7338-7347. DOI: 10.1021/acs.est.4c14255. Copyright 2025 American Chemical Society.

The PFAS pattern in the topsoil, characterized by a high diversity of precursors and a dominant fraction of cationic and zwitterionic PFAS, is consistent with contamination originating from AFFF use. The particularly diverse composition observed here likely reflects the historical application of foams from multiple manufacturers [61,136]. Comparable concentration levels have been reported for other AFFF-impacted locations, with Bigler et al. (2024) [71] documenting up to 31 µg/g and Nickerson et al. (2021) [61] reporting concentrations of up to 3.81 µg/g at firefighter training areas, alongside additional studies describing similar magnitudes of contamination [138].

The summed PFAS concentration of 15.19 µg/g corresponds to 7.96 µg F/g. Comparison with the EOF content of 7.8 µg F/g indicates that the fluorine mass balance for the topsoil is essentially closed (102%). This is notable considering the inherent uncertainty of semiquantification, and highlights the value of nontarget screening combined with a structured semiquantification workflow for site assessment.

Because cationic and zwitterionic PFAS were the dominant contributors to the PFAS burden, the extraction solvent suitability was evaluated. Extraction using MeOH + 0.4 M NH_4Ac recovered nearly twice as much EOF (7.8 µg F/g) compared to MeOH alone (4.1 µg F/g), demonstrating the importance of ammonium buffering for the efficient extraction of positively charged and zwitterionic AFFF constituents [92,139].

PFAS Concentrations in Deeper Soil Levels

Semiquantified and quantified PFAS concentrations generally decreased with depth. The top two soil layers contained the majority of the contamination, with 15.19 µg/g in the uppermost layer (0-0.5 m) and 13.34 µg/g in the second layer (0.5-1 m). In contrast, concentrations in the deeper layers were lower: 4.03 µg/g (1-1.5 m), 5.02 µg/g (1.5-2 m), 1.75 µg/g (2-2.5 m), and 0.39 µg/g (2.5-3 m). This indicates that the top 1 m of soil retains the majority of PFAS contamination, consistent with previous field observations [20,71,140], and may be attributed to retardation mechanisms such as adsorption to solids and at the air-water interface.

4.3. Distribution by Chemical Characteristics Across Soil Profiles and Groundwater

Topsoil PFAS Distribution

The chemical characteristics of PFAS within the topsoil were further assessed based on (semi)quantified concentrations. In contrast to peak-area-based patterns, the distribution by

concentration reveals that positive ionized PFAS constitute the largest fraction with 51.3% of the total concentration of all identified confidence level 1-3 PFAS, followed by zwitterionic compounds at 23.3% and negative ionized PFAS at 25.4% (Figure 4 a). This shift is mainly due to the particularly high concentrations of several positive ionized PFAS, including 6:2 FTSO-(2′)OHPr-TriMeAm, 6:2 FTSy-(2′)OHPr-TriMeAm, and various FTBs. Zwitterionic compounds are largely dominated by 6:2 FTSAm-Pr, while significant contributions of negative ionized PFAS originate from legacy compounds such as PFOS, and fluorotelomer-derived substances including 6:2 FTSAm and other FTSAs (Figure 3).

The distribution of PFAS in the topsoil according to perfluorinated chain length shows that C_6 compounds dominate with 66.5% of the total concentration, followed by C_8 at 22.2% (Figure 4 b). C_{10} and C_7 PFAS account for 4.4% and 2.0%, respectively. Shorter-chain PFAS (C_3-C_5) and longer-chain substances (C_9, C_{11}-C_{14}) together account for less than 3% of the total concentration. This pattern indicates that the applied AFFF formulations were primarily composed of C_6 and C_8 substances. This aligns with modern AFFF formulations, which are largely composed of C_6-based compounds [136].

Considering the structural classes of PFAS in the topsoil, FTSAm and derivatives represented the largest fraction at 27.5%, followed by FTBs (21.7%), FTSO derivatives (15.5%), FTSy derivatives (13.1%), and PFAAs (13.9%). Other classes contributed less than 5% each, with FTAAs at 4.8%, PFASAm & derivatives at 1.8%, PFSA and U-PFSA derivatives at 0.8%, and FTSA derivatives and other minor compounds each below 0.5% (Figure 4 c). This distribution indicates that modern fluorotelomer-based AFFFs dominate the contamination, reflecting the industry's shift toward short-chain polyfluorinated PFAS [58,135], which are partially degradable, while their TPs remain highly persistent in the environment.

To further contextualize the contamination pattern, identified confidence level 1-3 PFAS were assigned to specific categories as proposed by Yan et al. (2024) [136]. In this classification system, primary precursors are PFAS intentionally present in AFFF formulations as active agents, whereas secondary precursors include both TPs (excluding PFAAs) and by-products. Based on the concentration data, primary FT precursors represent the largest fraction in the topsoil, accounting for 42.8% of the total PFAS concentration, followed closely by secondary FT precursors at 40.7%. PFAAs contribute 13.9%, while primary and secondary ECF precursors together account for only ~1.3%, and other ECF compounds represent 1.4% of the total (Figure 4 d). Highly abundant primary precursors identified in soil are for example 6:2 FTSAm-Pr-B, multiple FTBs, and 6:2 FTTh-(2′)OHPr-TriMeAm. Secondary precursors, such as 6:2 FTSO-

(2′)OHPr-TriMeAm and 6:2 FTSy-(2′)OHPr-TriMeAm, were observed at high concentrations in soil, highlighting the transformation of primary precursors. For example, 6:2 FTSO-(2′)OHPr-TriMeAm and 6:2 FTSy-(2′)OHPr-TriMeAm occur at 35- and 29-fold higher concentrations than their corresponding primary precursor, 6:2 FTTh-(2′)OHPr-TriMeAm, suggesting high in situ transformation of primary precursors to secondary PFAS. Another well-known AFFF compound, 6:2 FTTh-Pr-Ad-(5′,5′)DiMeEtSA, was detected only at confidence level 4 due to low intensity and insufficient MS^2 spectra. Its corresponding secondary TPs, 6:2 FTSO-Pr-Ad-(5′,5′)DiMeEtSA and 6:2 FTSy-Pr-Ad-(5′,5′)DiMeEtSA, were observed at higher intensities, with FTSy-Pr-Ad-(5′,5′)DiMeEtSA present at 1.7-fold higher concentration than its precursor FTSO-Pr-Ad-(5′,5′)DiMeEtSA. Additionally, multiple homologues of n:2 FTSy-Pr-Ad-(5′,5′)DiMeEtSA (n = 6, 8, 10, 12) were detected, illustrating both the environmental transformation of primary precursors and their persistence as secondary PFAS. Overall, this distribution confirms that secondary precursors are present at levels comparable to primary precursors in the environment, even though primary precursors were originally applied in larger amounts in the AFFF formulations [136], indicating that the complex soil matrix and its active microbial community provide a favorable environment for PFAS transformation. This highlights the importance of including both primary and secondary PFAS in quantitative nontarget screening to fully characterize AFFF-impacted sites.

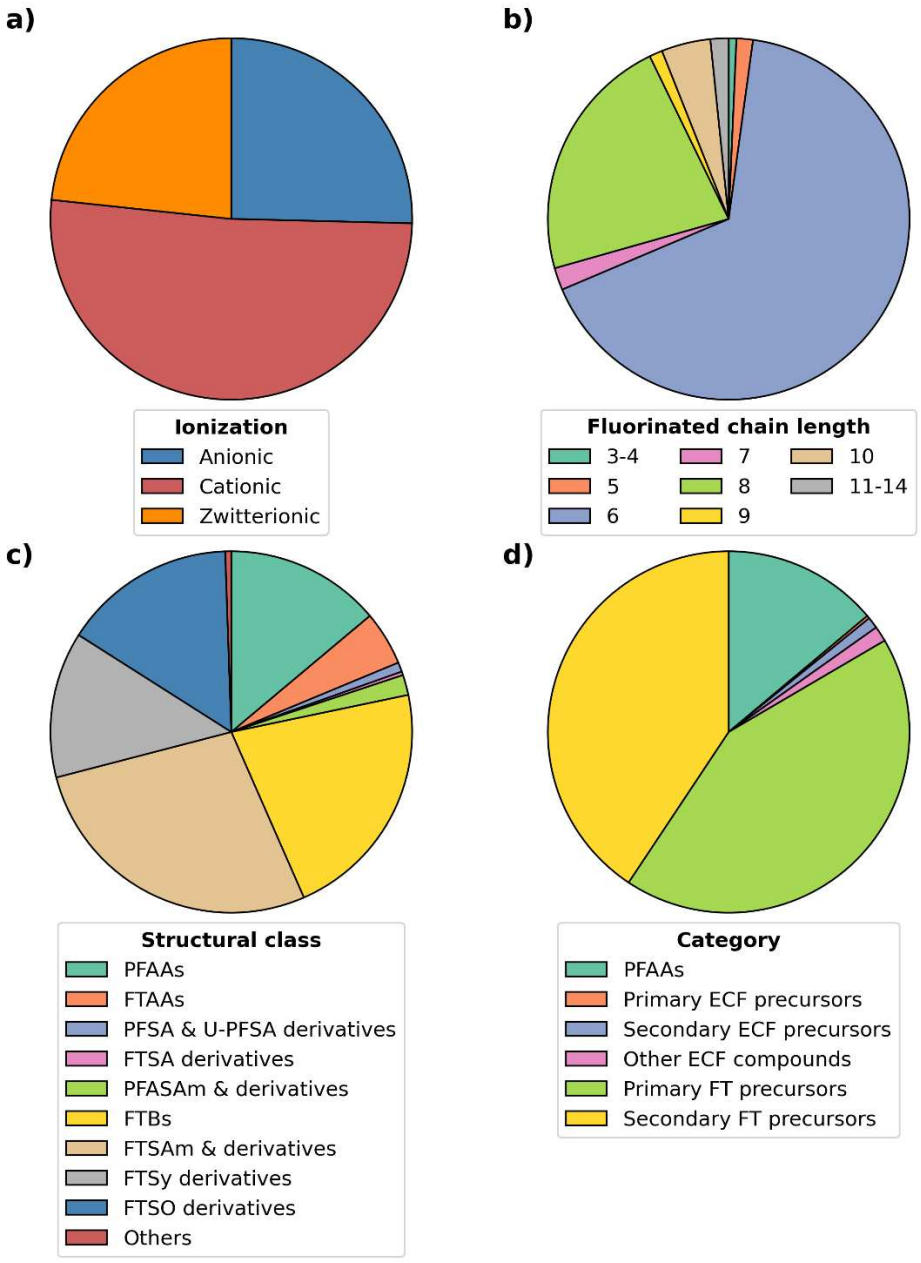

Figure 4: Distribution of (semi)quantified concentrations in µg/g in the extract of topsoil across a) ionization, b) fluorinated chain length distribution, c) structural classes, and d) categories PFAAs, primary, or secondary precursors.

Vertical PFAS Distribution

Across the soil profile, the highest concentrations of cationic and zwitterionic PFAS, as well as sulfonamide-based compounds, were found within the upper meter (Figure 5 a). Notably, several AFFF-related substances and potential TPs, including 5:2:1 FTB (1.68 µg/g), 5:3 FTB (0.29 µg/g), FTSAm-Pr-MeAm (0.30 µg/g), FTSAm-Pr-DiMeAm (0.91 µg/g), and 6:2 FTSA (0.85 µg/g), exhibited higher concentrations in the second layer (0.5-1 m) than in the surface layer. This enrichment may be linked to the increased cation exchange capacity and total organic

carbon in this layer, which can promote retention of positive ionized PFAS through electrostatic interactions [141,142]. Nevertheless, the sorption behavior of cationic and zwitterionic PFAS is known to be complex, influenced not only by soil properties [143] but also by co-occurring AFFF additives [144-146] and fluorophilic interactions among PFAS species [147].

In contrast, more mobile anionic TPs, including PFPeA, PFHxA, PFHpA, and PFHxS, were predominantly detected in deeper sections of the profile, with maximum concentrations occurring in the saturated zone (1.5-2 m; Figure 5 b). This vertical pattern is consistent with ongoing transformation of precursors in the upper layers combined with retarded downward migration of the resulting PFAAs with percolating water. The observed enrichment at depth aligns with known sorption behavior, as retention of anionic PFAAs decreases with shorter perfluoroalkyl chain length and lower organic carbon content, facilitating their transport through the soil [148,149].

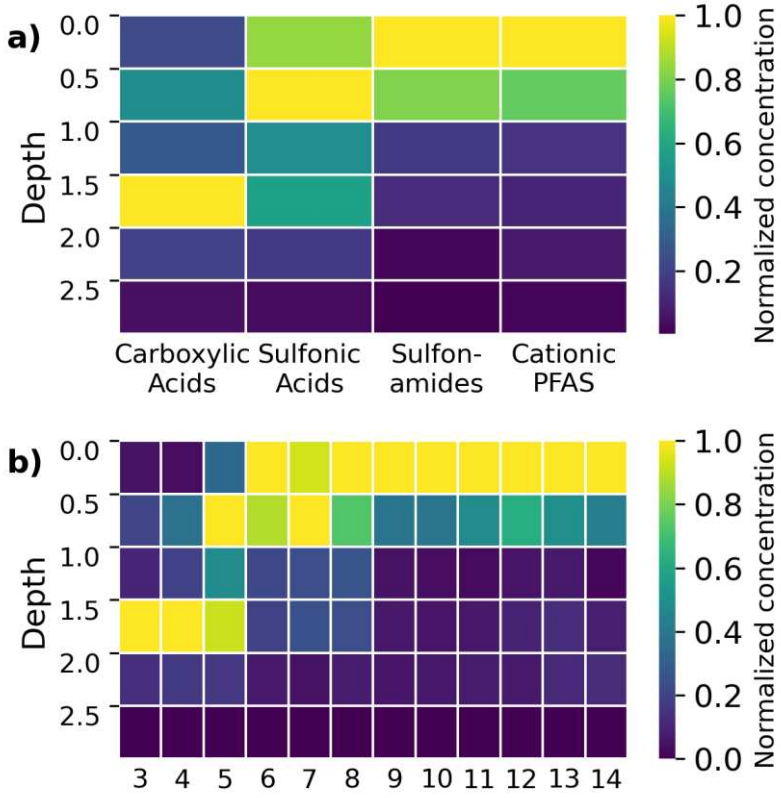

Figure 5: Depth distribution of the sum concentrations segmented by a) ionization class and b) chain length, depicted for a normalized scale based on the maximum concentration within an ionization class or chain length, respectively. Reprinted with permission from Capitain C, Schüßler M, Bugsel B, Zweigle J, Vogel C, Leube P, Zwiener C (2025). Implementation of Matrix-Matched Semiquantification of PFAS in AFFF-Contaminated Soil. *Environmental Science & Technology*, 59 (14), 7338-7347. DOI: 10.1021/acs.est.4c14255. Copyright 2025 American Chemical Society.

Soil-Groundwater PFAS Distribution

The groundwater sample collected a few meters downgradient from the soil profile (groundwater level: 1.3 m) contained representatives of twelve PFAS subclasses detected in the soil, including PFCA, PFSA, n:2 FTSA, K-n:2 FTSA, PFASAm, PFASAm-Me, PFASAm-EtA, n:1:2 and n:3 FTB, n:2 FTSAm, n:2 FTSAm-Pr-B, and n:2 FTTh-(2′)OHPr-TriMeAm (Figure 6). With the exception of PFASAm-Me and PFASAm-EtA, each subclass was represented in groundwater only by its shorter-chain homologues, whereas the soil contained both short- and long-chain members of the same subclasses, indicating preferential transport of low-molecular weight compounds. This trend is particularly evident for PFCAs: while only PFBA and longer PFCAs were detected in soil, the groundwater contained even the ultrashort-chain PFPrA, which was absent in the soil profile. The predominance of short-chain homologues in groundwater is consistent with their higher mobility and weaker sorption to soil organic matter and mineral surfaces [142]. A few longer-chain compounds detected in groundwater, such as PFASAm-Me, PFASAm-EtA, and n:2 FTSAm-Pr-B, likely reflect their comparatively high concentrations in soil, allowing trace amounts to reach groundwater despite their lower mobility. Their occurrence should therefore not be interpreted as high mobility, but rather as a consequence of the extreme concentrations at the site. While the migration of highly mobile PFAS such as short-chain PFAAs into groundwater is well established, the detection of precursors, particularly cationic and zwitterionic species, is unexpected from a mobility standpoint, as these substances typically exhibit strong sorption to soils [141]. Their detection in groundwater is therefore most plausibly attributed to the exceptionally high load of AFFF-derived PFAS in the soil, which exceeds the soil's retention capacity and allows minor fractions of otherwise immobile precursors to leach into the aquifer.

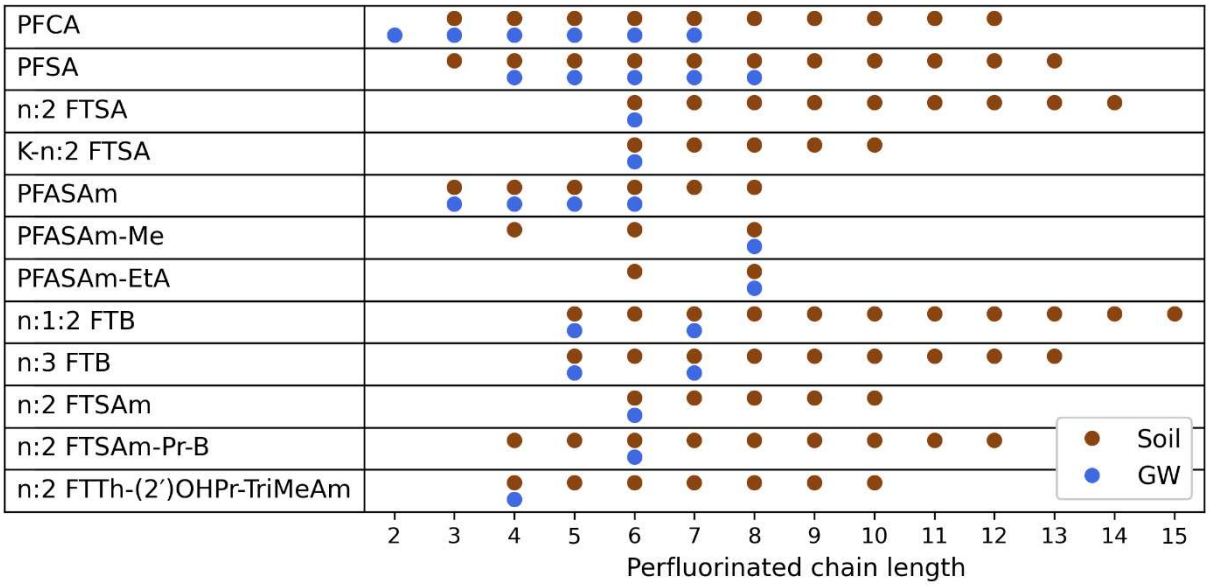

Figure 6: Distribution of PFAS chain lengths detected in soil (brown) and groundwater (blue).

4.4. Characterization via Photocatalytic Oxidation

Comprehensive PFAS characterization using qNTS approaches is often labor-intensive and may still remain incomplete, particularly when dealing with complex precursor mixtures. This poses substantial challenges for accurate PFAS identification and quantification in environmental samples. The PhotoTOP assay offers a complementary solution by employing photocatalytic oxidation to convert diverse precursors into a suite of quantifiable PFCAs. The PhotoTOP was applied for the first time to both AFFF-related PFAS standards and AFFF-contaminated soil. In addition, transformation kinetics were examined to provide deeper insight into the oxidative behavior and persistence of PFAS precursors during PhotoTOP treatment, thereby offering indications of their environmental fate.

Method Validation by Oxidative Conversion of AFFF Standards

To assess the performance of the PhotoTOP assay for the oxidative conversion of AFFF-related PFAS, seven known precursors were subjected to photocatalytic treatment. The test set included four fluorotelomer-based precursors (6:2 FTSAm-Pr-B, 6:2 FTSAm-Pr-DiMeNO, 5:3 FTB, and 5:1:2 FTB) and three perfluoroalkane sulfonamide-derived PFAS (PFHxSAm, PFOSAm, and PFHxSAm-Pr-DiMeAm). All target compounds, along with their intermediates, were efficiently degraded during the first hour of irradiation. The formation of the final PFCAs followed with a short delay, indicating the presence of short-lived intermediates that, however, could not be identified by NTS. The observed PhotoTOP transformation pattern showed a perfluorinated chain-shortening of n-1 for ECF-derived precursors, whereas fluorotelomer precursors yielded a product distribution of approximately 30% n, 55% n-1, and 15% n-2.

Martin et al. (2019) [150] reported the same major TPs for PFHxSAm, PFOSAm, and PFOSAm-Pr-DiMeAm when using the classical TOP assay. However, for 6:2 FTSAm-Pr-B they observed more extensive chain shortening, with PFBA and PFPeA as dominant products. In contrast, PhotoTOP treatment in the present study produced predominantly PFHxA and PFHpA. This difference is likely attributable to the milder oxidative conditions of PhotoTOP and the absence of sulfate radicals, which promotes less chain shortening [120].

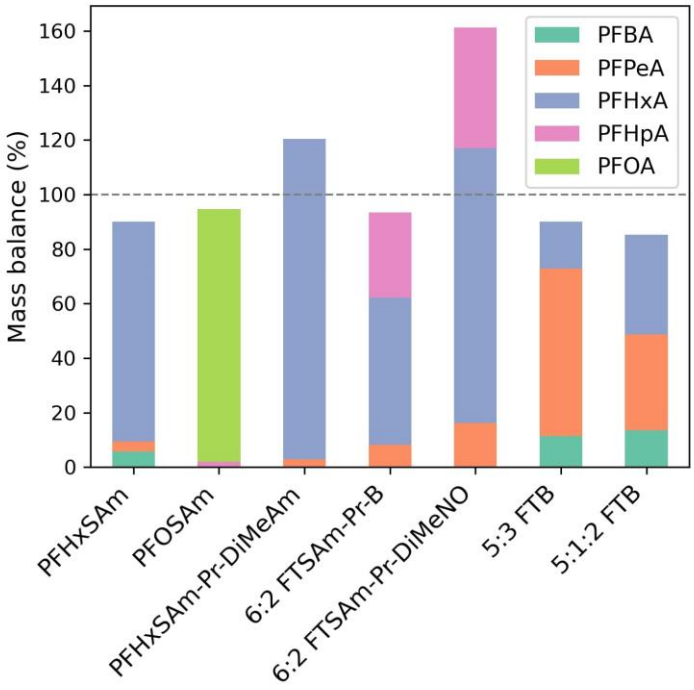

Figure 7: Molar contributions (%) of TPs to mass balance after Photo-TOP of AFFF standards.

Oxidative Conversion of Contaminated Soil

The PhotoTOP assay was applied to both the topsoil sample and its corresponding soil extract over a period of 46 h. Direct irradiation of soil has the advantage of avoiding extraction-related losses, but the substantially higher matrix load can impair oxidation efficiency. In contrast, irradiating the soil extract allows for much larger soil equivalents, approximately 90-fold more, due to reduced interfering matrix components.

After 46 h, the total concentration of TPs, stable PFAS, and residual precursors reached 27.6 nmol/g in the directly oxidized soil, whereas oxidation of the soil extract yielded only 9.5 nmol/g (Figure 8 a). This disparity clearly demonstrates that the methanolic extraction procedure used in this experimental setup did not fully recover the sorbed PFAS. The previously mentioned qNTS of the same soil (semi)quantified a summed PFAS concentration of 15.19 µg/g, corresponding to 29.6 nmol/g (Figure 8 b). Only 32.1% of these (semi)quantified PFAS

were recovered in the extract oxidation, largely due to the less efficient extraction protocol used here compared to the qNTS workflow, which relied on three sequential MeOH + 0.4 M NH_4Ac extractions, well-suited for strongly sorbing cationic and zwitterionic compounds. In contrast, the direct PhotoTOP treatment captured 93.2% of the (semi)quantified PFAS, demonstrating its enhanced ability to capture the full range of PFAS.

The molar chain-length distribution reported in the qNTS study was strongly dominated by PFAS with six (58%) and eight (16%) perfluorinated carbons. After PhotoTOP treatment, the distribution became more diffuse due to the expected chain-shortening reactions, particularly for fluorotelomer structures. When the PhotoTOP transformation pattern determined from standard oxidation experiments was applied to the qNTS dataset, the expected molar distribution aligned closely with the PhotoTOP results (Figure 8 b). The molar distributions from the direct PhotoTOP compared well with the predicted values (qNTS-derived), namely 13% vs. 15% (n = 4), 24% vs. 36% (n = 5), 22% vs. 23% (n = 6), 16% vs. 6% (n = 7), and 13% vs. 15% (n = 8), confirming that the observed oxidation behavior is consistent with precursor-specific transformation pathways.

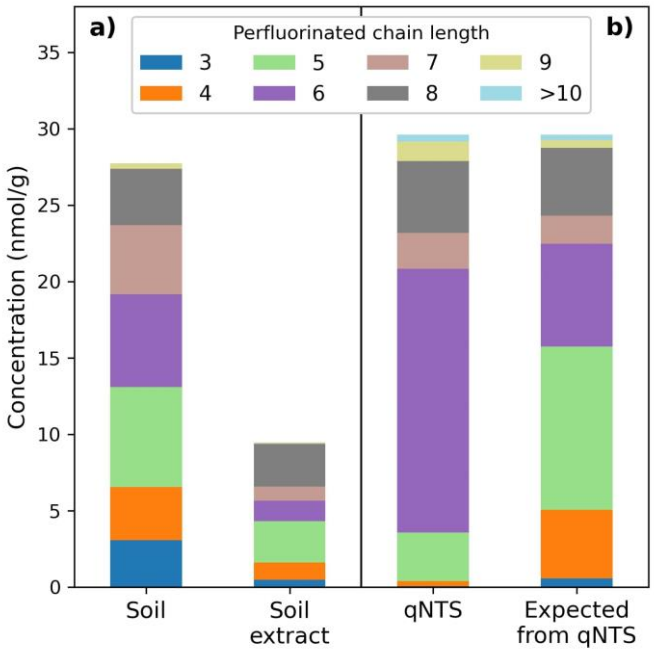

Figure 8: Molar concentrations (nmol/g) of a) TPs, stable compounds, and remaining precursors after PhotoTOP with 46-h oxidation of soil and soil extract and of b) all PFAS detected by target and qNTS, along with expected concentrations based on the observed PhotoTOP transformation patterns.

Transformation Kinetics of Precursors during Photocatalytic Oxidation

During 46 hours of PhotoTOP treatment on both soil and soil extract, PFAS precursors underwent transformation, intermediates were formed and subsequently transformed, and PFCAs emerged as the main terminal products (Figure 9 and 10).

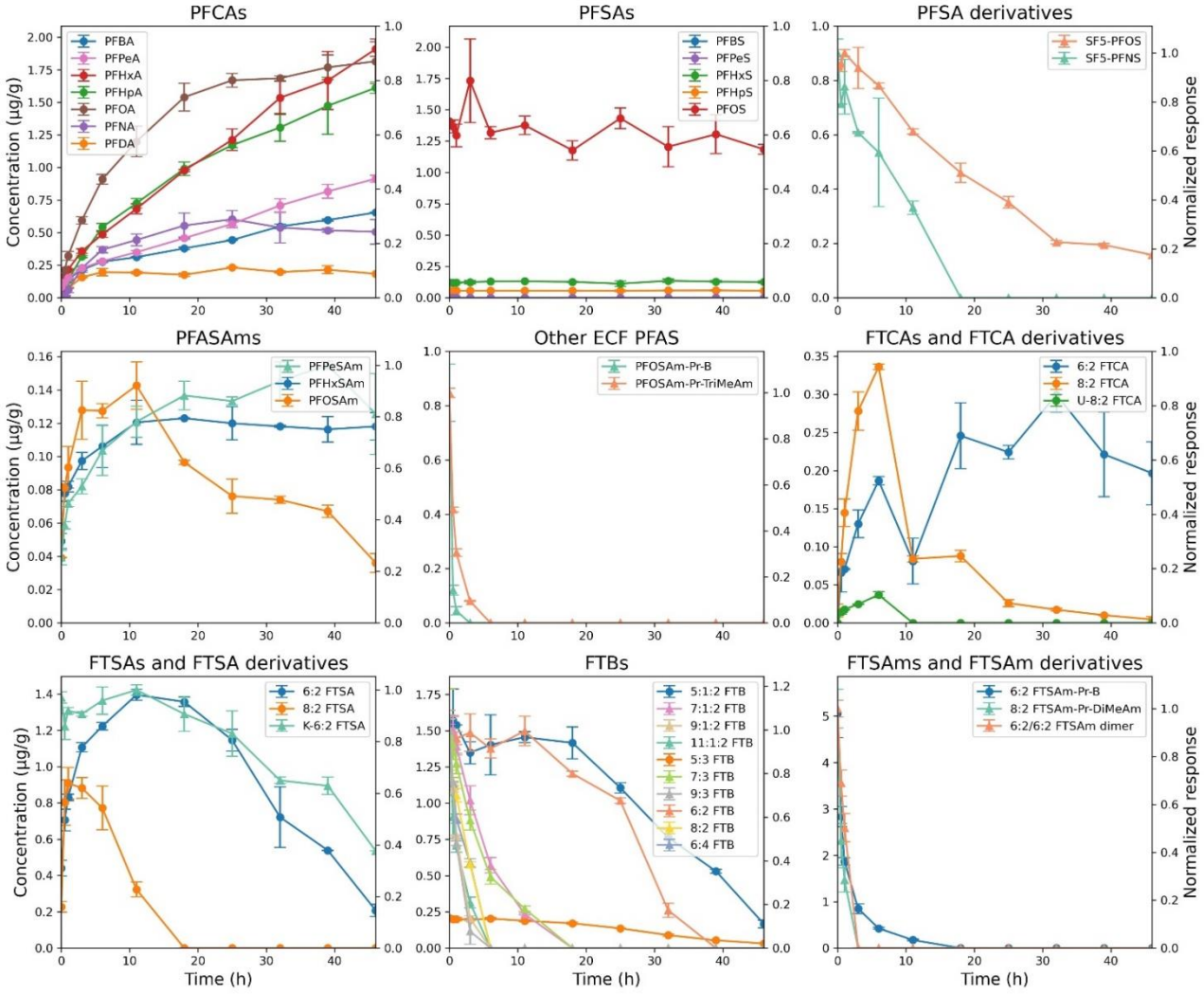

Figure 9: Direct PhotoTOP of topsoil. Time trends are shown for precursors, intermediates, and final TPs. Concentrations of confidence level 1 PFAS are plotted on the left axis (µg/g, circles), whereas normalized responses of confidence level 2 and 3 PFAS are plotted on the right axis (triangles). Error bars represent the standard deviation of duplicate measurements.

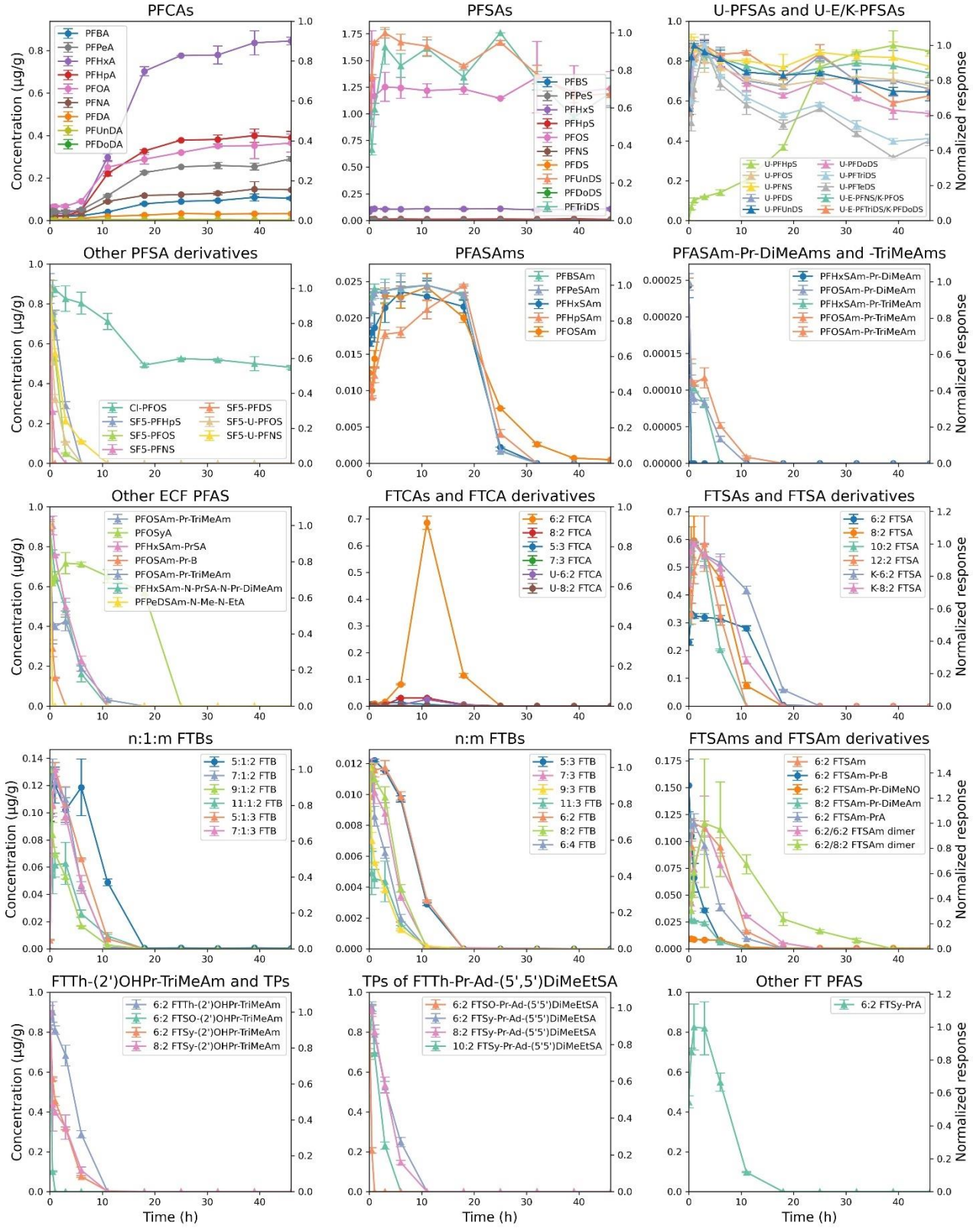

Figure 10: PhotoTOP of topsoil extract. Time trends are shown for precursors, intermediates, and final TPs. Concentrations of confidence level 1 PFAS are plotted on the left axis (µg/g, circles), whereas normalized responses of confidence level 2 and 3 PFAS are plotted on the right axis (triangles). Error bars represent the standard deviation of duplicate measurements.

For direct soil oxidation (Figure 9), some PFCAs, particularly those with perfluorinated chains shorter than six carbons, continued to increase in concentration at the end of the irradiation period. Intermediates such as PFASAms, FTCAs, and FTSAs were not fully transformed, suggesting incomplete oxidation and that the measured total PFAS concentration of 27.6 nmol/g likely underestimates the true PFAS burden. Precursors, including SF_5-PFSAs, PFOSAm-Pr-B, PFOSAm-Pr-TriMeAm, FTBs, 6:2 FTSAm-Pr-B, 8:2 FTSAm-Pr-DiMeAm, and 6:2/6:2 FTSAm dimers, were transformed, with some compounds (e.g. SF_5-PFOS, 5:1:2 FTB, 5:3 FTB) only partially but predominantly converted. This study is the first to demonstrate the transformation of SF_5-PFSAs, which were previously reported as stable under the TOP assay [151]. However, direct soil oxidation captured nearly all (semi)quantified PFAS, whereas soil extract oxidation required shorter reaction times due to the reduced matrix load and enabled higher response signals and detection of more compounds (91 vs. 42 for direct soil irradiation). By the end of extract oxidation (Figure 10), PFCAs had stabilized and most precursors and intermediates were nearly completely converted, allowing the investigation of transformation behavior for different PFAS classes.

Substances were categorized as precursors, intermediates, terminal TPs, or stable compounds based on their concentration/signal trends, though for some compounds it could not be clearly determined whether they acted as precursors or intermediates. For example, Cl-PFSA, K-n:2 FTSA, n:2, n:3, and n:1:2 FTB, and n:2 FTSy-Pr-Ad-(5′5′)DiMeEtSA exhibited slight initial concentration increases, likely due to desorption from surfaces or formation as intermediates. Precursors included ECF-derived PFAS (Cl-PFSA, SF_5-PFSA, PFASAm-PrSA, PFASAm-Pr-B, PFASAm-*N*-PrSA-*N*-Pr-DiMeAm, PFASAm-*N*-Me-*N*-EtA) and fluorotelomer-based PFAS (K-n:2 FTSA, n:1:2, n:2, n:3, and n:4 FTB, n:2 FTSAm-Pr-B, n:2 FTSAm-Pr-DiMeNO, n:2 FTTh-(2′)OHPr-TriMeAm, n:2 FTSO-(2′)OHPr-TriMeAm, FTSy-(2′)OHPr-TriMeAm, n:2 FTSO-Pr-Ad-(5′5′)DiMeEtSA, FTSy-Pr-Ad-(5′5′)DiMeEtSA). Intermediates included U-PFSAs, PFASAm, PFASyA, PFASAm-Pr-DiMeAm, PFASAm-Pr-TriMeAm, n:2 and n:3 FTCAs, U-n:2 FTCA, n:2 FTSA, n:1:3 FTB, n:2 FTSAm-PrA, and n:2/m:2 FTSAm dimers. Many intermediates were present before irradiation, reflecting environmental transformation processes such as biotic and abiotic transformation over the past 15 years [57,69,152,153]. Terminal PFCAs with n = 3-11 formed, predominantly PFHxA, while PFSAs (n = 4-13) remained stable, with PFOS at the highest concentration. This is the first application of PhotoTOP to AFFF-contaminated soil, revealing numerous previously uncharacterized precursors and intermediates.

Comparison with previous studies applying the PhotoTOP assay [120] and the TOP assay [117,150] shows similar formation of PFCAs as terminal products, and MEs influenced transformation dynamics, with higher matrix loads suppressing initial PFCA formation. Likewise, in this study, PFCA formation during soil PhotoTOP proceeded more slowly than during extract oxidation, which was less affected by matrix influences. Al Amin et al. (2023) [117] applied a modified TOP assay to several AFFF formulations and a PFAS-contaminated soil extract and used 6:2 and 8:2 FTSAs as oxidation indicators to track the progression of precursor transformation. In contrast, in the current study these compounds were already fully transformed after 18 h, while other substances such as PFASAm required substantially longer to degrade and would therefore represent more robust indicators of oxidation progress. Al Amin et al. (2023) [117] also observed various perfluorooctane sulfonamide-based PFAS that reached steady-state concentrations during the TOP assay, likely due to simultaneous formation and transformation processes.

To evaluate the kinetics and stability of the different PFAS during the PhotoTOP assay, the transformation and formation curves were fitted using four models: logistic formation, exponential decay, a combined logistic-exponential model, and a two-step exponential formation-decay model. These simplified models approximate the overall reaction as the sum of precursor transformation, intermediate formation and decay, and formation of final transformation products. Sorption and desorption processes on glass surfaces and TiO_2 particles, which can introduce delays, are also implicitly captured. Because multiple PFAS interact and compete for reactive sites, time shifts in the formation and decay patterns may occur, meaning that the models reflect the rate-limiting steps rather than fully resolving all underlying processes. The fitted curves and parameters (Appendix 3) show normalized RMSE values below 21% (median 4%), indicating good overall fit quality. Comparison of formation and decay rates provides insight into PFAS stability during PhotoTOP. Higher decay rates correspond to faster transformation, potentially caused by lower intrinsic stability or stronger sorption to TiO_2 particles where OH radicals are formed. The newly identified U-PFSAs showed particularly low decay rates (>0.7 h^{-1}), indicating high stability under PhotoTOP conditions. Similarly, Cl-PFSAs and K-PFSAs transformed only very slowly, confirming their pronounced resistance to degradation. These findings are consistent with environmental monitoring data, as Cl-PFSAs and K-PFSAs have been repeatedly detected in soil, wastewater treatment plant effluents, groundwater, and surface waters [60,65,154-156]. Cl-PFSAs and K-PFSAs have also been found in serum samples of firefighters as well as in wildlife [155,157,158]. Moreover, a recent mouse study demonstrated that K-PFOS, Cl-PFOS, and U-

PFOS accumulate in serum at levels comparable to or even exceeding those of PFOS, highlighting their potential for bioaccumulation and long-term exposure risks [159]. PFHxSAm, the perfluorinated analogue of 6:2 FTSAm, exhibited a higher decay rate than 6:2 FTSAm (0.49 h^{-1} vs. 0.17 h^{-1}), consistent with reduced simultaneous formation due to the greater abundance of fluorotelomer-based precursors relative to perfluorinated ones. This interpretation is supported by the higher formation rate of 6:2 FTSAm (2.08 h^{-1}) compared to PFHxSAm (0.51 h^{-1}). PFASAm-Pr-DiMeAm displayed decay rates approximately sevenfold higher than PFASAm-Pr-TriMeAm at n = 6, and threefold higher at n = 8, suggesting enhanced reactivity due to the presence of a free electron pair which can be oxidized. Pronounced structural effects were further observed: 6:2 FTSO-(2′)OHPr-TriMeAm and 6:2 FTSO-Pr-Ad-(5′5′)DiMeEtSA showed much higher decay rates than the corresponding sulfonyl analogues 6:2 FTSy-(2′)OHPr-TriMeAm and 6:2 FTSy-Pr-Ad-(5′5′)DiMeEtSA, which in turn degraded more rapidly than 6:2 FTTh-(2′)OHPr-TriMeAm. These patterns underscore the influence of easily oxidizable functional groups on transformation during PhotoTOP. While PhotoTOP-derived stability trends offer useful indicators, they may not directly translate to environmental behavior, where additional processes operate. For instance, n:2 FTTh-(2′)OHPr-TriMeAm is a precursor of n:2 FTSO-(2′)OHPr-TriMeAm, which subsequently forms n:2 FTSy-(2′)OHPr-TriMeAm. The previously shown qNTS data showed higher environmental concentrations of the latter two compounds relative to their precursor, meaning that under environmental conditions their decay cannot exceed that of n:2 FTTh-(2′)OHPr-TriMeAm. Contrasting trends with biotic systems further highlight the distinct nature of PhotoTOP chemistry. Fang et al. (2024) [132] showed that 6:2 FTSAm-Pr-B is more stable than 6:2 FTSAm-Pr-DiMeAm and 6:2 FTSAm-Pr-DiMeNO in aerobic sludge, consistent with the behavior of their perfluorinated analogues in aerobic soil [68]. Under PhotoTOP conditions, however, the opposite was observed: 6:2 FTSAm-Pr-B transformed faster than 6:2 FTSAm-Pr-DiMeNO, and PFOSAm-Pr-B faster than PFOSAm-Pr-DiMeAm. Additionally, although FTBs are generally regarded as resistant to microbial degradation [160], they transformed under OH-radical-dominated PhotoTOP conditions at rates comparable to other precursors. Zweigle et al. (2023) [151] previously reported that Cl-PFOS, SF_5-PFSA, SF_5-U-PFSA, U-PFSA, and U-E-PFSA were stable in the TOP assay. In contrast, the PhotoTOP assay revealed slow but measurable transformation of these compounds, with U-PFSAs, especially U-PFHpS, even appearing as intermediates. The observed difference may be due to the time-resolved design of the PhotoTOP assay, which captures transformation processes before they reach completion. Spearman correlations between perfluorinated chain length and formation/decay rates showed strong

positive relationships for soil oxidation, but both positive and negative relationships for soil extract oxidation (Appendix 3). The correlation in case of soil oxidation likely reflects stronger sorption of longer homologues to TiO_2 and thus faster transformation compared to shorter homologues. In soil extracts, however, strong initial sorption to the glass vials appears to distort the expected chain-length trends by delaying access to TiO_2 surfaces. These PhotoTOP correlations contrast with trends observed in microbial degradation, where longer perfluorinated chains generally exhibit greater stability [152]. This underlines that PhotoTOP behavior reflects oxidative reactivity rather than environmental persistence per se. Nevertheless, the assay provides valuable information on the relative stability of PFAS, as well as on intermediates and terminal products that can be expected.

4.5. Comparison of Analytical Methods

The combination of targeted analysis, NTS, (semi)quantification, EOF measurements, and PhotoTOP oxidation provides a comprehensive and mutually reinforcing characterization of the PFAS contamination in the Reilingen soil. Each method contributes complementary information, and their integration allows for a far more robust assessment than any single technique alone. Target and NTS revealed the exceptional chemical diversity of PFAS present in the impacted soil. Beyond some well-known primary AFFF-related PFAS and their terminal degradation products, NTS revealed a broad spectrum of other primary precursors as well as secondary precursors, including numerous intermediates and by-products that would not be detectable with targeted methods. This highlights the complexity of AFFF-derived PFAS contaminations and underscores the need for broad analytical approaches in contaminated sites. The semiquantification demonstrated that more than half of the total PFAS burden would remain undetected if analysis relied solely on targeted compounds. Importantly, the quantitative pattern also challenged initial assumptions: cationic and zwitterionic fluorotelomer PFAS, rather than PFOS, accounted for the largest share of the PFAS mass in this case. EOF measurements provided an essential independent validation of this semiquantitative estimate. EOF confirmed that the majority of fluorine-bearing substances were indeed captured by the qNTS workflow, thereby strengthening confidence in the results. PhotoTOP oxidation further corroborated the semiquantification results and provided critical dynamic information that static analytical measurements cannot capture. The assay enabled identification of intermediates and end products formed under oxidative conditions and delivered insights into the transformation kinetics and relative stability of both known and newly identified PFAS. But as emphasized by Wang et al. (2025) [107], mass balances after oxidative assays such as the

TOP assay often remain incomplete when compared with EOF due to non-oxidizable PFAS, incomplete conversion of unidentified precursors, and the formation of ultra-short-chain PFAS during oxidation. These considerations also apply to the PhotoTOP assay. Therefore, combining oxidative conversion with NTS and EOF, as implemented in this study, provides clear analytical advantages, supporting both identification and mass-balance closure. Overall, the combination of these analytical methods provides a thorough and mutually confirming picture of the contamination. Their complementarity not only strengthens the robustness of individual findings but also enables a holistic interpretation of PFAS sources, transformation pathways, and environmental persistence.

5. Conclusion and Outlook

This work provides several important contributions to PFAS research and environmental assessment. Using NTS, more than one hundred PFAS were identified in the Reilinger soil, including one previously unknown PFAS class and several additional classes detected for the first time in soil. The novel semiquantification approach developed here enables estimation of PFAS concentrations in the absence of matching analytical standards and could be adapted to other environmental matrices such as wastewater, surface water, biota, or human biological matrix [161]. The PhotoTOP assay was applied for the first time to AFFF standards and AFFF-impacted soils, revealing previously unrecognized intermediates, terminal products, and kinetic behavior in the PhotoTOP assay. These findings not only advance mechanistic understanding of precursor degradation but also demonstrate the potential of the PhotoTOP assay to be further optimized and commercialized as an alternative to the classical TOP assay, which still has inherent limitations. In the future, a refined PhotoTOP method could be applied across regulatory monitoring programs, for example, to support compliance with increasingly stringent PFAS regulations in environmental samples, food, and consumer products such as textiles [121]. These methodological advances and new chemical insights have direct implications for remediation strategies, monitoring frameworks, and regulatory decision-making.

Despite the broad data generated in this work, several methodological limitations must be acknowledged. NTS remains constrained by extraction selectivity, chromatographic separation, and ionization efficiency, all of which inherently limit chemical coverage and sensitivity and may bias detection toward certain PFAS while underrepresenting others. For example, very short-chain PFAS (< C_3/C_4), which are known to occur in AFFF-impacted environments [162],

were not included and therefore remain outside the analytical window. The semiquantification approach is restricted by the need for known structures, appropriate substance-class assignment, and matrix-specific calibration. Its performance depends on the availability of suitable analytical standards for each ionization class. The PhotoTOP assay also carries methodological limitations. Direct oxidation of soil led to strong matrix effects that reduced analytical sensitivity and hindered complete oxidation. Oxidation of soil extracts avoided these issues but is inherently limited by incomplete extraction efficiency. Although these constraints introduce uncertainty, combining qNTS, EOF analysis, and precursor oxidation, allowed for cross-validation of findings and substantially increased confidence in the overall assessment.

Future research on AFFF-derived PFAS should aim to broaden analytical coverage and capture currently overlooked compounds. In particular, including positive-mode electrospray ionization in suspect and non-target screening is critical, as significant fractions of PFAS may remain undetected if this mode is omitted. Complementary separation techniques, such as two-dimensional liquid chromatography coupled with differential mobility spectrometry (LC×DMS), have shown promise for enhancing resolution and detecting multiple PFAS species simultaneously [163]. Additionally, volatile PFAS, often missed by conventional LC-HRMS, can be accessed using emerging GC-HRMS methods, addressing gaps in the so-called "PFAS Dark Matter" [164]. Since there is "Not One Method to Rule Them All", combining reversed-phase LC with complementary techniques like supercritical fluid chromatography (SFC), hydrophilic interaction liquid chromatography (HILIC), or ion chromatography (IC) is recommended to extend chemical space in environmental non-target screening [165]. Alternatively, employing nonspecific, complementary techniques such as CIC or fluorine-19 nuclear magnetic resonance spectroscopy (^{19}F-NMR) [166] is essential to ensure accurate quantification and certification of total fluorine content. Further research on TOP and PhotoTOP assays is recommended, as these methods may produce terminal transformation products such as ultra-short-chain PFCAs and other end-products, that are not routinely captured in standard post-TOP PFAS analyses. Expanding the analytical panel to include additional products, such as trifluoroacetic acid (TFA) or HF, could provide deeper insights into degradation pathways and improve mass balance closure. Combining TOP or PhotoTOP with NTS is recommended to capture a broader range of intermediates and TPs. Moreover, the extent and efficiency of PFAS oxidation are influenced by factors such as pH, co-contaminants, inorganic ions, organic carbon content, and the chemical properties of the PFAS themselves [77], highlighting the need for further systematic studies to better understand these effects.

Artificial intelligence (AI) and machine learning (ML) offer promising new potentials for advancing PFAS detection, characterization, and management. Recent studies demonstrate their potential to overcome limitations of conventional analytical methods. For example, DeePFAS employs a deep-learning framework combining convolutional and transformer architectures to rapidly annotate PFAS from raw MS^2 spectra, projecting spectral data into a latent space representing chemical structural features [167]. Similarly, integrated non-target screening and ML approaches have been used to classify PFAS sources from high-resolution mass spectral data with high accuracy, improving source identification and contamination tracking [168,169]. Generative AI techniques have also expanded the known PFAS chemical space: a chemical language model assisted strategy generated over 1.4 million PFAS structures, increasing the PFAS chemical universe and enabling comprehensive suspect screening of previously uncharacterized compounds [170]. Moreover, AI-based models including random forests, gradient boosting decision trees, support vector machines, and artificial neural networks have been successfully applied to predict PFAS concentrations in environmental matrices, classify contamination sources, and optimize remediation processes with high predictive accuracy and efficiency [171]. Despite these advancements, challenges remain regarding data quality and model interpretability. Future research should focus on expanding publicly available datasets and using automated machine learning for model optimization. Collectively, AI and ML approaches hold game-changing potential to enhance efficiency, accuracy, and cost-effectiveness in PFAS monitoring, source tracking, and regulatory compliance.

Finally, expanding analytical platforms and data-sharing initiatives is crucial for advancing PFAS research. Tools such as enviPath illustrate this approach by providing standardized frameworks for reporting biotransformation data in a findable, accessible, interoperable, and reusable (FAIR) format [172]. Such platforms aim to improve the communication, standardize reporting of data, and increase both the quality and quantity of accessible data. Integrating NTS, qNTS, EOF, PhotoTOP, and other emerging techniques with FAIR-compliant data reporting could accelerate our understanding of PFAS fate and inform regulatory and remediation strategies globally.

The newly adopted EU restriction on PFAS in firefighting foams reflects a major shift, yet PFAS from AFFF applications continue to contaminate soils, where they accumulate and persist, and soils in turn act as long-term secondary sources to groundwater, surface waters, and biota [71,143,173]. Numerous studies have shown elevated PFAS levels in ecosystems, wildlife [157,174], and even firefighters [155], underscoring the human and environmental health relevance of AFFF-derived contamination. Importantly, the phase-out of legacy PFOS- and

PFOA-based foams has not eliminated risk. Many emerging PFAS used in modern foams are more toxic, more mobile, or more persistent than their predecessors, reinforcing the need for strict control of all PFAS classes, not only the traditionally regulated ones [119]. Recent global assessments further highlight the issue. Wei et al. (2025) [175] demonstrated that long-chain PFAS, particularly PFOS, still dominate soil contamination worldwide, with exceedances of health-based thresholds in many regions. PFHxS poses a growing health concern, especially in Europe and the U.S., while short-chain PFAS exhibit high mobility and greater leaching potential. Together, these findings show the necessity of establishing harmonized global soil quality standards for PFAS and adopting more proactive management strategies. Toxicity studies also emphasize the environmental risks. Multiple commercially used AFFFs have been shown to be toxic to marine invertebrates, even at environmentally relevant concentrations, confirming that foam releases pose ecological hazards beyond soil and groundwater contamination [176].

Moving forward, essential steps include phasing out PFAS production, preventing industrial emissions, mineralizing PFAS in waste streams, removing PFAS from drinking and surface waters, remediating contaminated hotspots, and accelerating the development of safer PFAS-free alternatives. The EU's ZeroPM initiative, which seeks to prevent, prioritize, and ultimately phase out persistent and mobile chemicals, reflects this shift toward a more holistic chemical management paradigm [177].

With this background, the analytical advances presented in this thesis, the identification of previously unreported PFAS classes, a transferable semiquantification approach, and the first application of the PhotoTOP assay to both AFFF standards and contaminated soil, support emerging regulatory needs by enabling more complete detection, improved mass balance assessment, and better precursor understanding. Such methodologies will be increasingly important for future compliance monitoring and environmental surveillance as PFAS regulations continue to tighten and extend across sectors.

6. References

1. Buck RC, Franklin J, Berger U, Conder JM, Cousins IT, de Voogt P, Jensen AA, Kannan K, Mabury SA, van Leeuwen SP (2011). Perfluoroalkyl and polyfluoroalkyl substances in the environment: terminology, classification, and origins. *Integrated Environmental Assessment and Management* 7 (4), 513-541. DOI: 10.1002/ieam.258

2. Schymanski EL, Zhang J, Thiessen PA, Chirsir P, Kondic T, Bolton EE (2023). Per- and Polyfluoroalkyl Substances (PFAS) in PubChem: 7 Million and Growing. *Environmental Science & Technology* 57 (44), 16918-16928. DOI: 10.1021/acs.est.3c04855

3. Wang Z, Buser AM, Cousins IT, Demattio S, Drost W, Johansson O, Ohno K, Patlewicz G, Richard AM, Walker GW, White GS, Leinala E (2021). A New OECD Definition for Per- and Polyfluoroalkyl Substances. *Environmental Science & Technology* 55 (23), 15575-15578. DOI: 10.1021/acs.est.1c06896

4. OECD (2021) Reconciling Terminology of the Universe of Per- and Polyfluoroalkyl Substances. OECD Series on Risk Management of Chemicals. DOI:10.1787/e458e796-en

5. Sigmund G, Venier M, Ågerstrand M, Cousins IT, DeWitt J, Diamond ML, Field J, Ford AT, Joudan S, van Leeuwen S, Lohmann R, Ng C, Scheringer M, Soehl A, Suzuki N, Trier X, Valsecchi S, Vlahos P, Young CJ, Wang ZY (2025). Scientists' Statement on the Chemical Definition of PFASs. *Environmental Science & Technology Letters*. DOI: 10.1021/acs.estlett.5c00478

6. Sigmund G, Venier M, Ågerstrand M, Cousins IT, Dewitt J, Diamond ML, Field J, Ford AT, Joudan S, Van Leeuwen S, Lohmann R, Ng C, Scheringer M, Soehl A, Suzuki N, Trier X, Valsecchi S, Vlahos P, Young CJ, Wang Z (2025). Rebuttal to "Correspondence on 'Scientists' Statement on the Chemical Definition of PFASs". *Environmental Science & Technology Letters*. DOI: 10.1021/acs.estlett.5c00819

7. Knepper TP, Lange FT (2011) Polyfluorinated Chemicals and Transformation Products. Springer Science & Business Media, Berlin

8. Lindstrom AB, Strynar MJ, Libelo EL (2011). Polyfluorinated compounds: past, present, and future. *Environmental Science & Technology* 45 (19), 7954-7961. DOI: 10.1021/es2011622

9. 3M Company (1999). Fluorochemical use, distribution and release overview. https://www.regulations.gov/document/EPA-HQ-OPPT-2002-0043-0008. Accessed: 25.06.2025

10. Alsmeyer YW, Childs WV, Flynn RM, Moore GGI, Smeltzer JC (1994). Electrochemical Fluorination and Its Applications. In: Banks RE, Smart BE, Tatlow JC (eds). Organofluorine Chemistry: Principles and Commercial Applications. Springer US, Boston, MA, pp 121-143. DOI:10.1007/978-1-4899-1202-2_5

11. Benskin JP (2011). Application of Perfluorinated Acid Isomer Profiles for Manufacturing and Exposure Source Determination. Doctoral dissertation, University of Alberta, Edmonton, Alberta

12. Umweltbundesamt (2020). Schwerpunkt 1-2020: PFAS. Gekommen, um zu bleiben. *Das Magazin des Umweltbundesamtes*

13. Evich MG, Davis MJB, McCord JP, Acrey B, Awkerman JA, Knappe DRU, Lindstrom AB, Speth TF, Tebes-Stevens C, Strynar MJ, Wang Z, Weber EJ, Henderson WM, Washington JW (2022). Per- and polyfluoroalkyl substances in the environment. *Science* 375 (6580), eabg9065. DOI: 10.1126/science.abg9065

14. Brunn H, Arnold G, Körner W, Rippen G, Steinhäuser KG, Valentin I (2023). PFAS: forever chemicals—persistent, bioaccumulative and mobile. Reviewing the status and the need for their phase out and remediation of contaminated sites. *Environmental Sciences Europe* 35 (1). DOI: 10.1186/s12302-023-00721-8

15. Tokranov AK, Hopkins ZR, Lindsey BD, Jurgens BC (2025). PFAS Are Widespread, Not Ubiquitous: Clarifying Misconceptions About the Prevalence of "Forever Chemicals". *Environmental Science & Technology* 59 (24), 11947-11949. DOI: 10.1021/acs.est.5c03878

16. Kurwadkar S, Dane J, Kanel SR, Nadagouda MN, Cawdrey RW, Ambade B, Struckhoff GC, Wilkin R (2022). Per- and polyfluoroalkyl substances in water and wastewater: A critical review of their global occurrence and distribution. *Science of the Total Environment* 809, 151003. DOI: 10.1016/j.scitotenv.2021.151003

17. Zhang H, Xu H, Qin B, Fu Y, Yao Y, Zhao Y, Qin C (2025). Review on the sources, distribution and treatment of per- and polyfluoroalkyl substances in global groundwater. *Environmental Research* 275, 121387. DOI: 10.1016/j.envres.2025.121387

18. Zhi Y, Lu X, Munoz G, Yeung LWY, De Silva AO, Hao S, He H, Jia Y, Higgins CP, Zhang C (2024). Environmental Occurrence and Biotic Concentrations of Ultrashort-Chain Perfluoroalkyl Acids: Overlooked Global Organofluorine Contaminants. *Environmental Science & Technology* 58 (49), 21393-21410. DOI: 10.1021/acs.est.4c04453

19. Rankin K, Mabury SA, Jenkins TM, Washington JW (2016). A North American and global survey of perfluoroalkyl substances in surface soils: Distribution patterns and mode of occurrence. *Chemosphere* 161, 333-341. DOI: 10.1016/j.chemosphere.2016.06.109

20. Brusseau ML, Anderson RH, Guo B (2020). PFAS concentrations in soils: Background levels versus contaminated sites. *Science of the Total Environment* 740, 140017. DOI: 10.1016/j.scitotenv.2020.140017

21. Jia X, Li X, Zhou L, Hui Y, Li W, Cai Y, Shi Y (2023). Variations of the Level, Profile, and Distribution of PFAS around POSF Manufacturing Facilities in China: An Overlooked Source of PFCA. *Environmental Science & Technology* 57 (13), 5264-5274. DOI: 10.1021/acs.est.2c08995

22. Liu S, Jin B, Arp HPH, Chen W, Liu Y, Zhang G (2022). The Fate and Transport of Chlorinated Polyfluorinated Ether Sulfonates and Other PFAS through Industrial Wastewater Treatment Facilities in China. *Environmental Science & Technology* 56 (5), 3002-3010. DOI: 10.1021/acs.est.1c04276

23. Savvidou EK, Sha B, Salter ME, Cousins IT, Johansson JH (2023). Horizontal and Vertical Distribution of Perfluoroalkyl Acids (PFAAs) in the Water Column of the Atlantic Ocean. *Environmental Science & Technology Letters* 10 (5), 418-424. DOI: 10.1021/acs.estlett.3c00119

24. Xie ZY, Kallenborn R (2023). Legacy and emerging per- and poly-fluoroalkyl substances in polar regions. *Current Opinion in Green and Sustainable Chemistry* 42, 100840. DOI: 10.1016/j.cogsc.2023.100840

25. Fujii Y, Shibata Y, Tokuda Y, Ito Y, Kudo N, Harada KH (2025). Human exposure and toxicity of per- and polyfluoroalkyl substances: Narrative review and perspectives. *Chemosphere* 385, 144508. DOI: 10.1016/j.chemosphere.2025.144508

26. Wang C, Magnuson JT, Zheng C, Qiu W (2025). Incidence of Pollution, Bioaccumulation, Biomagnification, and Toxic Effects of Per- and Polyfluoroalkyl Substances (PFAS) in Aquatic Ecosystems: A Review. *Aquatic Toxicology*, 107469. DOI: 10.1016/j.aquatox.2025.107469

27. Ajana R, Rachoń D, Gałęzowska G (2025). Reproductive toxicity of per- and polyfluoroalkyl substances. *Environmental Toxicology and Pharmacology* 117, 104740. DOI: 10.1016/j.etap.2025.104740

28. Arnesdotter E, Stoffels CBA, Alker W, Gutleb AC, Serchi T (2025). Per- and polyfluoroalkyl substances (PFAS): immunotoxicity at the primary sites of exposure. *Critical Reviews in Toxicology* 55 (4), 484-504. DOI: 10.1080/10408444.2025.2501420

29. Borghese MM, Feng J, Liang CL, Kienapple N, Manz KE, Fisher M, Arbuckle TE, Atlas E, Braun JM, Bouchard MF, Foster W, Ashley-Martin J (2025). Legacy, alternative, and precursor PFAS and associations with lipids and liver function biomarkers: results from a cross-sectional analysis of adult females in the MIREC-ENDO study. *International Journal of Hygiene and Environmental Health* 267, 114592. DOI: 10.1016/j.ijheh.2025.114592

30. Ames JL, Sharma V, Lyall K (2025). Effects of Early-life PFAS Exposure on Child Neurodevelopment: A Review of the Evidence and Research gaps. *Current Environmental Health Reports* 12 (1). DOI: 10.1007/s40572-024-00464-5

31. Cheng YT, Li JR, Yu HJ, Li S, Tychhon B, Cheng C, Weng YL (2025). Perfluoroalkyl substance pollutants disrupt microglia function and trigger transcriptional and epigenomic changes. *Toxicology* 517, 154198. DOI: 10.1016/j.tox.2025.154198

32. Sunderland EM, Hu XC, Dassuncao C, Tokranov AK, Wagner CC, Allen JG (2019). A review of the pathways of human exposure to poly- and perfluoroalkyl substances (PFASs) and present understanding of health effects. *Journal of Exposure Science & Environmental Epidemiology* 29 (2), 131-147. DOI: 10.1038/s41370-018-0094-1

33. Cousins IT, DeWitt JC, Glüge J, Goldenman G, Herzke D, Lohmann R, Miller M, Ng CA, Scheringer M, Vierke L, Wang Z (2020). Strategies for grouping per- and polyfluoroalkyl substances (PFAS) to protect human and environmental health. *Environmental Science: Processes & Impacts* 22 (7), 1444-1460. DOI: 10.1039/D0EM00147C

34. Renner R (2006). The long and the short of perfluorinated replacements. *Environmental Science & Technology* 40 (1), 12-13. DOI: 10.1021/es062612a

35. Ameduri B (2025). What Do We Know About Per- or Polyfluoroalkyl Substances (PFASs)? Issues, Challenges, Regulations, and Possible Alternatives. *Macromolecules* 58 (6), 2781-2791. DOI: 10.1021/acs.macromol.4c02993

36. Guo W, Hao W, Xiao W (2025). Emerging Perfluorinated Chemical GenX: Environmental and Biological Fates and Risks. *Environment & Health* 3 (4), 338-351. DOI: 10.1021/envhealth.4c00164

37. European Chemicals Agency (ECHA) (2025). List of substances proposed as POPs. https://echa.europa.eu/list-of-substances-proposed-as-pops. Accessed: 07.07.2025

38. Tyrrell ND (2023). A Proposal That Would Ban Manufacture, Supply, and Use of All Fluoropolymers and Most Fluorinated Reagents within the Entire EU. *Organic Process Research & Development* 27 (8), 1422-1426. DOI: 10.1021/acs.oprd.3c00199

39. Umweltbundesamt (2021). Ergänzung der Empfehlung „Umgang mit per- und polyfluorierten Alkylsubstanzen (PFAS) im Trinkwasser“ vom 26. August 2020. *Bundesgesundheitsblatt - Gesundheitsforschung - Gesundheitsschutz* 64 (10), 1328-1329. DOI: 10.1007/s00103-021-03411-z

40. Bundesministerium für Umwelt, Naturschutz, nukleare Sicherheit und Verbraucherschutz (2022). Guidelines for PFAS assessment - Recommendations for the uniform nationwide assessment of soil and water contamination and for the disposal of soil material containing PFAS.

https://www.bmuv.de/fileadmin/Daten_BMU/Download_PDF/Bodenschutz/pfas_leitfaden_2022_en_bf.pdf. Accessed: 11.07.2025

41. Umweltbundesamt (2023). Neue Trinkwasserverordnung sichert hohe Qualität unseres Trinkwassers. https://www.umweltbundesamt.de/presse/pressemitteilungen/neue-trinkwasserverordnung-sichert-hohe-qualitaet. Accessed: 11.07.2025

42. Klatt P (2023). PFAS in Mittelbaden – Auf der Suche nach Lösungen, Juli 2023. https://pfas-dilemma.info/images/PFAS-Broschuere-2023.pdf. Accessed: 11.07.2025

43. Bundesministerium für Gesundheit (2023). Bundesgesetzblatt - Zweite Verordnung zur Novellierung der Trinkwasserverordnung. https://www.recht.bund.de/bgbl/1/2023/159/VO.html. Accessed: 11.07.2025

44. Dorgerloh U, Becker R, Freeling F, Scheurer M, Gökçe E, Strack K, Sommerfeld T, Sauer A, Schneider J, Härtel C, Valkov V, Moser L, Geiß S, Junginger S, Schlittenbauer L, Suess E, Ruth K (2025). Standardising the quantification of trifluoroacetic acid in water: interlaboratory validation trial using liquid chromatography-mass spectrometric detection (LC–MS/MS). *Accreditation and Quality Assurance*. DOI: 10.1007/s00769-025-01640-2

45. Alghamdi W, Partington JM, Leung IKH, Clarke BO (2025). Premium Ultra-Trace Analytical Method for Part Per Quadrillion (ppq) PFAS Quantification in Drinking Water. *Analytica Chimica Acta* 1368, 344333. DOI: 10.1016/j.aca.2025.344333

46. Idowu IG, Ekpe OD, Megson D, Bruce-Vanderpuije P, Sandau CD (2025). A systematic review of methods for the analysis of total per- and polyfluoroalkyl substances (PFAS). *Science of the Total Environment* 967, 178644. DOI: 10.1016/j.scitotenv.2025.178644

47. Göckener B, Fliedner A, Rüdel H, Badry A, Koschorreck J (2022). Long-Term Trends of Per- and Polyfluoroalkyl Substances (PFAS) in Suspended Particular Matter from German Rivers Using the Direct Total Oxidizable Precursor (dTOP) Assay. *Environmental Science & Technology* 56 (1), 208-217. DOI: 10.1021/acs.est.1c04165

48. Moghadasi R, Mumberg T, Wanner P (2023). Spatial Prediction of Concentrations of Per- and Polyfluoroalkyl Substances (PFAS) in European Soils. *Environmental Science & Technology Letters*. DOI: 10.1021/acs.estlett.3c00633

49. Amen R, Ibrahim A, Shafqat W, Hassan EB (2023). A Critical Review on PFAS Removal from Water: Removal Mechanism and Future Challenges. *Sustainability* 15 (23), 16173. DOI: 10.3390/su152316173

50. Glüge J, Scheringer M, Cousins IT, DeWitt JC, Goldenman G, Herzke D, Lohmann R, Ng CA, Trier X, Wang Z (2020). An overview of the uses of per- and polyfluoroalkyl substances (PFAS). *Environmental Science: Processes & Impacts* 22 (12), 2345-2373. DOI: 10.1039/d0em00291g

51. Banerjee A, Liu Y (2021). Essential Factor of Perfluoroalkyl Surfactants Contributing to Efficacy in Firefighting Foams. *Langmuir* 37 (30), 8937-8944. DOI: 10.1021/acs.langmuir.1c00463

52. Houtz EF, Higgins CP, Field JA, Sedlak DL (2013). Persistence of perfluoroalkyl acid precursors in AFFF-impacted groundwater and soil. *Environmental Science & Technology* 47 (15), 8187-8195. DOI: 10.1021/es4018877

53. Liu M, Glover CM, Munoz G, Duy SV, Sauve S, Liu J (2024). Hunting the missing fluorine in aqueous film-forming foams containing per- and polyfluoroalkyl substances. *Journal of Hazardous materials* 464, 133006. DOI: 10.1016/j.jhazmat.2023.133006

54. Dauchy X, Boiteux V, Bach C, Rosin C, Munoz JF (2017). Per- and polyfluoroalkyl substances in firefighting foam concentrates and water samples collected near sites impacted by the use of these foams. *Chemosphere* 183, 53-61. DOI: 10.1016/j.chemosphere.2017.05.056

55. Weiner B, Yeung LWY, Marchington EB, D'Agostino LA, Mabury SA (2013). Organic fluorine content in aqueous film forming foams (AFFFs) and biodegradation of the foam component 6: 2 fluorotelomermercaptoalkylamido sulfonate (6: 2 FTSAS). *Environmental Chemistry* 10 (6), 486-493. DOI: 10.1071/En13128

56. Prevedouros K, Cousins IT, Buck RC, Korzeniowski SH (2006). Sources, fate and transport of perfluorocarboxylates. *Environmental Science & Technology* 40 (1), 32-44. DOI: 10.1021/es0512475

57. Choi YJ, Helbling DE, Liu J, Olivares CI, Higgins CP (2022). Microbial biotransformation of aqueous film-forming foam derived polyfluoroalkyl substances. *Science of the Total Environment* 824, 153711. DOI: 10.1016/j.scitotenv.2022.153711

58. Jahura FT, Mazumder NU, Hossain MT, Kasebi A, Girase A, Ormond RB (2024). Exploring the Prospects and Challenges of Fluorine-Free Firefighting Foams (F3) as Alternatives to Aqueous Film-Forming Foams (AFFF): A Review. *ACS Omega* 9 (36), 37430-37444. DOI: 10.1021/acsomega.4c03673

59. Place BJ, Field JA (2012). Identification of Novel Fluorochemicals in Aqueous Film-Forming Foams Used by the US Military. *Environmental Science & Technology* 46 (13), 7120-7127. DOI: 10.1021/es301465n

60. Nickerson A, Maizel AC, Kulkarni PR, Adamson DT, Kornuc JJ, Higgins CP (2020). Enhanced Extraction of AFFF-Associated PFASs from Source Zone Soils. *Environmental Science & Technology* 54 (8), 4952-4962. DOI: 10.1021/acs.est.0c00792

61. Nickerson A, Rodowa AE, Adamson DT, Field JA, Kulkarni PR, Kornuc JJ, Higgins CP (2021). Spatial Trends of Anionic, Zwitterionic, and Cationic PFASs at an AFFF-Impacted Site. *Environmental Science & Technology* 55 (1), 313-323. DOI: 10.1021/acs.est.0c04473

62. D'Agostino LA, Mabury SA (2017). Certain Perfluoroalkyl and Polyfluoroalkyl Substances Associated with Aqueous Film Forming Foam Are Widespread in Canadian Surface Waters. *Environmental Science & Technology* 51 (23), 13603-13613. DOI: 10.1021/acs.est.7b03994

63. Liu M, Munoz G, Vo Duy S, Sauvé S, Liu J (2022). Per- and Polyfluoroalkyl Substances in Contaminated Soil and Groundwater at Airports: A Canadian Case Study. *Environmental Science & Technology* 56 (2), 885-895. DOI: 10.1021/acs.est.1c04798

64. Backe WJ, Day TC, Field JA (2013). Zwitterionic, cationic, and anionic fluorinated chemicals in aqueous film forming foam formulations and groundwater from U.S. military bases by nonaqueous large-volume injection HPLC-MS/MS. *Environmental Science & Technology* 47 (10), 5226-5234. DOI: 10.1021/es3034999

65. Barzen-Hanson KA, Roberts SC, Choyke S, Oetjen K, McAlees A, Riddell N, McCrindle R, Ferguson PL, Higgins CP, Field JA (2017). Discovery of 40 Classes of Per- and Polyfluoroalkyl Substances in Historical Aqueous Film-Forming Foams (AFFFs) and AFFF-Impacted Groundwater. *Environmental Science & Technology* 51 (4), 2047-2057. DOI: 10.1021/acs.est.6b05843

66. Gonda N, Choyke S, Schaefer C, Higgins CP, Voelker B (2023). Hydroxyl Radical Transformations of Perfluoroalkyl Acid (PFAA) Precursors in Aqueous Film Forming Foams (AFFFs). *Environmental Science & Technology*. DOI: 10.1021/acs.est.2c08689

67. Moe MK, Huber S, Svenson J, Hagenaars A, Pabon M, Trümper M, Berger U, Knapen D, Herzke D (2012). The structure of the fire fighting foam surfactant Forafac®1157 and its

biological and photolytic transformation products. *Chemosphere* 89 (7), 869-875. DOI: 10.1016/j.chemosphere.2012.05.012

68. Liu M, Munoz G, Vo Duy S, Sauve S, Liu J (2021). Stability of Nitrogen-Containing Polyfluoroalkyl Substances in Aerobic Soils. *Environmental Science & Technology* 55 (8), 4698-4708. DOI: 10.1021/acs.est.0c05811

69. Cook EK, Olivares CI, Antell EH, Yi S, Nickerson A, Choi YJ, Higgins CP, Sedlak DL, Alvarez-Cohen L (2022). Biological and Chemical Transformation of the Six-Carbon Polyfluoroalkyl Substance N-Dimethyl Ammonio Propyl Perfluorohexane Sulfonamide (AmPr-FHxSA). *Environmental Science & Technology* 56 (22), 15478-15488. DOI: 10.1021/acs.est.2c00261

70. Harding-Marjanovic KC, Houtz EF, Yi S, Field JA, Sedlak DL, Alvarez-Cohen L (2015). Aerobic Biotransformation of Fluorotelomer Thioether Amido Sulfonate (Lodyne) in AFFF-Amended Microcosms. *Environmental Science & Technology* 49 (13), 7666-7674. DOI: 10.1021/acs.est.5b01219

71. Bigler MC, Brusseau ML, Guo B, Jones SL, Pritchard JC, Higgins CP, Hatton J (2024). High-Resolution Depth-Discrete Analysis of PFAS Distribution and Leaching for a Vadose-Zone Source at an AFFF-Impacted Site. *Environmental Science & Technology* 58 (22), 9863-9874. DOI: 10.1021/acs.est.4c01615

72. European Chemicals Agency (ECHA) (2023). ECHA's committees: EU-wide PFAS ban in firefighting foams warranted. https://echa.europa.eu/de/-/echa-s-committees-eu-wide-pfas-ban-in-firefighting-foams-warranted. Accessed: 11.07.2025

73. European Union (2025). Commission Regulation (EU) 2025/1988 of 2 October 2025 amending Annex XVII to Regulation (EC) No 1907/2006 of the European Parliament and of the Council as regards per- and polyfluoroalkyl substances in firefighting foams. http://data.europa.eu/eli/reg/2025/1988/oj.

74. Longwell AS, Hossain F, Subbiah S, Karnjanapiboonwong A, Suski JG, Anderson TA (2025). Chronic Reproductive Toxicity of Fomtec Enviro USP, a Fluorine-Free Firefighting Foam, to Northern Bobwhite (Colinus virginianus). *Toxics* 13 (6), 474. DOI: 10.3390/toxics13060474

75. Niaz K, McAtee D, Adhikari P, Rollefson P, Ateia M, Abdelmoneim A (2024). Assessing the effects of fluorine-free and PFAS-containing firefighting foams on development and behavioral responses using a zebrafish-based platform. *Chemosphere* 365, 143361. DOI: 10.1016/j.chemosphere.2024.143361

76. Schüßler M, Capitain C, Bugsel B, Zweigle J, Zwiener C (2024). Non-target screening reveals 124 PFAS at an AFFF-impacted field site in Germany specified by novel systematic terminology. *Analytical and Bioanalytical Chemistry* 417 (27), 6049-6064. DOI: 10.1007/s00216-024-05611-3

77. Shojaei M, Kumar N, Guelfo JL (2022). An Integrated Approach for Determination of Total Per- and Polyfluoroalkyl Substances (PFAS). *Environmental Science & Technology* 56 (20), 14517-14527. DOI: 10.1021/acs.est.2c05143

78. Wang Q, Van Hees P, Karlsson P, Jiao E, Filipovic M, Lam PKS, Yeung LWY (2025). Extractable Organofluorine Mass Balance Analysis of Aqueous Film-Forming Foam-Impacted Soils: Sample Pretreatment and a Combination of Target Analysis and Suspect Screening. *Environmental Science & Technology*. DOI: 10.1021/acs.est.4c11909

79. McDonough CA, Guelfo JL, Higgins CP (2019). Measuring total PFASs in water: The tradeoff between selectivity and inclusivity. *Current Opinion in Environmental Science & Health* 7, 13-18. DOI: 10.1016/j.coesh.2018.08.005

80. Mallet CR, Lu Z, Mazzeo JR (2004). A study of ion suppression effects in electrospray ionization from mobile phase additives and solid-phase extracts. *Rapid Communications in Mass Spectrometry* 18 (1), 49-58. DOI: 10.1002/rcm.1276

81. Bugsel B, Bauer R, Herrmann F, Maier ME, Zwiener C (2022). LC-HRMS screening of per- and polyfluorinated alkyl substances (PFAS) in impregnated paper samples and contaminated soils. *Analytical and Bioanalytical Chemistry* 414 (3), 1217-1225. DOI: 10.1007/s00216-021-03463-9

82. Janda J, Nödler K, Brauch H-J, Zwiener C, Lange FT (2019). Robust trace analysis of polar (C2-C8) perfluorinated carboxylic acids by liquid chromatography-tandem mass spectrometry: method development and application to surface water, groundwater and drinking water. *Environmental Science and Pollution Research* 26 (8), 7326-7336. DOI: 10.1007/s11356-018-1731-x

83. Ateia M, Maroli A, Tharayil N, Karanfil T (2019). The overlooked short- and ultrashort-chain poly- and perfluorinated substances: A review. *Chemosphere* 220, 866-882. DOI: 10.1016/j.chemosphere.2018.12.186

84. Camdzic D, Dickman RA, Joyce AS, Wallace JS, Ferguson PL, Aga DS (2023). Quantitation of Total PFAS Including Trifluoroacetic Acid with Fluorine Nuclear Magnetic Resonance Spectroscopy. *Analytical Chemistry*. DOI: 10.1021/acs.analchem.2c05354

85. Iannone A, Carriera F, Di Fiore C, Avino P (2024). Poly- and Perfluoroalkyl Substance (PFAS) Analysis in Environmental Matrices: An Overview of the Extraction and Chromatographic Detection Methods. *Analytica* 5 (2), 187-202. DOI: 10.3390/analytica5020012

86. Aßhoff N, Bernsmann T, Esselen M, Stahl T (2024). A sensitive method for the determination of per- and polyfluoroalkyl substances in food and food contact material using high-performance liquid chromatography coupled with tandem mass spectrometry. *Journal of Chromatography A* 1730, 465041. DOI: 10.1016/j.chroma.2024.465041

87. Shen Y, Wang L, Ding Y, Liu S, Li Y, Zhou Z, Liang Y (2024). Trends in the Analysis and Exploration of per- and Polyfluoroalkyl Substances (PFAS) in Environmental Matrices: A Review. *Critical Reviews in Analytical Chemistry* 54 (8), 3171-3195. DOI: 10.1080/10408347.2023.2231535

88. Interstate Technology and Regulatory Council (2023). Per- and Polyfluoroalkyl Substances (PFAS). https://pfas-1.itrcweb.org/wp-content/uploads/2023/12/Full-PFAS-Guidance-12.11.2023.pdf. Accessed: 15.09.2025

89. Zhang C, Gonda N, Kimble AN, Redman E, Grim CM, Gu S, Bednar A, Dahl K, Yuan C, Zhi Y, Cheng H, Higgins CP (2025). Quantification of per- and polyfluoroalkyl substances (PFASs) in aqueous film-forming foam (AFFF)-impacted water: Comparisons between methodologies and laboratories. *Journal of Hazardous materials* 499, 140142. DOI: 10.1016/j.jhazmat.2025.140142

90. Mejia-Avendaño S, Munoz G, Sauvé S, Liu J (2017). Assessment of the Influence of Soil Characteristics and Hydrocarbon Fuel Cocontamination on the Solvent Extraction of Perfluoroalkyl and Polyfluoroalkyl Substances. *Analytical Chemistry* 89 (4), 2539-2546. DOI: 10.1021/acs.analchem.6b04746

91. Dahlbom S, Bjarnemark F, Nguyen B, Petronis S, Mallin T (2024). Analysis of per- and polyfluoroalkyl substances (PFAS) extraction from contaminated firefighting materials: Effects of cleaning agent, temperature, and chain-length dependencies. *Emerging Contaminants* 10 (3), 100335. DOI: 10.1016/j.emcon.2024.100335

92. Munoz G, Ray P, Mejia-Avendano S, Vo Duy S, Tien Do D, Liu J, Sauve S (2018). Optimization of extraction methods for comprehensive profiling of perfluoroalkyl and polyfluoroalkyl substances in firefighting foam impacted soils. *Analytica Chimica Acta* 1034, 74-84. DOI: 10.1016/j.aca.2018.06.046

93. Enders JR, O'Neill GM, Whitten JL, Muddiman DC (2022). Understanding the electrospray ionization response factors of per-and poly-fluoroalkyl substances (PFAS). *Analytical and Bioanalytical Chemistry* 414 (3), 1227-1234. DOI: 10.1007/s00216-021-03545-8

94. Malm L, Liigand J, Aalizadeh R, Alygizakis N, Ng K, Fro Kjaer EE, Nanusha MY, Hansen M, Plassmann M, Bieber S, Letzel T, Balest L, Abis PP, Mazzetti M, Kasprzyk-Hordern B, Ceolotto N, Kumari S, Hann S, Kochmann S, Steininger-Mairinger T, Soulier C, Mascolo G, Murgolo S, Garcia-Vara M, Lopez de Alda M, Hollender J, Arturi K, Coppola G, Peruzzo M, Joerss H, van der Neut-Marchand C, Pieke EN, Gago-Ferrero P, Gil-Solsona R, Licul-Kucera V, Roscioli C, Valsecchi S, Luckute A, Christensen JH, Tisler S, Vughs D, Meekel N, Talavera Andujar B, Aurich D, Schymanski EL, Frigerio G, Macherius A, Kunkel U, Bader T, Rostkowski P, Gundersen H, Valdecanas B, Davis WC, Schulze B, Kaserzon S, Pijnappels M, Esperanza M, Fildier A, Vulliet E, Wiest L, Covaci A, Macan Schonleben A, Belova L, Celma A, Bijlsma L, Caupos E, Mebold E, Le Roux J, Troia E, de Rijke E, Helmus R, Leroy G, Haelewyck N, Chrastina D, Verwoert M, Thomaidis NS, Kruve A (2024). Quantification Approaches in Non-Target LC/ESI/HRMS Analysis: An Interlaboratory Comparison. *Analytical Chemistry* 96 (41), 16215-16226. DOI: 10.1021/acs.analchem.4c02902

95. Pu S, McCord JP, Dickman RA, Sayresmith NA, Sepman H, Kruve A, Aga DS, Sobus JR (2025). Examining environmental matrix effects on quantitative non-targeted analysis estimates of per- and polyfluoroalkyl substances. *Analytical and Bioanalytical Chemistry*. DOI: 10.1007/s00216-025-05796-1

96. Trufelli H, Palma P, Famiglini G, Cappiello A (2011). An overview of matrix effects in liquid chromatography–mass spectrometry. *Mass Spectrometry Reviews* 30 (3), 491-509. DOI: 10.1002/mas.20298

97. Bugsel B, Zweigle J, Zwiener C (2023). Nontarget screening strategies for PFAS prioritization and identification by high resolution mass spectrometry: A review. *Trends in Environmental Analytical Chemistry* 40, e00216. DOI: 10.1016/j.teac.2023.e00216

98. Zweigle J, Bugsel B, Fabregat-Palau J, Zwiener C (2024). PFΔScreen - an open-source tool for automated PFAS feature prioritization in non-target HRMS data. *Analytical and Bioanalytical Chemistry* 416 (2), 349-362. DOI: 10.1007/s00216-023-05070-2

99. Nason SL, Koelmel J, Zuverza-Mena N, Stanley C, Tamez C, Bowden JA, Godri Pollitt KJ (2021). Software Comparison for Nontargeted Analysis of PFAS in AFFF-Contaminated Soil. *Journal of the American Society for Mass Spectrometry* 32 (4), 840-846. DOI: 10.1021/jasms.0c00261

100. Koelmel JP, Stelben P, McDonough CA, Dukes DA, Aristizabal-Henao JJ, Nason SL, Li Y, Sternberg S, Lin E, Beckmann M, Williams AJ, Draper J, Finch JP, Munk JK, Deigl C, Rennie EE, Bowden JA, Godri Pollitt KJ (2022). FluoroMatch 2.0—making automated and comprehensive non-targeted PFAS annotation a reality. *Analytical and Bioanalytical Chemistry* 414 (3), 1201-1215. DOI: 10.1007/s00216-021-03392-7

101. McCord JP, Groff LC, Sobus JR (2022). Quantitative non-targeted analysis: Bridging the gap between contaminant discovery and risk characterization. *Environment International* 158, 107011. DOI: 10.1016/j.envint.2021.107011

102. McCord J, Newton S, Strynar M (2018). Validation of quantitative measurements and semi-quantitative estimates of emerging perfluoroethercarboxylic acids (PFECAs) and hexfluoroprolyene oxide acids (HFPOAs). *Journal of Chromatography A* 1551, 52-58. DOI: 10.1016/j.chroma.2018.03.047

103. Mejia-Avendaño S, Munoz G, Vo Duy S, Desrosiers M, BenoîT P, Sauvé S, Liu J (2017). Novel Fluoroalkylated Surfactants in Soils Following Firefighting Foam Deployment During the Lac-Mégantic Railway Accident. *Environmental Science & Technology* 51 (15), 8313-8323. DOI: 10.1021/acs.est.7b02028

104. Cao D, Schwichtenberg T, Duan C, Xue L, Muensterman D, Field J (2023). Practical Semiquantification Strategy for Estimating Suspect Per- and Polyfluoroalkyl Substance (PFAS) Concentrations. *Journal of the American Society for Mass Spectrometry* 34 (5), 939-947. DOI: 10.1021/jasms.3c00019

105. Pu S, McCord JP, Bangma J, Sobus JR (2024). Establishing performance metrics for quantitative non-targeted analysis: a demonstration using per- and polyfluoroalkyl substances. *Analytical and Bioanalytical Chemistry* 416 (5), 1249-1267. DOI: 10.1007/s00216-023-05117-4

106. Lauria MZ, Sepman H, Ledbetter T, Plassmann M, Roos AM, Simon M, Benskin JP, Kruve A (2024). Closing the Organofluorine Mass Balance in Marine Mammals Using Suspect Screening and Machine Learning-Based Quantification. *Environmental Science & Technology* 58 (5), 2458-2467. DOI: 10.1021/acs.est.3c07220

107. Wang Q, van Hees P, Karlsson P, Jiao E, Filipovic M, Lam PKS, Yeung LWY (2025). What we learn from using mass balance approach and oxidative conversion - A case study on PFAS contaminated soil samples. *Environmental Pollution* 376, 126420. DOI: 10.1016/j.envpol.2025.126420

108. Dubocq F, Wang T, Yeung LWY, Sjoberg V, Karrman A (2020). Characterization of the Chemical Contents of Fluorinated and Fluorine-Free Firefighting Foams Using a Novel Workflow Combining Nontarget Screening and Total Fluorine Analysis. *Environmental Science & Technology* 54 (1), 245-254. DOI: 10.1021/acs.est.9b05440

109. Roesch P, Vogel C, Huthwelker T, Wittwer P, Simon FG (2022). Investigation of per- and polyfluoroalkyl substances (PFAS) in soils and sewage sludges by fluorine K-edge XANES spectroscopy and combustion ion chromatography. *Environmental Science and Pollution Research International* 29 (18), 26889-26899. DOI: 10.1007/s11356-021-17838-z

110. Koch A, Yukioka S, Tanaka S, Yeung LWY, Kärrman A, Wang T (2021). Characterization of an AFFF impacted freshwater environment using total fluorine, extractable organofluorine and suspect per- and polyfluoroalkyl substance screening analysis. *Chemosphere* 276, 130179. DOI: 10.1016/j.chemosphere.2021.130179

111. Gehrenkemper L, Simon F, Roesch P, Fischer E, von der Au M, Pfeifer J, Cossmer A, Wittwer P, Vogel C, Simon FG, Meermann B (2021). Determination of organically bound fluorine sum parameters in river water samples-comparison of combustion ion chromatography (CIC) and high resolution-continuum source-graphite furnace molecular absorption spectrometry (HR-CS-GFMAS). *Analytical and Bioanalytical Chemistry* 413 (1), 103-115. DOI: 10.1007/s00216-020-03010-y

112. Jiao E, Larsson P, Wang Q, Zhu Z, Yin D, Karrman A, van Hees P, Karlsson P, Qiu Y, Yeung LWY (2023). Further Insight into Extractable (Organo)fluorine Mass Balance Analysis of Tap Water from Shanghai, China. *Environmental Science & Technology* 57 (38), 14330-14339. DOI: 10.1021/acs.est.3c02718

113. Karrman A, Yeung LWY, Spaan KM, Lange FT, Nguyen MA, Plassmann M, de Wit CA, Scheurer M, Awad R, Benskin JP (2021). Can determination of extractable organofluorine (EOF) be standardized? First interlaboratory comparisons of EOF and fluorine mass balance in sludge and water matrices. *Environmental Science: Processes & Impacts* 23 (10), 1458-1465. DOI: 10.1039/d1em00224d

114. Miaz LT, Plassmann MM, Gyllenhammar I, Bignert A, Sandblom O, Lignell S, Glynn A, Benskin JP (2020). Temporal trends of suspect- and target-per/polyfluoroalkyl substances (PFAS), extractable organic fluorine (EOF) and total fluorine (TF) in pooled serum from first-time mothers in Uppsala, Sweden, 1996-2017. *Environmental Science: Processes & Impacts* 22 (4), 1071-1083. DOI: 10.1039/c9em00502a

115. Houtz EF, Sedlak DL (2012). Oxidative conversion as a means of detecting precursors to perfluoroalkyl acids in urban runoff. *Environmental Science & Technology* 46 (17), 9342-9349. DOI: 10.1021/es302274g

116. Janda J, Nodler K, Scheurer M, Happel O, Nurenberg G, Zwiener C, Lange FT (2019). Closing the gap - inclusion of ultrashort-chain perfluoroalkyl carboxylic acids in the total oxidizable precursor (TOP) assay protocol. *Environmental Science: Processes & Impacts* 21 (11), 1926-1935. DOI: 10.1039/c9em00169g

117. Al Amin M, Luo Y, Shi F, Yu L, Liu Y, Nolan A, Awoyemi OS, Megharaj M, Naidu R, Fang C (2023). A modified TOP assay to detect per- and polyfluoroalkyl substances in aqueous film-forming foams (AFFF) and soil. *Frontiers in Chemistry* 11, 1141182. DOI: 10.3389/fchem.2023.1141182

118. Antell EH, Yi S, Olivares CI, Ruyle BJ, Kim JT, Tsou K, Dixit F, Alvarez-Cohen L, Sedlak DL (2023). The Total Oxidizable Precursor (TOP) Assay as a Forensic Tool for Per- and Polyfluoroalkyl Substances (PFAS) Source Apportionment. *ACS Environmental Science & Technology Water*. DOI: 10.1021/acsestwater.3c00106

119. Li M, Hu J, Cao X, Chen H, Lyu Y, Sun W (2024). Nontarget Analysis Combined with TOP Assay Reveals a Significant Portion of Unknown PFAS Precursors in Firefighting Foams Currently Used in China. *Environmental Science & Technology*. DOI: 10.1021/acs.est.4c07879

120. Zweigle J, Bugsel B, Capitain C, Zwiener C (2022). PhotoTOP: PFAS Precursor Characterization by UV/TiO(2) Photocatalysis. *Environmental Science & Technology* 56 (22), 15728-15736. DOI: 10.1021/acs.est.2c05652

121. Zweigle J, Capitain C, Simon F, Roesch P, Bugsel B, Zwiener C (2023). Non-extractable PFAS in functional textiles - characterization by complementary methods: oxidation, hydrolysis, and fluorine sum parameters. *Environmental Science: Processes & Impacts* 25 (8), 1298-1310. DOI: 10.1039/d3em00131h

122. Zweigle J, Bugsel B, Zwiener C (2023). Efficient PFAS prioritization in non-target HRMS data: systematic evaluation of the novel MD/C-m/C approach. *Analytical and Bioanalytical Chemistry* 415, 1791–1801. DOI: 10.1007/s00216-023-04601-1

123. Place BJ (2021). Suspect List of Possible Per- and Polyfluoroalkyl Substances (PFAS), National Institute of Standards and Technology. https://data.nist.gov/od/id/mds2-2387. Accessed: 15.12.2023

124. Zweigle J, Bugsel B, Zwiener C (2022). FindPFΔS: Non-Target Screening for PFAS─Comprehensive Data Mining for MS2 Fragment Mass Differences. *Analytical Chemistry* 94 (30), 10788-10796. DOI: 10.1021/acs.analchem.2c01521

125. Menin L, Ortiz D, Gasilova N, Sepulved F, Patiny L. MSTools. https://mstools.epfl.ch/monoisotopic/. Accessed: 2024-03-11

126. Patiny L, Borel A (2013). ChemCalc: A Building Block for Tomorrow's Chemical Infrastructure. *Journal of Chemical Information and Modeling* 53 (5), 1223-1228. DOI: 10.1021/ci300563h

127. Ruttkies C, Schymanski EL, Wolf S, Hollender J, Neumann S (2016). MetFrag relaunched: incorporating strategies beyond in silico fragmentation. *Journal of Cheminformatics* 8 (1), 3. DOI: 10.1186/s13321-016-0115-9

128. Charbonnet JA, McDonough CA, Xiao F, Schwichtenberg T, Cao D, Kaserzon S, Thomas KV, Dewapriya P, Place BJ, Schymanski EL, Field JA, Helbling DE, Higgins CP (2022). Communicating Confidence of Per- and Polyfluoroalkyl Substance Identification via High-Resolution Mass Spectrometry. *Environmental Science & Technology Letters* 9 (6), 473-481. DOI: 10.1021/acs.estlett.2c00206

129. Schymanski EL, Jeon J, Gulde R, Fenner K, Ruff M, Singer HP, Hollender J (2014). Identifying Small Molecules via High Resolution Mass Spectrometry: Communicating Confidence. *Environmental Science & Technology* 48 (4), 2097-2098. DOI: 10.1021/es5002105

130. Yukioka S, Tanaka S, Suzuki Y, Fujii S, Echigo S (2020). A new method to search for per- and polyfluoroalkyl substances (PFASs) by linking fragmentation flags with their molecular ions by drift time using ion mobility spectrometry. *Chemosphere* 239, 124644. DOI: 10.1016/j.chemosphere.2019.124644

131. Luo Y-S, Aly NA, McCord J, Strynar MJ, Chiu WA, Dodds JN, Baker ES, Rusyn I (2020). Rapid Characterization of Emerging Per- and Polyfluoroalkyl Substances in Aqueous Film-Forming Foams Using Ion Mobility Spectrometry–Mass Spectrometry. *Environmental Science & Technology* 54 (23), 15024-15034. DOI: 10.1021/acs.est.0c04798

132. Fang B, Zhang Y, Chen H, Qiao B, Yu H, Zhao M, Gao M, Li X, Yao Y, Zhu L, Sun H (2024). Stability and Biotransformation of 6:2 Fluorotelomer Sulfonic Acid, Sulfonamide Amine Oxide, and Sulfonamide Alkylbetaine in Aerobic Sludge. *Environmental Science & Technology* 58 (5), 2446-2457. DOI: 10.1021/acs.est.3c05506

133. D'Agostino LA, Mabury SA (2017). Aerobic biodegradation of 2 fluorotelomer sulfonamide–based aqueous film–forming foam components produces perfluoroalkyl carboxylates. *Environmental Toxicology and Chemistry* 36 (8), 2012-2021. DOI: 10.1002/etc.3750

134. D'Agostino LA, Mabury SA (2014). Identification of Novel Fluorinated Surfactants in Aqueous Film Forming Foams and Commercial Surfactant Concentrates. *Environmental Science & Technology* 48 (1), 121-129. DOI: 10.1021/es403729e

135. Ruyle BJ, Thackray CP, McCord JP, Strynar MJ, Mauge-Lewis KA, Fenton SE, Sunderland EM (2021). Reconstructing the Composition of Per- and Polyfluoroalkyl Substances in Contemporary Aqueous Film-Forming Foams. *Environmental Science & Technology Letters* 8 (1), 59-65. DOI: 10.1021/acs.estlett.0c00798

136. Yan PF, Dong S, Pennell KD, Capiro NL (2024). A review of the occurrence and microbial transformation of per- and polyfluoroalkyl substances (PFAS) in aqueous film-forming foam

(AFFF)-impacted environments. *Science of the Total Environment* 927, 171883. DOI: 10.1016/j.scitotenv.2024.171883

137. Hao S, Choi Y-J, Wu B, Higgins CP, Deeb R, Strathmann TJ (2021). Hydrothermal Alkaline Treatment for Destruction of Per- and Polyfluoroalkyl Substances in Aqueous Film-Forming Foam. *Environmental Science & Technology* 55 (5), 3283-3295. DOI: 10.1021/acs.est.0c06906

138. Ehsan MN, Riza M, Pervez MN, Li C-W, Zorpas AA, Naddeo V (2024). PFAS contamination in soil and sediment: Contribution of sources and environmental impacts on soil biota. *Case Studies in Chemical and Environmental Engineering* 9, 100643. DOI: 10.1016/j.cscee.2024.100643

139. Munoz G, Taxil-Paloc A, Desrosiers M, Vo Duy S, Liu M, Houde M, Liu J, Sauve S (2024). Zwitterionic, cationic, and anionic PFAS in freshwater sediments from AFFF-impacted and non-impacted sites of Eastern Canada. *Journal of Hazardous materials* 484, 136634. DOI: 10.1016/j.jhazmat.2024.136634

140. Baduel C, Mueller JF, Rotander A, Corfield J, Gomez-Ramos M-J (2017). Discovery of novel per- and polyfluoroalkyl substances (PFASs) at a fire fighting training ground and preliminary investigation of their fate and mobility. *Chemosphere* 185, 1030-1038. DOI: 10.1016/j.chemosphere.2017.06.096

141. Barzen-Hanson KA, Davis SE, Kleber M, Field JA (2017). Sorption of Fluorotelomer Sulfonates, Fluorotelomer Sulfonamido Betaines, and a Fluorotelomer Sulfonamido Amine in National Foam Aqueous Film-Forming Foam to Soil. *Environmental Science & Technology* 51 (21), 12394-12404. DOI: 10.1021/acs.est.7b03452

142. Nguyen TMH, Bräunig J, Thompson K, Thompson J, Kabiri S, Navarro DA, Kookana RS, Grimison C, Barnes CM, Higgins CP, McLaughlin MJ, Mueller JF (2020). Influences of Chemical Properties, Soil Properties, and Solution pH on Soil-Water Partitioning Coefficients of Per- and Polyfluoroalkyl Substances (PFASs). *Environmental Science & Technology* 54 (24), 15883-15892. DOI: 10.1021/acs.est.0c05705

143. Wanzek T, Stults JF, Johnson MG, Field JA, Kleber M (2023). Role of Mineral–Organic Interactions in PFAS Retention by AFFF-Impacted Soil. *Environmental Science & Technology*. DOI: 10.1021/acs.est.2c08806

144. Arshadi M, Garza-Rubalcava U, Guedes A, Capiro NL, Pennell KD, Christ J, Abriola LM (2024). Modeling 1-D aqueous film forming foam transport through the vadose zone under realistic site and release conditions. *Science of the Total Environment* 919, 170566. DOI: 10.1016/j.scitotenv.2024.170566

145. Guelfo JL, Higgins CP (2013). Subsurface transport potential of perfluoroalkyl acids at aqueous film-forming foam (AFFF)-impacted sites. *Environmental Science & Technology* 47 (9), 4164-4171. DOI: 10.1021/es3048043

146. Pan G, Jia C, Zhao D, You C, Chen H, Jiang G (2009). Effect of cationic and anionic surfactants on the sorption and desorption of perfluorooctane sulfonate (PFOS) on natural sediments. *Environmental Pollution* 157 (1), 325-330. DOI: 10.1016/j.envpol.2008.06.035

147. Wanzek TA, Field JA, Kostarelos K (2024). Repeated Aqueous Film-Forming Foams Applications: Impacts on Polyfluoroalkyl Substances Retention in Saturated Soil. *Environmental Science & Technology* 58 (3), 1659-1668. DOI: 10.1021/acs.est.3c04595

148. Higgins CP, Luthy RG (2006). Sorption of Perfluorinated Surfactants on Sediments. *Environmental Science & Technology* 40 (23), 7251-7256. DOI: 10.1021/es061000n

149. Maizel AC, Shea S, Nickerson A, Schaefer C, Higgins CP (2021). Release of Per- and Polyfluoroalkyl Substances from Aqueous Film-Forming Foam Impacted Soils. *Environmental Science & Technology* 55 (21), 14617-14627. DOI: 10.1021/acs.est.1c02871

150. Martin D, Munoz G, Mejia-Avendaño S, Duy SV, Yao Y, Volchek K, Brown CE, Liu J, Sauvé S (2019). Zwitterionic, cationic, and anionic perfluoroalkyl and polyfluoroalkyl substances integrated into total oxidizable precursor assay of contaminated groundwater. *Talanta* 195, 533-542. DOI: 10.1016/j.talanta.2018.11.093

151. Zweigle J, Bugsel B, Röhler K, Haluska AA, Zwiener C (2023). PFAS-Contaminated Soil Site in Germany: Nontarget Screening before and after Direct TOP Assay by Kendrick Mass Defect and FindPFΔS. *Environmental Science & Technology* 57 (16), 6647-6655. DOI: 10.1021/acs.est.2c07969

152. Dong S, Yan PF, Manz KE, Abriola LM, Pennell KD, Capiro NL (2024). Fate and Transformation of 15 Classes of Per- and Polyfluoroalkyl Substances in Aqueous Film-Forming Foam (AFFF)-Amended Soil Microcosms. *Environmental Science & Technology* 58 (51), 22777-22789. DOI: 10.1021/acs.est.4c08665

153. Fang B, Chen H, Zhao M, Qiao B, Zhou Y, Wang Y, Zhang Y, Gao M, Wang Y, Yao Y, Sun H (2025). Biotic and abiotic transformations of aqueous film-forming foam (AFFF)-derived emerging polyfluoroalkyl substances in aerobic soil slurry. *Water Research* 276, 123284. DOI: 10.1016/j.watres.2025.123284

154. Liu Y, Pereira ADS, Martin JW (2015). Discovery of C5–C17 Poly- and Perfluoroalkyl Substances in Water by In-Line SPE-HPLC-Orbitrap with In-Source Fragmentation Flagging. *Analytical Chemistry* 87 (8), 4260-4268. DOI: 10.1021/acs.analchem.5b00039

155. Rotander A, Kärrman A, Toms L-ML, Kay M, Mueller JF, Gómez Ramos MJ (2015). Novel Fluorinated Surfactants Tentatively Identified in Firefighters Using Liquid Chromatography Quadrupole Time-of-Flight Tandem Mass Spectrometry and a Case-Control Approach. *Environmental Science & Technology* 49 (4), 2434-2442. DOI: 10.1021/es503653n

156. Houtz E, Wang M, Park J-S (2018). Identification and Fate of Aqueous Film Forming Foam Derived Per- and Polyfluoroalkyl Substances in a Wastewater Treatment Plant. *Environmental Science & Technology* 52 (22), 13212-13221. DOI: 10.1021/acs.est.8b04028

157. Ecke F, Ytrehus B, Evander M, Hörnfeldt B, Leijon A, Malmsten J, Skrobonja A, Ahrens L (2025). Biomagnification and potential health effects of per- and polyfluoroalkyl substances (PFAS) in a terrestrial food web. *Scientific Reports* 15 (1). DOI: 10.1038/s41598-025-16395-6

158. Khan B, Burgess RM, Cantwell MG (2023). Occurrence and Bioaccumulation Patterns of Per- and Polyfluoroalkyl Substances (PFAS) in the Marine Environment. *Environmental Science & Technology Water* 3 (5), 1243-1259. DOI: 10.1021/acsestwater.2c00296

159. McDonough CA, Choyke S, Ferguson PL, Dewitt JC, Higgins CP (2020). Bioaccumulation of Novel Per- and Polyfluoroalkyl Substances in Mice Dosed with an Aqueous Film-Forming Foam. *Environmental Science & Technology* 54 (9), 5700-5709. DOI: 10.1021/acs.est.0c00234

160. Fang B, Chen H, Zhou Y, Qiao B, Baqar M, Wang Y, Yao Y, Sun H (2024). Fluorotelomer betaines and sulfonic acid in aerobic wetland soil: Stability, biotransformation, and bacterial community response. *Journal of Hazardous materials* 477, 135261. DOI: 10.1016/j.jhazmat.2024.135261

161. Dewapriya P, Nilsson S, Ghorbani Gorji S, O'Brien JW, Bräunig J, José Gómez Ramos M, Samanipour S, Martin JW, Toms L-ML, Mueller JF, Kaserzon SL, Thomas KV (2025).

Discovery of Previously Unreported Per- and Polyfluoroalkyl Substances (PFAS) in Pooled Australian Human Serum Using Nontarget Analysis. *Environmental Science & Technology*. DOI: 10.1021/acs.est.5c04623

162. Sture M, Valdersnes S, Boitsov S, Grøsvik BE, Ali A (2025). Source and fate of ultra-short-chain PFAS in water and biota from an AFFF impacted site. *Journal of Chromatography B* 1268, 124848. DOI: 10.1016/j.jchromb.2025.124848

163. Ryan CRM, Nazdrajić E, Campbell JL, Bell KY, Hopkins WS (2025). Two-Dimensional LC × DMS Analysis of 34 PFAS Compounds. *Analytical Chemistry* 97 (38), 21050-21059. DOI: 10.1021/acs.analchem.5c04119

164. Koelmel JP, Lin EZ, Chang P, Johnson E, Stelben P, Liu S, Nishida K, Tsugawa H, Lin A, Newton S, Casey JS, Nikiforov V, Roberts D, Aksenov A, Okeme J, Metayer C, Vieira VM, Manz KE, Braun JM, Pennell KD, Robey NM, Bangma J, Strynar M, Townsend TG, Bowden JA, Godri Pollitt KJ (2025). Shedding Light on PFAS Dark Matter Using a Novel GC-HRMS Approach. *Environmental Science & Technology*. DOI: 10.1021/acs.est.5c11712

165. Zweigle J, Schlüsener M, Flottmann J, Bader T, Vidkjær NH, Bollmann UE, Christensen JH, Tisler S (2025). Not One Method to Rule Them All: A Comparative Study of Chromatographic Platforms (RP-LC-, HILIC-, SFC-, and IC-HRMS) for Water Analysis. *Analytical Chemistry* 97 (45), 25099-25110. DOI: 10.1021/acs.analchem.5c04114

166. Faber KA, Pomerantz WCK, Gray JL, Hubbard LE, Kolpin DW, Arnold WA (2025). Revealing Organofluorine Contamination in Effluents and Surface Waters with Complementary Analytical Approaches: Fluorine-19 Nuclear Magnetic Resonance Spectroscopy (19F-NMR) and Liquid Chromatography-Tandem Mass Spectrometry (LC-MS/MS). *Environmental Science & Technology* 59 (28), 14695-14706. DOI: 10.1021/acs.est.5c05079

167. Wang H, Kuo T-C, Tseng YJ (2025). DeePFAS: Deep-Learning-Enabled Rapid Annotation of PFAS: Enhancing Nontargeted Screening through Spectral Encoding and Latent Space Analysis. *Environmental Science & Technology* 59 (46), 24841-24852. DOI: 10.1021/acs.est.5c09769

168. Joseph NT, Schwichtenberg T, Cao D, Jones GD, Rodowa AE, Barlaz MA, Charbonnet JA, Higgins CP, Field JA, Helbling DE (2023). Target and Suspect Screening Integrated with Machine Learning to Discover Per- and Polyfluoroalkyl Substance Source Fingerprints. *Environmental Science & Technology* 57 (38), 14351-14362. DOI: 10.1021/acs.est.3c03770

169. Joseph NT, Droz B, Schwichtenberg T, Oetjen K, Sühnholz S, Jones GD, Field JA, Higgins CP, Helbling DE (2025). Discovery of Comprehensive Sets of Chemical Constituents as Markers of PFAS Sources through a Nontarget Screening and Machine Learning Approach. *Environmental Science & Technology* 59 (42), 22852-22865. DOI: 10.1021/acs.est.5c07560

170. Liu Y, Wang H, Xie H, Zhang Y, Chen J (2025). Generative AI-Empowered Screening Strategy for Chemical Pollutants: A Case on Per- and Polyfluoroalkyl Substances. *Environmental Science & Technology* 59 (46), 24976-24986. DOI: 10.1021/acs.est.5c07495

171. Park J, Baik J-H, Adjei-Nimoh S, Lee WH (2025). Advancements in artificial intelligence-based technologies for PFAS detection, monitoring, and management. *Science of the Total Environment* 980, 179536. DOI: 10.1016/j.scitotenv.2025.179536

172. Rich SL, Hafner J, Salz M, Qanbarzadeh M, Geng F, Yan L, Liu J, Helbling DE, Higgins CP, Fenner K (2025). FAIR and Effective Communication of Data on Chemical Contaminant Biotransformation in the Environment. *Environmental Science & Technology Letters* 12 (11), 1462-1470. DOI: 10.1021/acs.estlett.5c00753

173. Nickerson A, Maizel AC, Schaefer CE, Ranville JF, Higgins CP (2023). Effect of geochemical conditions on PFAS release from AFFF-impacted saturated soil columns. *Environmental Science: Processes & Impacts* 25 (3), 405-414. DOI: 10.1039/d2em00367h

174. Liu J-J, Li F, Zhao Q, Jiang W-Y, Zhang P-D (2025). Bioaccumulation and trophic transfer characteristics of emerging and legacy per- and polyfluoroalkyl substances in Laizhou Bay, China. *Ecotoxicology and Environmental Safety* 306, 119339. DOI: 10.1016/j.ecoenv.2025.119339

175. Wei M, Chen Z, Yang K, Cao L, Qiu C, Zhou L, Shi Z, Chen S (2025). Global ecological and health risks of PFAS in surface soil. *Environment International* 206, 109925. DOI: 10.1016/j.envint.2025.109925

176. Ueda de Carvalho M, Buruaem Moreira L, Alves Maranho L, Moledo de Souza Abessa D (2025). Aqueous film-forming foams used in Brazil are toxic to neotropical invertebrates. *Marine Environmental Research* 212, 107581. DOI: 10.1016/j.marenvres.2025.107581

177. Chaubey AK, Pratap T, Mohan D (2025). Growing Concern about Per- and Polyfluoroalkyl Substance (PFAS) Contamination: An Emerging Environmental Challenge and Its Management. *ACS Sustainable Resource Management*. DOI: 10.1021/acssusresmgt.5c00376

Appendix 1

Publication 1

Non-target screening reveals 124 PFAS at an AFFF-impacted field site in Germany specified by novel systematic terminology

Melanie Schüßler[+‖], Catharina Capitain[+‖], Boris Bugsel[+], Jonathan Zweigle[+], Christian Zwiener[+]

[+]Environmental Analytical Chemistry, Department of Geosciences, University of Tübingen, Schnarrenbergstraße 94-96, 72076 Tübingen, Germany

[‖]The authors contributed equally to this work and share first authorship.

Published in: Analytical and Bioanalytical Chemistry, 417 (27), 6049-6064

DOI: 10.1007/s00216-024-05611-3

Analytical and Bioanalytical Chemistry
https://doi.org/10.1007/s00216-024-05611-3

RESEARCH PAPER

Non-target screening reveals 124 PFAS at an AFFF-impacted field site in Germany specified by novel systematic terminology

Melanie Schüßler[1] · Catharina Capitain[1] · Boris Bugsel[1] · Jonathan Zweigle[1] · Christian Zwiener[1]

Received: 5 August 2024 / Revised: 13 October 2024 / Accepted: 15 October 2024

Abstract

The uncontrolled release of aqueous film-forming foam (AFFF) ingredients during a major fire incident in Reilingen, Germany, in 2008 led to significant soil and groundwater contamination. As the identity of fluorochemical surfactants in AFFF are often veiled due to company secrets, it is important to characterize AFFF contaminations and their impact on the environment comprehensively. In this study, we adapted a systematic approach combining a suitable extraction method with liquid chromatography high-resolution quadrupole time-of-flight mass spectrometry (LC-QTOF-MS) for an extensive non-targeted analysis. Our analysis identified 124 per- and polyfluoroalkyl substances (PFAS) from 42 subclasses in the contaminated soil (confidence levels of identification between 1 and 3). Typical for AFFF-impacted field sites, these included anionic, cationic, and zwitterionic substances with perfluoroalkyl chains spanning from 3 to 14 carbon atoms. Furthermore, we identified 1 previously unreported substance, and detected 9 PFAS subclasses for the first time in soil. AFFFs have long been employed to extinguish large hydrocarbon fires, yet their environmental consequences remain a concern. This study sheds light on the complex composition of AFFFs at this particularly contaminated area, emphasizing the necessity for extensive contaminant characterization as sound basis for informed management strategies to mitigate their adverse effects. AFFF PFAS are often named differently in the literature, leading to inconsistency in terminology. To address this issue, we introduced partially new terminology for AFFF-related PFAS to establish consistent terminology, to facilitate communication of identified compounds, and to ensure that the chemical structure can be directly derived from acronyms.

Keywords AFFF · PFAS · Terminology · HRMS · Non-target screening · Identification · Soil

Introduction

In 2021, a new definition for the group of per- and polyfluoroalkyl substances (PFAS) was released by the Organisation for Economic Co-Operation and Development (OECD), which categorizes all substances with a CF_2 or CF_3 group (excluded CF_2H and CF_2-halogens) as PFAS, resulting in more than 7 million single substances that fall into the PFAS category [1–3]. Another definition of PFAS by Buck et al. [4] from 2011 includes all compounds with perfluoroalkyl moieties (C_nF_{2n+1}), where *n* denotes the number of carbon atoms. This results in more than 4700 substances [4]. Due to an increasing awareness of PFAS even outside the research community and extensive application combined with human and environmental health concerns, the European Union aspires to a ban of the entire PFAS class [5]. Earlier regulations of PFAS on international level comprise the three popular PFAS representatives, perfluorooctanoic acid (PFOA), perfluorooctane sulfonic acid (PFOS), and perfluorohexane sulfonic acid (PFHxS), into the Stockholm Convention of persistent organic pollutants [6].

These regulations were enacted since various PFAS are increasingly associated with adverse human health effects such as thyroid disorder, liver damage, kidney and testicular cancer, and lower birth weight, [7] as well as environmental

Published in the topical collection highlighting *Computational Mass Spectrometry for Exposomics in Non-Target Screening* with guest editors Gerrit Renner, Saer Samanipour, and Torsten C. Schmidt.

Melanie Schüßler and Catharina Capitain contributed equally to this work and share first authorship.

✉ Christian Zwiener
christian.zwiener@uni-tuebingen.de

[1] Environmental Analytical Chemistry, Department of Geosciences, University of Tübingen, Schnarrenbergstraße 94-96, 72076 Tübingen, Germany

Published online: 28 October 2024

concerns due to potential bioaccumulation [8–10] and high persistence in the environment [11, 12].

However, due to their unique chemistry, PFAS show attractive properties for industrial applications such as high surface activity, hydro- and oleophobicity, as well as high chemical and thermal stability [13]. Produced since the 1950s, PFAS are now used in nearly every branch of industry and are ingredients in numerous everyday consumer products [14].

A major field of PFAS application is the use in fluorosurfactant-based firefighting foams such as aqueous film-forming foams (AFFFs), which are used for extinguishing class B fires caused by hydrocarbon-based liquids [15]. PFAS ensure stability of the foam and the formation of a water film between the burning material and the foam, preventing reignition [14]. AFFFs are produced by various manufacturers and formulations differ in composition [16, 17]. In the past, perfluorocarboxylic and sulfonic acids (PFCAs and PFSAs) and their derivatives were often employed in AFFF formulations and PFOS was the substantial component in the AFFF brand Lightwater from 3M, a former major AFFF producer, until 3M phased-out PFOS in the early 2000s [15, 18–20]. 3M ceased AFFF production in 2002 but was known to utilize both perfluorinated and polyfluorinated substances generated by electrochemical fluorination (ECF) over the years, while other manufacturers usually employ polyfluorinated fluorotelomer-based PFAS in their formulations [16, 20, 21]. Common, well-known AFFF PFAS include perfluoroalkyl sulfonamides propyl dimethylamines (PFASAm-Pr-DiMeAms, e.g., in 3M AFFF, Angus), fluorotelomer sulfonamide propyl betaines (FTSAm-Pr-Bs, e.g., in National Foam, Fireade, Angus), and n:1:2 fluorotelomer betaines (n:1:2 FTBs, e.g., in Buckeye, Ansulite) (Electronic Supplementary Material, ESM 2). Due to the phase-out from C_8-based PFAS chemistry, the trend in AFFF formulations shifted towards short-chain PFAS [14]. As AFFF formulations do not have to be disclosed by manufacturers, large fractions of PFAS in AFFFs remain unknown [16, 17]. Since AFFFs are directly discharged into the environment during a fire or training event, sites impacted by AFFFs are often heavily contaminated [18, 22, 23].

Numerous studies showed that various AFFF PFAS can ultimately transform to legacy PFAS such as perfluoroalkyl acids (PFAAs), fluorotelomer sulfonic acids (FTSAs), or fluorotelomer sulfonamides (FTSAms) by photochemical oxidation [24, 25] or biodegradation [25–28]. PFAAs are not further transformed under environmental conditions and can thus accumulate in soil and groundwater over time [29]. While short-chain PFAS are more mobile and can migrate into groundwater, longer chain PFAS are mostly retained in the top layers of soil [29, 30]. This is especially true for zwitterionic and cationic AFFF compounds due to electrostatic interaction with negatively charged soil particles [31, 32]. Thus, for risk assessment and remediation management of AFFF-impacted field sites, a comprehensive characterization of the contaminant pattern is crucial. To accurately characterize the contamination pattern in AFFF-impacted soils, it is essential to select an appropriate extraction method. A simple methanolic extraction, as is often used for soil samples contaminated with anionic PFAS, is insufficient for cationic and zwitterionic AFFF-PFAS [33]. Thus, more exhaustive methods have been developed for soils contaminated with AFFF, employing the combination of acidic and basic extraction solvents [33] or various additives to methanol [34].

Non-target screening (NTS) by high-resolution mass spectrometry (HRMS) is an important tool to identify unknown PFAS in AFFF formulations and impacted field sites, especially since analytical reference standards are often not commercially available which considerably limits target analysis [35]. NTS approaches enabled to identify novel PFAS in AFFF formulations [17, 21, 23, 36, 37] which were then also increasingly detected in groundwater [22, 23, 38], surface water [15], and soils [33, 38, 39] from AFFF-impacted field sites.

One of the challenges in NTS is to achieve appropriate data reduction without losing features of interest. Various strategies for PFAS have been described that utilize the intrinsic compound properties [40]. Since PFAS often occur in homologous series with characteristic repeating units of CF_2, C_2F_4, or CF_2O moieties, Kendrick-mass defect analysis can be applied [41]. Mass defects of PFAS usually fall into a range from − 0.2 to + 0.1 Da which also offers a filtering possibility. Furthermore, it was shown that the novel MD/C-m/C approach, where for each substance the mass defect per carbon number (MD/C) is plotted against the mass per carbon number (m/C), can reliably separate potential PFAS from many common organic compounds coextracted from the sample matrix [42, 43]. On the MS^2 level, diagnostic fragments or recurring fragment mass differences can be utilized for identification and structure elucidation [44].

The terminology of PFAS has largely followed the conventions established by Buck et al. [4]. However, typical PFAS in AFFF formulations are anionic, cationic, or zwitterionic and can contain multiple functional groups and novel structures are frequently employed, diverging from those described by Buck et al. [4]. These AFFFs often receive varied, inconsistent acronyms and names in the literature. For instance, the major AFFF component Capstone B/Forafac 1157 (CAS 34455–29-3) is commonly abbreviated as 6:2 FTAB [25], 6:2 FTSaB [22], or CMAmP-6:2 FASA [23]. To address this issue, we propose a consistent and easy identifiable system for acronyms of AFFF PFAS and their transformation products (TPs) based on the terminology of Buck et al. [4].

In Reilingen, southwest Germany, a major fire incident occurred in a mattress warehouse in 2008. Various fire departments from the region were involved in firefighting activities, which led to a massive deployment of different AFFF formulations. The AFFFs drained into an irrigation trench across the street and an adjacent agricultural area. An extensive characterization of AFFF PFAS in this area was still pending. The goals of this study were therefore to (i) identify the prevailing PFAS contamination in soil and groundwater by target and non-target screening and to (ii) introduce consistent and identifiable acronyms for AFFF PFAS. This includes by-products and transformation products of AFFF compounds.

Materials and methods

Chemicals and reagents

Methanol (MeOH), ammonium acetate (NH_4Ac), and water were of optima LC–MS grade and were purchased from Thermo Fisher Scientific. A PFAS standard mixture containing 51 authentic reference standards was used for identification of level 1 substances. Detailed information on the reference standards can be found in the ESM 1.A (Table S1).

Sampling and processing of soil and water samples

Soil and groundwater samples were taken in May 2023. Soil samples (*S1*) were collected using drill core probing to a depth of 3 m within the *Nachtwaidgraben* field site (for detailed information, see ESM 1.B, Fig. S1). Four drill cores were obtained at location *S1* (*S1-1*, *S1-2*, *S1-3*, *S1-4*) arranged on a 1 × 1 m square. Drill cores were divided vertically into six sections of 0.5 m each and composite samples of the four drill cores were prepared for each depth section. In this study, only the first depth section (*S1 0–0.5 m*) is discussed. Composite samples were dried at 40 °C, ground, and sieved to a remaining fraction of ≤ 1.6 mm. The water content was 12.6 w/w%. A groundwater sample was taken from a monitoring well along the roadside (*GW*, Fig. S1). Prior to analysis, the water sample was centrifuged for 30 min at 20,817 relative centrifugal forces (rcf) and decanted.

To determine the most suitable extraction method for the soil, four different methods were tested: a simple methanolic extraction, two extractions with methanol plus additives (MeOH + 0.1 M NH_4OH and MeOH + 0.4 M NH_4Ac [34]), and the extraction method described by Nickerson et al. [33], which combines acidic and basic extraction solutions. Sequential extraction with MeOH + 0.4 M NH_4Ac was chosen as the final extraction method. Five grams of dried soil was weighed into 40-mL centrifuge tubes and mixed with 5 mL of the extraction agent. The suspensions were vortexed for 1 min, sonicated for 15 min, and placed on an overhead shaker for approximately 24 h. The tubes were centrifuged for 15 min at 7197 rcf, and the supernatant was transferred and centrifuged again for 30 min at 20817 rcf. A second and third extraction was processed likewise, but with 3 mL extraction agent only as the soil was already soaked. Extracts from multiple extractions were combined with proportional shares (0.5, 0.3, and 0.3 mL). An extraction blank consisting of pure extraction solvent was processed the same way as the soil samples to check for background contamination during the extraction process.

Instrumental analysis

Soil extracts and the groundwater sample were analyzed using high-performance liquid chromatography (1290 HPLC from Agilent Technologies, Waldbronn, Germany) coupled to a quadrupole time-of-flight mass spectrometer with an electrospray ionization source (6550 QTOF, Agilent Technologies, Santa Clara, USA, HPLC-ESI-QTOF-MS). Separation was achieved on an Agilent C_{18} column (Poroshell 120 EC-C_{18}, 2.1 mm × 100 mm, particle size 2.7 µm) with a flow rate of 0.3 mL/min and a column temperature of 40 °C. A 23-min gradient elution was employed with eluent A (95/5 H_2O/MeOH + 2 mM NH_4Ac) and eluent B (95/5 MeOH/H_2O + 2 mM NH_4Ac). The injection volume was 5 µL. The gradient started at 15% B followed by a linear increase to 100% B within 10 min and kept isocratic conditions for 5 min. A post time of 8 min was used to equilibrate the column for initial conditions (15% B). The ionization source was operated separately in negative and positive ionization mode (ESI −/ESI +) due to the presence of anionic, cationic, and zwitterionic substances. For higher MS^2 coverage, QTOF data acquisition was performed in an iterative data-dependent MS^2 mode ($ddMS^2$), injecting each sample five times with a dynamic exclusion list to prevent MS^2 triggering of precursors already selected for MS^2 in previous injections of the sample. The threshold for MS^2 triggering was 1000 counts and after recording 3 MS^2 spectra, the respective precursor m/z was excluded for the next 0.5 min. The acquisition rate was 3 spectra/s in both MS^1 and MS^2, and a narrow isolation window was chosen (1.3 m/z). A linear m/z-dependent collision energy (CE) was applied for collision-induced dissociation according to the following equation: CE (m/z) = 3 $\frac{m/z}{100}$ + 15 eV. For prioritized substances with unsatisfactory MS^2 spectra, additional targeted MS^2 measurements were performed with fixed CE (10, 20, 40 eV) and an acquisition rate of 2 spectra/s. Samples were run together with an extraction blank.

Data evaluation

Identification of target analytes

Target analytes (confidence level 1) were identified by matching the accurate mass, retention time (RT) and MS^2 spectra with an analytical reference standard. For target analysis, 51 PFAS reference standards including 20 PFAAs and 5 AFFF substances were available (ESM 1.A, Table S1).

Feature prioritization

For prioritization of features and identification of potential PFAS, the in-house developed open-source, Python-based software PFΔ*Screen* was used [45]. Feature finding was performed with a mass error of 10 ppm and an intensity threshold of 1000 counts for the peak finding algorithm. An isotope model for small molecules was applied for isotope clustering. For alignment of MS^2 fragments to their respective MS^1 peaks, a mass tolerance of 5 mDa and a RT tolerance of 12 s (±6 s) from the MS^1 peak was used. Features were removed in the blank correction procedure when a feature in the sample aligned with a feature in the extraction blank within a mass tolerance of 2 mDa and a RT tolerance of 6 s. The applied values were chosen according to the peak width of the signals. Furthermore, features were only considered if the peak area was 5 times higher in the sample than in the extraction blank. For prioritization of possible PFAS features, the output feature table of PFΔ*Screen* was sliced, keeping only features with an m/C value > 23 and a RT > 4 min. The cut-off of the m/C value was chosen according to the typical m/C value range of PFAS (m/C = 30–60) [43], depending on the degree of fluorination with highly fluorinated PFAS such as PFAAs exhibiting higher m/C values (e.g., 46 for PFOA and 62.5 for PFOS) than less fluorinated PFAS such as 4:4 fluorotelomer betaine (4:4 FTB) with m/C = 31.5. Since PFΔ*Screen* calculates the m/C values based on the abundance of the M + 1 isotope, which can lead to errors in cases of peak saturation, peak overlap, or too low abundance of the M + 1 peak, the threshold was set slightly lower to ensure that all relevant PFAS are detected. This conservative value still proved viable as more than 90% of the features were removed from the data with a cut-off at a value of m/C = 23 alone (ESM 1.C, Fig. S2a). With the applied reversed-phase chromatography method, highly polar substances typically elute in the first 4 min of the method, while the PFAS of interest are moderately polar to non-polar substances that elute only after 4 min.

Further data reduction was achieved with the help of the extracted ion chromatogram (EIC) correlator in the "Raw Data Visualization" tool within PFΔ*Screen* [45] which correlates EICs at a certain RT-window with an individually adjustable coefficient of determination R^2 ($R^2 > 0.97$). Several substances in the soil samples formed various in-source fragments and/or adducts which appeared in the output table of PFΔ*Screen* as separate compounds but could be assigned to a respective molecular ion ($[M\text{-}H]^-$, $[M\text{-}2H]^-$, $[M+H]^+$, or $[M]^+$) with the help of the EIC correlator.

Identification of suspect- and non-target features

After prioritization, a PFAS suspect screening was conducted with PFΔ*Screen* [45] for which the suspect list from the National Institute of Standards and Technology (NIST) [46] together with an in-house prepared suspect list was used. Additional to the suspect screening with PFΔ*Screen*, the literature was manually searched for m/z values of relevant AFFF-related PFAS. This resulted in the inclusion of some features that were not yet included in the PFΔ*Screen* output table. These manually detected features of interest often showed relatively low abundances, which is probably why they were not detected by the feature detection algorithm of PFΔ*Screen* as their intensities were below the selected intensity threshold.

Prioritized features (m/C > 23, RT > 4 min) that did not produce a suspect hit in the PFΔ*Screen* output table, as well as features that were manually prioritized by literature research but for which no structure was proposed in the literature, were subject to a non-target screening workflow.

The identification process of PFAS started by checking for presence of all possible molecular ions in both ionization modes (ESI−/ESI+) and determining if a suspected PFAS or feature of interest was anionic, cationic, or zwitterionic. Then the presence of further homologues belonging to the feature was checked by searching for repeating CF_2 units with the help of the "Raw Data Visualization" tool in PFΔS*creen*. Homologues which show mass spacing of Δm = 49.9968 (CF_2 repeating unit) indicate an ECF-based structure, while homologues with a mass difference of Δm = 99.9936 (C_2F_4 repeating unit) indicate a fluorotelomer (FT)-derived homologous series [44]. The peak shape of a feature can provide further information about the manufacturing process of the supposed PFAS. A non-baseline separated split peak usually indicates the presence of differently branched and/or linear isomers which suggests an ECF-based structure.

Isotopic patterns were checked against the proposed structure in case of a suspect hit and the structure either was matched or discarded. If no structure was proposed, isotopic patterns and exact mass were used to determine possible molecular formulae with *MSTools* [47] and *ChemCalc* [48]. The isotopic pattern match was calculated according to Eq. 1:

$$\text{Isotopic pattern match} = \left(1 - \left|\left(I_{M+1}^{\text{theoretical}}\right) - \left(I_{M+1}^{\text{measured}}\right)\right|\right) \bullet \left(1 - \left|\left(I_{M+2}^{\text{theoretical}}\right) - \left(I_{M+2}^{\text{measured}}\right)\right|\right) \quad (1)$$

where I is the peak area of the theoretical and measured M + 1 and M + 2 peak, normalized to the M peak (similar to Pluskal et al. [49]).

If MS^2 information was available for suspect hits, MS^2 spectra were investigated manually for the occurrence of matching fragments to the proposed structure. Features with available MS^2 information and no suspect hit were investigated for typical PFAS fragments and fragment differences. The software tool *MetFrag* [50] was also utilized to verify potential chemical structures. In negative ionization mode, FT-based PFAS often show losses of HF (Δm = 20.0062). Fragments of the perfluoroalkyl chain $(C_nF_{2n+1})^-$ with fragment mass differences of 49.9968 (CF_2) indicate a PFAS. Frequently occurring diagnostic fragments for AFFF PFAS in negative mode such as $[SO_3]^-$, $[HO_3S]^-$, $[SO_3F]^-$, $[SO_2F]^-$, $[CH_3O_3S]^-$, $[NO_2S]^-$, $[H_2NO_2S]^-$, and $[C_5H_{11}N_2O_2S]^-$ can further provide information about functional groups and PFAS structures.

In positive ionization mode, fragments of the per- and polyfluoroalkyl chain only and their characteristic mass fragment differences do not occur, but informative positive ionizing fragments of the non-fluorinated molecule part can give valuable information on molecule structure. Frequent diagnostic fragments of positive ionizing AFFF PFAS are for example $[C_4H_{11}N]^{\cdot+}$, $[C_5H_{11}N]^{\cdot+}$, $[C_4H_8N]^+$, $[C_5H_{14}N_2]^{\cdot+}$, $[C_4H_{10}NO_2]^+$, $[C_4H_8NO_2]^+$, and $[C_5H_{12}NO_2]^+$ and can indicate for example the presence of a betaine or trimethylamine moiety in a molecule [23].

Classification into confidence levels

To classify the identified substances into confidence levels, a scheme adapted from Charbonnet et al. [51] is introduced here (ESM 1.D, Table S2). Since PFAS are rare in MS^2 libraries, the criterion for library MS^2 matching was discarded. Instead, the m/C value was included as a criterion (m/C > 25) and experimental data from the literature (e.g., provided MS^2 spectra in peer-reviewed publications) can also be considered in determining the confidence level of a feature similar to the initially proposed confidence level for small molecules by Schymanski et al. [52].

Results and discussion

Terminology

Perfluorohexane sulfonamide propyl dimethylamine (PFHxSAm-Pr-DiMeAm), the most predominant PFAS species in AFFF apart from PFHxS and PFOS [53], and its fluorotelomer analogue 6:2 fluorotelomer sulfonamide propyl dimethylamine (6:2 FTSAm-Pr-DiMeAm) have both received multiple names in literature, which are not necessarily consistent or describe the structure unambiguously (PFHxSaAm [22], AmPr-FHxSA [33], N-AP-FHxSA [54], PFHxSAm [16], and PFHxSAA [14] for PFHxSAm-Pr-DiMeAm (Table 3, row 5) and 6:2 FtSaAm [22], N-AP-6:2 FASA [23], 6:2 FTSAPr-DiMeAn [33], 6:2 FTAA [55], and 6:2 FTA [39] for 6:2 FTSAm-Pr-DiMeAm (Table 3, row 7)). In an effort to counteract this development, the new terminology for AFFF PFAS was established and applied to all identified PFAS. The naming approach incorporates the terminology conventions of Buck et al. [4] and aligns with multiple designations found in the literature, ensuring a consistent terminology where the structure can be derived from the acronym. All rules and acronyms for specific moieties are specified in Table 1. In short:

- The acronyms for the different parts of the chemical structure are assembled stepwise, starting from the per-/polyfluoroalkyl moiety on the left and progressing to the right. Each subsequent moiety is added sequentially and separated by hyphens (e.g., 6:2 FTSAm-Pr-B, 6:2 fluorotelomer sulfonamide propyl betaine, Table 1).
- The acronyms for side chains and substitutions are placed directly in front of the respective acronym to which they are attached. The positions of side chains, as well as keto, ether, unsaturated, H-substituted, and OH-substituted moieties, are indicated by numbers in parentheses (e.g., (6)U-(5)E-PFHpS, Table 1).
- If the main chain branches at the sulfonamide nitrogen into chains X and Y, this is denoted as *N*-X-*N*-Y (e.g., PFHxSAm-*N*-Et-*N*-EtA, Table 1).

A table with all acronyms of subclasses/compounds with an example structure, formula, International Chemical Identifier (InChI), and alternative names in literature can be found in ESM 2.

Choice of extraction method

We investigated the performance of four different extraction methods: extraction employing neutral and basic methanol (MeOH, MeOH + 0.1 M NH_4OH, MeOH + 0.4 M NH_4Ac) as extraction solvents, along with the method described by Nickerson et al. [33] which employs the combination of acidic and basic extraction solvents. The extraction efficiencies were compared for 19 anionic, zwitterionic, and cationic PFAS (ESM 1.E, Fig. S3). For

Table 1 Rules for the new systematic terminology with acronyms of specific moieties and examples

Rules	Explanations/Examples	
Order and link	**Acronym**	**Moiety**
All moieties are abbreviated as indicated here.	Me/Et/Pr	Methyl/Ethyl/Propyl
Acronyms for the different parts of the chemical structure assembled stepwise from the per-/polyfluoroalkyl moiety (left) to right.	A	Acid (e.g. EtA)
	Ad	Amide
	Al	Aldehyde
	Am	Amine
The per- or polyfluoroalkyl moiety and the directly following functional group are building the base structure and are combined without a separator, e.g. FTSAm.	B	Betaine
	CA	Carboxylic acid
	E	Ether
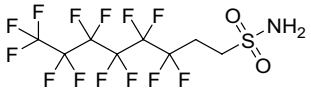	FT	Fluorotelomer
	H/Cl	H/Cl-substitution
	K	Ketone
All subsequent moieties are added sequentially and separated by hyphens, e.g. FTSAm-Pr-B.	NO	Amine oxide
	OH	Hydroxy
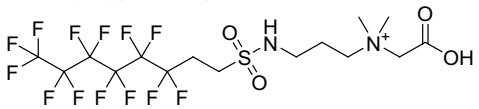	PF	Perfluoro
	SA	Sulfonic acid (e.g. PrSA)
	SAm	Sulfonamide
	SF_5	Pentafluoro-sulfanyl
	Sy	Sulfonyl
	SO	Sulfoxide
	Th	Thio
	U	Unsaturation
Per-/polyfluoroalkyl chain length	PFOA	
In perfluorinated compounds, the length of the alkyl chain is expressed by the corresponding acronym of an alkane based on the chain length n (e.g. O for octane if n = 8). The chain length of fluorotelomers is denoted by n:p FT, where n represents the length of the perfluorinated alkyl chain and p represents the length of the hydrocarbon chain. Additionally, n:1:p fluorotelomers include one extra CHF moiety [4].		
	6:2 FTCA	
	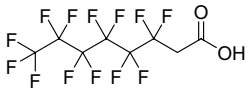	
Numbering	PFHxSAm-Pr-DiMeAm	
The numbering starts from the atoms next to the functional group attached to the per-/polyfluoroalkyl chain in both directions. All heteroatoms in the main chain are included in the numbering. Numbers in the non-fluorinated chain are marked with an apostrophe.	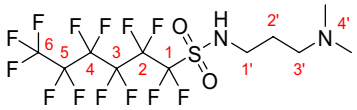	
Side chains	PFHxSAm-Pr-DiMeAm	
The acronyms of side chains are added in front of the respective acronym to which the side chain is attached, without any separator (no blank, no hyphen).	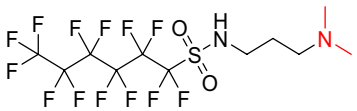	
Positions	(6)U-(5)E-PFHpS	
The positioning of side chains, keto, ether, unsaturated, H-substituted, and OH-substituted moieties is denoted by numbers in parentheses. These moieties are integrated into the counting of carbon atoms.	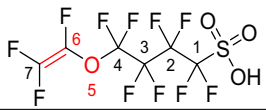	
Branching at SAm moiety	PFHxSAm-*N*-Et-*N*-EtA	
For example, if the main chain is branched at the sulfonamide N into chains X and Y, this is denoted as *N*-X-*N*-Y.	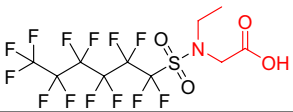	

anionic PFAS, all of the enhanced extraction methods only showed a small improvement or even a decrease in extraction efficiency. For cationic and zwitterionic PFAS, MeOH + 0.1 M NH_4OH performed worst for 7 out of 9 zwitterionic and cationic substances and was therefore not used. Therefore, in a next step, we conducted a three-step sequential extraction with MeOH + 0.4 M NH_4Ac and compared it to the method of Nickerson et al. [33] (ESM 1.E, Fig. S4). Extraction efficiencies were similar for both methods, but the extraction with MeOH + 0.4 M NH_4Ac showed slightly better recoveries for 7 out of 19 substances. Due to the reduced workload compared to the method from Nickerson et al. [33], the three-step sequential extraction with MeOH + 0.4 M NH_4Ac as extraction

solvent was chosen as the final extraction method. No contamination could be detected in the extraction blank.

PFAS prioritization

The extract of soil sample *S1* in the upper horizon (0–0.5 m) was analyzed by LC-HRMS in ESI + and ESI − and data evaluation was performed with the open-source tool PFΔ*Screen* [45]. The output tables of PFΔ*Screen* for soil yielded a total of 2262 and 1921 non-target features in ESI − and ESI +, respectively (after componentization of isotope clusters). Prioritization of features was reached by cutting off the output tables of PFΔS*creen* and only keeping features with m/C > 23 and RT > 4 min. The m/C threshold was chosen to separate hydrocarbon-dominated substances in the sample matrix from highly fluorinated PFAS [43] and the RT threshold to separate early eluting polar compounds from the moderately polar to non-polar PFAS. This led to a significant reduction in total peak areas of 79% for ESI − and 82% for ESI +, corresponding to a reduction of total number of features of 95%. Ninety-two and 94% of the respective prioritized peak areas (5% of total features) could be identified as PFAS (levels 1–3, 124 features) in ESI − and ESI +, respectively. An additional 6% and 3% of the prioritized peak areas in ESI − and ESI +, respectively, were classified as potential PFAS (levels 4 and 5, 114 features in total, Fig. 1).

Prioritizing via the m/C and RT dimension led to significant feature reduction (Fig. S2a) and major fractions of the prioritized peak areas could be identified as PFAS. PFAS prioritization via the MD/C-m/C approach was proven to be effective before [43] and the performance of the prioritization workflow applied in this work (RT > 4 min and m/C < 23) was validated by application to a standard mix (ESM 1.C). A histogram of the m/C values of all PFAS of the NIST suspect list [46] (ESM 1.C, Fig. S2b) reveals that only a small fraction (0.9%) of specific PFAS with low fluorine percentage show a m/C below 23, indicating a low probability to exclude PFAS (false negatives) via this prioritization technique. We did not consider PFAAs with chain length shorter than perfluoropentanoic acid (PFPeA) and perfluoropropane sulfonic acid (PFPrS) and similar highly polar PFAS due to RT cut-off at 4 min. Further limitations result from the choice of extraction and ionization methods.

Identified PFAS in soil and groundwater samples

Suspect hits and non-target features were identified according to the identification workflow described above. In total, 124 features of 42 subclasses were identified as PFAS in soil (levels 1–3, Tables 2 and 3). Ten of the 42 identified subclasses were identified as level 1, 28 at level 2, and 4 at level 3, corresponding to 52.7%, 41.7%, and 0.3% of the total peak area, respectively (Fig. 2a). Twelve of the 42 identified subclasses in soil were also present in the groundwater sample (25 individual compounds, Tables 2 and 3).

At level 1, substances in soil were confirmed with corresponding reference standards (target compounds). For level 2 substances, a possible structure is proposed that is supported by meaningful MS^2 fragments. At level 3, one molecular formula is proposed but various chemical structures can

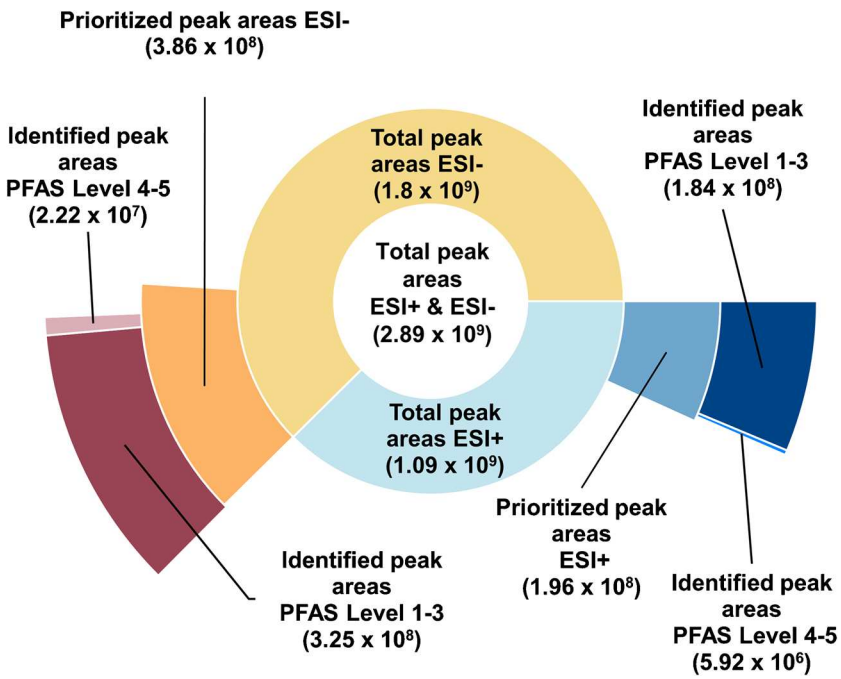

Fig. 1 Cumulative peak areas of all features from the PFΔS*creen* output tables (inner sections), peak areas of prioritized features filtered for RT > 4 min and m/C > 23 (middle sections), and peak areas of features identified as PFAS in negative and positive ESI mode (outer sections), respectively. Peak areas of in-source fragments and adducts were first combined with the respective parent ion

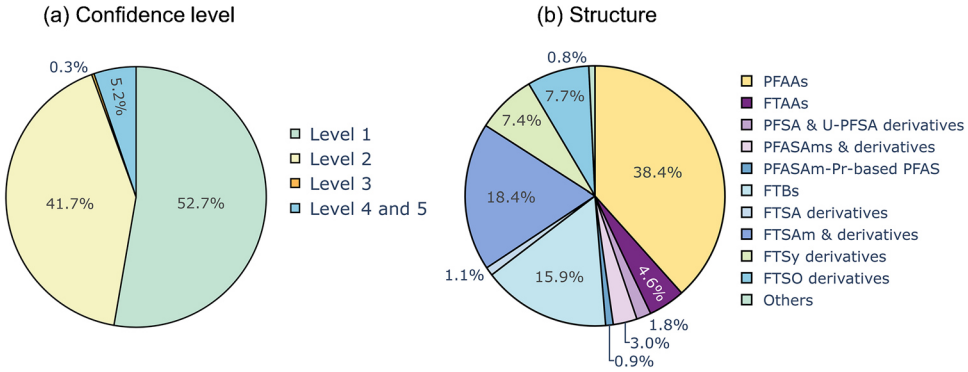

Fig. 2 Distribution of peak areas in soil across the identification levels (**a**) and for different PFAS subclasses (**b**; levels 1–3; see also Tables 2 and 3)

be possible due to the lack of meaningful MS^2 fragments. The poor quality of MS^2 spectra often results from low peak intensity of the respective substances. All substances identified at levels 1, 2, and 3 are included with (possible) structure, name, and additional information in ESM 2. For level 4 substances, a molecular formula is proposed according to accurate mass and isotopic pattern match and level 5 substances are features of interest that are potentially PFAS due to a suitable m/C value and the occurrence of homologous series. In total, 114 individual compounds were categorized into levels 4 and 5, including 17 homologous series. Level 4 and level 5 substances together contribute to 5.2% to the total peak area of all level 1–5 substances in the soil (for more details on the classification of confidence levels and fragmentation evidence, refer to ESM 1.D and G; for more detailed information on all identified substances, explanations of all acronyms, molecular formula, ionization polarity, alternative names in the literature, additional information from the literature, and criteria used for assigning the single substances to specific confidence levels, refer to the ESM 2). Note: In some cases, corresponding homologues within one subclass were assigned at different confidence levels. A subclass is described in the following section at the level of the homologue with the highest confidence level.

Newly identified substances and substances identified for the first time in soil

One PFAS subclass with two homologues (n:2/m:2 FTSAm dimers) was newly identified in the soil samples (red font in Table 2). To the best of our knowledge, 9 further PFAS subclasses were detected in soil for the first time (three fluorotelomer betaines, three fluorotelomer sulfonamides, one fluorotelomer sulfone, and two fluorotelomer sulfonic acids, Table 2). All subclasses discussed in this section were identified at level 2, except for n:1:2 FTB which was identified at level 3.

Fluorotelomer sulfonamide dimer (n:2/m:2 FTSAm dimer, Table 2, row 1) Two homologues of the newly identified n:2/m:2 fluorotelomer sulfonamide dimer (n:2/m:2 FTSAm dimer) were detected (6:2/6:2 at 9.36 min, exact mass m/z 835.9485 and 6:2/8:2 at 10.38 min, m/z 935.9421) which can be considered as fluorotelomer derivatives of the anion bistriflimide (bis(trifluoromethane)sulfonimide, also known as NTf2). Yukioka et al. [56] and Luo et al. [37] already detected this compound as unknown. Our MS^2 data strongly support the proposed structures with 6 and 10 meaningful fragments, respectively (level 2, Fig. 3, S5b, and S5c). Both compounds show the diagnostic fragment $[SO_2NH_2]^-$ (exact mass m/z 79.9812), indicating the presence of a sulfonamide group which is also detected for other sulfonamide-based PFAS like 6:2 FTSAm (Fig. S36b), [M-H-HF]- ions (at exact mass m/z 815.9423 and m/z 915.9539) indicative for fluorotelomer-based PFAS and fragments resulting from a cleavage of one fluorotelomer side chain (m/z 405.9777 and m/z 505.9713) combined with further three consecutive HF losses (exact mass m/z 405.9777 → 385.9714 → 365.9645 → 345.9652, Fig. 3 and S5c). In the case of the asymmetrically substituted 6:2/8:2 FTSAm dimer, both series of HF losses occur from the 6:2 FTSAm fragment (exact mass m/z 405.9777) and the 8:2 FTSAm fragment (exact mass m/z 505.9713). Formation of the dimer from n:2 FTSAm as ionization artifact can be ruled out due to chromatographic separation of n:2/m:2 FTSAm dimers compared to the corresponding fluorotelomer sulfonamides which elute much earlier (RT 7.77 min and 8.88 min, respectively; Fig. S36a and S5a).

Fluorotelomer sulfonamide–based PFAS (n:2 FTSAm-based subclasses, Table 2, row 1) The three FTSAm-based subclasses n:2 fluorotelomer sulfonamide *N*-methyl *N*-propanoic acid (6:2 FTSAm-*N*-Me-*N*-PrA), n:2 fluorotelomer sulfonamide unsaturated propyl dimethylamine (6:2 FTSAm-U-Pr-DiMeAm), and n:2 fluorotelomer sulfonamide propanoic acid (6:2 FTSAm-PrA) were identified for the first time in soil. Various series of HF losses support a fluorotelomer structure for 6:2 FTSAm-*N*-Me-*N*-PrA and diagnostic fragments such as $[SO_2NH_2]^-$ and $[C_4H_8NO_4S]^-$ (exact mass m/z 166.0180) are indicative for the functional groups and

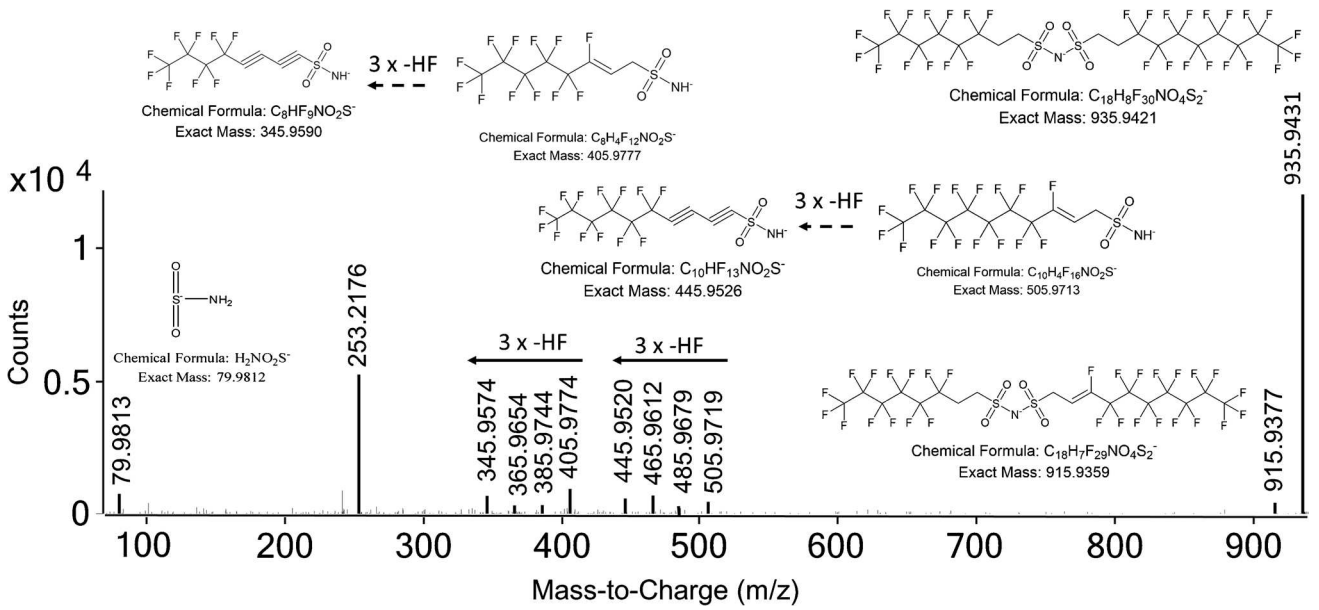

Fig. 3 Annotated MS^2 fragmentation spectrum of 6:2/8:2 FTSAm dimer (m/z = 935.9431, RT = 10.2 min) in ESI − at a collision energy of 43 eV

the non-fluorinated part of the molecules (Fig. S6c). 14 MS^2 fragments could be matched to the proposed structures, of which 11 fragments could be matched with those reported by Fang et al. [57]. For 6:2 FTSAm-U-Pr-DiMeAm, three MS^2 fragments could be matched to the structure including the fragment $[C_{10}H_9F_{13}NO_2S]^+$ (due to the loss of the terminal C_3H_7N moiety) and fragments of the quaternary ammonium moiety (Fig. S7b), all in accordance with the fragments observed by Fang et al. [57]. For 6:2 FTSAm-PrA (Fig. S8b), several fragments could be assigned to the polyfluorinated carbon moiety ($[C_3F_7]^-$, $[C_4F_9]^-$, $[C_8F_9]^-$) and the functional group ($[NSO_2]^-$, $[FSO_2]^-$, $[C_3H_6NO_4S]^-$) and loss of HF. The $n = 6$ homologues of all three subclasses were detected as biotransformation products of 6:2 fluorotelomer sulfonamide propyl dimethylamine oxide (6:2 FTSAm-Pr-DiMeNO) in aerobic sludge by Fang et al. [57]. In addition, 6:2 FTSAm-PrA was also observed as an intermediate in aerobic biodegradation of 6:2 fluorotelomer sulfonamide propyl dimethylamine (6:2 FTSAm-Pr-DiMeAm) in sludge [55].

Fluorotelomer betaines (n:2 FTB, n:1:3 FTB, n:4 FTB, Table 2, row 2) The diagnostic fragments $[C_4H_{10}NO_2]^+$ (exact mass m/z 104.0706) and $[C_5H_{12}NO_2]^+$ (exact mass m/z 118.0831) are indicative for the FTB class (Fig. S9b) and were detected for at least one homologue of the two FTB subclasses (n:2 and n:4 FTB; Fig. S9b,c and S10b). For n:1:3 FTB, only m/z 118.0863 was detected (Fig. S11b). In general, the MS^2 spectra of FTBs are rather poor in fragments due to the fixed positive charge at the quaternary ammonium moiety. Therefore, correct and accurate mass match and isotope patterns are crucial parameters in this case. All three FTB subclasses were previously identified in Ansulite AFFF in lower abundance compared to n:1:2 and n:3 FTBs [17]. This corresponds very well with the results of the homologue analysis. Whereas less homologues occurred for n:2 FTB ($n = 6$, 8, 10, 12), n:4 FTB ($n = 6$, 8, 10), and n:1:3 FTB ($n = 6$, 8, 10), an extended range was found for n:3 FTB ($n = 5$, 7, 9, 11, 13) and n:1:2 FTB ($n = 5$, 7, 9, 11, 13, 15).

Fluorotelomer sulfonic acids (K-n:2 FTSA and U-n:2 FTSA, Table 2, row 3) Ketone-n:2 fluorotelomer sulfonic acids (K-n:2 FTSAs) and unsaturated-n:2 FTSAs (U-n:2-FTSAs) both show fragments of the unsaturated fluorinated carbon chain as well as the diagnostic fragment $[SO_3H]^-$ (exact mass m/z 80.9652) which is characteristic for the sulfonic acid moiety in the vicinity of a hydrogen atom. For both subclasses, at least three fragments (e.g., $[C_2F_5]^-$, $[C_2F_7]^-$, $[C_7F_9]^-$, $[C_7F_{11}]^-$) could be matched with the proposed structures (Fig. S12b, S13b). All MS^2 fragments of both subclasses were also observed by Fang et al. [57] who detected both, K-6:2 FTSA and U-6:2 FTSA as biotransformation products of 6:2 FTSA in aerobic sludge. U-n:2 FTSAs resulting from in-source fragmentation (loss of water) of K-n:2 FTSAs could be excluded due to chromatographic separation of the two subclasses (e.g., U-6:2 FTSA at 7.03 min; K-6:2-FTSA at 6.92 min, Fig. S12a and S13a).

Fluorotelomer sulfones (n:2 FTSy-(2′)OHPr-TriMeAm, Table 2, row 4) n:2 fluorotelomer sulfone (2′)-propanol

Table 2 Summary of newly identified PFAS (red font) and newly in soil identified PFAS (black font) at the field site in Reilingen (soil, S1 and groundwater, GW). Identified homologues are denoted in brackets. Note that some homologues might have a lower confidence level (ESM 2)

Row	Substances
1	**Fluorotelomer sulfonamides (FTSAm-based)** **n:2/m:2 FTSAm dimer** (S1: n = 6/m = 6, 8) **n:2 FTSAm-U-Pr-DiMeAm** (S1: n=6) **n:2 FTSAm-*N*-Me-*N*-PrA** (S1: n = 6) **n:2 FTSAm-PrA** (S1: n = 6)
2	**Fluorotelomer Betaines (FTB)** **n:2 FTB** (S1: n = 6-12) **n:1:3 FTB** (S1: n = 5-9) **n:4 FTB** (S1: n = 4-10)
3	**Fluorotelomer sulfonic acid derivatives (FTSA derivatives)** **K-n:2 FTSA** (S1: n = 6-10, GW: n = 6) **U-n:2 FTSA** (S1: n = 6, 8)
4	**Fluorotelomer sulfone derivatives (FTSy derivatives)** **n:2 FTSy-(2')OHPr-TriMeAm** (S1: n = 4-8)

trimethylamine (n:2 FTSy-(2′)OHPr-TriMeAm, Fig. S14b,c) was identified at level 2 according to matches of five meaningful MS^2 fragments for $n = 6$ and $n = 8$ homologues. The fragments m/z 469.0138 and m/z 412.9875 are formed by losses of the terminal moieties C_3H_9N and further C_3H_4O from the molecular ion $[M\text{-}H]^+$ ($[C_{14}H_{19}F_{13}NO_3S]^+$). Further MS fragments are ions from the terminal end of the molecule, $[C_6H_{16}NO_3S]^+$ (exact mass m/z 182.0845), $[C_3H_7O_3S]^+$ (exact mass m/z 123.0110), and $[C_5H_{12}NO]^+$ (exact mass m/z 102.0913). This subclass was already identified in various AFFF formulations [17, 21, 36, 58], but to the best of our knowledge never in soil.

Further PFAS in soil and groundwater

Fragmentation evidence for all identified level 2 and level 3 substances can be obtained from ESM 1.G.

PFCA, PFSA, FTCA, and FTSA (Table 3, row 1) PFAAs such as PFCAs and PFSAs as well as n:3 fluorotelomer carboxylic acids (n:3 FTCAs) and n:2 FTSAs were detected at level 1. The group of PFAAs constitutes the largest portion of the contamination based on peak area, contributing to 38.4% of the total peak area of all level 1–3 substances (Fig. 2b). This is not surprising since both PFCAs and PFSAs were mainly used in various AFFFs from 3 M and Angus [18, 21, 22]. FTCAs and FTSAs comprise only 4.6% of the total peak area of all level 1–3 substances, although n:2 FTSAs are also known to be found in various AFFF formulations [53, 58].

PFSA- and U-PFSA-derivatives (Table 3; rows 2, 3, and 10) PFSA derivatives include Cl-substituted PFSAs (Cl-PFSAs), pentafluorosulfanyl PFSAs (SF_5-PFSAs), H-substituted PFSAs (H-PFSAs), ketone PFSAs (K-PFSAs)/unsaturated ether PFSAs (U-E-PFSAs), and perfluoro

Table 3 Summary of further identified PFAS at the Reilingen site in soil (S1) and groundwater (GW). The table shows all previously detected subclasses in soil where at least one homologue was assigned level 1–3. Note that for the sake of simplicity, only one positional isomer is depicted even if the correct position is unclear. K-PFSA/U-E-PFSA are in brackets indicating that both structures may be possible

Row	Common base structure	Subclass defining moiety (R)
1	PFAA & FTAA	PFCA (S1: C_4-C_{12}, GW: C_3-C_7); PFSA (S1: C_3-C_{13}, GW: C_4-C_8); n:3 FTCA (S1: n = 3-9); n:2 FTSA (S1: n = 6-14, GW: n = 6)
2	PFSA derivatives	Cl-PFSA (S1:C_6, C_8); K-PFSA (S1: C_6-C_{14}); SF_5 -PFSA (S1:C_7-C_{10}); H-PFSA (S1:C_8, C_{10})
3	U-PFSA derivatives	U-PFSA (S1:C_6-C_{15}); U-E-PFSA (S1: C_7-C_{15}); SF_5-U-PFSA (S1:C_8-C_{10})
4	PFASAm and derivatives	PFASAm (S1: C_3-C_8, GW: C_3-C_6); PFASAm-Me (S1: C_4, C_6, C_8, GW: C_8); PFASAm-EtA (S1: C_6, C_8, GW: C_8)
5	PFASAm-Pr-based AFFF PFAS	PFASAm-PrSA (S1: C_4-C_6); PFASAm-Pr-B (S1: C_4-C_6, C_8); PFASAm-Pr-DiMeAm (S1: C_6, C_8); PFASAm-Pr-TriMeAm (S1: C_6, C_8)

Row	Common base structure	Subclass defining moiety (R)
6	FTBs	n:3 FTB (S1: n = 5-13GW: n = 5,7); n:1:2 FTB (S1: n = 5-15, GW: n = 5,7)
7	FTSAm and derivatives	n:2 FTSAm (S1: n = 6-10, GW: n =6); n:2 FTSAm-Pr-MeAm (S1: n = 6); n:2 FTSAm-Pr-DiMeAm (S1: n = 6, 8); n:2 FTSAm-Pr-B (S1: n = 4-12,GW = 6); n:2 FTSAm-Pr-DiMeNO (S1: n = 6, 8)
8	FTSy derivatives	n:2 FTSy-PrA (S1: n = 4-8); n:2 FTSy-Pr-Ad-(5',5')DiMeEtSA (S1: n = 6-12)
9	FTSO derivatives	n:2 FTSO-(2')OHPr-TriMeAm (S1: n = 4-8); n:2 FTSO-Pr-Ad-(5',5')DiMeEtSA (S1: n = 6)
10	Others	PFASAm-*N*-PrSA-*N*-Pr-DiMeAm (S1: C_4-C_6); PFASyA (S1: C_8); OH-n:2 FTSA (S1: n = 6, 8); n:2 FTTh-(2')OHPr-TriMeAm (S1: n = 4-10, GW: n = 4)

sulfinic acids (PFASyAs). Unsaturated PFSA (U-PFSA) derivatives include U-PFSAs and pentafluorosulfanyl unsaturated PFSAs (SF_5-U-PFSAs). All above listed subclasses were determined at level 2 besides K-PFSAs/U-E-PFSAs which were identified at level 3 due to the lack of meaningful MS^2 spectra. PFSA and U-PFSA derivatives only represent minor fractions of the total peak area of all identified level 1–3 substances (1.8%, Fig. 2b). All PFSA derivatives but SF_5-U-PFSAs have been detected in 3 M AFFF [23].

PFASAm-based subclasses (Table 3; rows 4, 5, and 10) Perfluoroalkyl sulfonamide–based PFAS (PFASAms) and perfluoroalkyl sulfonamides propyl dimethylamines (PFASAm-Pr-DiMeAms) were identified at level 1. PFASAm-Pr-DiMeAms is one of the most predominant compounds in AFFF [53]. At level 2, perfluoroalkane sulfonamide ethanoic acids (PFASAm-EtAs), perfluoroalkane sulfonamide propyl sulfonic acids (PFASAm-PrSAs), perfluoroalkane sulfonamide propyl betaines (PFASAm-Pr-Bs), and perfluoroalkane sulfonamide propyl trimethylamines (PFASAm-Pr-TriMeAms) were identified. The PFASAm-based perfluoroalkane sulfonamide methyl (PFASAm-Mes) and perfluoroalkane sulfonamide *N*-propyl sulfonic acid *N*-propyl dimethylamine (PFASAm-*N*-PrSA-*N*-Pr-DiMeAm, Table 3, row 10) were identified at level 3. An isomer of PFASAm-*N*-PrSA-*N*-Pr-DiMeAm was previously detected in AFFF from 3 M (class 2 (*N*-SPAmP-FASAs) according to Barzen-Hanson et al. [23]). In this study, MS^2 data (m/z 519.9564, $[C_9H_7F_{13}NO_5S_2]^-$, Fig. S33c) suggest branching at the first nitrogen moiety, which still needs to be validated by further analyses. PFASAm and PFASAm-Pr-based substances together only contribute to 1.2% of the total peak area (Fig. 2b).

FTBs (Table 3, row 6) FTBs represent a significant portion of the total peak area (15.9%, Fig. 2b) and include five subclasses in total of which three subclasses were identified for the first time in soil (discussion in previous section). The remaining two subclasses were assigned level 1: n:1:2 FTBs and n:3 FTBs. Both have been detected abundantly in various AFFF formulations [16, 17, 21, 22, 36] and therefore contribute to a significant portion to the total FTB peak area (97.7%). In contrast, n:2, n:1:3, and n:4 FTBs contribute only to a minor fraction and have been detected with less frequency in AFFF [17, 23].

n:2 FTSAm derivatives (Table 3, row 7) Identified PFAS, sharing a common n:2 FTSAm-based structure, represent the second largest group of substances based on peak area after PFAAs (18.4%, Fig. 2b) and include eight substance subclasses of which two were identified at level 1: the two, well-known AFFF compounds n:2 fluorotelomer sulfonamide propyl betaines (n:2 FTSAm-Pr-Bs) and n:2 FTSAm-Pr-DiMeNOs. All other FTSAm-derivatives were identified at level 2 of which n:2-FTSAm-*N*-Me-*N*-PrAs n:2 FTSAm-PrAs and n:2 FTSAm-U-Pr-DiMeAms (Table 2, row 1) were detected for the first time in soil in this study, to the best of our knowledge (discussion in previous section). n:2 FTSAm-Pr-MeAms and n:2 FTSAm-Pr-DiMeAms both were detected in AFFF and AFFF-impacted environment before [17, 36, 37] and are possible TPs or synthetic intermediates of n:2 FTSAm-Pr-Bs and n:2 FTSAm-Pr-DiMeNOs [17, 25, 57].

n:2 FTSy-based PFAS (Table 3, row 8) Two further PFAS subclasses sharing a fluorotelomer sulfonyl (FTSy)-based structure were detected and identified at level 2. All FTSy-based PFAS together, including the previously discussed 6:2 FTSy-(2′)OHPr-TriMeAm, which was detected for the first time in soil in this study contribute to 7.4% of the total peak area of all level 1–3 substances (Fig. 2b). 6:2 FTSy-(2′)OHPr-TriMeAm is among the top three most abundant substances in the soil based on peak area and contributes with 90% alone to the fraction of the FTSy-based substances of all identified level 1–3 substances, consequently contributing to 6.9% of the total peak area of all level 1–3 substances.

n:2 FTSO-based PFAS (Table 3, row 9) Two PFAS subclasses sharing a fluorotelomer sulfoxide (FTSO)–based structure were detected at level 2. Though only consisting of two subclasses corresponding to 4 single substances, this group represents 7.7% of the total peak area of all level 1–3 substances. This is largely due to 6:2 fluorotelomer sulfoxide (2′)-propanol trimethylamine (6:2 FTSO-(2′)OHPr-TriMeAm) which contributes 98.6% alone to the peak area of the FTSO-based PFAS. Both subclasses have previously been detected in AFFF-impacted soil [39] and AFFF [21].

n:2 FTTh-based PFAS (Table 3, row 10) n:2 fluorotelomer thio (2′)-propanol trimethylamine (n:2 FTTh-(2′)OHPr-TriMeAms) was identified at level 2 in soil. 6:2 FTTh-(2′)OHPr-TriMeAm contributes to 36.5% of the total peak areas of the "other" category (Fig. 2b) and is a well-known AFFF compound which was detected in various AFFF formulations before [16, 21, 22, 36].

n:2 FTSA derivatives (Table 3, row 10) n:2 FTSA derivatives include hydroxy-n:2 FTSAs (OH-n:2 FTSAs), ketone-n:2 FTSAs (K-n:2 FTSAs), and unsaturated n:2 FTSAs (U-n:2 FTSAs). U-n:2 FTSAs and K-n:2 FTSAs both were detected in soil for the first time in this study (discussion in previous section). n:2 FTSA derivatives only represent a minor fraction of the total peak area of all identified level 1–3 substances (1.1%, Fig. 2b). As was shown that U-n:2 FTSAs and K-n:2 FTSAs can originate from n:2 FTSA biotransformation, OH-n:2 FTSA likely are either TPs or synthetic

by-products of fluorotelomer-based AFFF substances such as n:2 FTSA as well [23, 57].

Characteristics of identified level 1–3 substances

Negative ionizable PFAS are dominating the contamination pattern, representing 62.8% of the total peak area of all identified level 1–3 PFAS (Fig. 4a). This can be partly attributed to the high proportion of PFAAs present in the contaminated soil (38.4%, Figs. 2b and 4c), especially PFOS and PFHxS, which are the most abundant PFAAs based on peak area in soil. But also 6:2 FTSA and 6:2 FTSAm contribute to large parts of the fraction of negative ionizable compounds. Positive ionizable substances represent the second largest fraction comprising 31.5% of the total peak area. Substances dominating this group of substances are 5:1:2 and 7:1:2 FTB, 6:2 FTSO-(2′)OHPr-TriMeAm, and 6:2 FTSy-(2′)OHPr-TriMeAm. Zwitterionic substances make up 5.7% of the total peak area. The fraction of the zwitterionic substances is clearly dominated by 6:2 FTSAm-Pr-B, solely contributing to 80% of the total peak area of zwitterionic substances.

Considering the perfluorinated chain length distribution of the level 1–3 substances, PFAS with $n=6$ represent the largest fraction of the total peak area (43.4%), followed by $n=8$ (33.1%), $n=7$ (10.7%), and $n=5$ (7.2%) (Fig. 4b). PFAS with chain lengths of 3 and 4 and more than 10 fluorinated carbon atoms together only contribute to less than 3% of the total peak area. Compounds with shorter perfluorinated chain lengths than 3 (PFPrS) or 4 (PFPeA) have not been considered in this work. The $n=8$ substances are dominated by PFOS (82.2%), followed by 8:2 FTSA and PFOSAm, all three together contributing 95% to the $n=8$ fraction. The high abundance of $n=5$ and $n=7$ substances can be attributed to the n:1:2 and n:3 FTBs. The $n=6$ and $n=8$ fractions also include the highest numbers of single substances compared to all other chain lengths indicating that mainly C_6 and C_8 substances dominated the AFFFs applied for the firefighting activities. This is in compliance with most contemporary AFFF formulations, which are mainly based on C_6-chemistry [53].

Occurrence of identified PFAS in AFFF and the environment

Six out of the 14 most abundant PFAS in contemporary AFFF formulations [58] could be identified in the contaminated soil. These are all 6:2 FT-based PFAS and include 6:2 FTSA, 6:2 FTTh-Pr-(2′)OHPr-TriMeAm, two FTSO-based AFFF (6:2 FTSO-Pr-Ad-(5′,5′)DiMeEtSA, 6:2 FTSO-(2′)OHPr-TriMeAm), and two FTSAm-based AFFFs (6:2 FTSAm-Pr-DiMeNO, 6:2 FTSAm-Pr-B). The occurrence of FT-based and ECF-based precursors in soil at the Reilingen site clearly indicates that AFFF formulations from various manufacturers were used for firefighting activities. Despite the presence of numerous precursors, PFAAs represent a large part of the contamination (38.4%) and may originate either from the used AFFFs itself or have been formed in situ during transformation of precursors.

A recent review by Yan et al. [53] proposed a novel classification system for AFFF-derived PFAS precursors. In this system, primary precursors are defined as PFAS intended to be present in AFFF formulations as active agents. Secondary precursors encompass both transformation products (excluding PFAAs) and by-products resulting from primary precursors. Identified level 1–3 PFAS were assigned to the respective category (primary precursors/secondary precursor) based on literature review (Fig. 4c). While primary precursors (ECF + FT based) make up only about 21.3% of the total peak area, secondary precursors (ECF + FT) represent 38.3% of the total peak area similar to PFAAs accounting for 38.4% of the peak area. Highly abundant primary precursors identified in soil are for example 5:1:2 FTB, 7:1:2 FTB, 5:3 FTB, 7:3 FTB, 6:2 FTSAm-Pr-B, 6:2 FTTh-(2′)OHPr-TriMeAm, and PFOSAm-Pr-DiMeAm.

These findings are consistent with the review by Yan et al. [53] who determined that secondary precursors are more frequently detected in AFFF-contaminated areas, despite

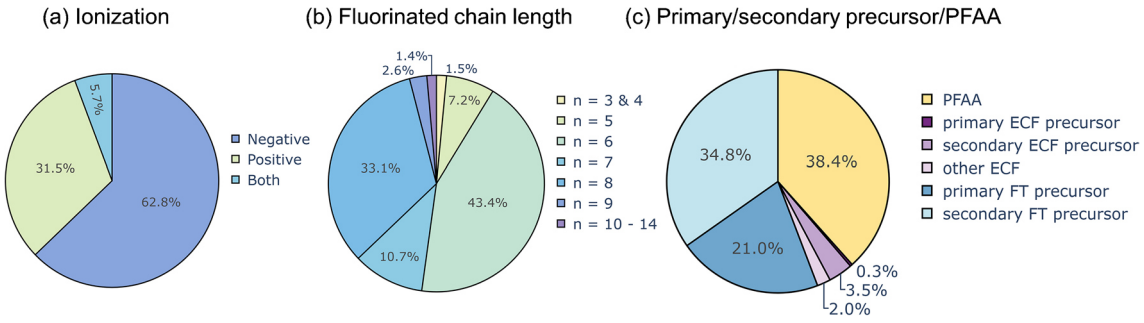

Fig. 4 Distribution of peak areas of identified level 1–3 substances in soil characterized by the ionization mode (**a**), the perfluorinated chain length distribution (**b**), and the categories primary or secondary precursors, and PFAAs (**c**)

primary precursors being present in larger quantities in the original AFFF formulations [53]. This discrepancy can be explained by in situ biotransformation of primary precursors to secondary precursors [53]. At the field site in Reilingen, a signal of 6:2 fluorotelomer thio propyl amide dimethylethyl sulfonic acid (6:2 FTTh-Pr-Ad-(5′,5′)DiMeEtSA, structure in ESM 2), a widely used AFFF substance and primary precursor [17, 21, 22, 36, 53, 58], was detected but identified only at confidence level 4 due to low intensity and insufficient MS^2 spectra. 6:2 FTTh-Pr-Ad-(5′,5′)DiMeEtSA is known to be readily biodegraded under environmental conditions and yields two known intermediate thio oxidation products, 6:2 FTSO-Pr-Ad-(5′,5′)DiMeEtSA and 6:2 FTSy-Pr-Ad-(5′,5′) DiMeEtSA [27, 59]. The latter two compounds both were detected in soil at level 2. Additionally, for n:2 FTSy-Pr-Ad-(5′,5′)DiMeEtSA, three more homologues were present in the soil ($n = 8$, 10, 12) while for n:2 FTTh-Pr-Ad-(5′,5′) DiMeEtSA and n:2 FTSO-Pr-Ad-(5′,5′)DiMeEtSA, only the $n = 6$ homologue could be detected. Similarly, n:2 FTTh-(2′) OHPr-TriMeAms also contain an oxidizable thio moiety, and its oxidation products (n:2 FTSO-(2′)OHPr-TriMeAms, n:2 FTSy-(2′)OHPr-TriMeAms) both were also present in soil. Both oxidation products have been detected in AFFF formulations [17, 21, 36]. While 6:2 FTSO-(2′)OHPr-TriMeAm is one of the most abundant PFAS in contemporary AFFF formulations [58], 6:2 FTSy-(2′)OHPr-TriMeAm mostly was detected at low concentrations, likely as impurity [21, 36]. However, in soil, 6:2 FTSy-(2′)OHPr-TriMeAm is one of the most abundant peaks and shows a 24 times higher peak area compared to the precursor compound (6:2 FTTh-(2′)OHPr-TriMeAm). This indicates its potential origin from in situ transformation of the precursor (6:2 FTTh-(2′) OHPr-TriMeAm) rather than from impurities in the AFFF formulation.

Conclusions

The results of this study indicate that even after more than 15 years, sites contaminated with AFFF substances exhibit a wide variety of PFAS and their TPs and are therefore a long-term source for PFAAs due to biotransformation of precursors. To assess remediation measures and risk management, characterization of the PFAS pattern and its potential TPs has to be considered during planning, realization, and completion. A significant proportion of PFAS can easily be overlooked when applying targeted analytical methods, since analytical standards for AFFF PFAS, especially cationic ones, are lacking. NTS and suitable workflows for efficient data-prioritization are viable tools for the characterization of AFFF-contaminated sites. Data prioritization by the m/C dimension proofed to be rather efficient in this study. Nevertheless, still limited coverage of the chemical space has to be considered for NTS approaches due to a limited analytical window (choice of extraction method, ionization technique, chromatographic method, etc.). The lack of analytical standards also limits quantitative results. Therefore, robust semi-quantification approaches are needed to obtain quantitative information on the contaminant levels.

Supplementary Information The online version contains supplementary material available at https://doi.org/10.1007/s00216-024-05611-3.

Acknowledgements The authors acknowledge the Federal Ministry of Education and Research (BMBF) for funding the project PFClean (02WGW1665C) and the Deutsche Bundesstiftung Umwelt (DBU) for the scholarship of JZ.

Author contribution MS: conceptualization, writing of original draft (focus on soil sampling and processing, instrumental analysis, NTS workflow, data evaluation, PFAS identification, distributions, AFFF manufacturer). CC: conceptualization, writing of original draft (focus on extraction method, terminology, confidence level, PFAS identification). JZ and BB contributed to PFAS identification and reviewed the manuscript. CZ supervised the study, supported data interpretation, and reviewed and revised the manuscript.

Funding Open Access funding enabled and organized by Projekt DEAL.

Data availability Data will be made available on request.

Declarations

Competing interests The authors declare no competing interests.

References

1. Organisation for Economic Co-operation and Development (OECD). Reconciling terminology of the universe of per- and polyfluoroalkyl substances: recommendations and practical guidance. Paris: OECD Publishing. 2021. https://doi.org/10.1787/e458e796-en.
2. Wang Z, Buser AM, Cousins IT, Demattio S, Drost W, Johansson O, Ohno K, Patlewicz G, Richard AM, Walker GW, White GS, Leinala E. A new OECD definition for per- and polyfluoroalkyl substances. Environ Sci Technol. 2021;55(23):15575–8. https://doi.org/10.1021/acs.est.1c06896.
3. Schymanski EL, Zhang J, Thiessen PA, Chirsir P, Kondic T, Bolton EE. Per- and polyfluoroalkyl substances (PFAS) in PubChem:

7 million and growing. Environ Sci Technol. 2023;57(44):16918–28. https://doi.org/10.1021/acs.est.3c04855.
4. Buck RC, Franklin J, Berger U, Conder JM, Cousins IT, de Voogt P, Jensen AA, Kannan K, Mabury SA, van Leeuwen SP. Perfluoroalkyl and polyfluoroalkyl substances in the environment: terminology, classification, and origins. Integr Environ Assess Manag. 2011;7(4):513–41. https://doi.org/10.1002/ieam.258.
5. European Chemicals Agency (ECHA) (2023) Annex XV restriction report: proposal for a restriction. https://echa.europa.eu/documents/10162/f605d4b5-7c17-7414-8823-b49b9fd43aea. Accessed 2023–12–21
6. UN environment programm (UNEP) The 16 new POPS - an introduction to the chemicals added to the Stockholm Convention as persistant organic pollutants by the Conference of the Parties. https://www.pops.int/TheConvention/ThePOPs/TheNewPOPs/tabid/2511/Default.aspx. Accessed 2023–12–21.
7. Fenton SE, Ducatman A, Boobis A, DeWitt JC, Lau C, Ng C, Smith JS, Roberts SM. Per- and polyfluoroalkyl substance toxicity and human health review: current state of knowledge and strategies for informing future research. Environ Toxicol Chem. 2021;40(3):606–30. https://doi.org/10.1002/etc.4890.
8. Haukas M, Berger U, Hop H, Gulliksen B, Gabrielsen GW. Bioaccumulation of per- and polyfluorinated alkyl substances (PFAS) in selected species from the Barents Sea food web. Environ Pollut. 2007;148(1):360–71. https://doi.org/10.1016/j.envpol.2006.09.021.
9. Dai Z, Xia X, Guo J, Jiang X. Bioaccumulation and uptake routes of perfluoroalkyl acids in Daphnia magna. Chemosphere. 2013;90(5):1589–96. https://doi.org/10.1016/j.chemosphere.2012.08.026.
10. Sun JM, Kelly BC, Gobas F, Sunderland EM. A food web bioaccumulation model for the accumulation of per- and polyfluoroalkyl substances (PFAS) in fish: how important is renal elimination? Environ Sci Process Impacts. 2022;24(8):1152–64. https://doi.org/10.1039/d2em00047d.
11. Brunn H, Arnold G, Körner W, Rippen G, Steinhäuser KG, Valentin I. PFAS: forever chemicals—persistent, bioaccumulative and mobile. Reviewing the status and the need for their phase out and remediation of contaminated sites. Environ Sci Eur. 2023;35(1):20. https://doi.org/10.1186/s12302-023-00721-8.
12. Cousins IT, DeWitt JC, Gluge J, Goldenman G, Herzke D, Lohmann R, Ng CA, Scheringer M, Wang Z. The high persistence of PFAS is sufficient for their management as a chemical class. Environ Sci Process Impacts. 2020;22(12):2307–12. https://doi.org/10.1039/d0em00355g.
13. Kissa E. Fluorinated surfactants and repellents. New York: Marcel Dekker. 2001.
14. Glüge J, Scheringer M, Cousins IT, Dewitt JC, Goldenman G, Herzke D, Lohmann R, Ng CA, Trier X, Wang Z. An overview of the uses of per- and polyfluoroalkyl substances (PFAS). Environ Sci Process Impacts. 2020;22(12):2345–73. https://doi.org/10.1039/d0em00291g.
15. Dauchy X, Boiteux V, Bach C, Rosin C, Munoz JF. Per- and polyfluoroalkyl substances in firefighting foam concentrates and water samples collected near sites impacted by the use of these foams. Chemosphere. 2017;183:53–61. https://doi.org/10.1016/j.chemosphere.2017.05.056.
16. Houtz EF, Higgins CP, Field JA, Sedlak DL. Persistence of perfluoroalkyl acid precursors in AFFF-impacted groundwater and soil. Environ Sci Technol. 2013;47(15):8187–95. https://doi.org/10.1021/es4018877.
17. Liu M, Glover CM, Munoz G, Duy SV, Sauve S, Liu J. Hunting the missing fluorine in aqueous film-forming foams containing per- and polyfluoroalkyl substances. J Hazard Mater. 2024;464:133006. https://doi.org/10.1016/j.jhazmat.2023.133006.
18. Weiner B, Yeung LW, Marchington EB, D'Agostino LA, Mabury SA. Organic fluorine content in aqueous film forming foams (AFFFs) and biodegradation of the foam component 6: 2 fluorotelomermercaptoalkylamido sulfonate (6: 2 FTSAS). Environ Chem. 2013;10(6):486–93.
19. Prevedouros K, Cousins IT, Buck RC, Korzeniowski SH. Sources, fate and transport of perfluorocarboxylates. Environ Sci Technol. 2006;40(1):32–44. https://doi.org/10.1021/es0512475.
20. Choi YJ, Helbling DE, Liu J, Olivares CI, Higgins CP. Microbial biotransformation of aqueous film-forming foam derived polyfluoroalkyl substances. Sci Total Environ. 2022;824:153711. https://doi.org/10.1016/j.scitotenv.2022.153711.
21. Place BJ, Field JA. Identification of novel fluorochemicals in aqueous film-forming foams used by the US military. Environ Sci Technol. 2012;46(13):7120–7. https://doi.org/10.1021/es301465n.
22. Backe WJ, Day TC, Field JA. Zwitterionic, cationic, and anionic fluorinated chemicals in aqueous film forming foam formulations and groundwater from U.S. military bases by nonaqueous large-volume injection HPLC-MS/MS. Environ Sci Technol. 2013;47(10):5226–34. https://doi.org/10.1021/es3034999.
23. Barzen-Hanson KA, Roberts SC, Choyke S, Oetjen K, McAlees A, Riddell N, McCrindle R, Ferguson PL, Higgins CP, Field JA. Discovery of 40 classes of per- and polyfluoroalkyl substances in historical aqueous film-forming foams (AFFFs) and AFFF-impacted groundwater. Environ Sci Technol. 2017;51(4):2047–57. https://doi.org/10.1021/acs.est.6b05843.
24. Gonda N, Choyke S, Schaefer C, Higgins CP, Voelker B. Hydroxyl radical transformations of perfluoroalkyl acid (PFAA) precursors in aqueous film forming foams (AFFFs). Environ Sci Technol. 2023;57(21):8053–64. https://doi.org/10.1021/acs.est.2c08689.
25. Moe MK, Huber S, Svenson J, Hagenaars A, Pabon M, Trumper M, Berger U, Knapen D, Herzke D. The structure of the fire fighting foam surfactant Forafac(R)1157 and its biological and photolytic transformation products. Chemosphere. 2012;89(7):869–75. https://doi.org/10.1016/j.chemosphere.2012.05.012.
26. Cook EK, Olivares CI, Antell EH, Yi S, Nickerson A, Choi YJ, Higgins CP, Sedlak DL, Alvarez-Cohen L. Biological and chemical transformation of the six-carbon polyfluoroalkyl substance N-dimethyl ammonio propyl perfluorohexane sulfonamide (AmPr-FHxSA). Environ Sci Technol. 2022;56(22):15478–88. https://doi.org/10.1021/acs.est.2c00261.
27. Harding-Marjanovic KC, Houtz EF, Yi S, Field JA, Sedlak DL, Alvarez-Cohen L. Aerobic biotransformation of fluorotelomer thioether amido sulfonate (Lodyne) in AFFF-amended microcosms. Environ Sci Technol. 2015;49(13):7666–74. https://doi.org/10.1021/acs.est.5b01219.
28. Liu M, Munoz G, Vo Duy S, Sauve S, Liu J. Stability of nitrogen-containing polyfluoroalkyl substances in aerobic soils. Environ Sci Technol. 2021;55(8):4698–708. https://doi.org/10.1021/acs.est.0c05811.
29. Röhler K, Susset B, Grathwohl P. Production of perfluoroalkyl acids (PFAAs) from precursors in contaminated agricultural soils: batch and leaching experiments. Sci Total Environ. 2023;902:166555. https://doi.org/10.1016/j.scitotenv.2023.166555.
30. Higgins CP, Luthy RG. Sorption of perfluorinated surfactants on sediments. Environ Sci Technol. 2006;40(23):7521–7256. https://doi.org/10.1021/es061000n.
31. Xiao F, Jin B, Golovko SA, Golovko MY, Xing B. Sorption and desorption mechanisms of cationic and zwitterionic per- and polyfluoroalkyl substances in natural soils: thermodynamics and hysteresis. Environ Sci Technol. 2019;53(20):11818–27. https://doi.org/10.1021/acs.est.9b05379.
32. Maizel AC, Shea S, Nickerson A, Schaefer C, Higgins CP. Release of per- and polyfluoroalkyl substances from aqueous film-forming

foam impacted soils. Environ Sci Technol. 2021;55(21):14617–27. https://doi.org/10.1021/acs.est.1c02871.
33. Nickerson A, Maizel AC, Kulkarni PR, Adamson DT, Kornuc JJ, Higgins CP. Enhanced extraction of AFFF-associated PFASs from source zone soils. Environ Sci Technol. 2020;54(8):4952–62. https://doi.org/10.1021/acs.est.0c00792.
34. Munoz G, Ray P, Mejia-Avendano S, Vo Duy S, Tien Do D, Liu J, Sauve S. Optimization of extraction methods for comprehensive profiling of perfluoroalkyl and polyfluoroalkyl substances in fire-fighting foam impacted soils. Anal Chim Acta. 2018;1034:74–84. https://doi.org/10.1016/j.aca.2018.06.046.
35. Cao D, Schwichtenberg T, Duan C, Xue L, Muensterman D, Field J. Practical semiquantification strategy for estimating suspect per- and polyfluoroalkyl substance (PFAS) concentrations. J Am Soc Mass Spectrom. 2023. https://doi.org/10.1021/jasms.3c00019.
36. D'Agostino LA, Mabury SA. Identification of novel fluorinated surfactants in aqueous film forming foams and commercial surfactant concentrates. Environ Sci Technol. 2014;48(1):121–9. https://doi.org/10.1021/es403729e.
37. Luo Y-S, Aly NA, McCord J, Strynar MJ, Chiu WA, Dodds JN, Baker ES, Rusyn I. Rapid characterization of emerging per- and polyfluoroalkyl substances in aqueous film-forming foams using ion mobility spectrometry–mass spectrometry. Environ Sci Technol. 2020;54(23):15024–34. https://doi.org/10.1021/acs.est.0c04798.
38. Liu M, Munoz G, Vo Duy S, Sauve S, Liu J. Per- and polyfluoroalkyl substances in contaminated soil and groundwater at airports: a Canadian case study. Environ Sci Technol. 2022;56(2):885–95. https://doi.org/10.1021/acs.est.1c04798.
39. Mejia-Avendaño S, Munoz G, Vo Duy S, Desrosiers M, BenoıTSauvéLiu PSJ. Novel fluoroalkylated surfactants in soils following firefighting foam deployment during the Lac-Mégantic Railway Accident. Environ Sci Technol. 2017;51(15):8313–23. https://doi.org/10.1021/acs.est.7b02028.
40. Bugsel B, Zweigle J, Zwiener C. Nontarget screening strategies for PFAS prioritization and identification by high resolution mass spectrometry: A review. Trends Environ Anal Chem. 2023;40. https://doi.org/10.1016/j.teac.2023.e00216.
41. Bugsel B, Zwiener C. LC-MS screening of poly- and perfluoroalkyl substances in contaminated soil by Kendrick mass analysis. Anal Bioanal Chem. 2020;412(20):4797–805. https://doi.org/10.1007/s00216-019-02358-0.
42. Kaufmann A, Butcher P, Maden K, Walker S, Widmer M. Simplifying nontargeted analysis of PFAS in complex food matrixes. J AOAC Int. 2022;105(5):1280–7. https://doi.org/10.1093/jaoacint/qsac071.
43. Zweigle J, Bugsel B, Zwiener C. Efficient PFAS prioritization in non-target HRMS data: systematic evaluation of the novel MD/C-m/C approach. Anal Bioanal Chem. 2023;415:1791–801. https://doi.org/10.1007/s00216-023-04601-1.
44. Zweigle J, Bugsel B, Zwiener C. FindPFΔS: non-target screening for PFAS—comprehensive data mining for MS2 fragment mass differences. Anal Chem. 2022;94(30):10788–96. https://doi.org/10.1021/acs.analchem.2c01521.
45. Zweigle J, Bugsel B, Fabregat-Palau J, Zwiener C. PFΔScreen - an open-source tool for automated PFAS feature prioritization in non-target HRMS data. Anal Bioanal Chem. 2024;416(2):349–62. https://doi.org/10.1007/s00216-023-05070-2.
46. Place B. Suspect list of possible per- and polyfluoroalkyl substances (PFAS). National Inst Stand Technol. 2021. https://data.nist.gov/od/id/mds2-2387. Accessed 2023–12–15.
47. Menin L, Ortiz D, Gasilova N, Sepulved F, Patiny L MSTools. https://mstools.epfl.ch/monoisotopic/. Accessed 2024–03–11.
48. Patiny L, Borel A. ChemCalc: a building block for tomorrow's chemical infrastructure. J Chem Inf Model. 2013;53(5):1223–8. https://doi.org/10.1021/ci300563h.
49. Pluskal T, Uehara T, Yanagida M. Highly accurate chemical formula prediction tool utilizing high-resolution mass spectra, MS/MS fragmentation, heuristic rules, and isotope pattern matching. Anal Chem. 2012;84(10):4396–403. https://doi.org/10.1021/ac3000418.
50. Ruttkies C, Schymanski EL, Wolf S, Hollender J, Neumann S. MetFrag relaunched: incorporating strategies beyond in silico fragmentation. J Cheminform. 2016;8(1):3. https://doi.org/10.1186/s13321-016-0115-9.
51. Charbonnet JA, McDonough CA, Xiao F, Schwichtenberg T, Cao D, Kaserzon S, Thomas KV, Dewapriya P, Place BJ, Schymanski EL, Field JA, Helbling DE, Higgins CP. Communicating confidence of per- and polyfluoroalkyl substance identification via high-resolution mass spectrometry. Environ Sci Technol Lett. 2022;9(6):473–81. https://doi.org/10.1021/acs.estlett.2c00206.
52. Schymanski EL, Jeon J, Gulde R, Fenner K, Ruff M, Singer HP, Hollender J. Identifying small molecules via high resolution mass spectrometry: communicating confidence. Environ Sci Technol. 2014;48(4):2097–8. https://doi.org/10.1021/es5002105.
53. Yan PF, Dong S, Pennell KD, Capiro NL. A review of the occurrence and microbial transformation of per- and polyfluoroalkyl substances (PFAS) in aqueous film-forming foam (AFFF)-impacted environments. Sci Total Environ. 2024;927:171883. https://doi.org/10.1016/j.scitotenv.2024.171883.
54. Li Z, Lu Y, Chen T, He A, Huang Y, Li L, Pan W, Li J, Zhu N, Wang Y, Jiang G. Generation mechanism of perfluorohexanesulfonic acid from polyfluoroalkyl sulfonamide derivatives during chloramination in drinking water. Environ Sci Technol. 2023;57(47):18462–72. https://doi.org/10.1021/acs.est.2c07881.
55. D'Agostino LA, Mabury SA. Aerobic biodegradation of 2 fluorotelomer sulfonamide-based aqueous film-forming foam components produces perfluoroalkyl carboxylates. Environ Toxicol Chem. 2017;36(8):2012–21. https://doi.org/10.1002/etc.3750.
56. Yukioka S, Tanaka S, Suzuki Y, Fujii S, Echigo S. A new method to search for per- and polyfluoroalkyl substances (PFASs) by linking fragmentation flags with their molecular ions by drift time using ion mobility spectrometry. Chemosphere. 2020;239:124644. https://doi.org/10.1016/j.chemosphere.2019.124644.
57. Fang B, Zhang Y, Chen H, Qiao B, Yu H, Zhao M, Gao M, Li X, Yao Y, Zhu L, Sun H. Stability and biotransformation of 6:2 fluorotelomer sulfonic acid, sulfonamide amine oxide, and sulfonamide alkylbetaine in aerobic sludge. Environ Sci Technol. 2024;58(5):2446–57. https://doi.org/10.1021/acs.est.3c05506.
58. Ruyle BJ, Thackray CP, McCord JP, Strynar MJ, Mauge-Lewis KA, Fenton SE, Sunderland EM. Reconstructing the composition of per- and polyfluoroalkyl substances in contemporary aqueous film-forming foams. Environ Sci Technol Lett. 2021;8(1):59–65. https://doi.org/10.1021/acs.estlett.0c00798.
59. Olivares CI, Yi S, Cook EK, Choi YJ, Montagnolli R, Byrne A, Higgins CP, Sedlak DL, Alvarez-Cohen L. Aerobic BTEX biodegradation increases yield of perfluoroalkyl carboxylic acids from biotransformation of a polyfluoroalkyl surfactant, 6:2 FtTAoS. Environ Sci Process Impacts. 2022;24(3):439–46. https://doi.org/10.1039/d1em00494h.

Analytical and Bioanalytical Chemistry

Electronic Supplementary Material 1

Non-target Screening reveals 124 PFAS at an AFFF impacted field site in Germany specified by a novel systematic terminology

Melanie Schüßler[1], Catharina Capitain[1], Boris Bugsel[1], Jonathan Zweigle[1], Christian Zwiener[1]

1 Environmental Analytical Chemistry, Department of Geosciences, University of Tübingen, Schnarrenbergstraße 94-96, 72076 Tübingen, Germany

Table of content

ESM 1.A Chemicals

Table S1: Overview about all PFAS reference standards that were included in the PFAS standard mixture and where they were purchased. PFAS originated either from Wellington Laboratories, Guelph, Ontario, Canada (1), Toronto Research Chemicals, North York, Ontario, Canada (2), Dr. Ehrenstorfer, Augsburg, Bavaria, Germany (3) or were custom-synthesized in-house (4).

Acronym	Used standard / purchased chemical	Origin
PFCAs		
PFBA	Perfluorobutanoic acid / perfluoro-n-butanoic acid	(1)
PFPeA	Perfluoropentanoic acid / perfluoro-n-pentanoic acid	(1)
PFHxA	Perfluorohexanoic acid / perfluoro-n-hexanoic acid	(1)
PFHpA	Perfluoroheptanoic acid / perfluoro-n-heptanoic acid	(1)
PFOA	Perfluorooctanoic acid / perfluoro-n-octanoic acid	(1)
PFNA	Perfluorononanic acid / perfluoro-n-nonanic acid	(1)
PFDA	Perfluorodecanoic acid / perfluoro-n-decanoic acid	(1)
PFUnDA	Perfluoroundecanoic acid / perfluoro-n-undecanoic acid	(1)
PFDoDA	Perfluorododecanoic acid / perfluoro-n-dodecanoic acid	(1)
PFTriDA	Perfluorotridecanoic acid / perfluoro-n-tridecanoic acid	(1)
PFTeDA	Perfluorotetradecanoic acid / perfluoro-n-tetradecanoic acid	(1)
PFHxDA	Perfluorohexadecanoic acid / perfluoro-n-hexadecanoic acid	(1)
PFODA	Perfluorooctadecanoic acid / perfluoro-n-octadecanoic acid	(1)
PFSAs		
PFBS	Perfluorobutanesulfonic acid / potassium perfluoro-1-butanesulfonate	(1)
PFPeS	Perfluoropentanesulfonic acid / sodium perfluoro-1-pentanesulfonate	(1)
PFHxS	Perfluorohexanesulfonic acid / sodium perfluoro-1-hexanesulfonate	(1)
PFHpS	Perfluoroheptanesulfonic acid / sodium perfluoro-1-heptanesulfonate	(1)
PFOS	Perfluorooctanesulfonic acid / sodium perfluoro-1-octanesulfonate	(1)
PFNS	Perfluorononanesulfonic acid / sodium perfluoro-1-nonanesulfonate	(1)
PFDS	Perfluorodecanesulfonic acid / sodium perfluoro-1-decanesulfonate	(1)
PFDoDS	Perfluorododecanesulfonic acid / sodium perfluoro-1-dodecanesulfonate	(1)
PFPAs		
PFOPA	Perfluorooctylphosphonic acid	(1)
PFDPA	Perfluorodecylphosphonic acid	(1)
PAPs		
6:2/6:2 diPAP	6:2/6:2 phosphoric acid diester / Bis[2-(perfluorohexyl)ethyl] phosphate	(2)
8:2/8:2 diPAP	6:2/6:2 polyfluoroalkyl phosphoric acid diester / Sodium bis (1H, 1H, 2H, 2H-perfluorodecyl) phosphate	(1)
6:2 PAP	6:2 polyfluoroalkyl phosphoric ester / Mono[2-(perfluorohexyl)ethyl] phosphate	(2)

8:2 PAP	6:2 polyfluoroalkyl phosphoric ester / Sodium 1H, 1H, 2H, 2H-perfluorodecyl phosphate	(1)
PFPiAs		
C6/C6 PFPiA	C6/C6 Perfluoroalkyl phosphinic acid	(2)
PASF-based PFAS		
PFHxSAm	Perfluorohexane sulfonamide	(3)
PFOSAm	Perfluorooctane sulfonamide	(1)
PFOSAm-*N*-Et-*N*-EtA	Perfluorooctane sulfonamide *N*-ethyl *N*-ethanoic acid	(1)
SamPAP	Perfluorooctane sulfonamide ethanol-based phosphate diester /Sodium-2-(N-ethylperfluorooctane-1-sulfonamido) ethyl phosphate	(1)
diSAmPAP	Perfluorooctane sulfonamide ethanol-based phosphate diester/ Sodium bis[2-(N-ethylperfluorooctane-1-sulfonamido) ethyl] phosphate	(1)
FTCAs		
6:2 FTCA	6:2 fluorotelomer carboxylic acid / 2-Perfluorohexyl ethanoic acid (6:2)	(1)
8:2 FTCA	8:2 fluorotelomer carboxylic acid / 2-Perfluorooctyl ethanoic acid (6:2)	(1)
5:3 FTCA	5:3 fluorotelomer carboxylic acid/ 3-Perfluoropentyl propanoic acid	(1)
7:3 FTCA	7:3 fluorotelomer carboxylic acid/ 3-Perfluoroheptyl propanoic acid	(1)
FTUCAs		
6:2 FTUCA	6:2 fluorotelomer unsaturated carboxylic acid/ 2H-Perfluoro-2-octenoic acid (6:2)	(1)
8:2 FTUCA	8:2 fluorotelomer unsaturated carboxylic acid/ 2H-Perfluoro-2-decenoic acid (8:2)	(1)
FTSAs		
6:2 FTSA	6:2 fluorotelomer sulfonic acid / Sodium 1H, 1H,2H,2H-perfluorooctanesulfonate	(1)
8:2 FTSA	8:2 fluorotelomer sulfonic acid / Sodium 1H, 1H,2H,2H-perfluorodecanesulfonate	(1)
FTMAPs		
6:2 FTMAP	6:2 Fluorotelomer mercapto alkyl phosphate	(4)
PFECAs		
HFPO-Da	2,3,3,3-Tetrafluoro-2-(1,1,2,2,3,3,3-heptafluoropropoxy) propanoic acid	(1)
ADONA	Sodium dodecafluoro-3H-4,8-dioxanonanoate	(1)
PFESAs		
9Cl-PF3ONS	Potassium 9-chlorhexadecafluoro-3-oxanonane-1-sulfonate	(1)
11Cl-PF3OUdS	Potassium 11-chloroeicosafluoro-3-oxaundecane-1-sulfonate	(1)
AFFF-substances		
6:2 FTSAm-Pr-DiMeNO	6:2 fluorotelomer sulfonamide propyl methylamineoxide / Capstone product A	(3)
6:2 FTSAm-Pr-B	6:2 fluorotelomer sulfonamide propyl betaine / Capstone product B	(3)
PFHxSAm-Pr-DiMeAm	N-[3(dimethylamino)propyl] perfluoro-1-hexanesulfonamide	(3)

5:3 FTB	5:3 Fluorotelomer betaine / 2-[4,4,5,5,6,6,7,7,8,8,8-Undecafluorooctyl) dimethylammonio] acetate	(1)
5:1:2 FTB	5:1:2 Fluorotelomer etaine / 2-[(3,4,4,5,5,6,6,7,7,8,8,8-Dodecafluorooctyl) dimethylammonio] acetate	(1)

ESM 1.B Sampling site

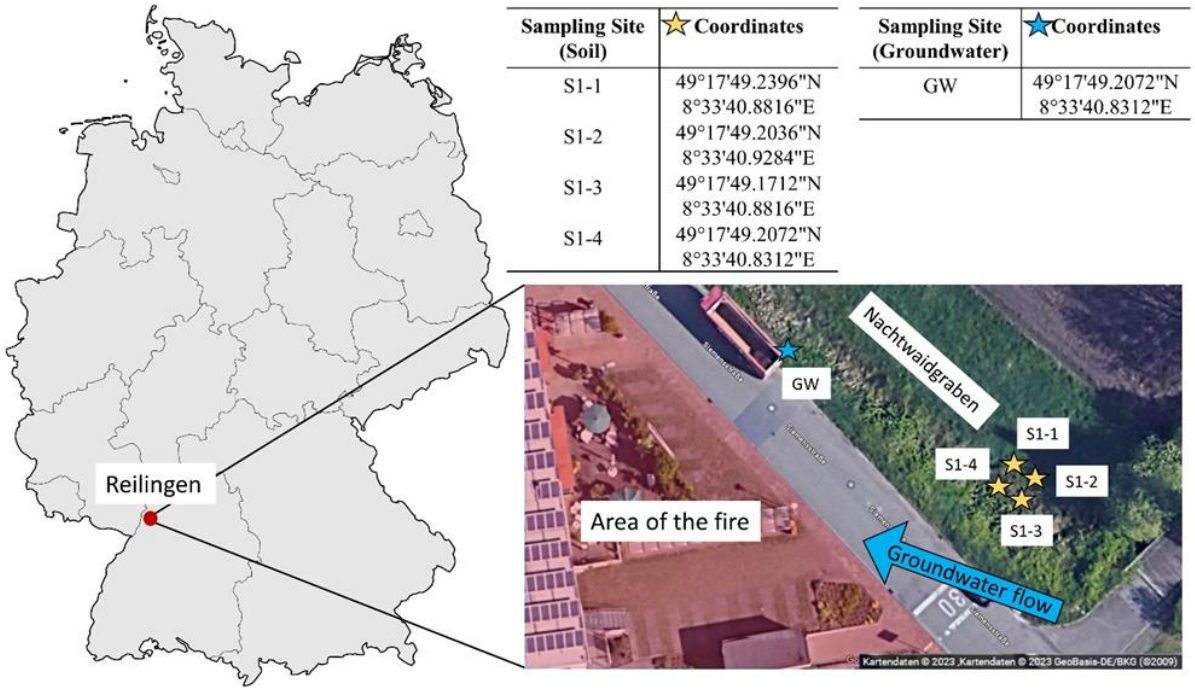

Sampling Site (Soil)	Coordinates
S1-1	49°17'49.2396"N 8°33'40.8816"E
S1-2	49°17'49.2036"N 8°33'40.9284"E
S1-3	49°17'49.1712"N 8°33'40.8816"E
S1-4	49°17'49.2072"N 8°33'40.8312"E

Sampling Site (Groundwater)	Coordinates
GW	49°17'49.2072"N 8°33'40.8312"E

Fig. S1: Overview of the sampling site *Nachtwaidgraben* in Reilingen, Baden Württemberg and coordinates of the respective sampling points. Yellow stars represent soil sampling and blue stars represent groundwater sampling. The screenshot of the field site was taken from Google Maps (15.12.2023). Groundwater flow was determined by Arcadis.

ESM 1.C Feature prioritization

The prioritization workflow (RT > 4 min, m/C > 23) was validated by application to a standard mix sample consisting of 49 negative and 5 positive ionizable PFAS. For negative ionizable PFAS the false positive rate was 8.3% and the false negative rate 0.034% (related to peak areas). For positive ionizable PFAS the false positive rate was 31.8% and the false negative rate 2.4%. The high false positive rate likely results from the low number of available positively ionizing PFAS standards. Manual inspection of the false positively prioritized features revealed that most of them did not show a gaussian peak shape and thus would not have been further considered for identification.

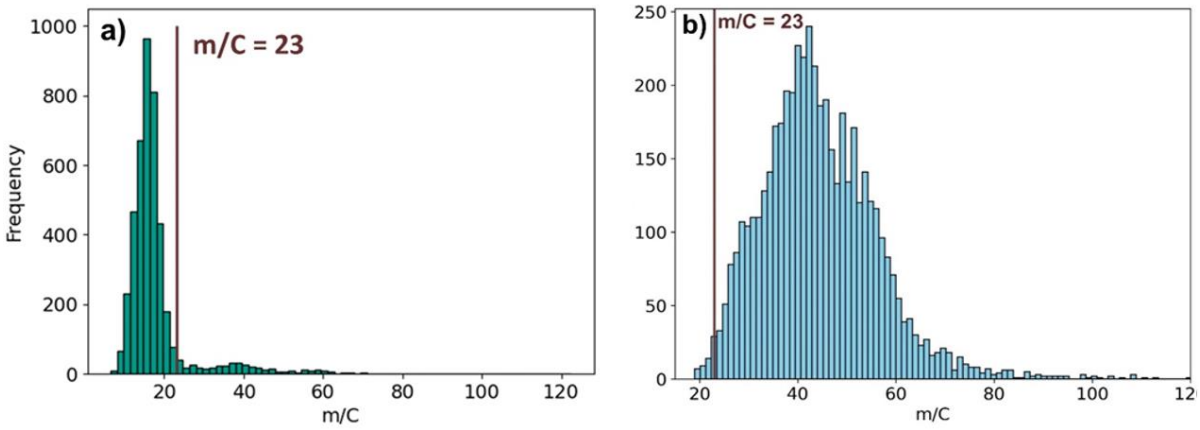

Fig. S2: a) Histogram of m/C values of all features of soil *S1* in the output table of PFΔ*Screen* before prioritization. The red line at m/C = 23 represents the cutoff for the prioritization. b) Histogram of m/C values of all PFAS included in the NIST suspect list [1]. The red line indicates an m/C value of 23, revealing that only a small fraction of PFAS from the list would be missed with a cutoff at m/C = 23.

ESM 1.D Confidence level

The classification into confidence levels considered matching reference standards, accurate mass (< 10 ppm) and isotopic pattern match (Eq. 1, > 95%) for proposed formulas, m/C (> 25), diagnostic fragments, homologous series, and experimental data (see Table S2). The type of MS^2 fragment is not specifically named, but diagnostic fragments are expected to provide evidence for the proposed structure. PFAS that are ionizable in both ESI- and ESI+ mode give extra evidence for the proposed structure. Therefore, matching MS^2 fragments from positive and negative measurements are summed for the determination of the confidence level. Experimental data from the literature or from own experiments (e.g. the presence of similar structures) may be additionally available to support the proposed structure.

Level 1 compounds are confirmed by analytical reference standards. For all substances classified at level 2, a molecular formula and a specific structure are assigned, supported by accurate mass, isotopic pattern matching, diagnostic fragments (minimum of 3 fragments), and/or homologues (minimum of 3 homologues, with at least one at level 2 or higher). For all substances classified at level 3, a molecular formula and one or more structures are suggested, evidenced by accurate mass, isotopic pattern matching, diagnostic fragments (minimum of 2 fragments), and/or homologues (minimum of 2 homologues, with at least one at level 3 or higher). Level 2 PFAS are more reliable than level 3 PFAS, as more evidence is available. In addition, only one structure is suggested for level 2 PFAS, whereas several structures are possible for level 3. Unlike constitutional isomers, positional isomers only differ by the position of the same moiety or substituent (unsaturated bond, keto-/methyl-/hydroxy-group, SF_5-/Cl-/H-substitution). Positional isomers with varying possible structures are therefore grouped together and one exemplary structure is shown (ESM 2). The only uncertainty in the structure is the exact position of the moiety or substituent and can therefore still be assigned a confidence level of 2. The same approach was applied to ECF-based substances where

different variations of a structure are possible due to branching in the perfluoroalkyl chain. Level 4 compounds are assigned a matching molecular formula with accurate mass and isotopic pattern match. Although no structures can be directly inferred from MS^2 spectra, structures can still be proposed for some compounds that have already been found in the literature and thus are evidently TPs or precursors of other identified (level 1 – 3) compounds that were identified in the samples. Features are selected as level 5 PFAS due to matching mass defects (-0.15 – 0.15 Da), PFAS typical m/C ratios (m/C > 30), homologous series, and/or typical MS^2 fragments.

Table S2: Applied confidence level modified according to Charbonnet et al. [2]. Only one structure is suggested for level 2 PFAS, whereas several structures are possible for level 3. Positional isomers or branched perfluoroalkyl chains are grouped together.

Level	Definition	Reference Standard	Accurate Mass (< 10 ppm)	Isotopic Pattern Match (> 95%)	m/C (> 25)	Homologues (number) with consistent RT	MS^2 Fragments (number)	Experimental Data
1	Confirmed by reference standard	✓	✓	✓	✓	(✓)	(✓)	(✓)
2	Probable structure by diagnostic fragmentation evidence	**x**	✓	✓	✓	**x**	**≥ 3**	(✓)
	Probable structure by diagnostic homologue evidence	**x**	✓	✓	✓	**≥ 3** (at least one homologue at level ≥ 2)	**x**	(✓)
3	Circumstantial candidates with fragmentation evidence	**x**	✓	✓	✓	**x**	**≥ 2**	(✓)
	Circumstantial candidates with homologue evidence	**x**	✓	✓	✓	**≥ 2** (at least one homologue at level ≥ 3)	**x**	(✓)
4	Matching molecular formula	**x**	✓	✓	✓	**x**	**x**	(✓)
5	Nontarget PFAS exact mass of interest	At least one of condition must apply: PFAS typical mass defect, PFAS typical m/C ratio, homologous series, typical MS^2 fragments						

ESM 1.E Extraction method

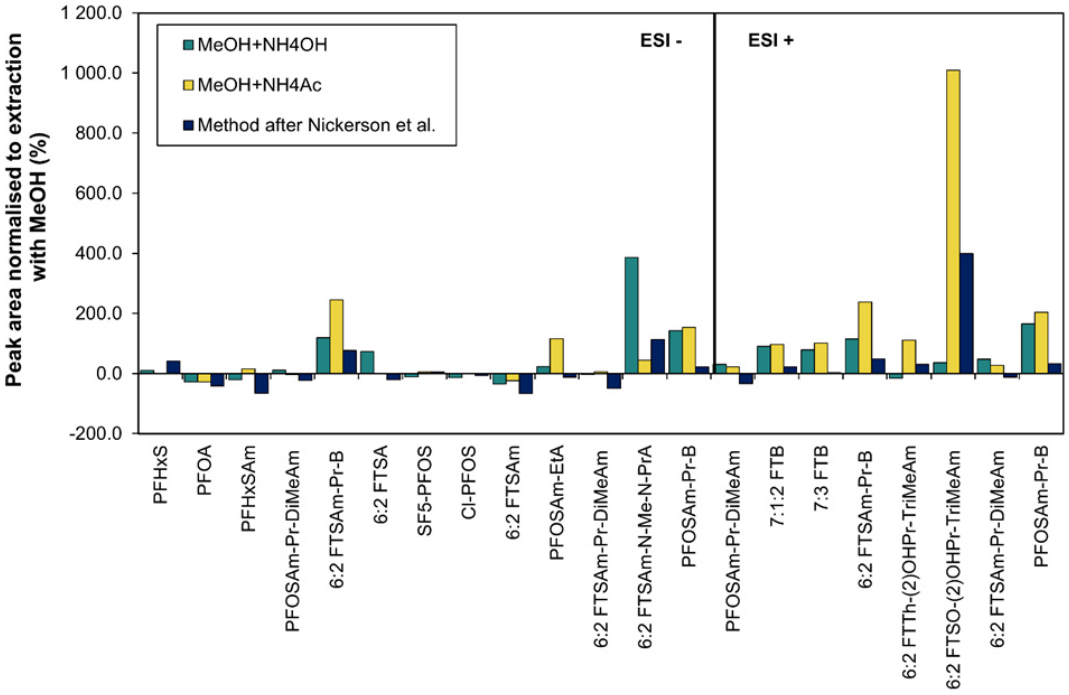

Fig. S3: Comparison of extraction efficiencies for 19 different PFAS with MeOH+NH_4OH or MeOH+NH_4Ac as extraction solvent and the extraction method after Nickerson et al. [3] relative to the extraction with pure MeOH in negative ionization mode (ESI-, left side) and positive ionization mode (ESI+, right side). Note: substances that appear in both ionization modes are zwitterionic substances.

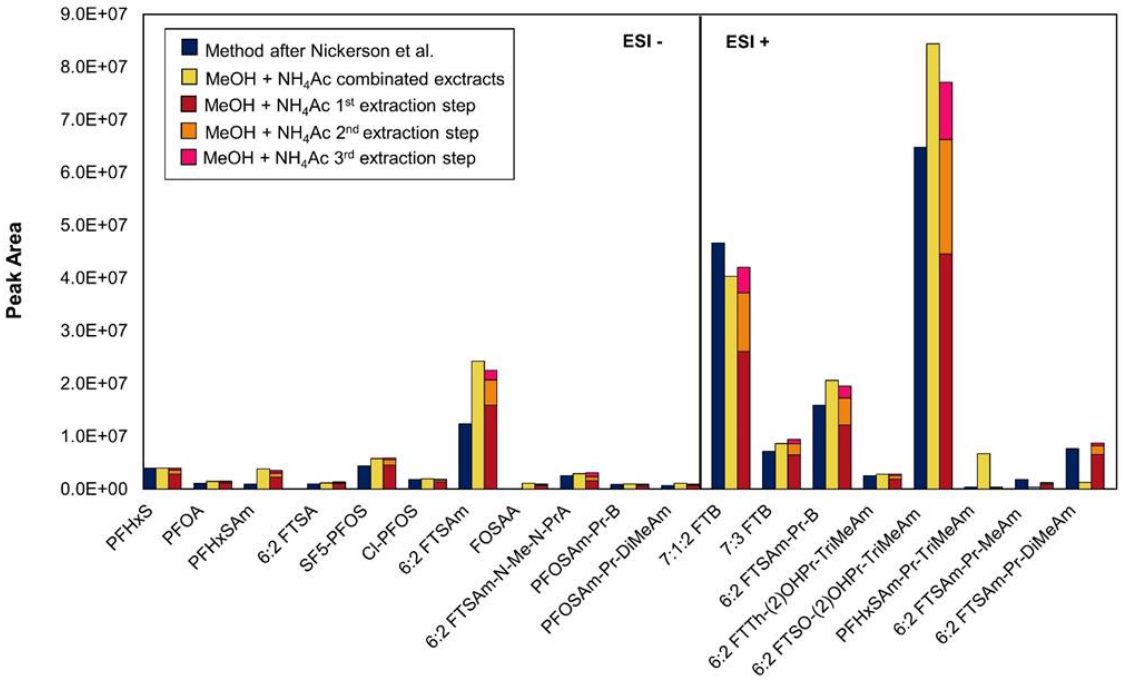

Fig. S4: Comparison of extraction efficiencies for 19 different PFAS with MeOH+NH_4Ac as extraction solvent and a three-step extraction and the extraction method after Nickerson et al. [3] in negative ionization mode (ESI-, left side) and positive ionization mode (ESI+, right side).

ESM 1.G Fragmentation evidence, chromatograms, and MS^2 spectra

PFSA and U-PFSA derivatives (Table 3, row 2, 3, and 11): Cl-PFSAs, SF_5-PFSAs, H-PFSAs, U-PFSAs, and SF_5-U-PFSAs, PFASyAs (all ESI-)

The diagnostic fragment $[SO_3]^-$ indicates a sulfonic acid in a molecule and the fragments $[SO_3F]^-$ or $[SO_2F]^-$ indicate a SO_3 or SO_2 group being located in direct vicinity to the fluorinated part of the molecule. All PFSA derivatives but PFASyA show the diagnostic fragment $[SO_3]^-$. The $[SO_2F]^-$ fragment was observed for PFOSyA (Fig. S23b) and the $[SO_3F]^-$ fragment was observed for all other PFSA subclasses but SF_5-U-PFSAs. Fragments of the fluorinated chain with mass fragment differences of $\Delta = 49.9968$ (CF_2) are also indicative for PFSA fragmentation. This was observed for SF_5-PFSAs (Fig. S20b, c), U-PFSAs (Fig. S24b, c), SF_5-U-PFSAs (Fig. S25b, c), Cl-PFSAs (Fig. S19c) and PFOSyA (Fig. S23b). In addition, attached moieties to the fluorinated chain such as $[SO_3Cl]^-$ (Cl-PFOS, Fig. S19c), $[SF_5]^-$/$[M\text{-}SF_5]^-$ (SF_5-PFSAs and SF_5-U-PFSAs, Fig. S20b, c and S24b, c) or $[SO_3H]^-$ (H-PFOS, Fig. S21b) can reveal valuable structural information and be matched to the proposed structure.

For Cl-PFOS, which shows a split peak two possible positional isomers could be identified due of differing MS^2 spectra (Fig. S19a-c). The spectrum obtained from the second peak indicates that the Cl-substitution is located directly next to the sulfonic acid group (fragment $[SO_3Cl]^-$ Fig. S19c, [4]), while the spectrum obtained from the first peak does not show this fragment (Fig. S19b), indicating the position of the Cl-substitution being at the end of the perfluoroalkyl chain. However, since it is unlikely that an RT shift of this magnitude results from the occurrence of only two positional isomers, it is possible that a mixture of linear and branched Cl-PFOS isomers is present, which is responsible for the split peak.

PFASAm and PFASAm-Pr-based AFFF PFAS (Table 3, row 4 and 5): PFASAm-EtA (ESI-), PFASAm-PrSA (ESI-), PFASAm-Pr-B (ESI-/ESI+), PFASAm-Pr-TriMeAm (ESI+)

PFASAm-EtA and PFASAm-PrSA both show the diagnostic fragment $[SO_2N]^-$ indicating the presence of the sulfonamide group (Fig. S28b, c and S29b) and fragments of the fluorinated chain with characteristic mass differences of ΔCF_2. Also, both subclasses show fragments of PFASAm itself (e.g. $[C_6HF_{13}NO_2S]^-$ for n = 6, Fig. S26b and S29b), corresponding to $[M\text{-}CH_2COO]^-$ for PFASAm-EtA and $[M\text{-}C_3H_6SO_3]^-$ for PFASAm-PrSA. As both subclasses do not coelute with PFASAm itself, interference of PFASAm with the MS^2 spectra of the 2 subclasses can be excluded.

PFASAm-Pr-B is zwitterionic but ionizes better in positive mode (Fig. S30a, b). Thus, fragmentation spectra are only available in ESI+ for PFASAm-Pr-B. Fragments distinctive for the betaine moiety ($[C_4H_8NO_2]^+$, $[C_4H_{10}NO_2]^+$, $[C_5H_{12}NO_2]^+$) were observed (Fig. S30c, d) and three further insightful fragments such as $[M\text{-}CO_2]^-$ (599.0656 Da) could be assigned to the structure (Fig. S30d). For PFASAm-Pr-TriMeAm three diagnostic fragments confirming the presence of the sulphonamide and propyl trimethylamine moieties could be observed for the n = 8 homologue (Fig. S31b).

FTBs (Table 2, row 2 and Table 3, row 6): n:2 FTBs, n:1:3 FTBs, n:4 FTBs, n:3 FTBs, n:1:2 FTBs (all ESI+)

Fragmentation evidence for FTBs is discussed in the main document.

FTSA derivatives (Table 2, row 3 and Table 3, row 10): K-n:2 FTSAs, U-n:2 FTSAs, OH-n:2 FTSAs (all ESI-)

Fragmentation evidence for K-n:2 and U-n:2 FTSAs is discussed in the main document. OH-n:2 FTSA shows diagnostic fragments of the sulfonic acid group ($[SO_3]^-$ and $[CH_3SO_3]^-$) as

well as the sulfonic acid group plus the OH-substitution ($[C_2H_3O_4S]^-$, Fig. S46b, c). Fragments of the fluorinated chain were also observed. Further, a neutral loss of water ($[M\text{-}H_2O]^-$) could be identified in the MS^2 spectra of both homologues, matching the proposed structure (e.g. $[C_8H_2F_{13}O_3S]^-$ for OH-6:2 FTSA, Fig. S46b).

FTSAm derivatives (Table 2, row 1 and Table 3, row 7): n:2/m:2 FTSAm dimer, n:2 FTSAm-PrA, n:2 FTSAm-U-Pr-DiMeAm, n:2 FTSAm-*N*-Me-*N*-PrA, n:2 FTSAm-PrA (ESI-), n:2 FTSAm-Pr-MeAm (ESI+), n:2 FTSAm-Pr-DiMeAm (ESI-/ESI+), and n:2 FTSAm-U-Pr-DiMeAm (ESI-)

Fragmentation evidence for n:2/m:2 FTSAm dimer, n:2 FTSAm-PrA, n:2 FTSAm-U-Pr-DiMeAm, and n:2 FTSAm-*N*-Me-*N*-PrA is discussed in the main document.

Three diagnostic fragments reveal the presence of a sulfonamide propyl trimethylamine moiety ($[C_4H_{11}N^{\cdot}]^+$, $[C_5H12N]^+$ and $[C_6H_{16}N_2]^+$) for the n = 8 homologue of n:2 FTSAm-Pr-MeAm (Fig. S39b).

n:2 FTSAm-Pr-DiMeAm is a zwitterionic substance but ionizes much better in ESI+ (Fig. S40a). Fragmentation evidence could be retrieved from both ionization modes for the n = 6 homologue (Fig. S40b, c). In ESI-, the fragmentation spectra is characterized by a series of 4 HF losses starting from the molecular precursor ion ($[M\text{-}2H]^-$, Fig. S40b) as well as the diagnostic fragment $[C_5H_{13}N_2O_2S]^-$ which is indicative for the sulfonamide propyl dimethyl amine moiety. In ESI+ n:2 FTSAm-Pr-DiMeAm shows various diagnostic fragments indicative for the propyl dimethylamine moiety (Fig. S35c, d) as well as two further fragments supporting the structure for the n = 6 homologue (Fig. S40c).

FTSy derivatives (Table 2, row 4 and Table 3, row 8): n:2 FTSy-PrA, n:2 FTSy-(2')OHPr-TriMeAm, n:2 FTSy-Pr-Ad-(5',5')DiMeEtSA

Fragmentation evidence of n:2 FTSy-(2')OHPr-TriMeAm is discussed in the main document. For the n = 8 homologue of n:2 FTSy-PrA a series of 4 HF losses could be observed, matching the proposed structure. In addition, the diagnostic fragment $[C_3H_5O_2]^-$ could be identified confirming the presence of the propanoic acid group (Fig. S41c).

For n:2 FTSy-Pr-Ad-(5',5')DiMeEtSA a total of four diagnostic fragments matching the proposed structure was identified for the n = 6 and n = 8 homologues, respectively ($[SO_3]^-$, $[C_4H_7O_3S]^-$, $[C_4H_{10}NO_3S]^{-\cdot}$, $[C_7H_{12}NO_4S]^-$, Fig. S42b, c).

FTSO derivatives (Table 3, row 9): n:2 FTSO-(2')OHPr-TriMeAm (ESI+) and n:2 FTSO-Pr-Ad-(5',5')DiMeEtSA (ESI-)

For the n = 6 and n = 8 homologues of n:2 FTSO-(2')OHPr-TriMeAm, a total of 10 MS^2 fragments could be matched to the proposed structure, respectively (Fig. S43b, c). The most prominent two diagnostic fragments being $[C_6H_{16}NO_2S]^+$ (166.0896 Da) and $[C_6H_{14}NO]^+$ (116.1070).

For n:2 FTSO-Pr-Ad-(5',5')DiMeEtSA a total of 5 fragments could be matched the proposed structure for the n = 6 homologue (Fig. S44b). The fragment with the highest intensity nearly reveals the complete non-fluorinated part of the molecule ($[C_7H_{14}NO_5S_2]^-$, 256.0319 Da).

FTTh derivatives (Table 2, row 11): n:2 FTTh-(2')OHPr-TriMeAm (ESI+)

The n = 6 and n = 8 homologues of n:2 FTTh-(2')OHPr-TriMeAm do not show any diagnostic fragments but 3 expressive fragments with higher molecular weights, respectively (Fig. S45b, c).

Chromatograms and MS² spectra

Chromatograms of all confirmed and potential PFAS with proposed names are displayed below (chromatograms of "unknown" potential PFAS not shown) as well as MS² spectra of all level 2 and 3 PFAS subclasses, if available with two homologues and in positive and negative ionization mode. The precursor ions are indicated by blue diamonds. The best chromatograms/MS² spectra from site *S1*, depths, and extracts (first extract/combined extract) were displayed.

Newly identified Substances

n:2/m:2 FTSAm dimers (n = 6, 8 / m = 6)

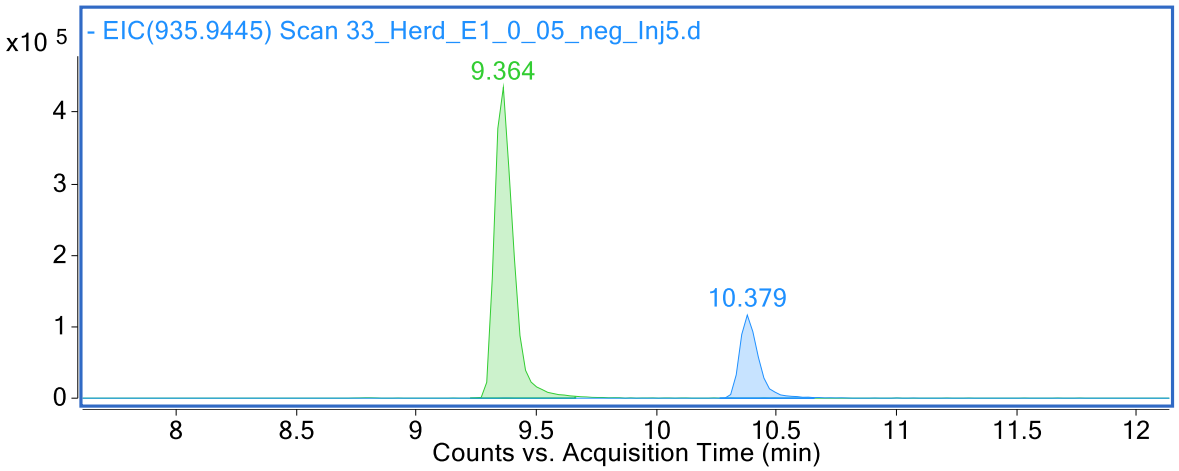

Fig. S5a: Chromatogram (ESI⁻, soil *S1*, 0 – 0.5 m, first extract) of n:2/6:2 FTSAm dimers (n = 6 (green, m/z 835.9485, 9.364 min) and 8 (blue, m/z 935.9421, 10.379 min)).

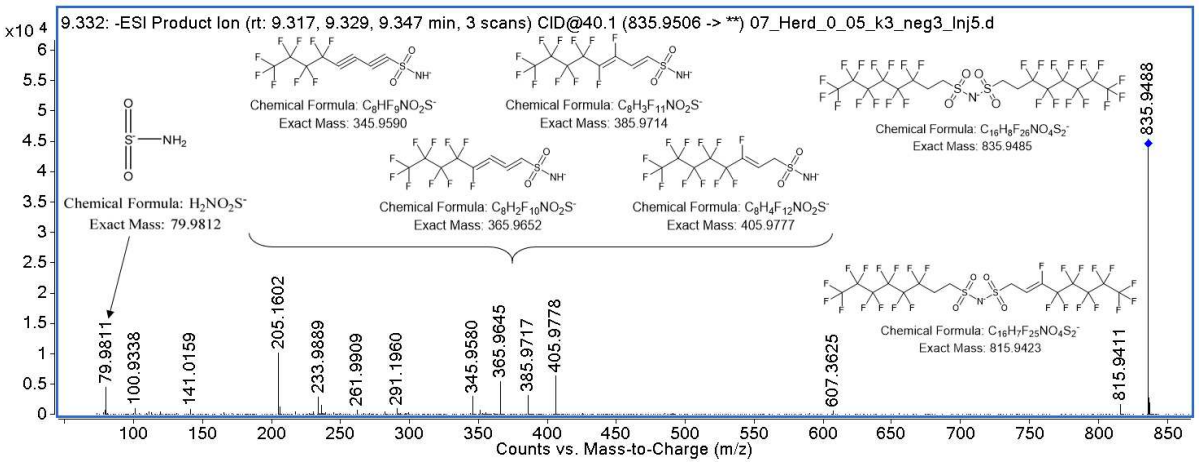

Fig. S5b: MS² spectrum (ESI⁻, 40.1 eV, soil *S1*, 0 – 0.5 m, combined extract, iterative MS²) of 6:2/6:2 FTSAm dimer (m/z 835.9485, 9.317, 9.329, and 9.347 min).

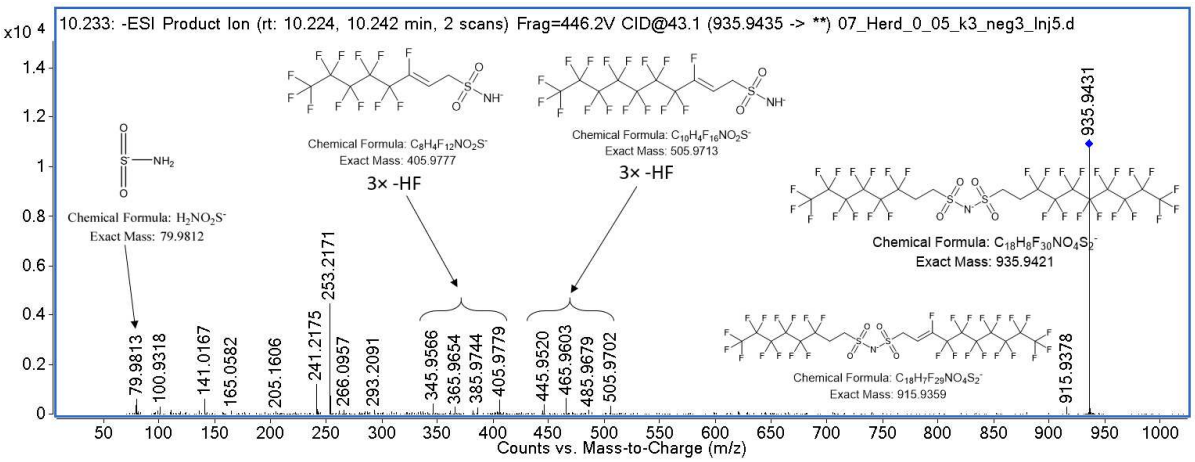

Fig. S5c: MS^2 spectrum (ESI^-, 43.1 eV, soil *S1*, 0 – 0.5 m, combined extract, iterative MS^2) of 6:2/8:2 FTSAm dimer (m/z 935.9421, 10.224 and 10.242 min).

Substances detected for the first time in soil

n:2 FTSAm-*N*-Me-*N*-PrAs (n = 6)

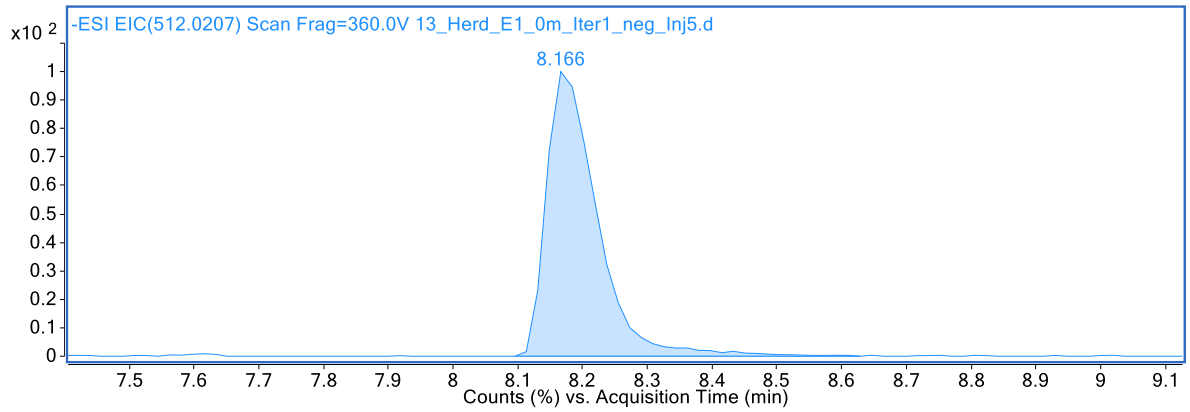

Fig. S6a: Chromatogram (ESI$^-$, soil *S1*, 0 – 0.5 m, first extract, iterative MS^2) of 6:2 FTSAm-*N*-Me-*N*-PrA (m/z 512.0207, 8.166 min).

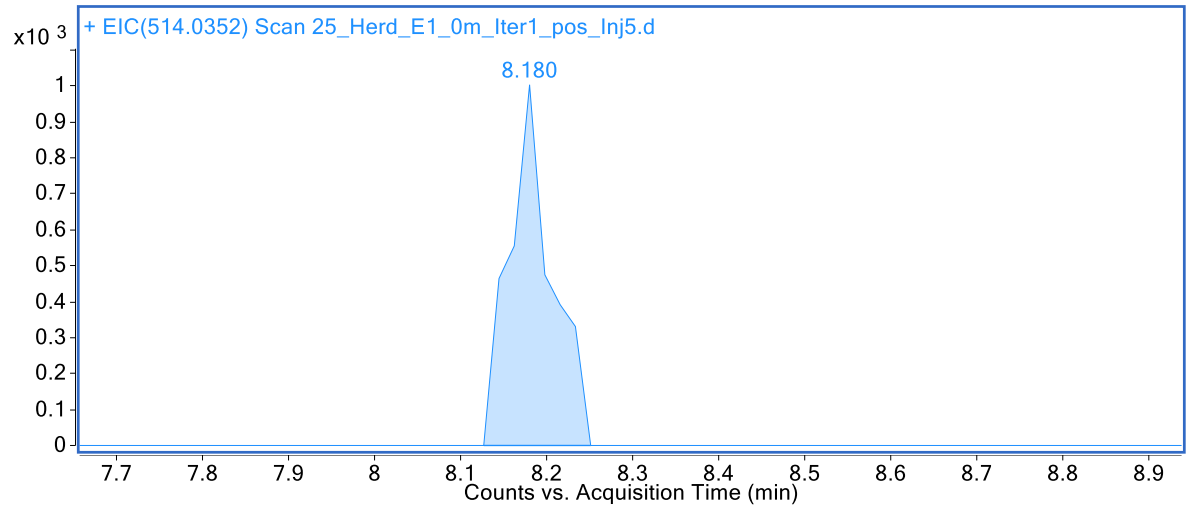

Fig. S6b: Chromatogram (ESI$^+$, soil *S1*, 0 – 0.5 m, first extract) of 6:2 FTSAm-*N*-Me-*N*-PrA (m/z 514.0352, 8.180 min).

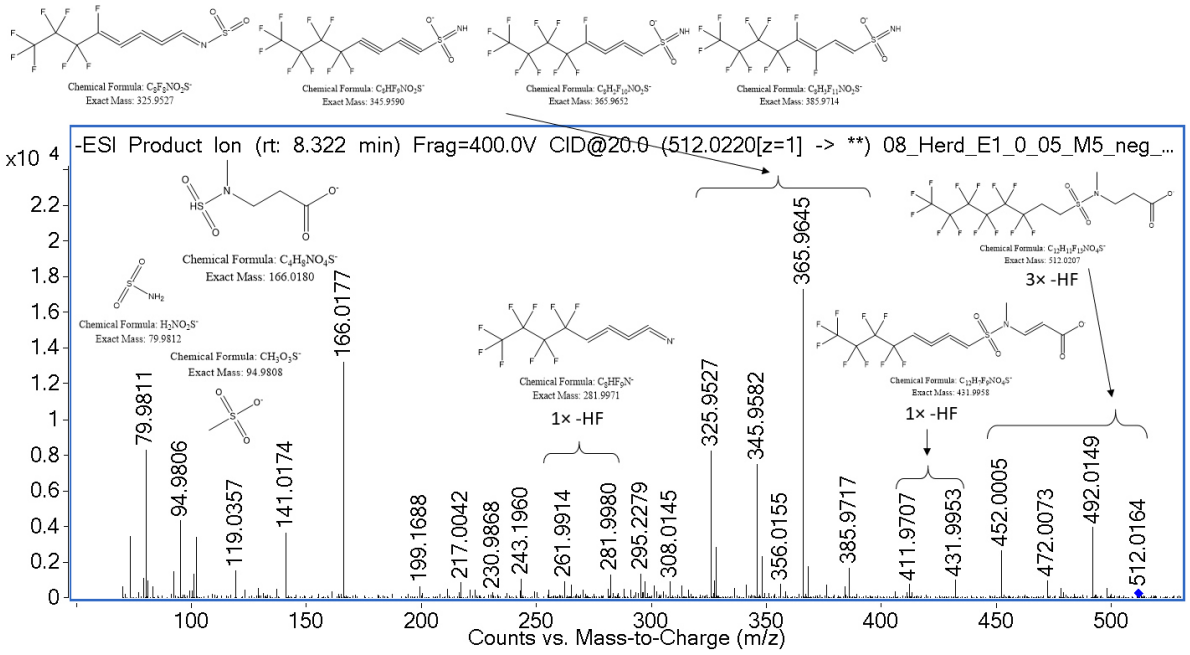

Fig. S6c: MS^2 spectrum (ESI^-, 20.0 eV, soil *S1*, 0 – 0.5 m, first extract, targeted MS^2) of 6:2 FTSAm-*N*-Me-*N*-PrA (m/z 512.0207, 8.322 min).

n:2 FTSAm-U-Pr-DiMeAms (n = 6)

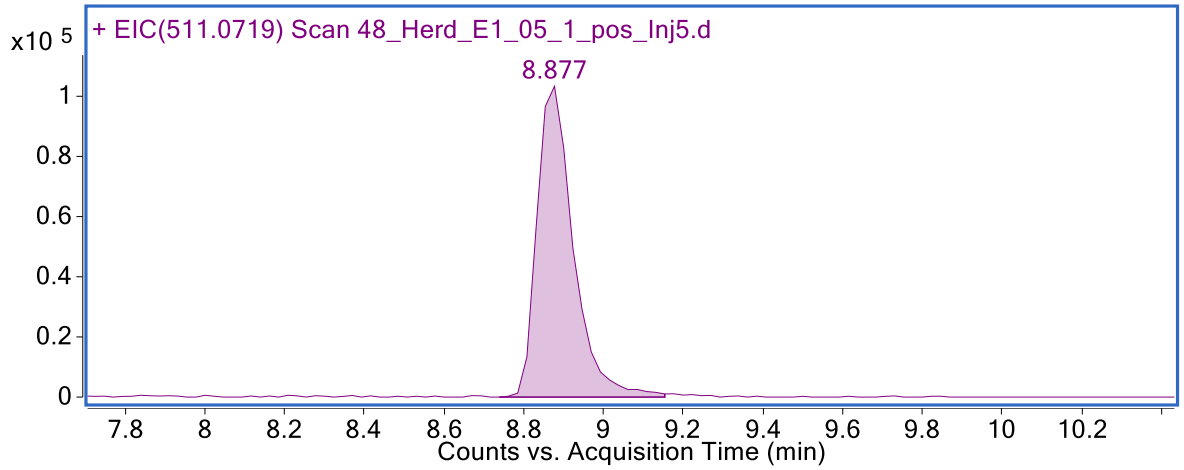

Fig. S7a: Chromatogram (ESI$^+$, soil *S1*, 0.5 – 1 m, first extract) of 6:2 FTSAm-U-Pr-DiMeAm (m/z 511.0719, 8.877 min).

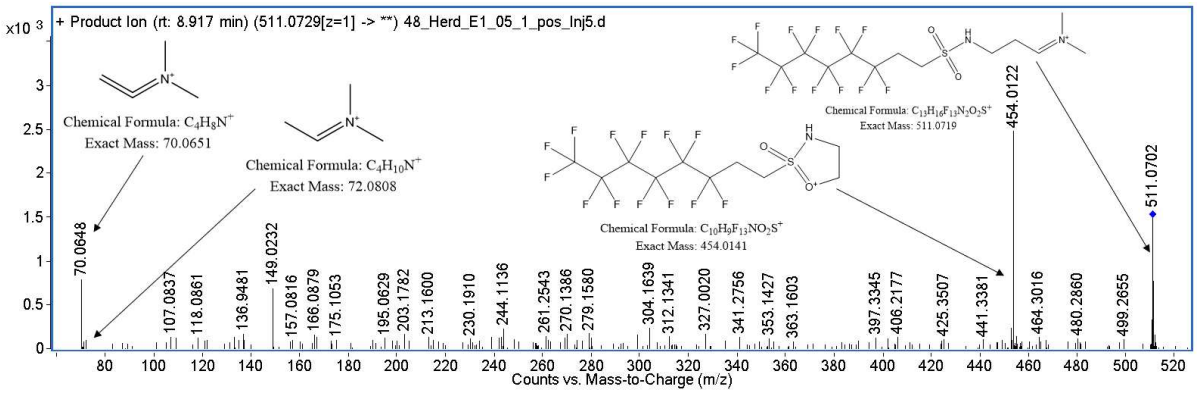

Fig. S7b: MS^2 spectrum (ESI$^+$, 30.3 eV, soil *S1*, 0.5 – 1 m, first extract) of 6:2 FTSAm-U-Pr-DiMeAm (m/z 511.0719, 8.917 min).

n:2 FTSAm-PrAs (n = 6)

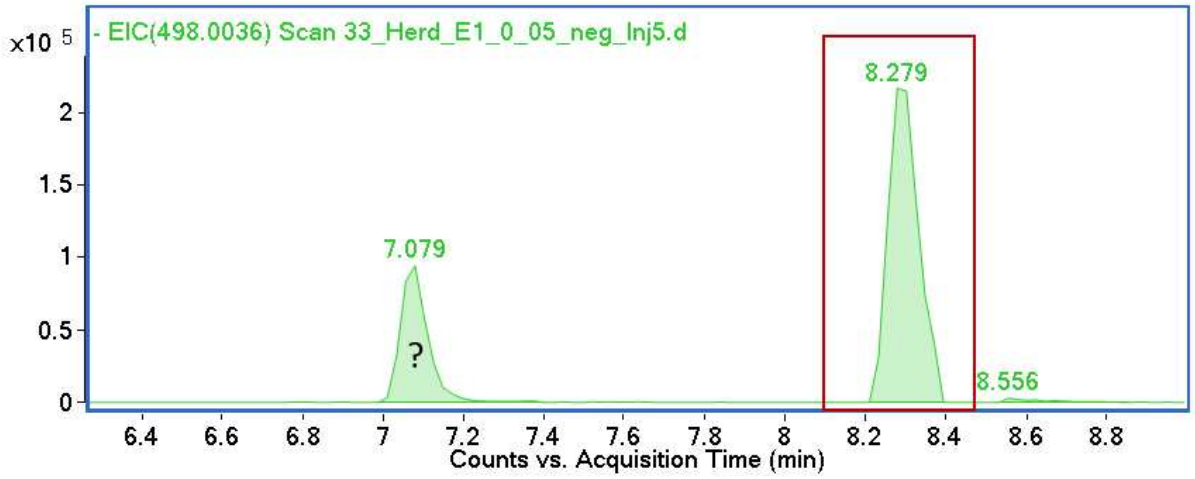

Fig. S8a: Chromatogram (ESI$^-$, soil *S1*, 0 – 0.5 m, first extract) of 6:2 FTSAm-PrA (m/z 498.0050, 8.279 min). First peak is possibly an isomer.

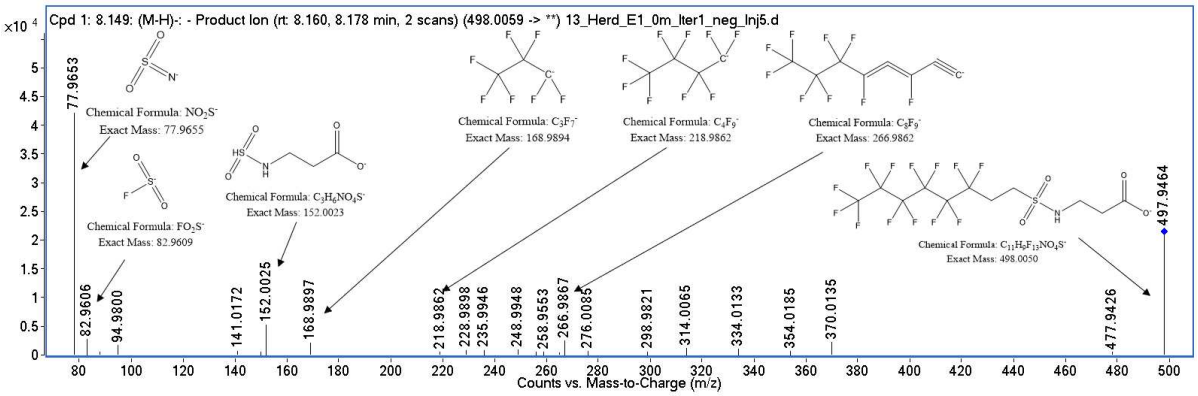

Fig. S8b: MS^2 spectrum (ESI$^-$, 29.9 eV, soil *S1*, 0 – 0.5 m, first extract, iterative MS^2) of 6:2 FTSAm-PrA (m/z 498.0050, 8.160 and 8.178 min).

n:2 FTBs (n = 6, 8, 10, 12)

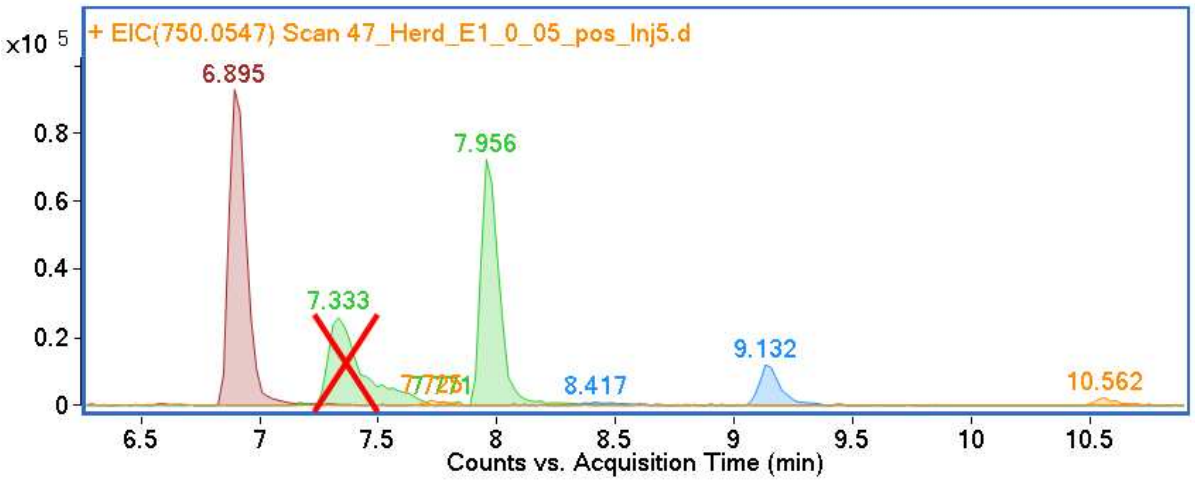

Fig. S9a: Chromatogram (ESI$^+$, soil *S1*, 0 – 0.5 m, first extract) of n:2 FTBs (n = 6 (red, m/z 450.0733, 6.895 min), 8 (green, m/z 550.0669, 7.956 min), 10 (blue, m/z 650.0605, 9.132 min), and 12 (orange, m/z 750.0542, 10.562 min)). Note: The first peak of 8:2 FTB (green, 7.333 min) is crossed out as it belongs to the Na-adduct of 6:2 FTSy-(2')OHPr-TriMeAm.

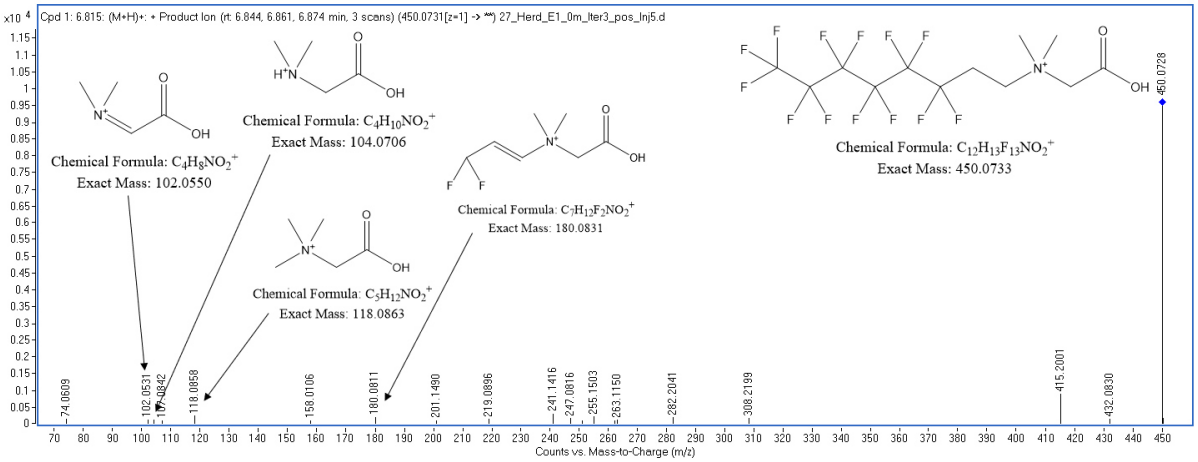

Fig. S9b: MS^2 spectrum (ESI$^+$, 28.5 eV, soil *S1*, 0 – 0.5 m, first extract, iterative MS^2) of 6:2 FTB (m/z 450.0733, 6.844, 6.861, and 6.874 min).

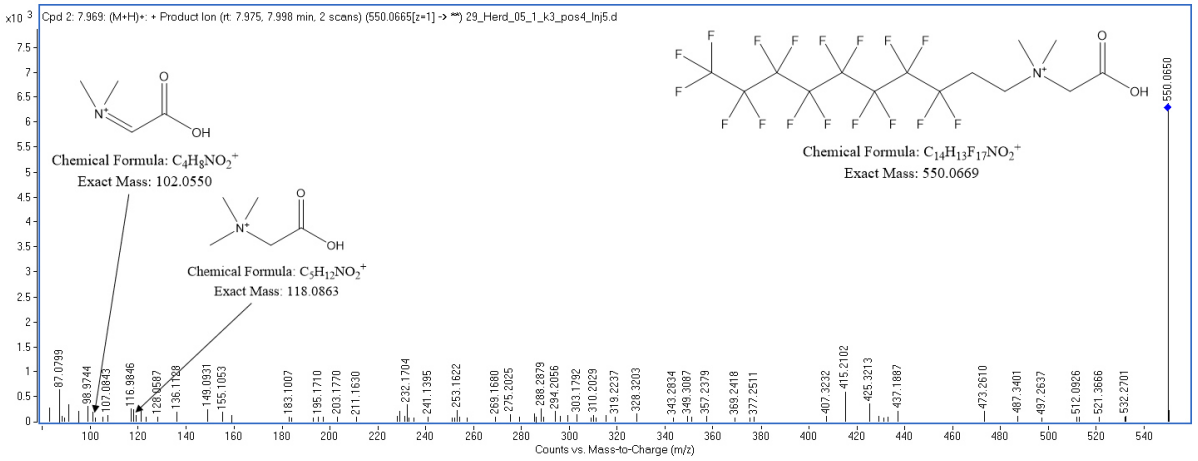

Fig. S9c: MS^2 spectrum (ESI$^+$, 31.5 eV, soil *S1*, 0.5 – 1 m, combined extract, iterative MS^2) of 8:2 FTB (m/z 550.0669, 7.975 and 7.998 min).

n:4 FTBs (n = 4, 6, 8, 10)

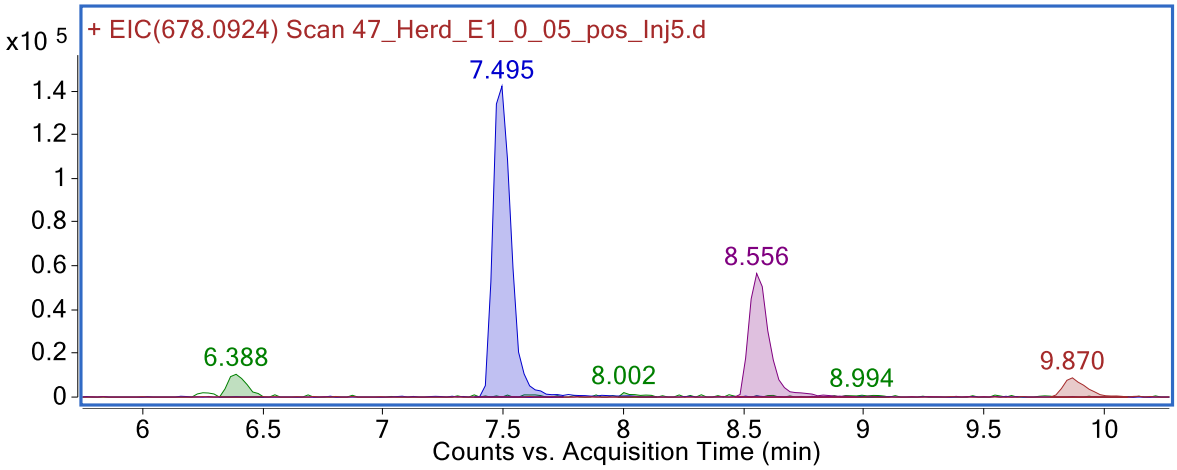

Fig. S10a: Chromatogram (ESI$^+$, soil *S1*, 0 – 0.5 m, first extract) of n:4 FTBs (n = 4 (green, m/z 378.1110, 6.388 min), 6 (blue, m/z 478.1046, 7.495 min), 8 (violet, m/z 578.0982, 8.556 min), and 10 (red, m/z 678.0918, 9.870 min)).

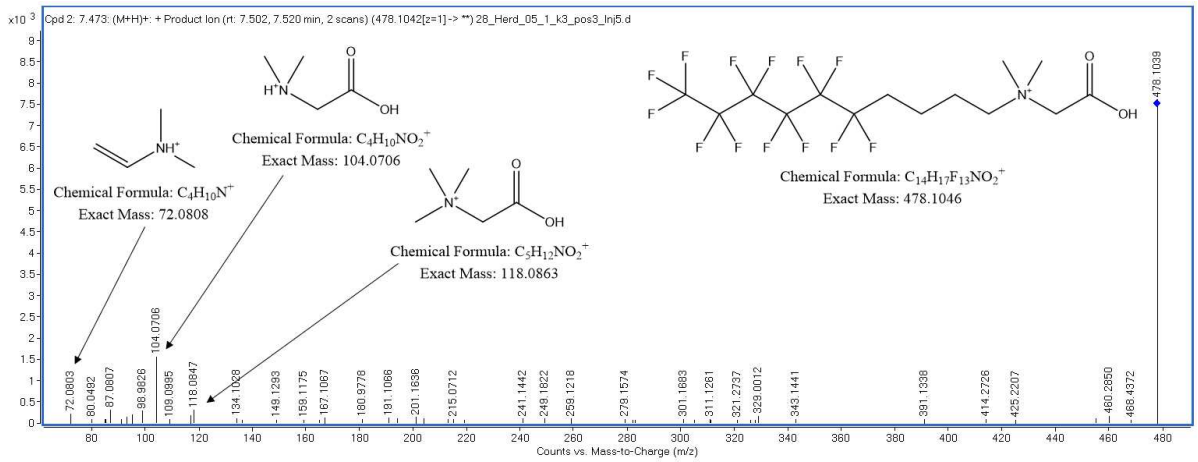

Fig. S10b: MS^2 spectrum (ESI$^+$, 29.3 eV, soil *S1*, 0.5 – 1 m, combined extract, iterative MS^2) of 6:4 FTB (m/z 478.1046, 7.502 and 7.520 min).

n:1:3 FTBs (n = 5, 7, 9)

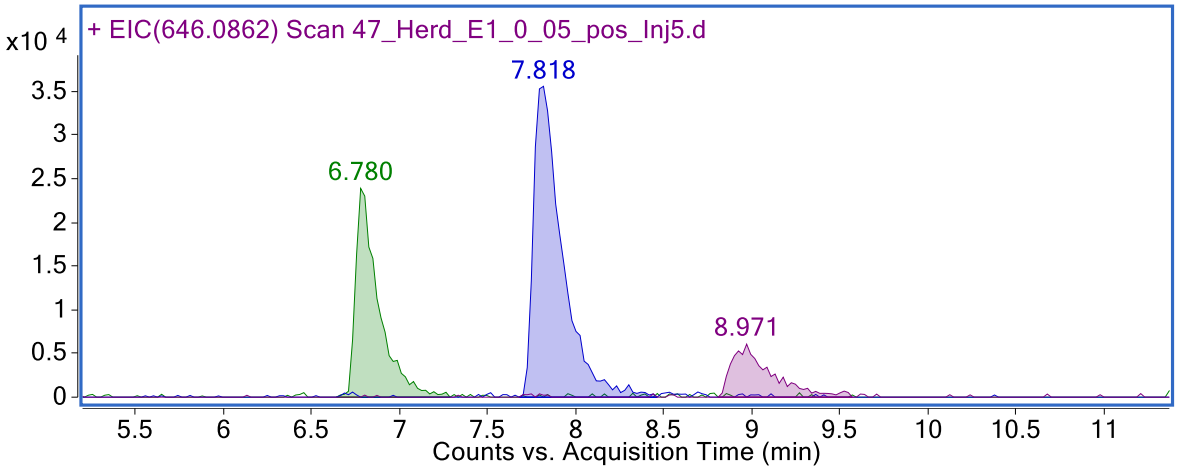

Fig. S11a: Chromatogram (ESI$^+$, soil *S1*, 0 – 0.5 m, first extract) of n:1:3 FTBs (n = 5 (green, m/z 446.0984, 6.780 min), 7 (blue, m/z 546.0920, 7.818 min), and 9 (violet, m/z 646.0856, 8.971 min)).

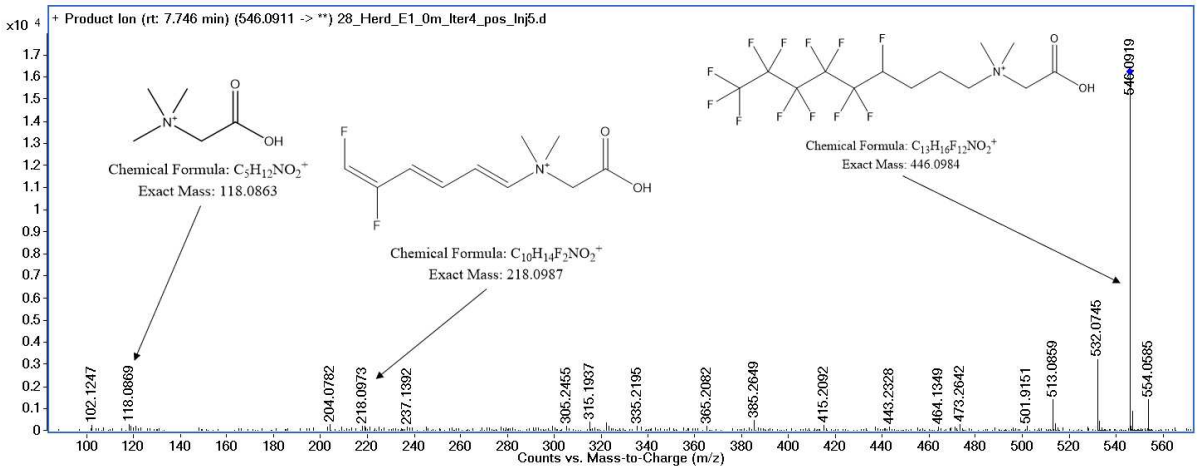

Fig. S11b: MS^2 spectrum (ESI^+, 28.4 eV, soil *S1*, 0 – 0.5 m, first extract, iterative MS^2) of 7:1:3 FTB (m/z 546.0920, 7.746 min).

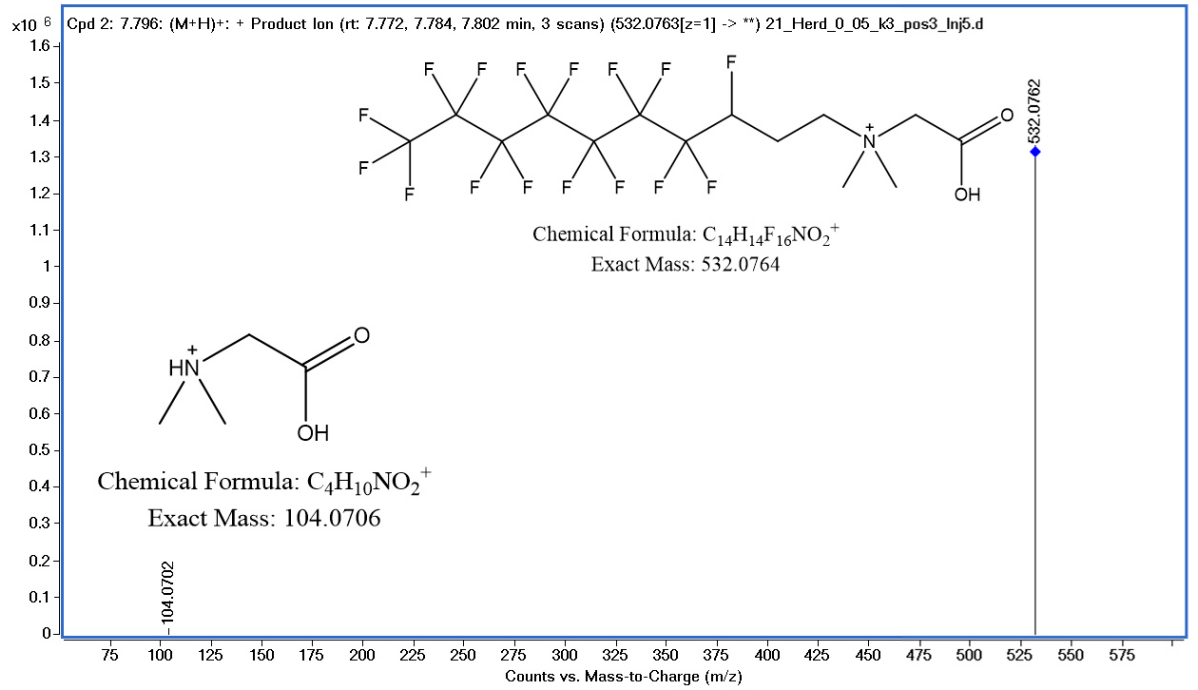

Fig. S11d: MS^2 spectrum (ESI^+, 31.0 eV, soil *S1*, 0 – 0.5 m, combined extract, iterative MS^2) of 7:1:2 FTB (m/z 532.0764, 7.772, 7.784 and 7.802 min).

K-n:2 FTSAs (n = 6, 8, 10)

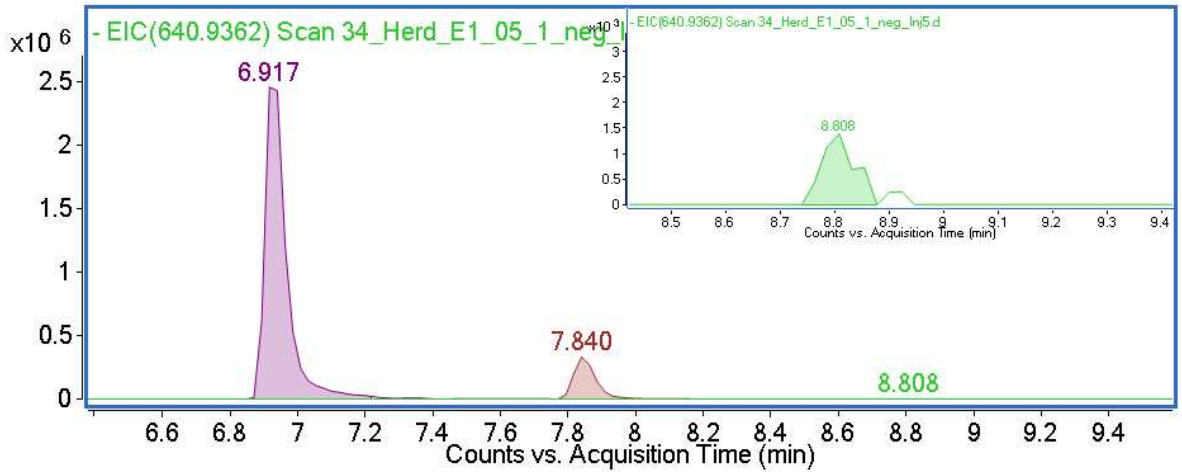

Fig. S12a: Chromatogram (ESI$^-$, soil *S1*, 0.5 – 1 m, first extract) of K-n:2 FTSAs (n = 6 (violet, m/z 440.9472, 6.917 min), 8 (red, m/z 540.9408, 7.840 min), and 10 (green, m/z 640.9344, 8.808 min)). Scale-up in top right corner.

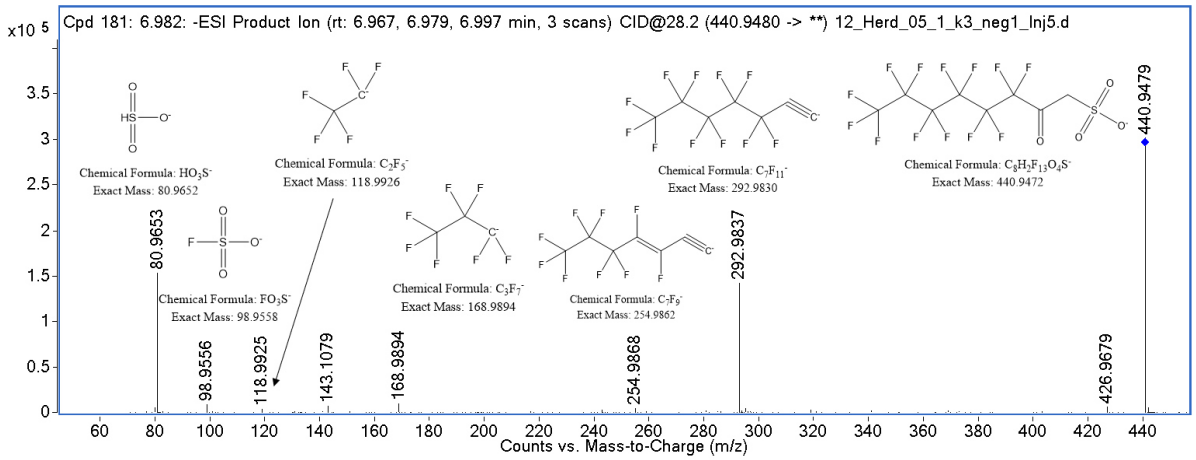

Fig. S12b: MS^2 spectrum (ESI$^-$, 28.2 eV, soil *S1*, 0.5 – 1 m, combined extract, iterative MS^2) of K-6:2 FTSA (m/z 440.9472, 6.967, 6.979, and 6.997 min).

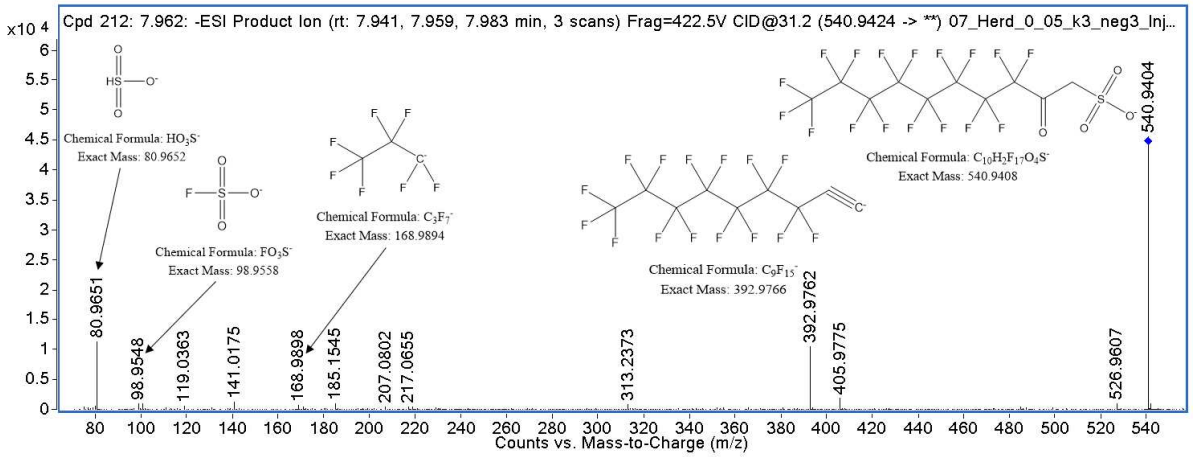

Fig. S12c: MS^2 spectrum (ESI$^-$, 31.2 eV, soil *S1*, 0 – 0.5 m, combined extract, iterative MS^2) of K-8:2 FTSA (m/z 540.9408, 7.941, 7.959, and 7.983 min).

U-n:2 FTSAs (n = 6, 8)

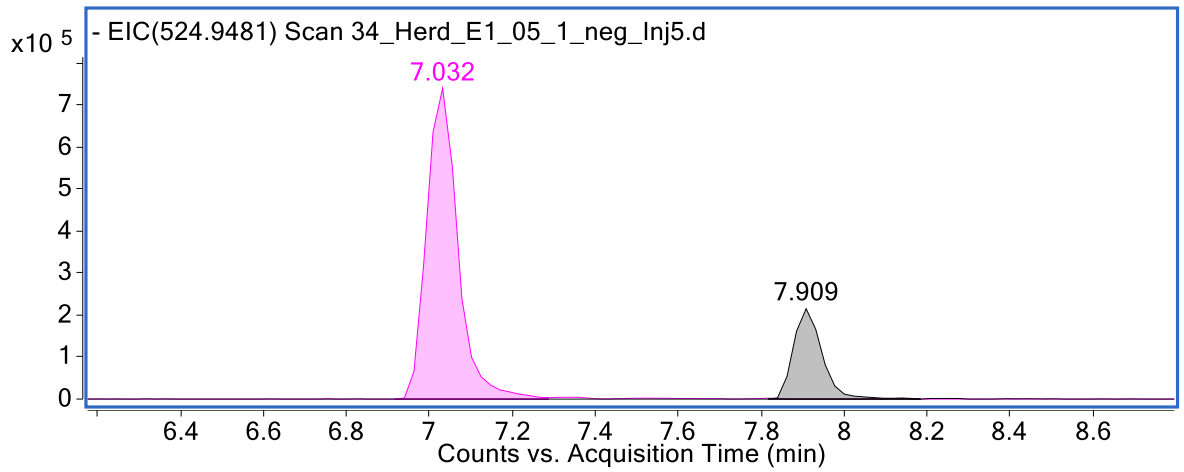

Fig. S13a: Chromatogram (ESI$^-$, soil *S1*, 0.5 – 1 m, first extract) of U-n:2 FTSAs (n = 6 (pink, m/z 424.9523, 7.032 min) and 8 (grey, m/z 524.9459, 7.909 min)).

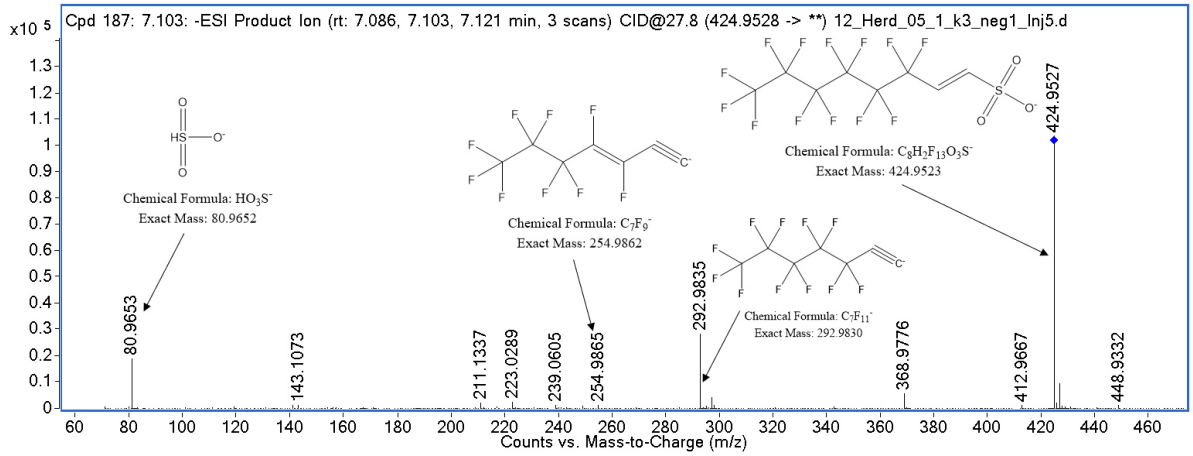

Fig. S13b: MS^2 spectrum (ESI$^-$, 27.8 eV, soil *S1*, 0.5 – 1 m, combined extract, iterative MS^2) of U-6:2 FTSA (m/z 424.9523, 7.086, 7.103, and 7.121 min).

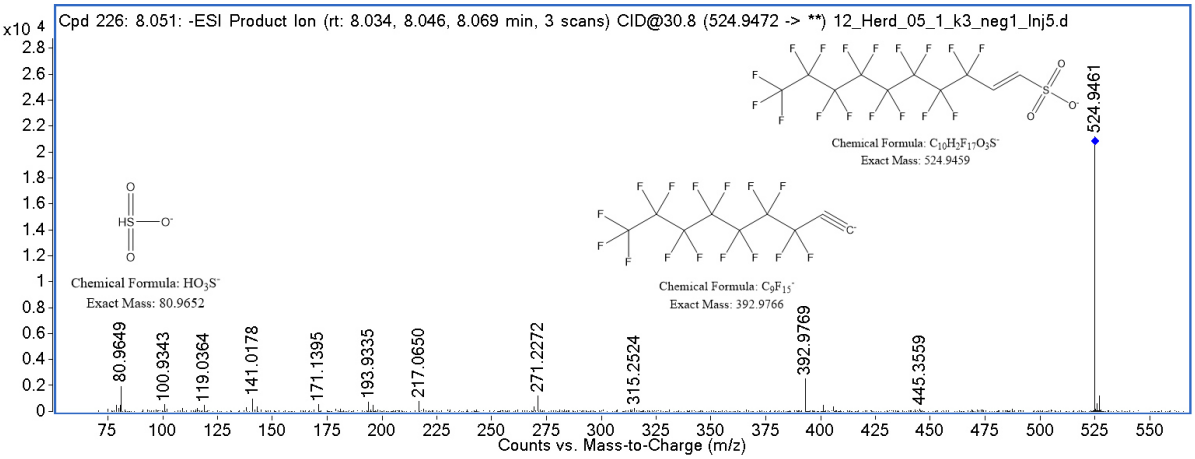

Fig. S13c: MS^2 spectrum (ESI$^-$, 30.8 eV, soil *S1*, 0.5 – 1 m, combined extract, iterative MS^2) of U-8:2 FTSA (m/z 524.9459, 8.034, 8.046, and 8.069 min).

n:2 FTSy-(2')OHPr-TriMeAms (n = 4, 6, 8)

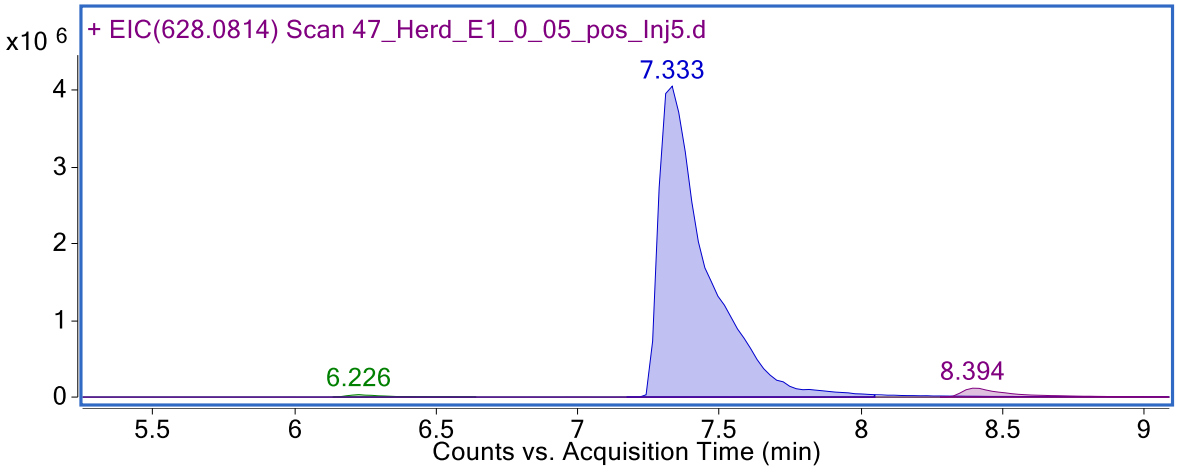

Fig. S14a: Chromatogram (ESI$^+$, soil *S1*, 0 – 0.5 m, first extract) of n:2 FTSy-(2')OHPr-TriMeAms (n = 4 (green, m/z 428.0936, 6.226 min), 6 (blue, m/z 528.0873, 7.333 min), and 8 (violet, m/z 628.0809, 8.394 min)).

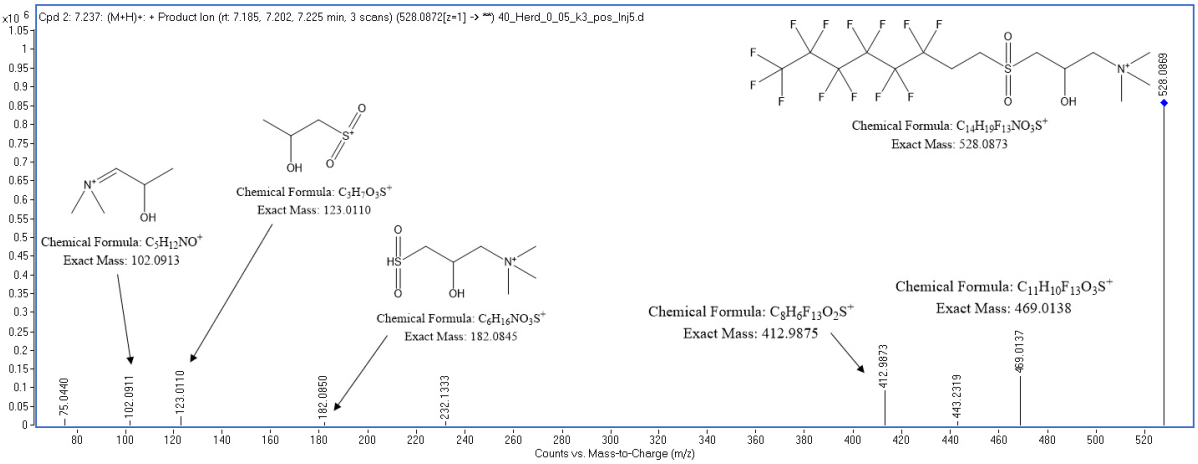

Fig. S14b: MS^2 spectrum (ESI$^+$, 30.8 eV, soil *S1*, 0 – 0.5 m, combined extract) of 6:2 FTSy-(2')OHPr-TriMeAm (m/z 528.0873, 7.185, 7.202, and 7.225 min).

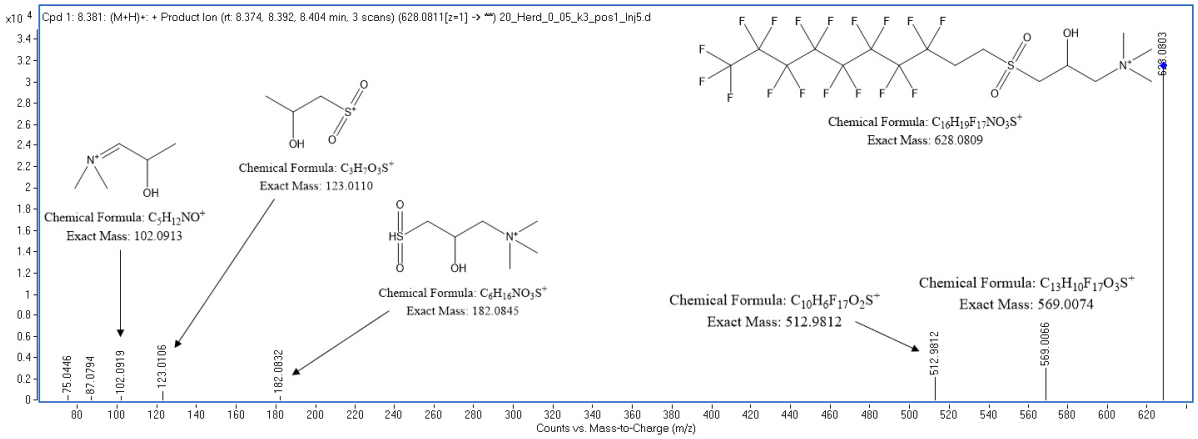

Fig. S14c: MS^2 spectrum mode (ESI$^+$, 33.8 eV, soil *S1*, 0 – 0.5 m, combined extract, iterative MS^2) of 8:2 FTSy-(2')OHPr-TriMeAm (m/z 628.0809, 8.374, 8.392, and 8.404 min).

Previously identified Substances

1. PFCA, PFSA, FTCA, FTSA

PFCAs (n = 3 - 11)

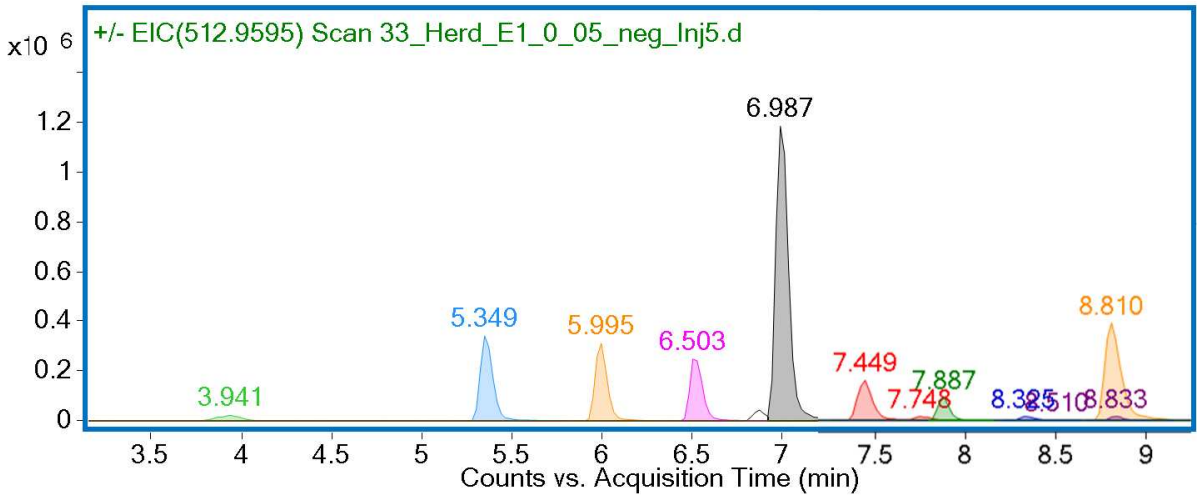

Fig. S15: Chromatogram (ESI$^-$, soil *S1*, 0 – 0.5 m, first extract) of PFCAs (n = 3 (green, m/z 212.9792, 3.941 min), 4 (blue, m/z 262.9760, 5.349 min), 5 (orange, m/z 312.9728, 5.995 min), 6 (pink, m/z 362.9696, 6.503 min), 7 (grey, m/z 412.9664, 6.987 min), 8 (red, m/z 462.9632, 7.449 min), 9 (dark green, m/z 512.9600, 7.887 min), 10 (dark blue, m/z 562.9568, 8.325 min), and 11 (violet, m/z 612.9537, 8.833 min)). Note: PFHxA (orange) shows a second peak at a retention time of 8.810 min. No MS^2 spectra are shown as fragmentation of PFCAs is already well known.

PFSAs (n = 3-13)

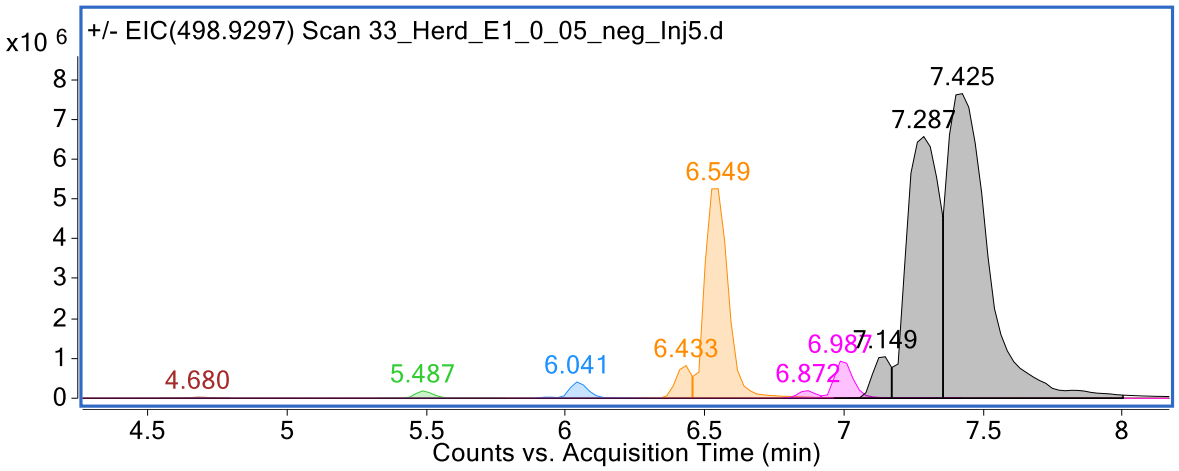

Fig. S16a: Chromatogram (ESI$^-$, soil *S1*, 0 – 0.5 m, first extract) of PFSAs (n = 3 – 8; n = 3 (dark red, m/z 248.9462, 4.680 min), 4 (green, m/z 298.9430, 5.487 min), 5 (blue, m/z 348.9398, 6.041 min), 6 (orange, m/z 398.9366, 6.433 and 6.549 min), 7 (pink, m/z 448.9334, 6.872 and 6.987 min), and 8 (grey, m/z 498.9302, 7.149, 7.287, and 7.425 min)). Note: The PFOS (n = 8) peak is in saturation. No MS^2 spectra are shown as fragmentation of PFSAs is already well known.

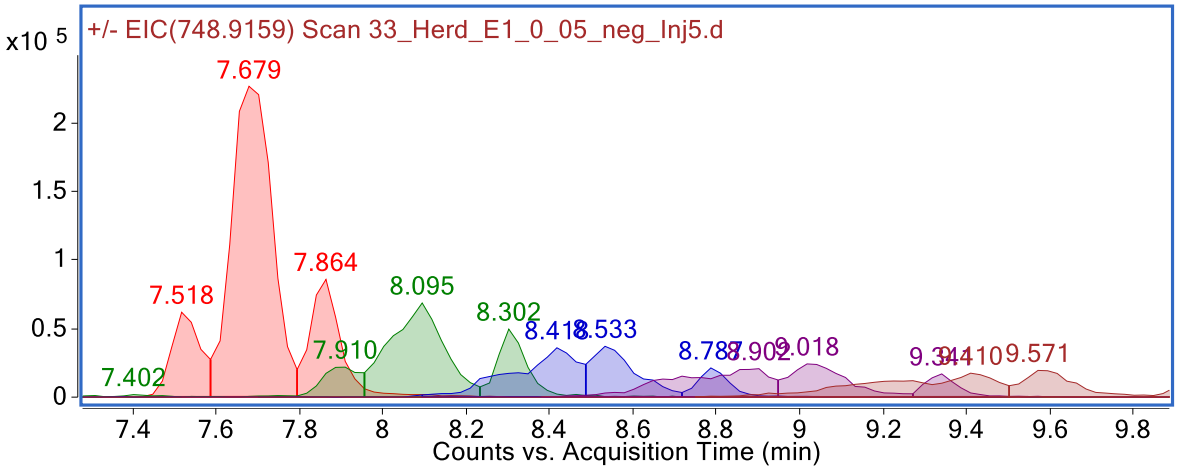

Fig. S16b: Chromatogram (ESI$^-$, soil *S1*, 0 – 0.5 m, first extract). of PFSAs (n = 9 – 13); n = 9 (red, m/z 548.9270, 7.518, 7.679, and 7.864 min), 10 (dark green, m/z 598.9238, 7.910, 8.095, and 8.302 min), 11 (dark blue, m/z 648.9206, 8.418, 8.533, and 8.787 min), 12 (violet, m/z 698.9174, 8.902, 9.018, and 9.341 min), and 13 (dark red, m/z 748.9143, 9.419 and 9.571 min)).

n:3 FTCAs (n = 3 - 9)

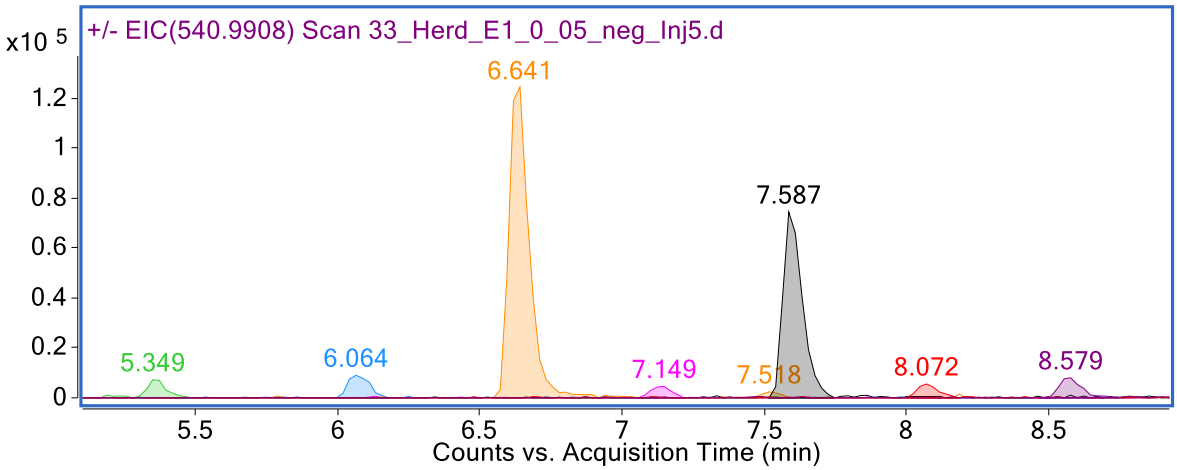

Fig. S17: Chromatogram (ESI$^-$, soil *S1*, 0 – 0.5 m, first extract) of n:3 FTCAs (n = 3 (green, m/z 241.0105, 5.349 min), 4 (blue, m/z 291.0073, 6.064 min), 5 (orange, m/z 341.0041, 6.641 min), 6 (pink, m/z 391.0009, 7.149 min), 7 (gray, m/z 440.9977, 7.587 min), 8 (red, m/z 490.9945, 8.072 min), and 9 (violet, m/z 540.9913, 8.579 min)).

n:2 FTSAs (n = 6, 8, 10, 12, 14)

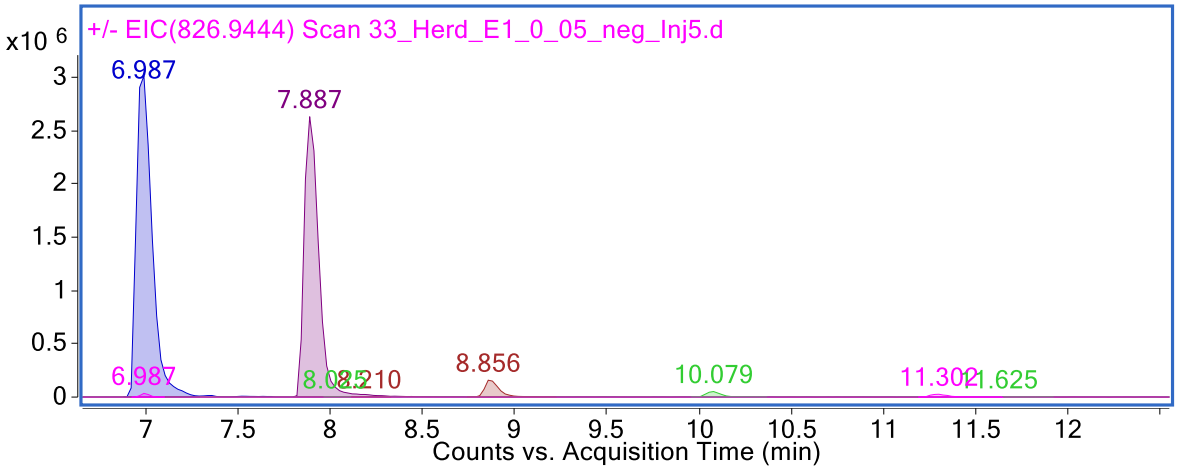

Fig. S18: Chromatogram (ESI$^-$, soil *S1*, 0 – 0.5 m, first extract) of n:2 FTSAs (n = 6 (blue, m/z 426.9679, 6.987 min), 8 (violet, m/z 526.9615, 7.887 min), 10 (red, m/z 626.9551, 8.856 min), 12 (green, m/z 726.9487, 10.079 min), and 14 (pink, m/z 826.9424, 11.302 min)).

2. PFSA- and U-PFSA derivatives

Cl-PFSAs (n = 6, 8)

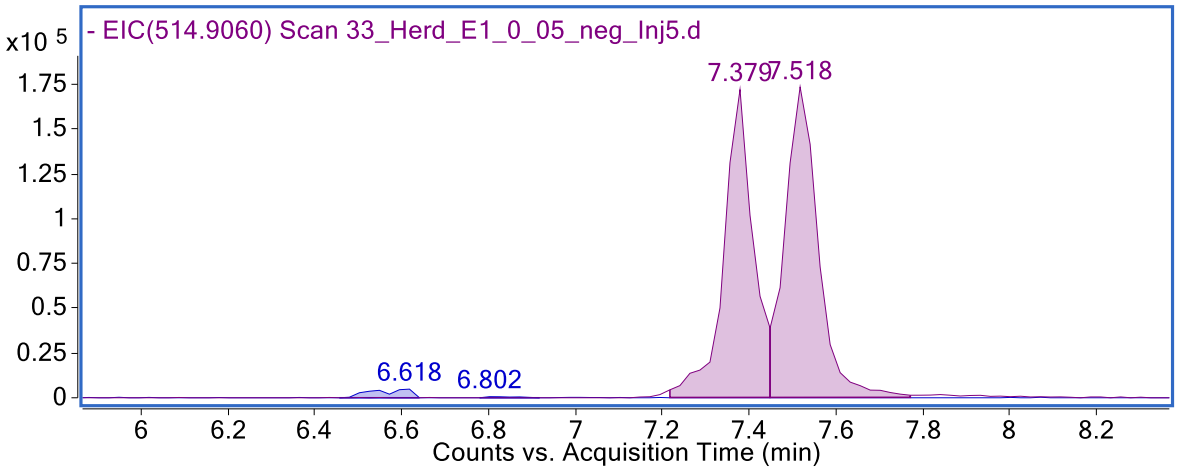

Fig. S19a: Chromatogram (ESI$^-$, soil *S1*, 0 – 0.5 m, first extract) of Cl-PFSAs (n = 6 (blue, m/z 414.9071, 6.618 and 6.802 min) and 8 (violet, m/z 514.9007, 7.379 and 7.518 min)).

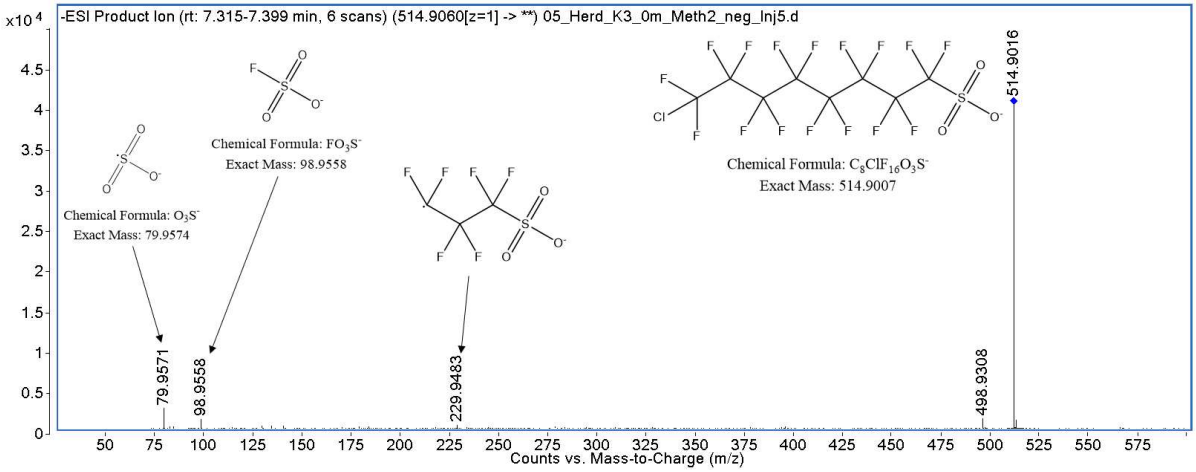

Fig. S19b: MS^2 spectrum (ESI$^-$, different CEs (10 – 40 eV), soil *S1*, 0 – 0.5 m, combined extract, targeted MS^2) of (8)Cl-PFOS (m/z 514.9007, 7.315 – 7.399 min).

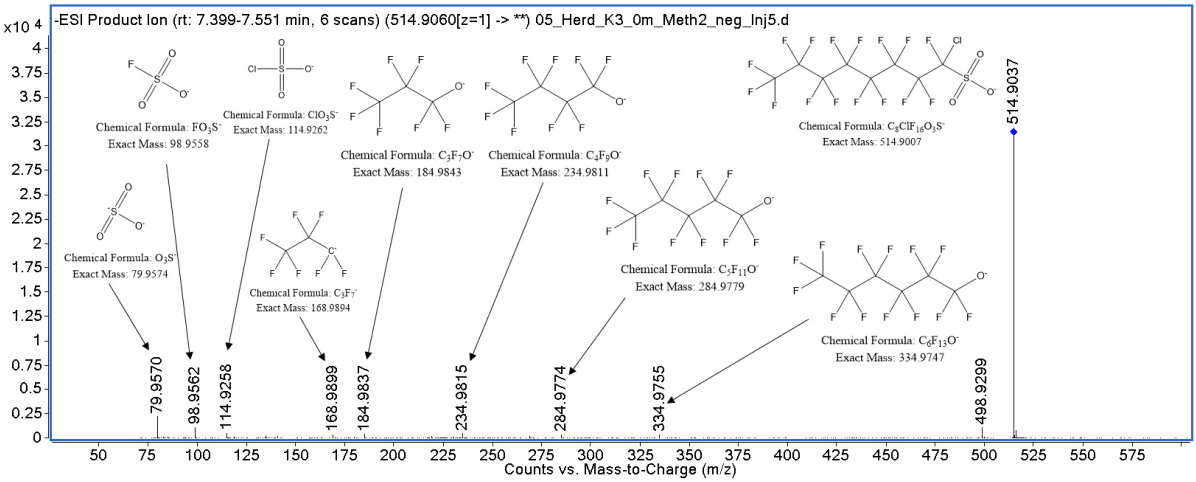

Fig. S19c: MS^2 spectrum (ESI$^-$, different CEs (10 – 40 eV), soil *S1*, 0 – 0.5 m, combined extract, targeted MS^2) of (1)Cl-PFOS (m/z 514.9007, 7.399 – 7.551 min).

SF_5-PFSAs (n = 7 - 10)

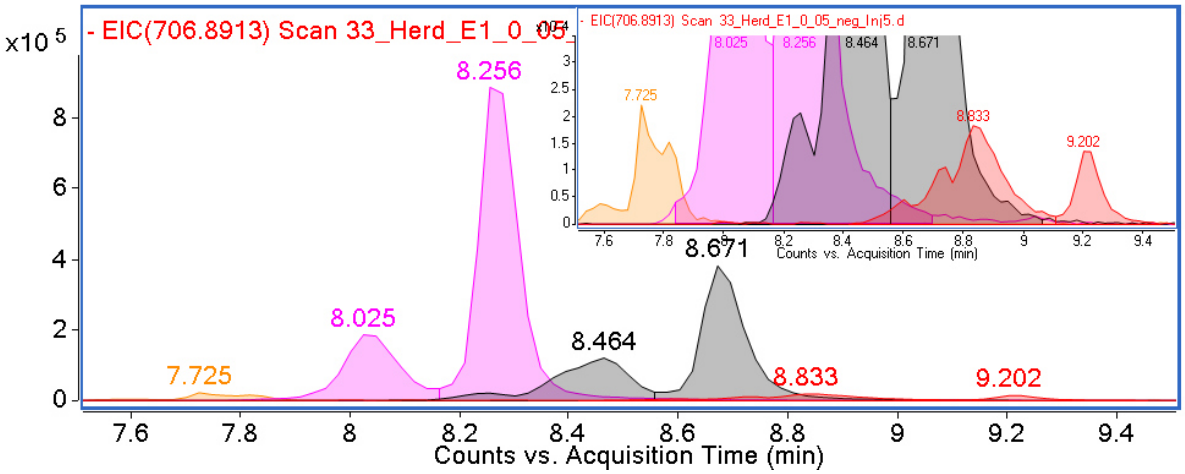

Fig. S20a: Chromatogram (ESI$^-$, soil *S1*, 0 – 0.5 m, first extract) of SF_5-PFSAs (n = 7 (orange, m/z 556.8991, 7.725 min), 8 (pink, m/z 606.8959, 8.025 and 8.256 min), 9 (grey, m/z 656.8927, 8.464 and 8.671 min), and 10 (red, m/z 706.8895, 8.833 nad 9.202 min)). Scale-up in top right corner.

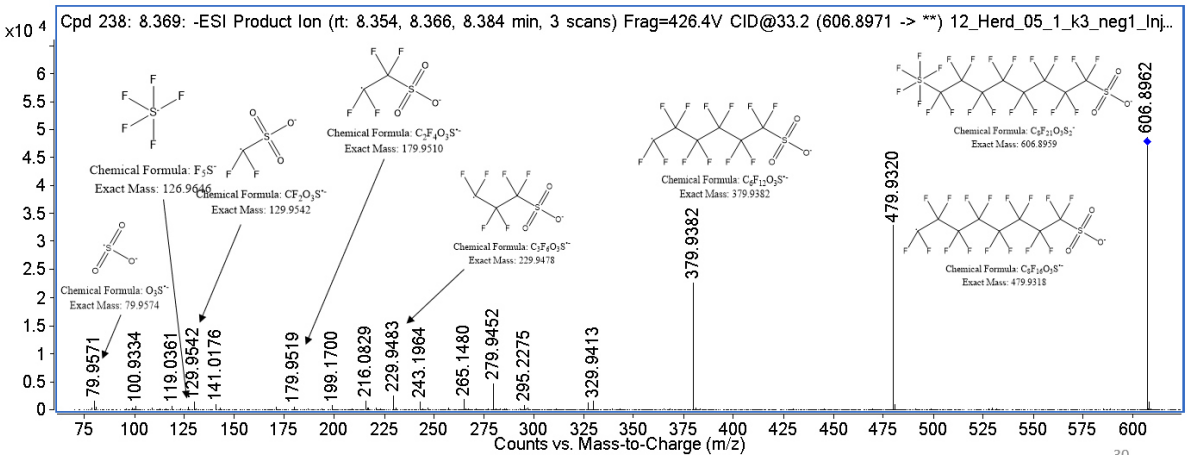

Fig. S20b: MS^2 spectrum (ESI$^-$, 33.2 eV, soil *S1*, 0.5 – 1 m, combined extract, iterative MS^2) of SF_5-PFOS (m/z 606.8959, 8.354, 8.366, and 8.384 min).

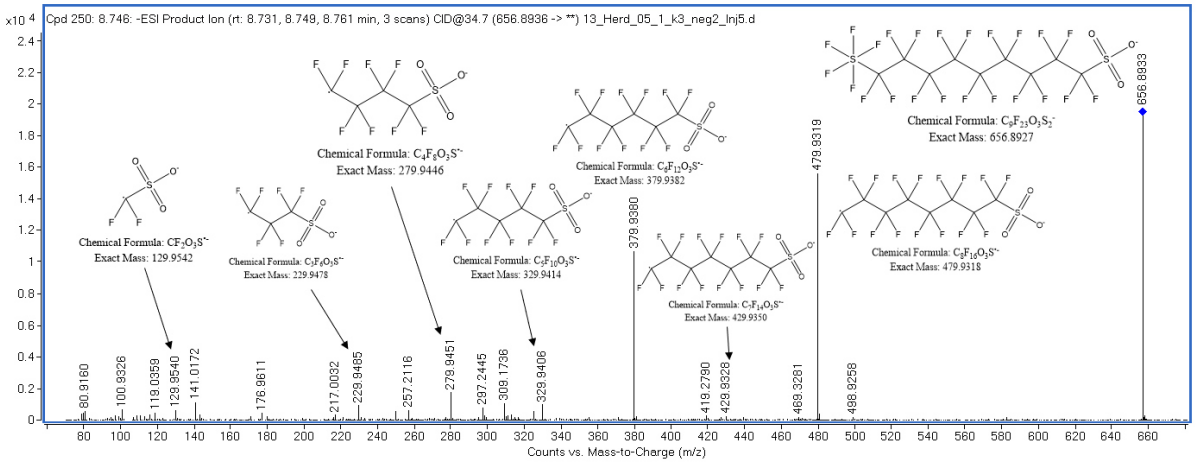

Fig. S20c: MS^2 spectrum (ESI$^-$, 34.7 eV, soil *S1*, 0.5 – 1 m, combined extract, iterative MS^2) of SF_5-PFNS (m/z 656.8927).

H-PFSAs (n = 8, 10)

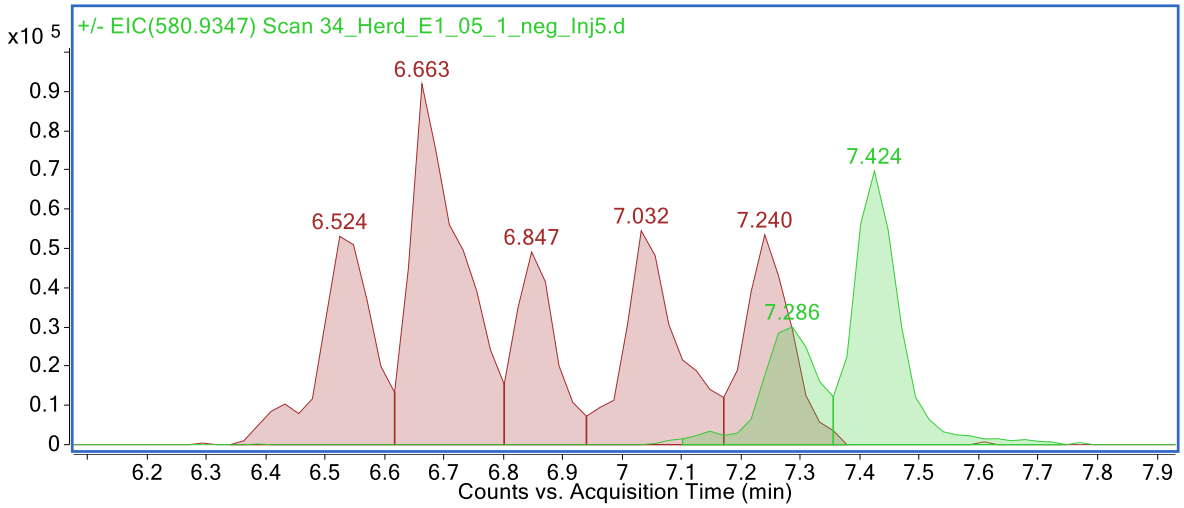

Fig. S21a: Chromatogram (ESI$^-$, soil *S1*, 0.5 – 1 m, first extract) of H-PFSAs (n = 8 (red, m/z 480.9396, 6.524, 6.663, 6.847, 7.032, and 7.240 min) and 10 (green, m/z 580.9333, 7.286 and 7.424 min)).

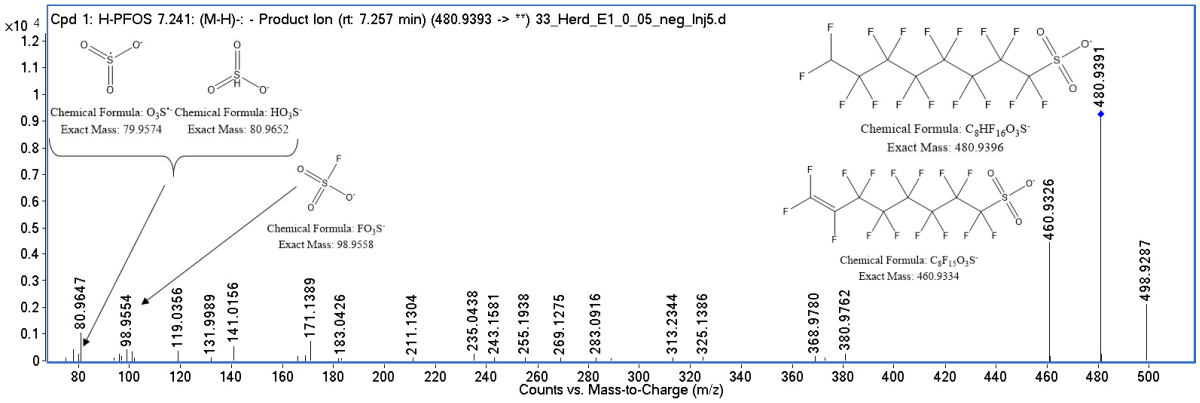

Fig. 21b: MS^2 spectrum (ESI$^-$, 29.4 eV, soil *S1*, 0 – 0.5 m, first extract) of H-PFOS (m/z 480.9396, 7.257 min).

K-PFSAs/U-E-PFSAs (n = 6/7, 7/8, 8/9, 9/10, 10/11, 11/12, 12/13, 13/14, 14/15)

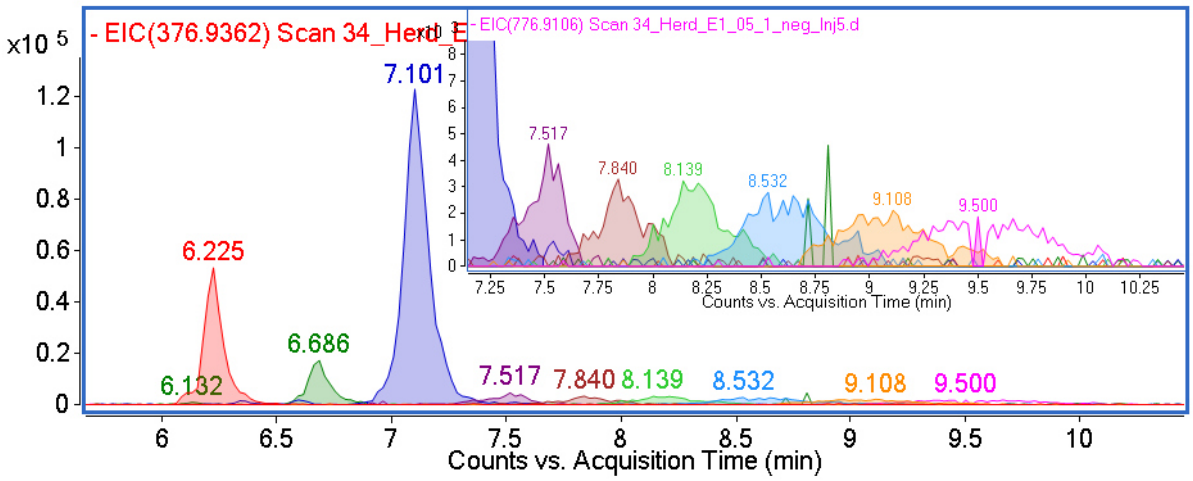

Fig. S22a: Chromatogram (ESI$^-$, soil *S1*, 0.5 – 1 m, first extract) of K-PFSAs/U-E-PFSAs (n = 6/7 (red, m/z 376.9347, 6.225 min), 7/8 (dark green, m/z 426.9315, 6.686 min), 8/9 (dark blue, m/z 476.9283, 7.101 min), 9/10 (violet, m/z 526.9251, 7.517 min), 10/11 (dark red, m/z 576.9219, 7.840 min), 11/12 (green, m/z 626.9187, 8.139 min), 12/13 (blue, m/z 676.9156, 8.532 min), 13/14 (orange, m/z 726.9124, 9.108 min), and 14/15 (pink, m/z 776.9092, 9.500 min)). Scale-up in top right corner.

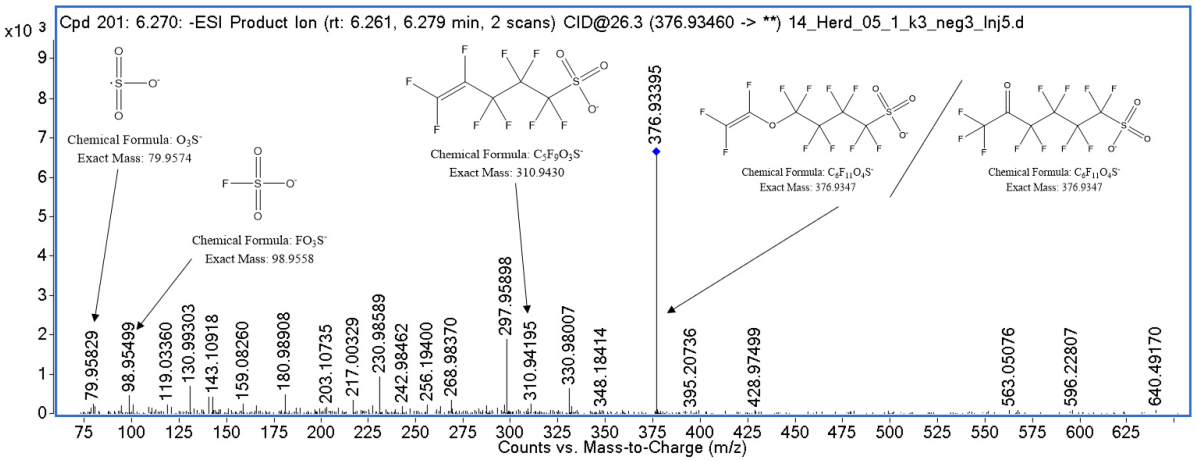

Fig. S22b: MS^2 spectrum (ESI$^-$, 26.3 eV, soil *S1*, 0.5 – 1 m, combined extract, iterative MS^2) of U-E-PFHpS/K-PFHxS (m/z 376.9347, 6.261 and 6.279 min).

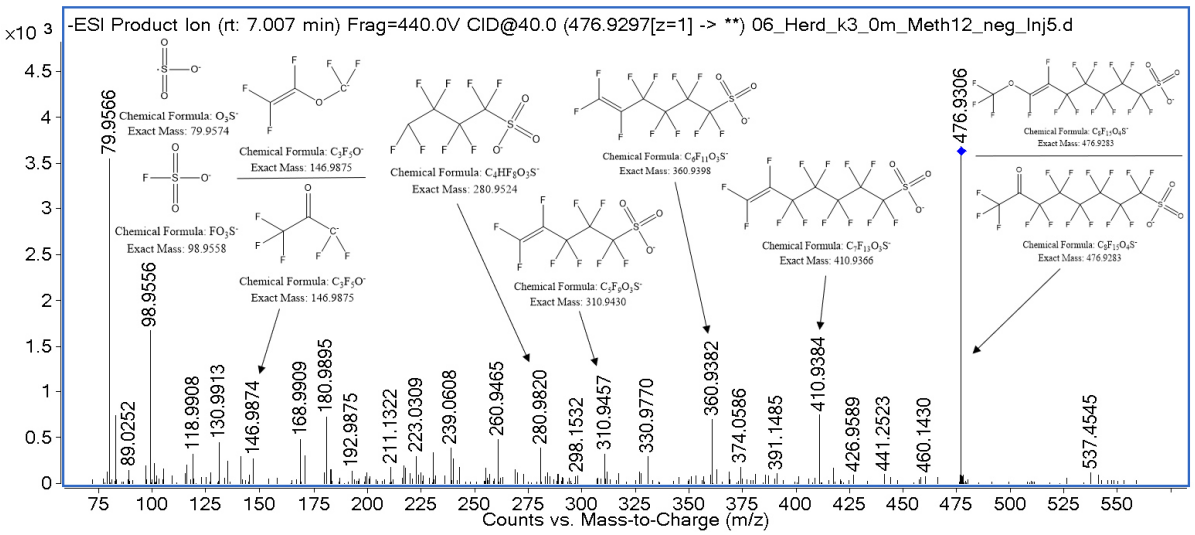

Fig. S22c: MS^2 spectrum (ESI^-, 40.0 eV, soil *S1*, 0 – 0.5 m, combined extract, targeted MS^2) of U-E-PFNS/K-PFOS (m/z 476.9283, 7.007 min).

PFASyAs (n = 8)

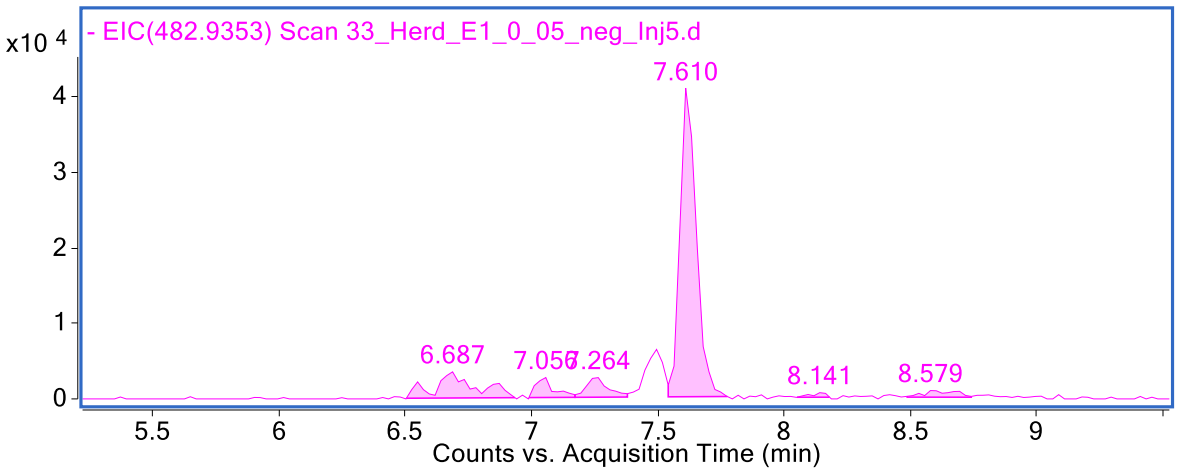

Fig. S23a: Chromatogram (ESI^-, soil *S1*, 0 – 0.5 m, first extract) of PFOSyA (m/z 482.9353, 7.610 min).

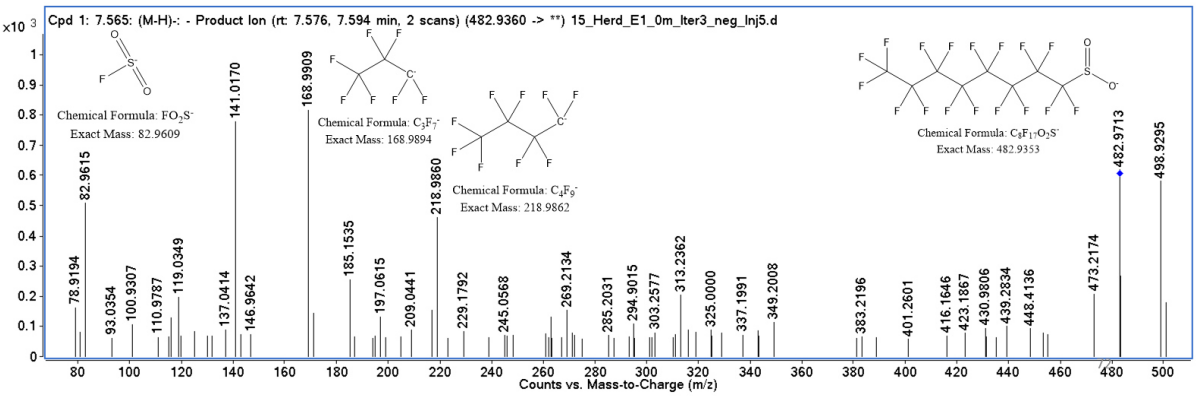

Fig. S23b: MS^2 spectrum (ESI^-, 29.5 eV, soil *S1*, 0 – 0.5 m, first extract, iterative MS^2) of PFOSyA (m/z 482.9353, 7.576 and 7.594 min).

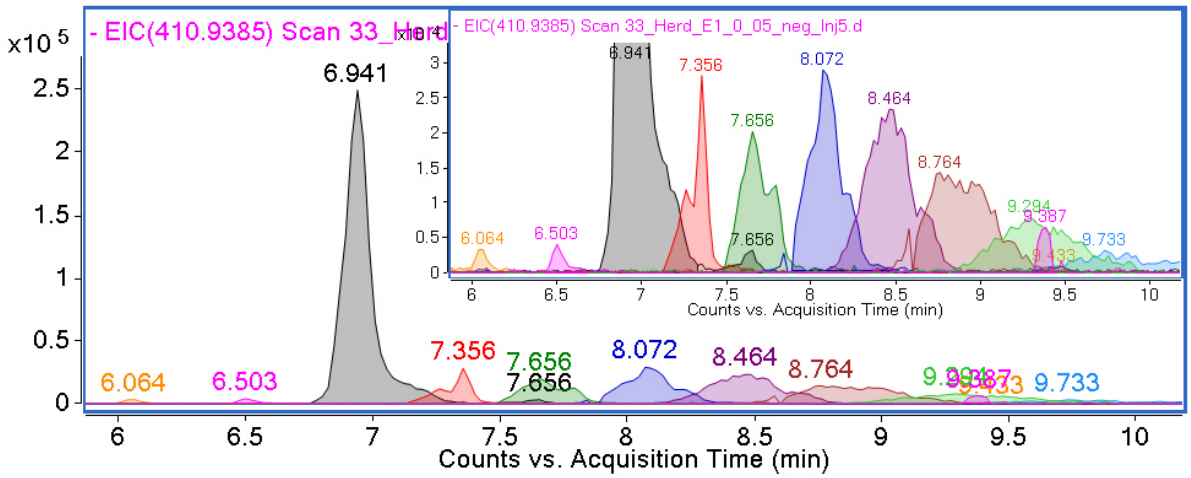

Fig. S24a: Chromatogram (ESI$^-$, soil *S1*, 0 – 0.5 m, first extract) of U-PFSAs (n = 6 (orange, m/z 360.9398, 6.064 min), 7 (pink, m/z 410.9366, 6.503 min), 8 (grey, m/z 460.9334, 6.941 min), 9 (red, m/z 510.9302, 7.356 min), 10 (dark green, m/z 560.9270, 7.656 min), 11 (dark blue, m/z 610.9238, 8.072 min), 12 (violet, m/z 660.9206, 8.464 min), 13 (dark red, m/z 710.9174, 8.764 min), 14 (green, m/z 760.9143, 9.294 min), and 15 (blue, m/z 810.9111, 9.733 min)). Scale-up in top right corner.

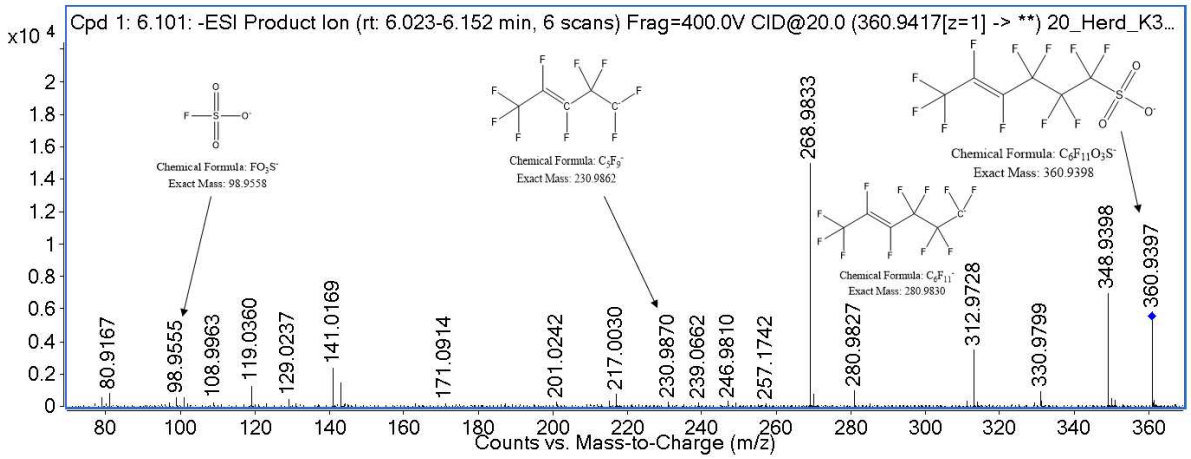

Fig. S24b: MS^2 spectrum (ESI$^-$, 20.0 eV, soil *S1*, 1.5 – 2 m, combined extract, targeted MS^2) of U-PFHxS (m/z 360.9398, 6.023 – 6.152 min).

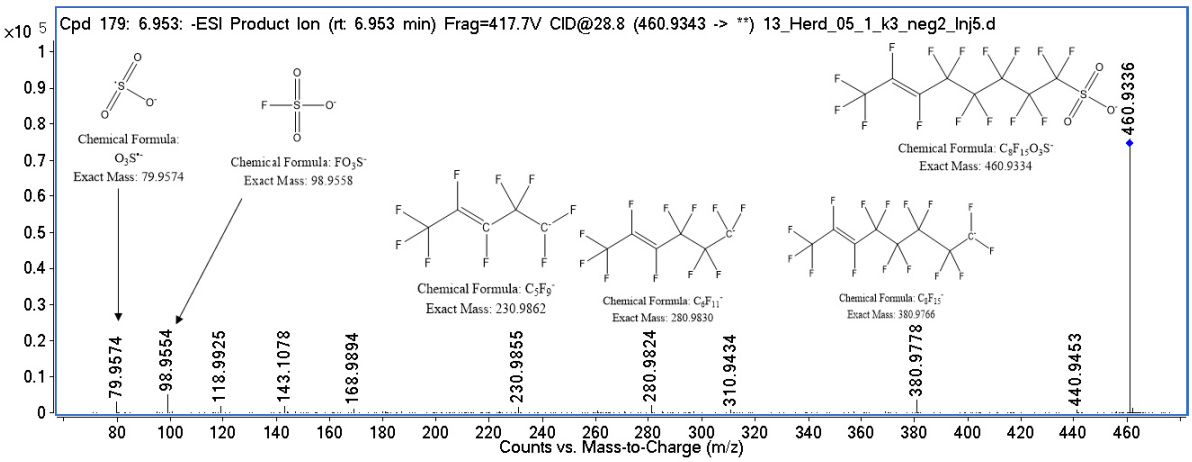

Fig. S24c: MS^2 spectrum (ESI$^-$, 28.8 eV, soil *S1*, 0.5 – 1 m, combined extract, iterative MS^2) of U-PFOS (m/z 460.9334, 6.953 min).

SF_5-U-PFSAs (n = 8, 9, 10)

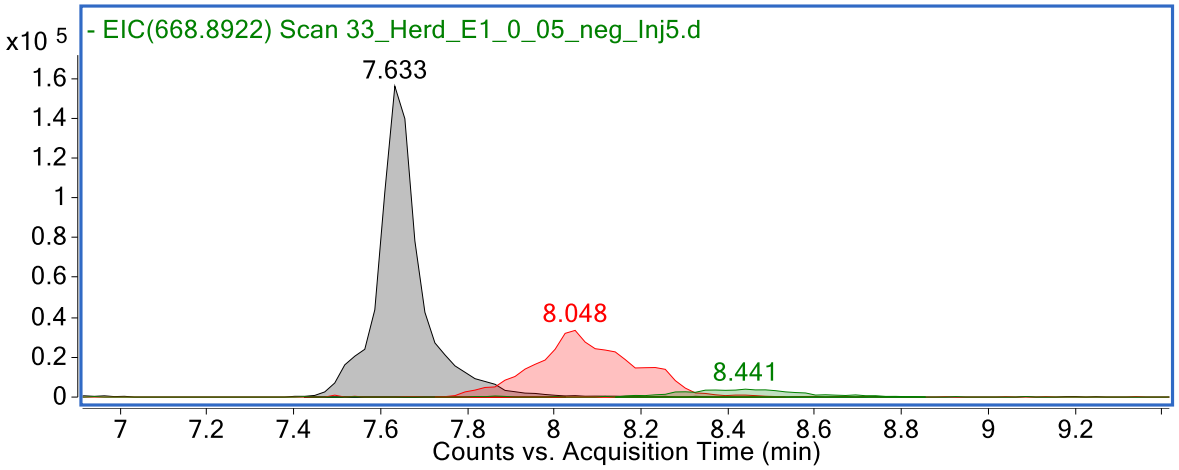

Fig. S25a: Chromatogram (ESI$^-$, soil *S1*, 0 – 0.5 m, first extract) of SF_5-U-PFSAs (n = 8 (grey, m/z 568.8991, 7.633 min), 9 (red, m/z 618.8959, 8.048 min), and 10 (green, m/z 668.8927, 8.441 min)).

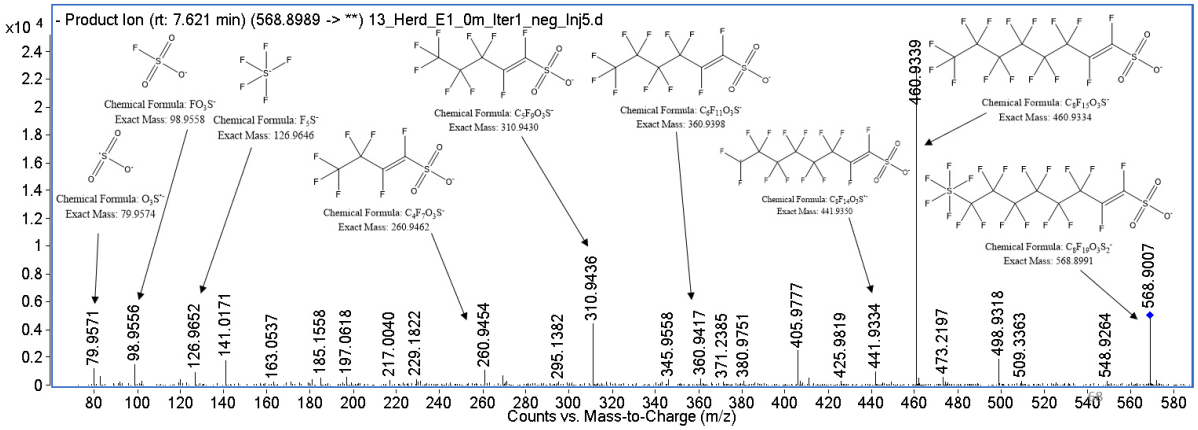

Fig. S25b: MS^2 spectrum (ESI$^-$, 32.1 eV, soil *S1*, 0 – 0.5 m, first extract, iterative MS^2) of SF_5-U-PFOS (m/z 568.8991, 7.621 min).

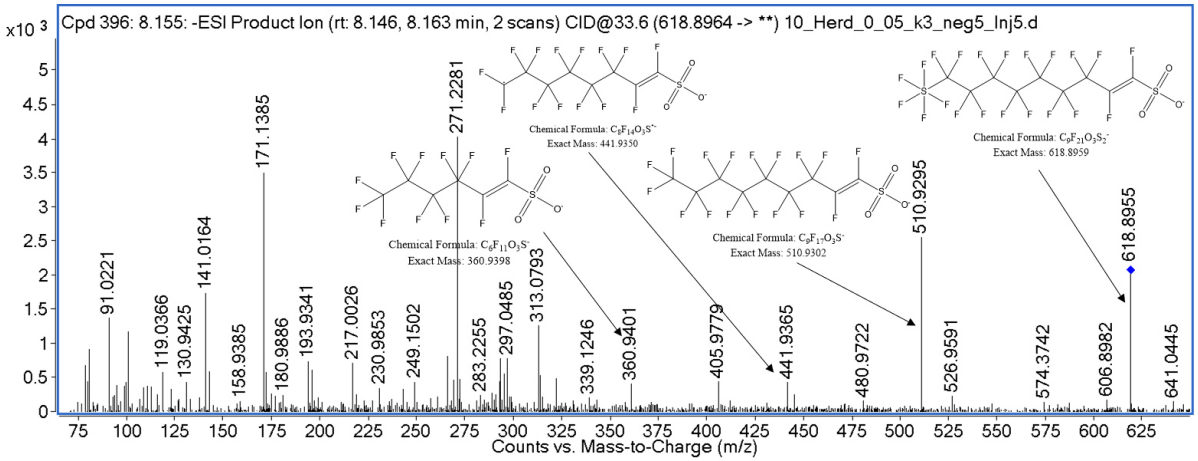

Fig. S25c: MS^2 spectrum (ESI$^-$, 33.6 eV, soil *S1*, 0 – 0.5 m, combined extract, iterative MS^2) of SF_5-U-PFNS (m/z 618.8959, 8.146 and 8.163 min).

3. PFASAm and PFASAm-Pr derivatives

PFASAms (n = 3-8)

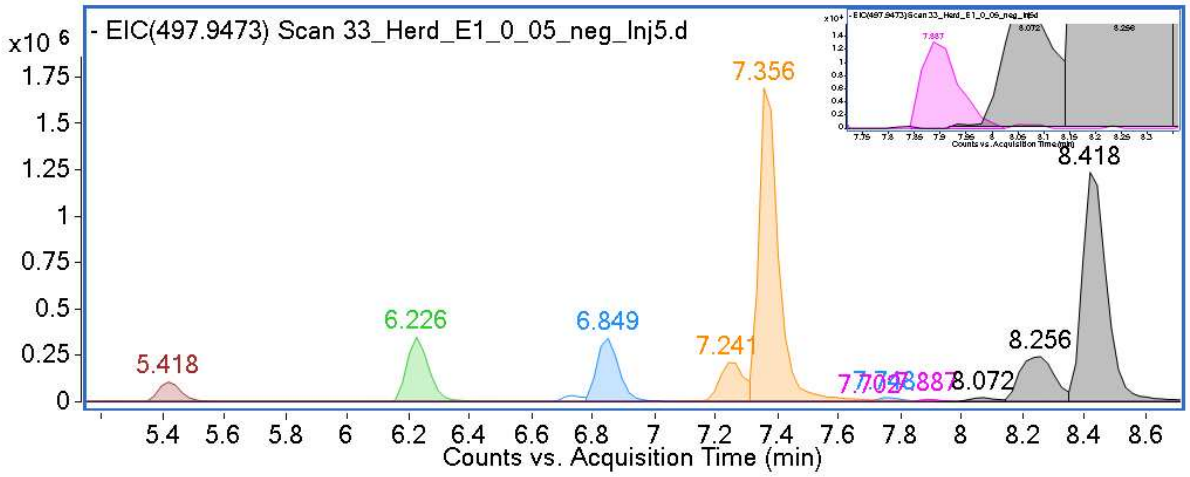

Fig. S26a: Chromatogram (ESI$^-$, soil *S1*, 0 – 0.5 m, first extract) of PFASAms (n = 3 (red, m/z 247.9622, 5.418 min), 4 (green, m/z 297.9590, 6.226 min), 5 (blue, m/z 347.9558, 6.849 min), 6 (orange, m/z 397.9526, 7.241 and 7.356 min), 7 (pink, m/z 447.9494, 7.887 min), and 8 (grey, m/z 497.9462, 8.072, 8.256, and 8.418 min)). Scale-up in top right corner.

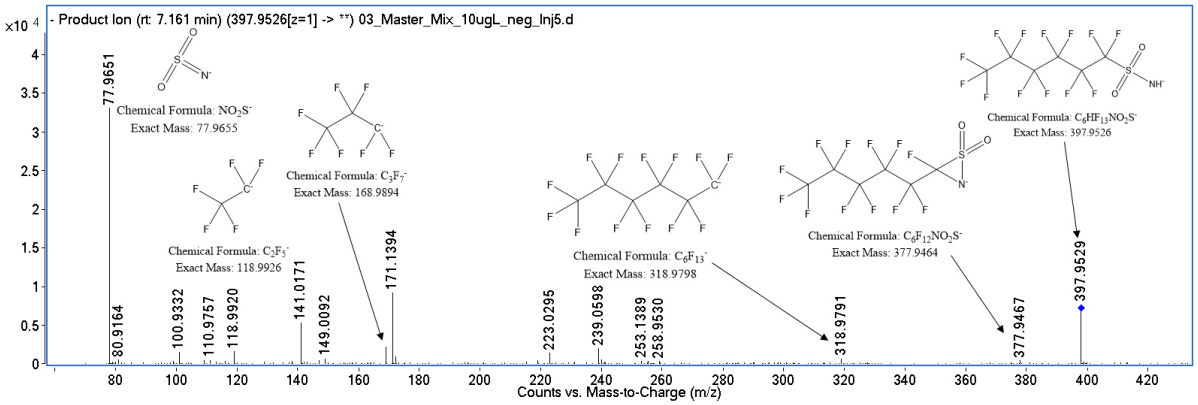

Fig. S26b: MS^2 spectrum (ESI$^-$, 26.9 eV, reference standard) of PFHxSAm (m/z 397.9526, 7.161 min).

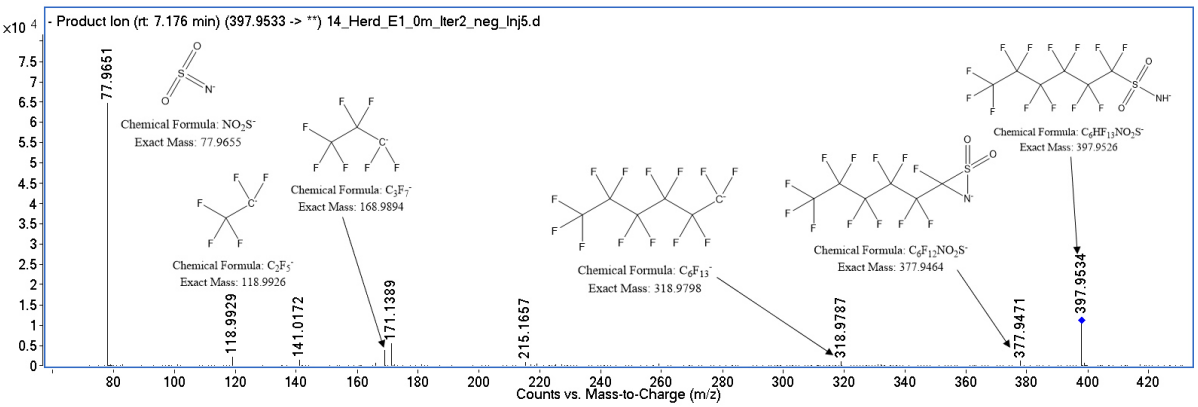

Fig. S26c: MS^2 spectrum (ESI$^-$, 26.9 eV, soil *S1*, 0 – 0.5 m, first extract, iterative MS^2) of PFHxSAm (m/z 397.9526, 7.176 min).

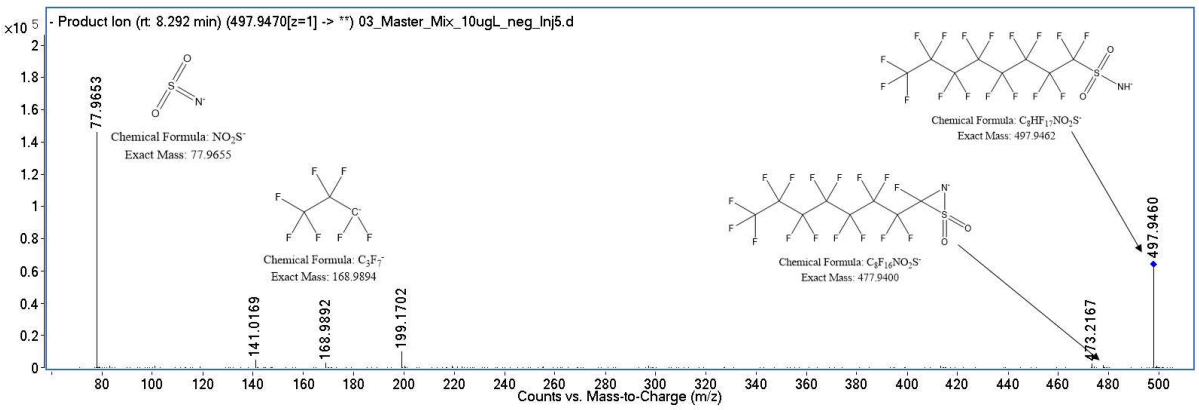

Fig. S26d: MS^2 spectrum (ESI$^-$, 29.9 eV, reference standard) of PFOSAm (m/z 497.9462, 8.292 min).

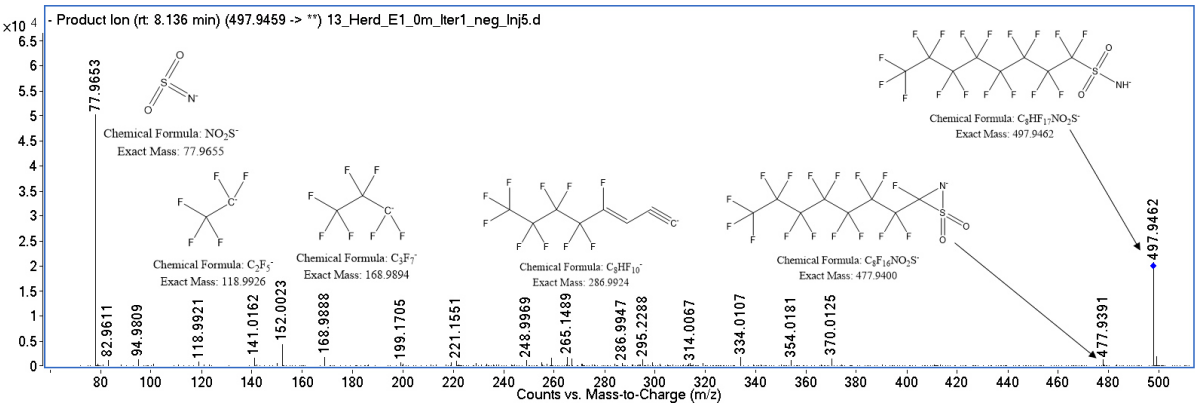

Fig. S26e: MS^2 spectrum (ESI$^-$, 29.9 eV, soil *S1*, 0 – 0.5 m, first extract, iterative MS^2) of PFOSAm (m/z 497.9462, 8.136 min).

PFASAm-Pr-DiMeAm (n = 6, 8)

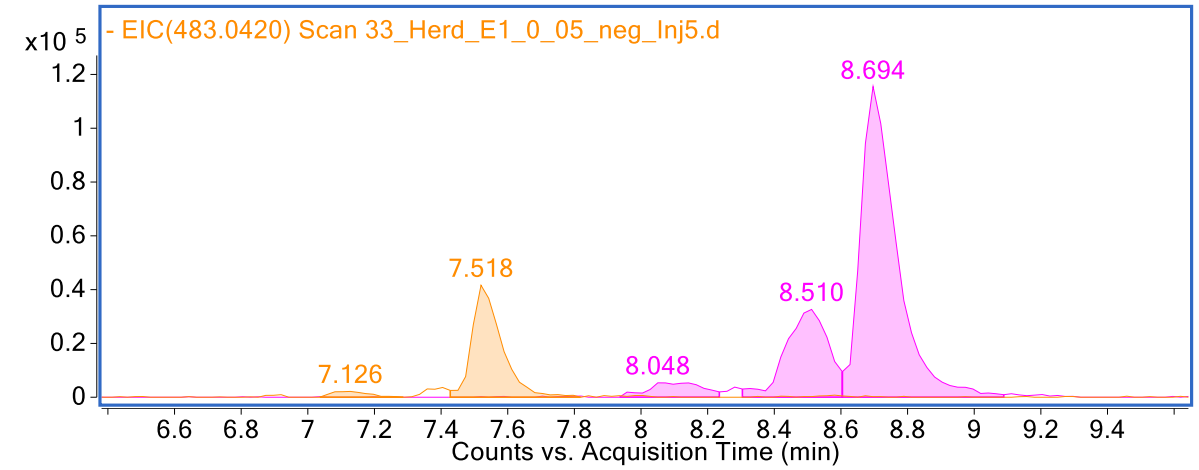

Fig. S27a: Chromatogram (ESI$^-$, soil *s*, 0 – 0.5 m, first extract) of PFHxSAm-Pr-DiMeAm (orange peak, m/z 483.0417, 7.126 and 7.518 min) and PFOSAm-Pr-DiMeAm (pink peak, m/z 583.0353, 8.510 and 8.694 min).

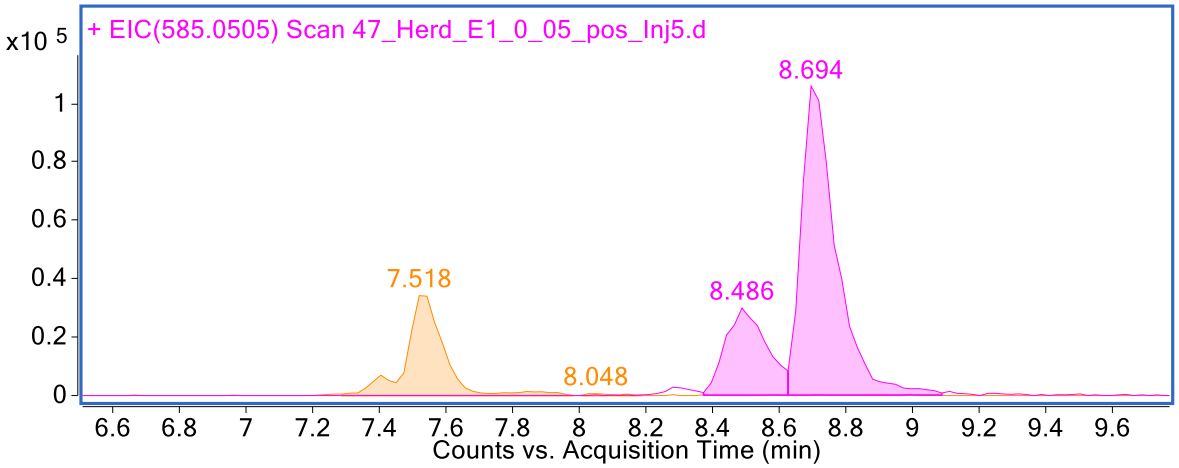

Fig. S27b: Chromatogram (ESI$^+$, soil *S1*, 0 – 0.5 m, first extract) of PFHxSAm-Pr-DiMeAm (orange peak, m/z 485.0563, 7.518 min) and PFOSAm-Pr-DiMeAm (pink peak, m/z 585.0499, 8.486 and 8.694 min).

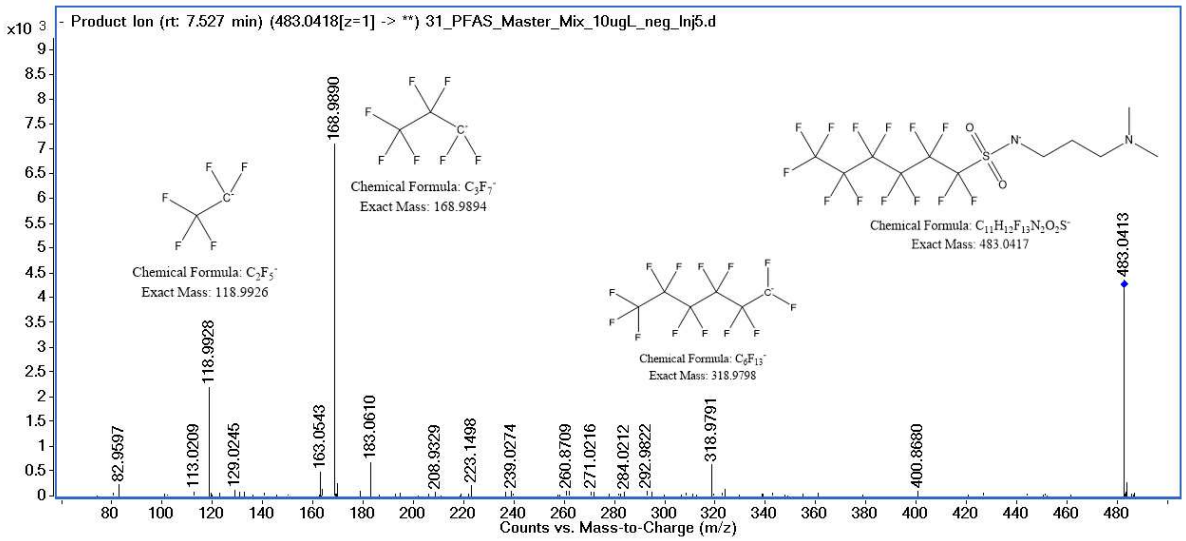

Fig. S27c: MS^2 spectrum (ESI$^-$, 29.5 eV, reference standard) of PFHxSAm-Pr-DiMeAm (m/z 483.0417, 7.527 min).

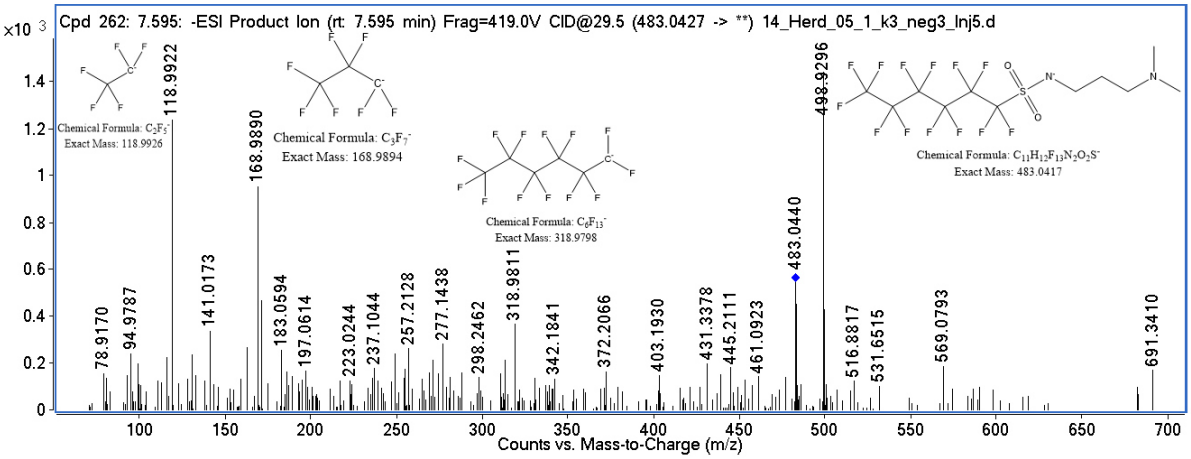

Fig. S27d: MS^2 spectrum (ESI$^-$, 29.5 eV, soil *S1*, 0.5 – 1 m, combined extract, iterative MS^2) of PFHxSAm-Pr-DiMeAm (m/z 483.0417, 7.595 min).

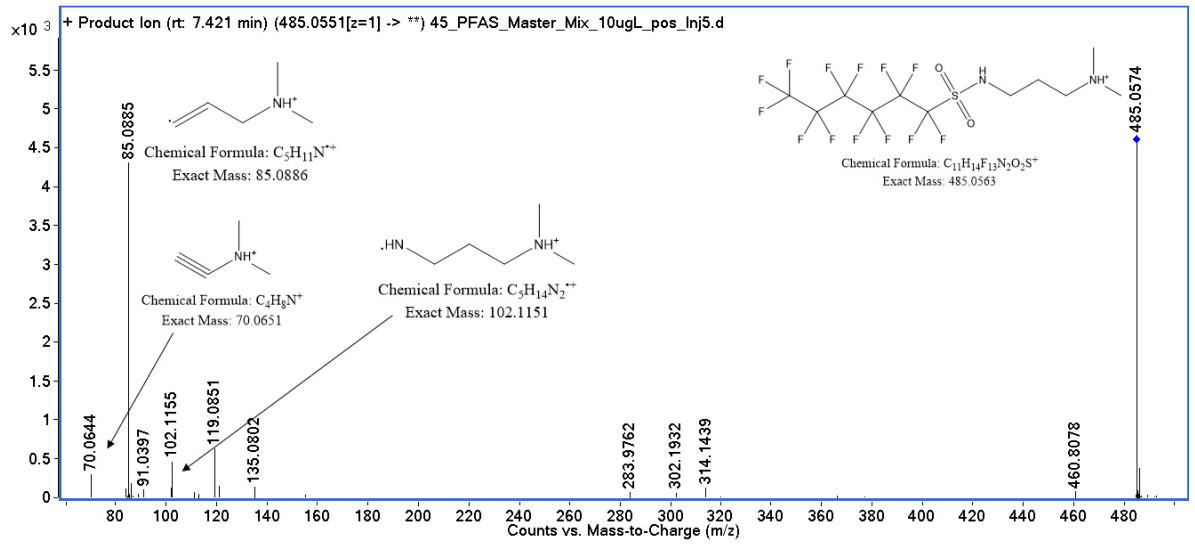

Fig. S27e: MS^2 spectrum (ESI$^+$, 29.6 eV, reference standard) of PFHxSAm-Pr-DiMeAm (m/z 485.0563, 7.421 min).

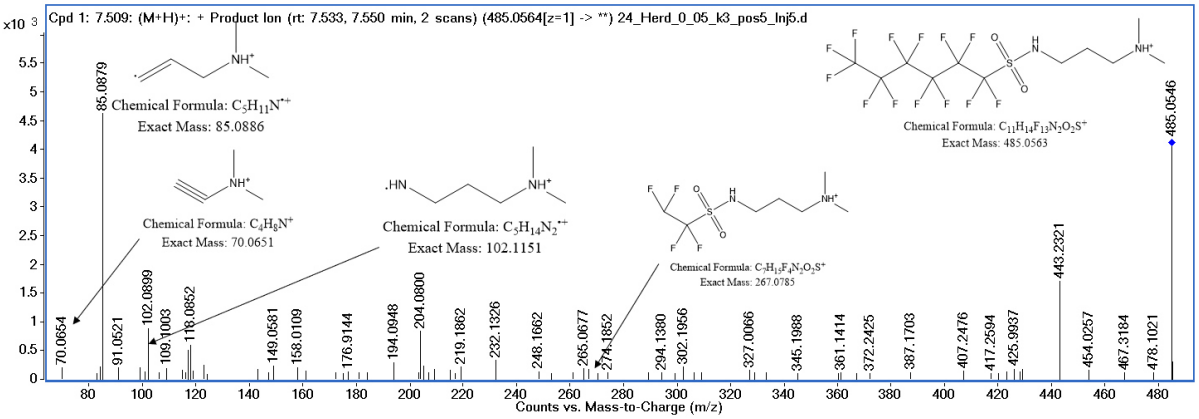

Fig. S27f: MS^2 spectrum (ESI$^+$, 29.6 eV, soil *S1*, 0 – 0.5 m, combined extract, iterative MS^2) of PFHxSAm-Pr-DiMeAm (m/z 485.0563, 7.533 and 7.550 min).

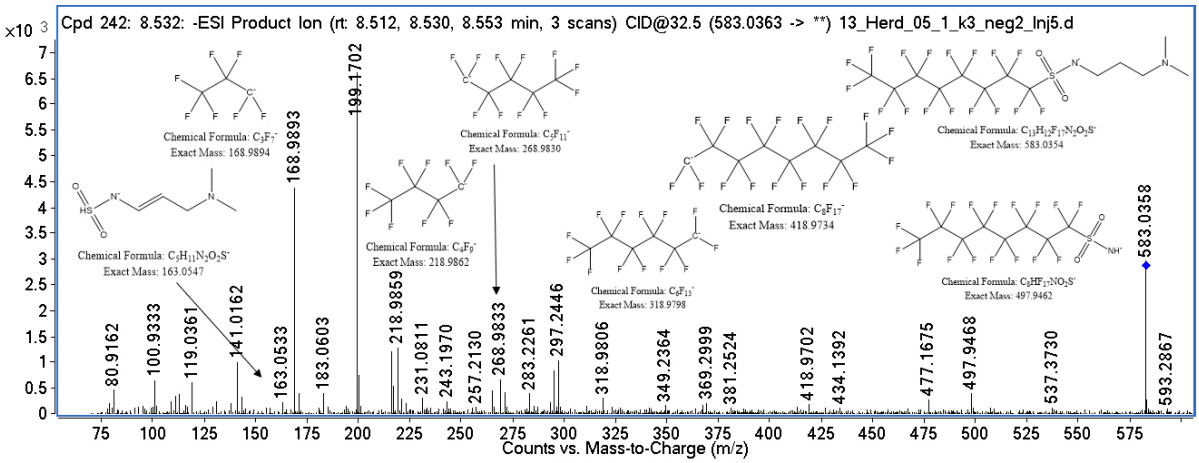

Fig. S27g: MS^2 spectrum (ESI$^-$, 32.5 eV, soil *S1*, 0.5 – 1 m, combined extract, iterative MS^2) of PFOSAm-Pr-DiMeAm (m/z 583.0353, 8.512, 8.530 and 8.553 min).

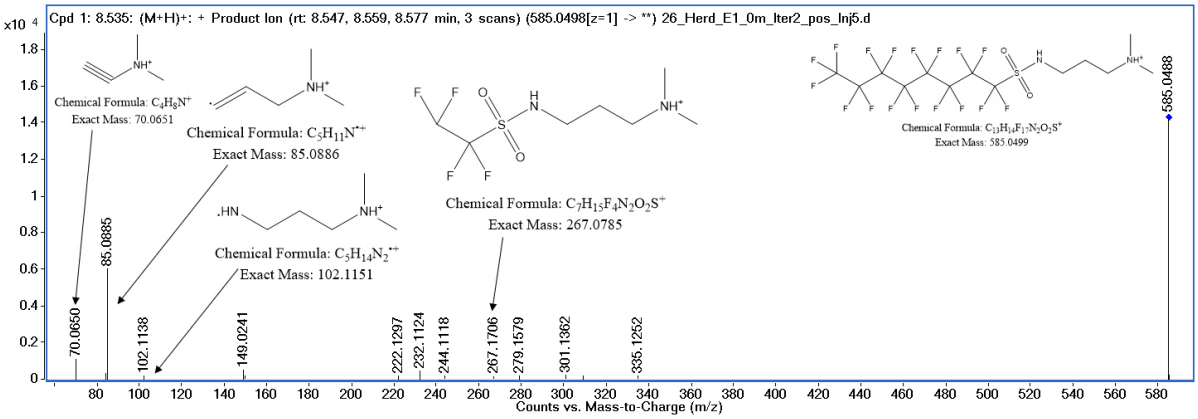

Fig. S27h: MS^2 spectrum (ESI^+, 32.6 eV, soil *S1*, 0 – 0.5 m, first extract, iterative MS^2) of PFOSAm-Pr-DiMeAm (m/z 585.0499, 8.547, 8.559 and 8.577 min).

PFASAm-EtAs (n = 6, 8)

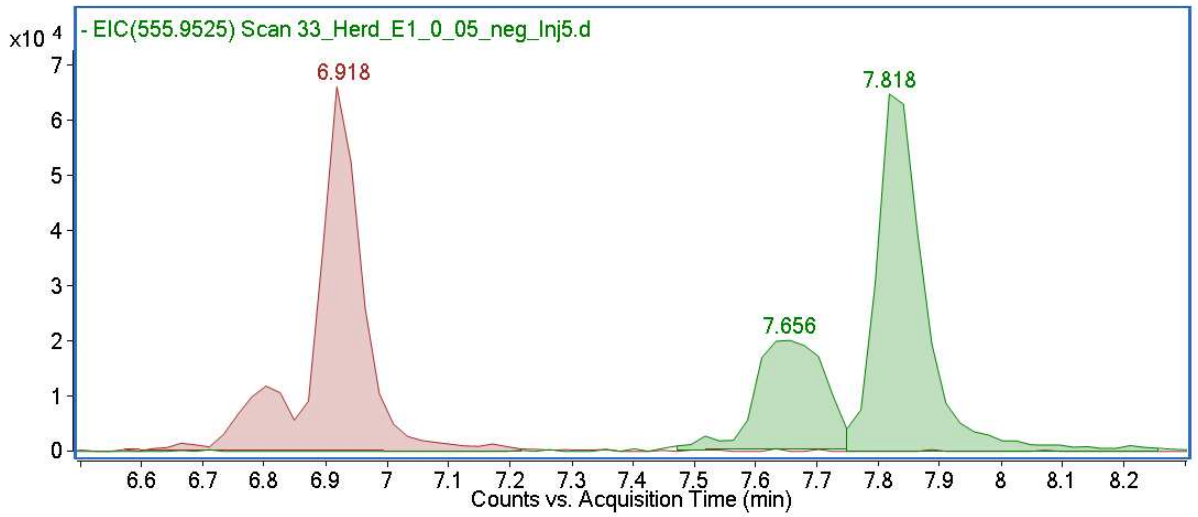

Fig. S28a: Chromatogram (ESI^-, soil *S1*, 0 – 0.5 m, first extract) of PFASA-EtA (n = 6 (red, m/z 455.9581, 6.918 min) and 8 (green, m/z 555.9517, 7.656 and 7.818 min)).

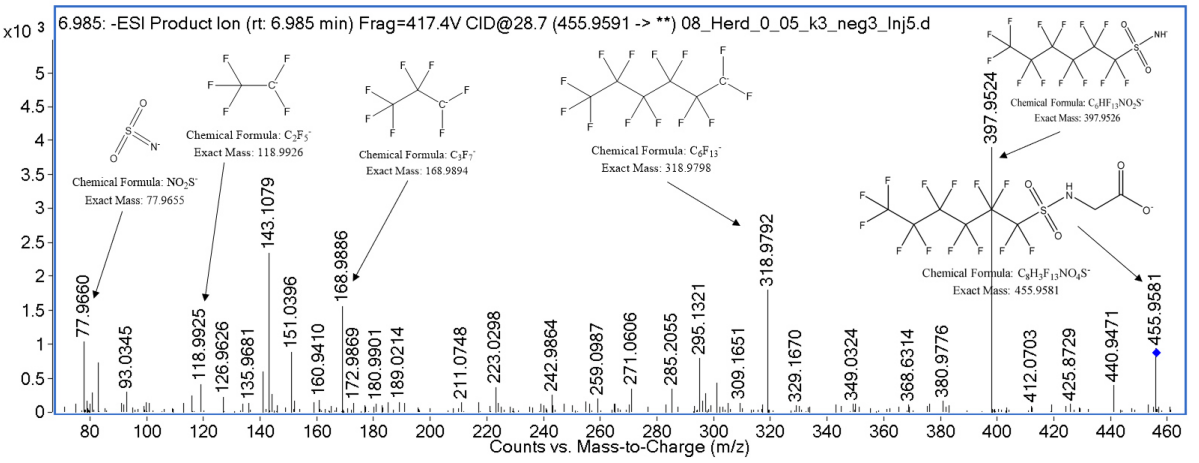

Fig. S28b: MS^2 spectrum (ESI^-, 28.7 eV, soil *S1*, 0 – 0.5 m, combined extract, iterative MS^2) of PFHxSAm-EtA (m/z 455.9581, 6.985 min).

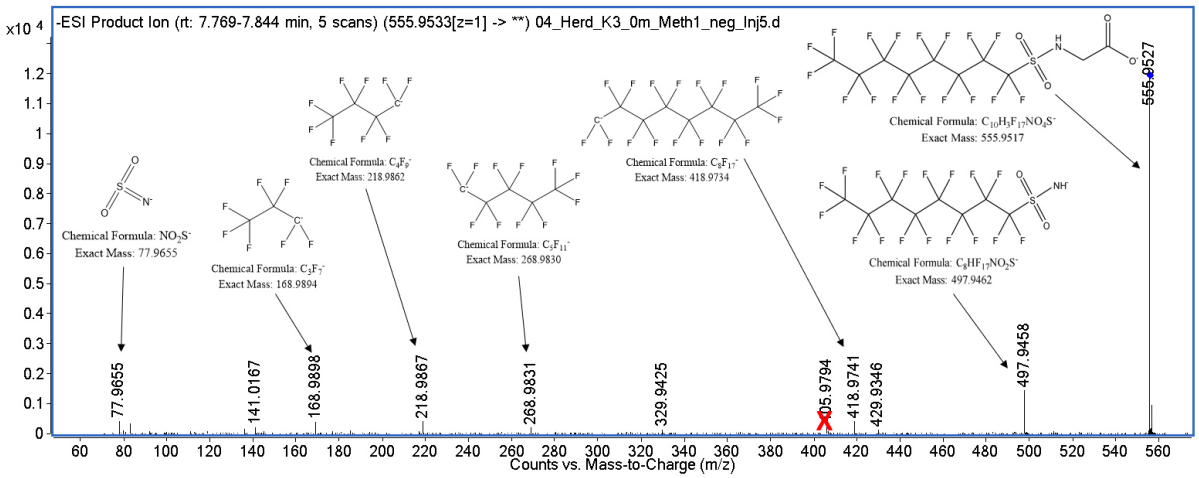

Fig. S28c: MS^2 spectrum (ESI^-, different CEs (10 – 40 eV), soil *S1*, 0 – 0.5 m, combined extract, targeted MS^2) of PFOSAm-EtA (m/z 555.9517, 7.769 – 7.844 min).

PFASAm-PrSAs (n = 4, 5, 6)

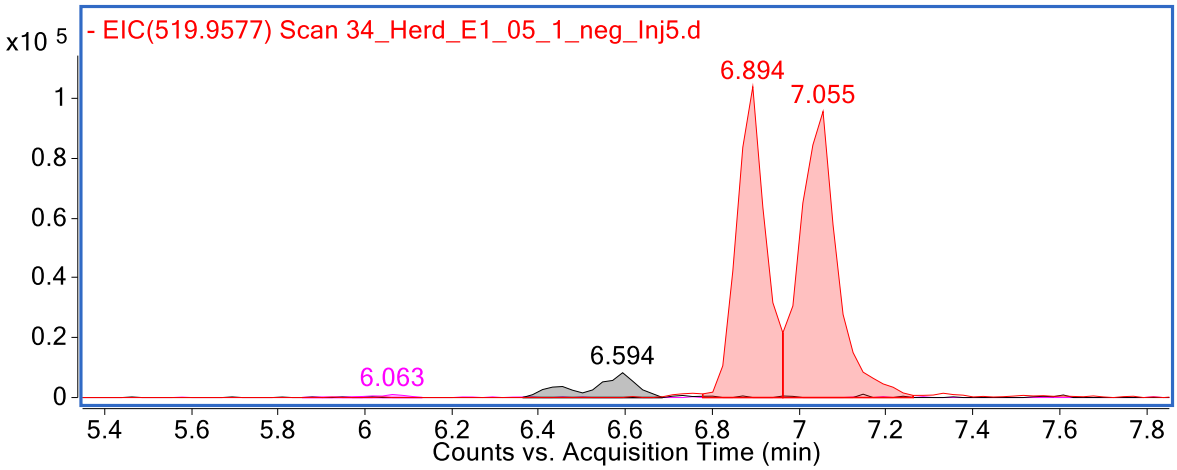

Fig. S29a: Chromatogram (ESI^-, soil *S1*, 0.5 – 1 m, first extract) of PFASAm-PrSAs (n = 4 (pink, m/z 419.9627, 6.063 min), 5 (grey, m/z 469.9595, 6.594 min), and 6 (red, m/z 519.9564, 6.894 and 7.055 min)).

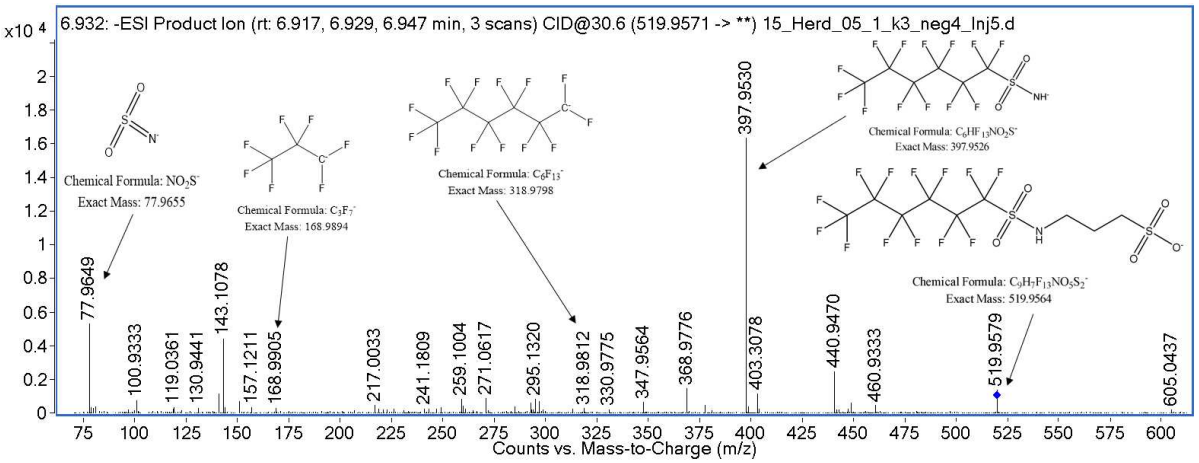

Fig. S29b: MS^2 spectrum (ESI^-, 30.6 eV, soil *S1*, 0.5 – 1 m, combined extract, iterative MS^2) of PFHxSAm-PrSA (m/z 519.9564, 6.917, 6.929, and 6.947 min).

PFASAm-Pr-Bs (n = 6, 8)

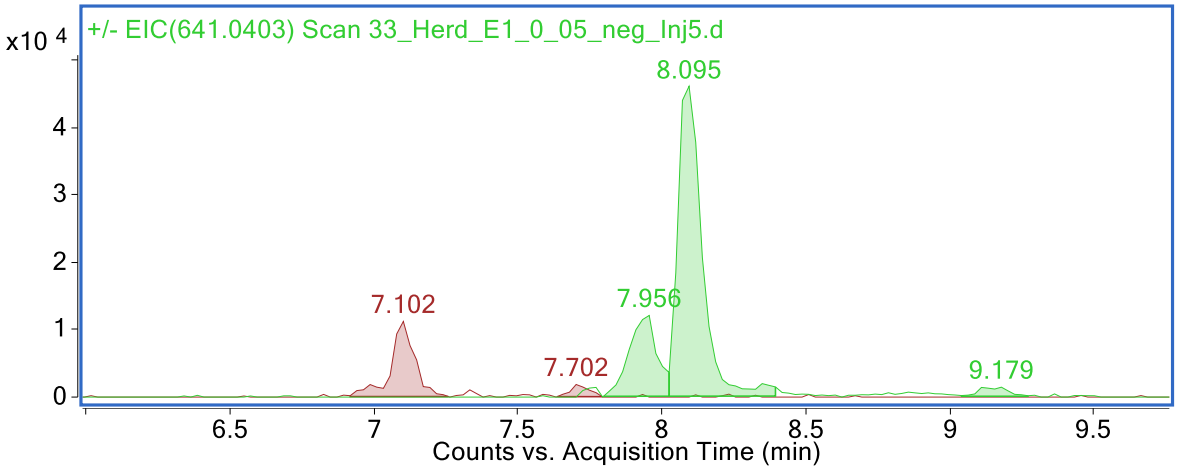

Fig. S30a: Chromatogram (ESI$^-$, soil *S1*, 0 – 0.5 m, first extract) of PFASAm-Pr-Bs (n = 6 (red, m/z 541.0472, 7.102 min) and 8 (green, m/z 641.0408, 7.956 and 8.095 min)).

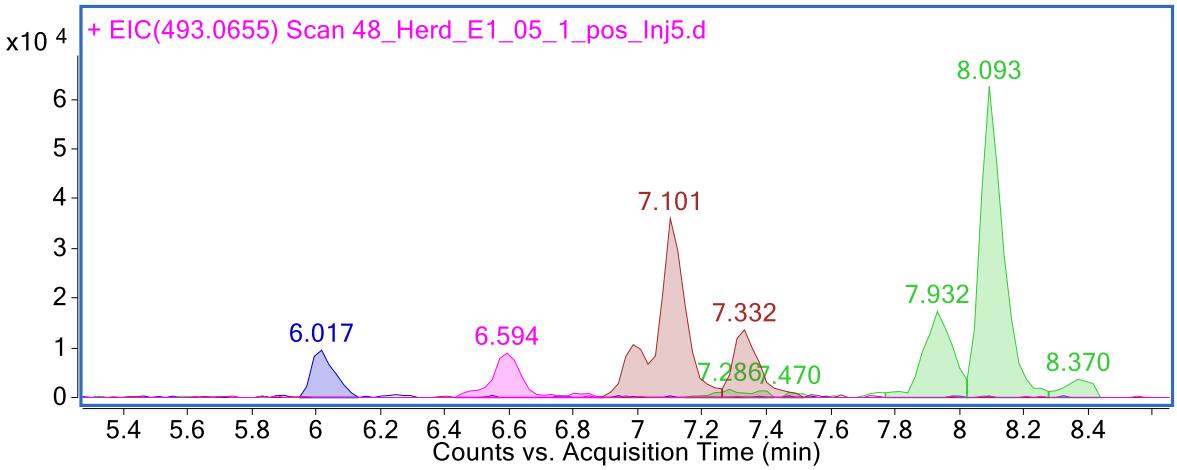

Fig. S30b: Chromatogram (ESI$^+$, soil *S1*, 0.5 – 1 m, first extract) of PFASAm-Pr-Bs (n = 4 (blue, m/z 443.0682, 6.017 min), 5 (pink, m/z 493.0650, 6.594 min), 6 (red, m/z 543.0618, 7.101 and 7.332 min), and 8 (green, m/z 643.0554, 7.932, 8.093, and 8.370 min)).

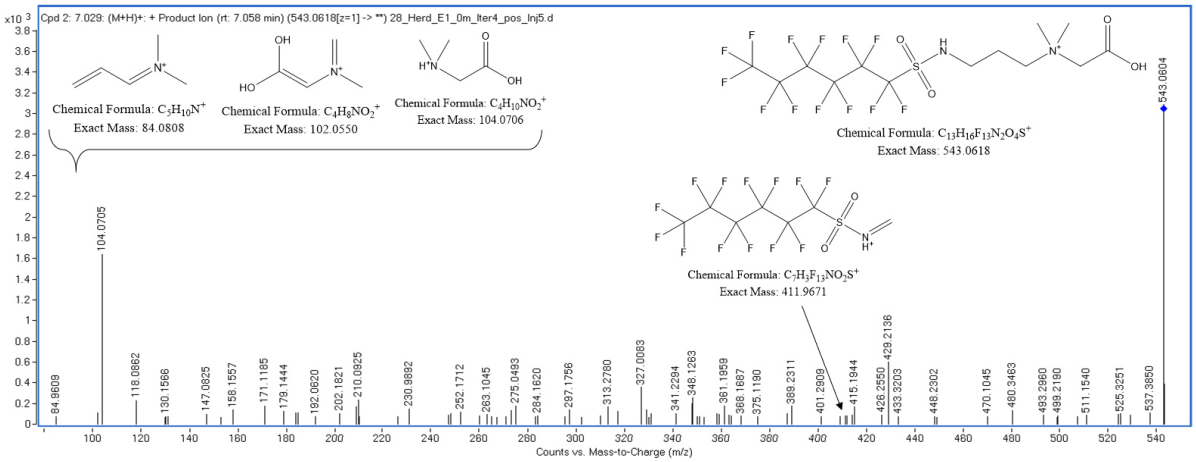

Fig. S30c: MS^2 spectrum (ESI$^+$, 31.3 eV, soil *S1*, 0 – 0.5 m, first extract, iterative MS^2) of PFHxSAm-Pr-B (m/z 543.0618, 7.058 min).

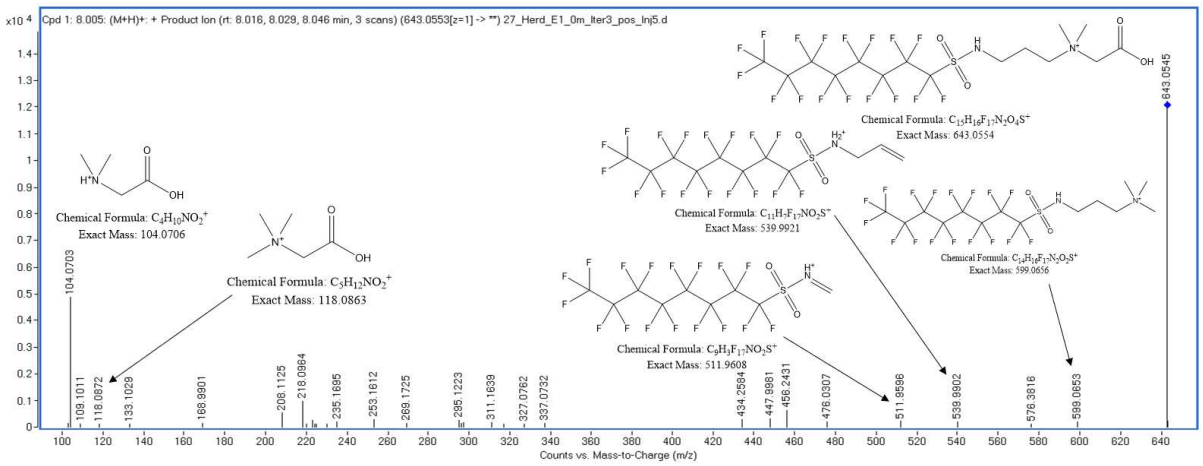

Fig. S30d: MS^2 spectrum (ESI$^+$, 34.3 eV, soil *S1*, 0 – 0.5 m, first extract, iterative MS^2) of PFOSAm-Pr-B (m/z 643.0554, 8.016, 8.029, and 8.046 min).

PFASAm-Pr-TriMeAms (n = 6, 8)

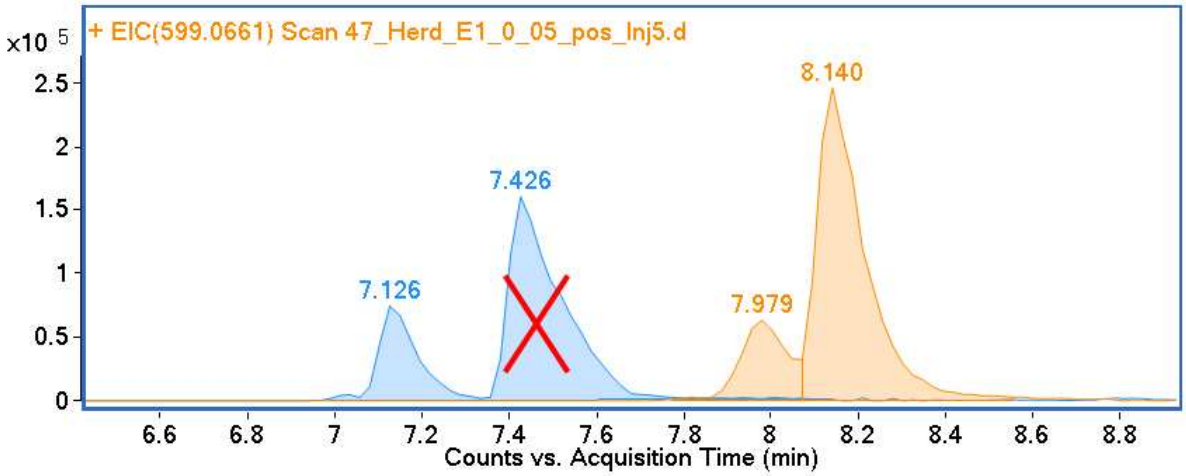

Fig. S31a: Chromatogram (ESI$^+$, soil *S1*, 0 – 0.5 m, first extract) of PFASAm-Pr-TriMeAms (n = 6 (blue, m/z 499.0719, 7.126 min) and 8 (orange, m/z 599.0656, 7.979 and 8.140 min)). Note: The second peak of PFHxSAm-Pr-TriMeAm (blue) is crossed out as it belongs to 6:2 FTSAm-Pr-MeAm.

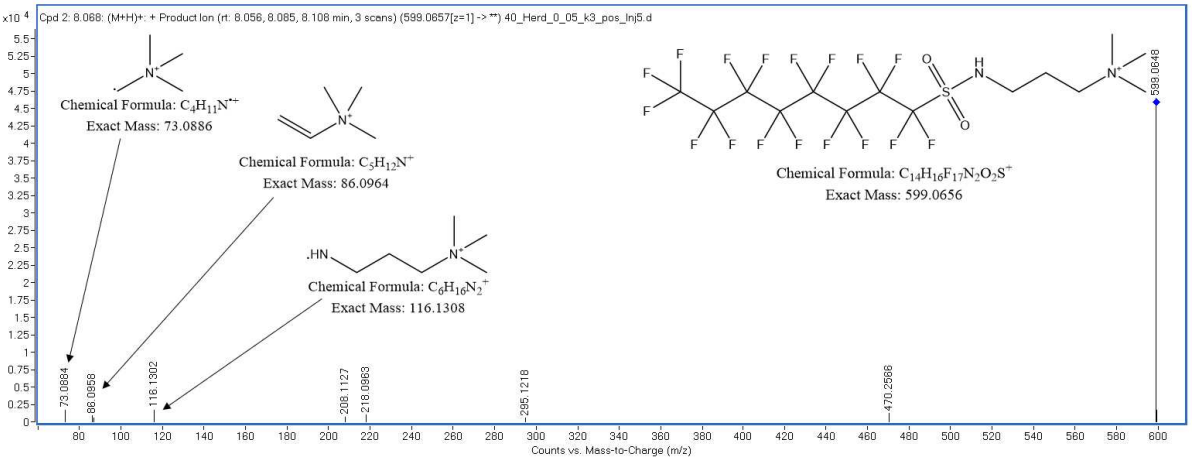

Fig. S31b: MS^2 spectrum (ESI$^+$, 33.0 eV, soil *S1*, 0 – 0.5 m, combined extract) of PFOSAm-Pr-TriMeAm (m/z 599.0656, 8.056, 8.085, and 8.108 min).

PFASAm-Mes (n = 4, 6, 8)

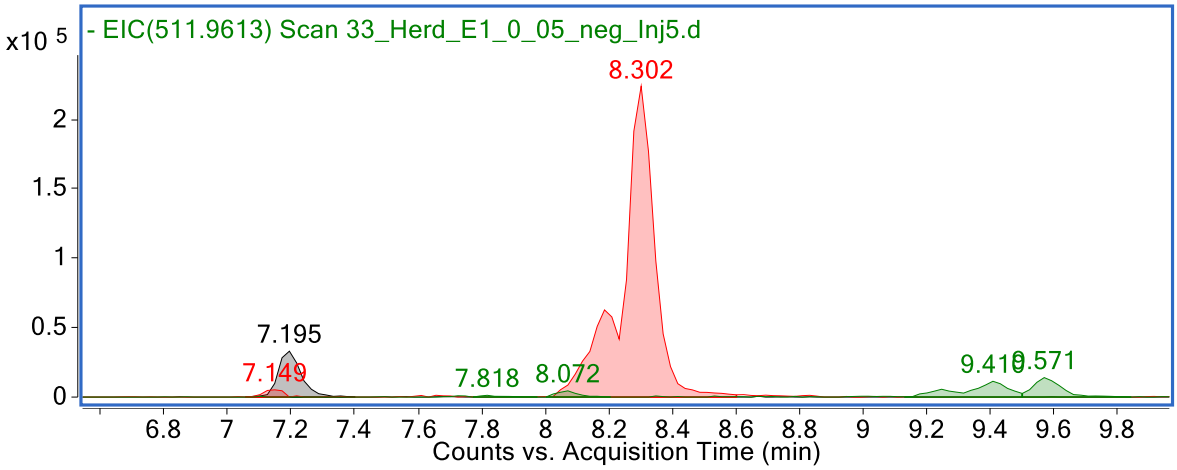

Fig. S32a: Chromatogram (ESI$^-$, soil *S1*, 0 – 0.5 m, first extract) of PFASAm-Mes (n = 4 (grey, m/z 311.9746, 7.195 min), 6 (red, m/z 411.9682, 8.302 min), and 8 (green, m/z 511.9619, 9.410 min)).

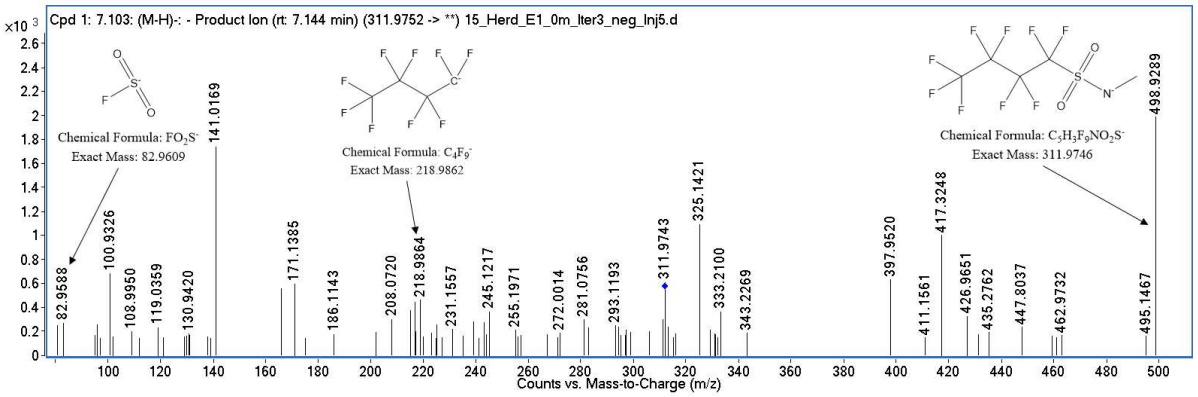

Fig. S32b: MS^2 spectrum (ESI$^-$, 24.4 eV, soil *S1*, 0 – 0.5 m, first extract, iterative MS^2) of PFBSAm-Me (m/z 311.9746, 7.144 min).

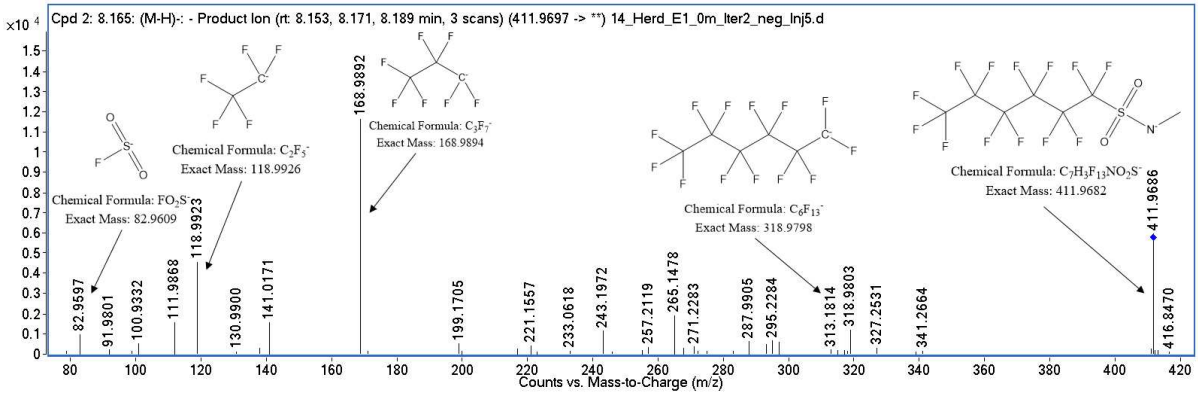

Fig. S32c: MS^2 spectrum (ESI$^-$, 27.4 eV, soil *S1*, 0 – 0.5 m, first extract, iterative MS^2) of PFHxSAm-Me (m/z 411.9682, 8.153, 8.171, and 8.189 min).

PFASAm-*N*-PrSA-*N*-Pr-DiMeAms (n = 4, 5, 6)

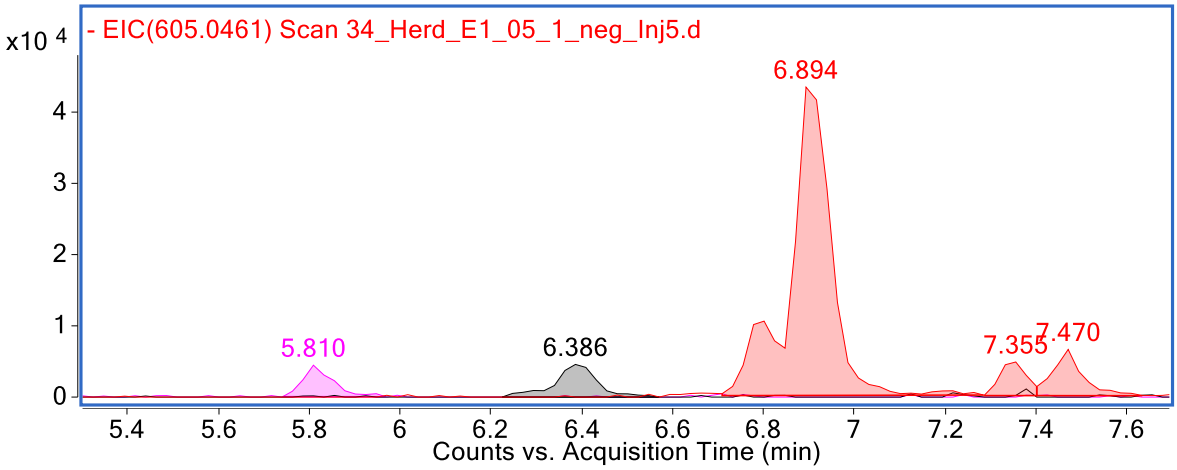

Fig. S33a: Chromatogram (ESI$^-$, soil *S1*, 0.5 – 1 m, first extract) of PFASAm-*N*-PrSA- -*N*-Pr-DiMeAms (n = 4 (pink, m/z 505.0519, 5.810 min), 5 (grey, m/z 555.0487, 6.386 min), and 6 (red, m/z 605.0455, 6.894 min)).

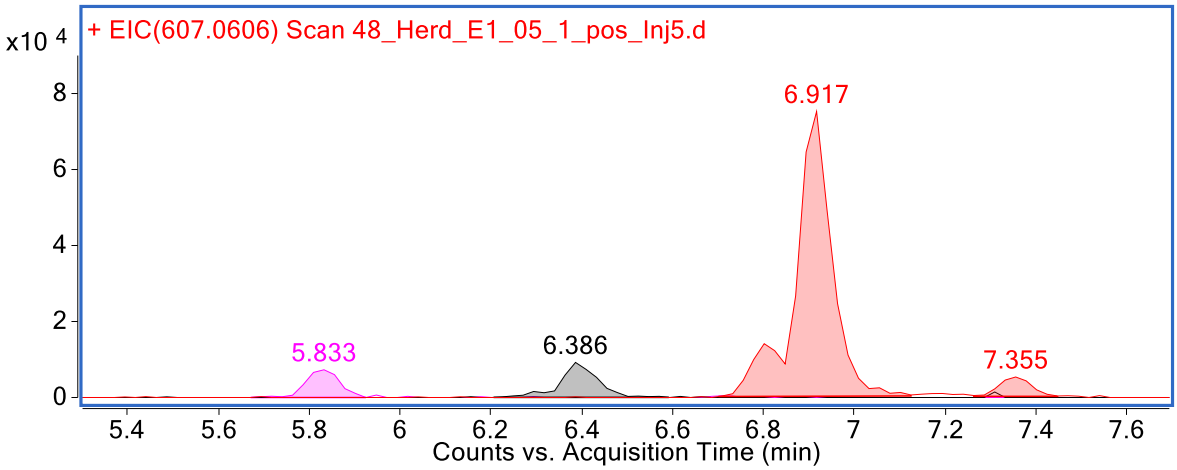

Fig. S33b: Chromatogram (ESI$^+$, soil *S1*, 0.5 – 1 m, first extract) of PFASAm-*N*-PrSA--*N*-Pr-DiMeAms (n = 4 (pink, m/z 557.0633, 5.833 min), 5 (grey, m/z 557.0633, 6.386 min), and 6 (red, m/z 607.0601, 6.917 min)).

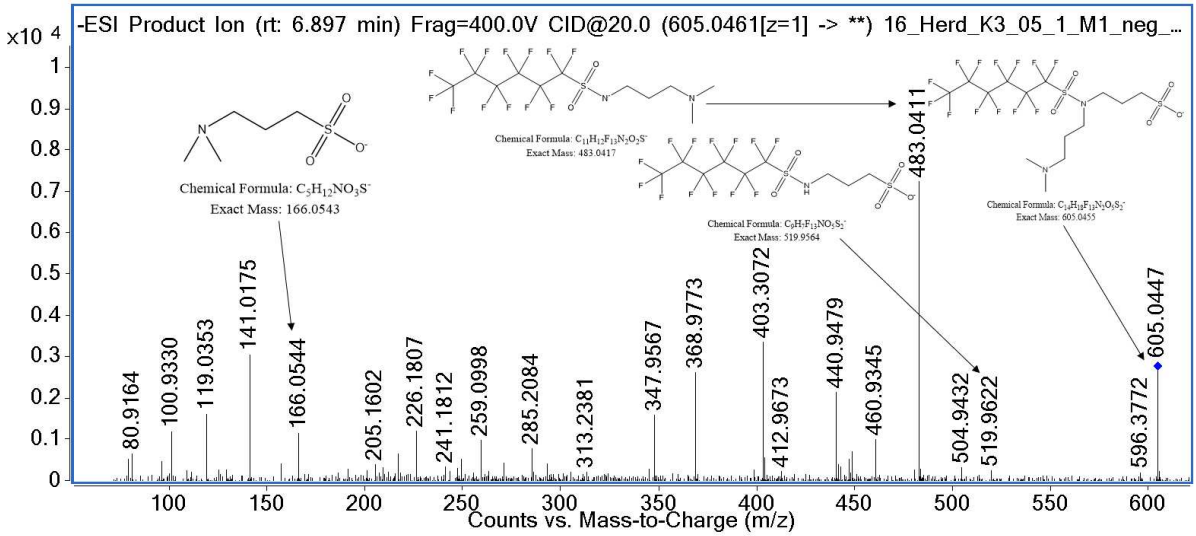

Fig. S33c: MS^2 spectrum (ESI$^-$, 20.0 eV, soil *S1*, 0.5 – 1 m, combined extract, targeted MS^2) of PFHxSAm-*N*-PrSA--*N*-Pr-DiMeAm (m/z 605.0455, 6.897 min).

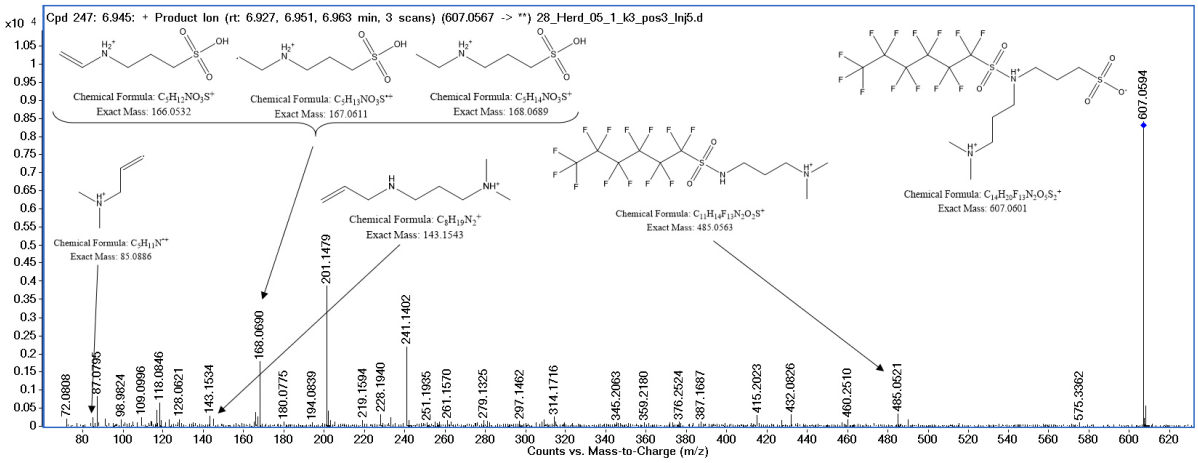

Fig. S33d: MS^2 spectrum (ESI^+, 33.2 eV, soil *S1*, 0.5 – 1 m, combined extract, iterative MS^2) of PFHxSAm-*N*-PrSA--*N*-Pr-DiMeAm (m/z 607.0601, 6.927, 6.951, and 6.963 min).

4. FTBs

n:1:2 FTBs (n = 5, 7, 9, 11, 13, 15)

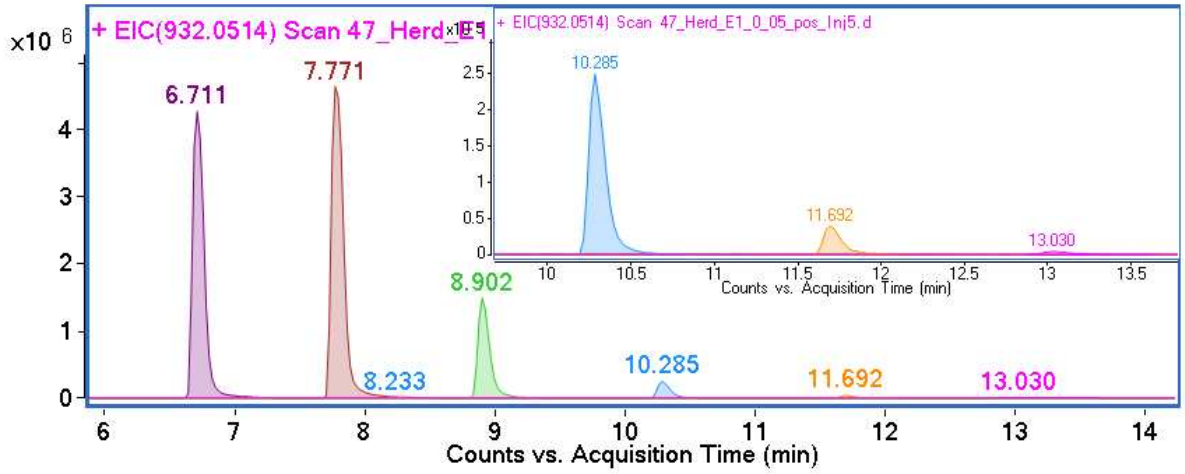

Fig. S34a: Chromatogram (ESI^+, soil *S1*, 0 – 0.5 m, first extract) of n:1:2 FTBs (n = 5 (violet, m/z 432.0827, 6.711 min), 7 (red, m/z 532.0764, 7.771 min), 9 (green, m/z 632.0700, 8.902 min), 11 (blue, m/z 732.0636, 10.285 min), 13 (orange, m/z 832.0572, 11.692 min), and 15 (pink, m/z 932.0508, 13.030 min)). Scale-up in top right corner.

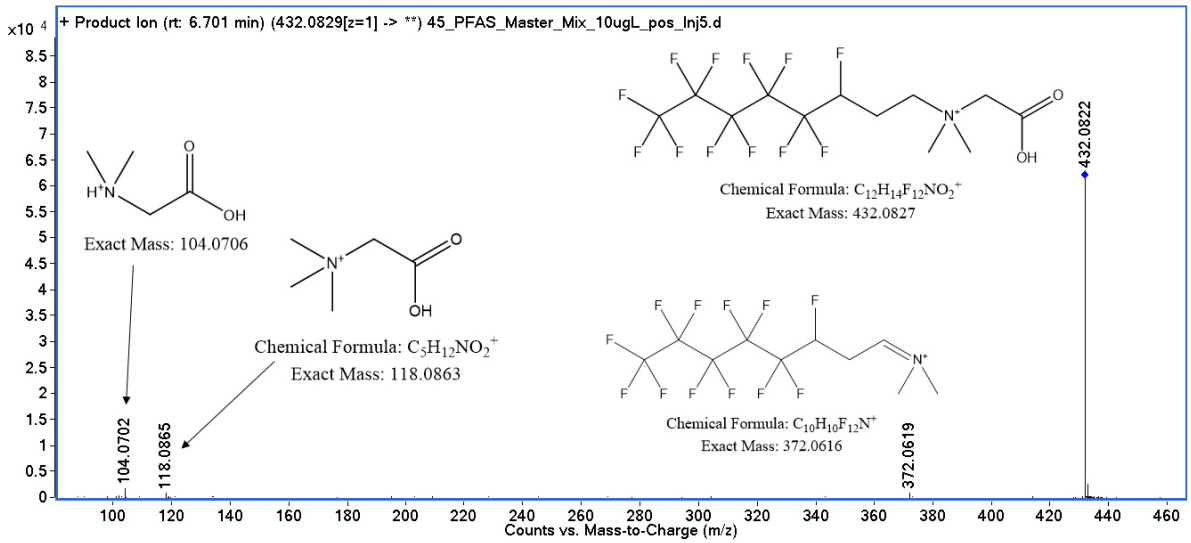

Fig. S34b: MS^2 spectrum (ESI$^+$, 28.0 eV, reference standard) of 5:1:2 FTB (m/z 432.0827, 6.701 min).

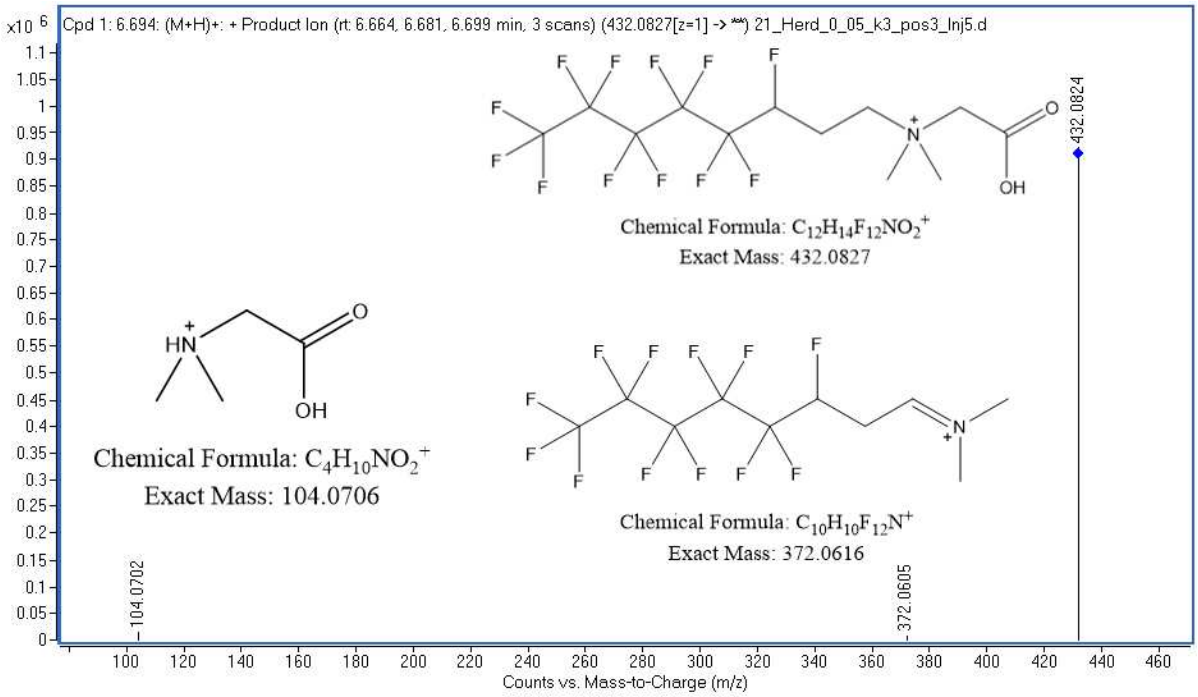

Fig. S34c: MS^2 spectrum (ESI$^+$, 28.0 eV, soil *S1*, 0 – 0.5 m, combined extract, iterative MS^2) of 5:1:2 FTB (m/z 432.0827, 6.694 min).

n:3 FTBs (n = 5, 7, 9, 11, 13)

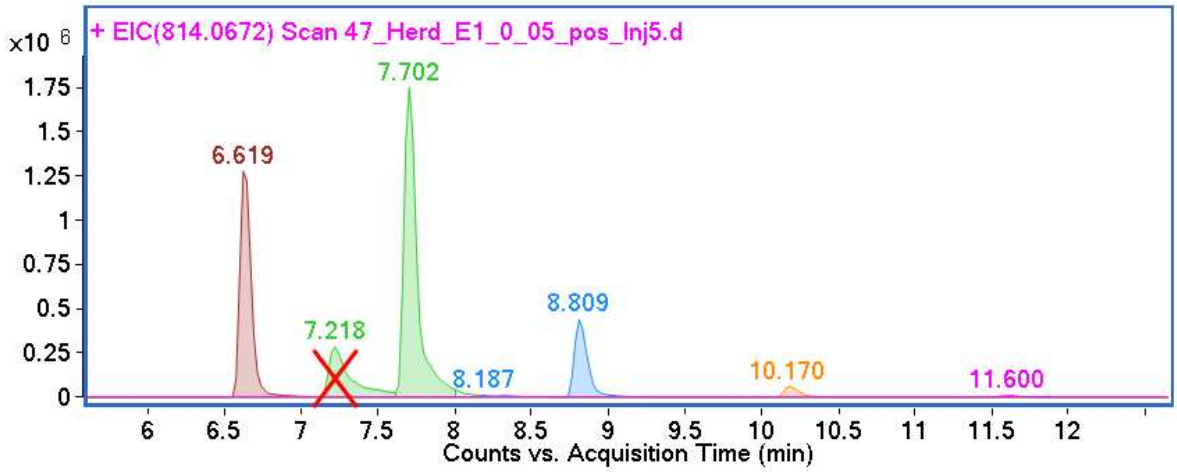

Fig. S35a: Chromatogram (ESI$^+$, soil *S1*, 0 – 0.5 m, first extract) of n:3 FTBs (n = 5 (red, m/z 414.0922, 6.619 min), 7 (green, m/z 514.0858, 7.702 min), 9 (blue, m/z 614.0794, 8.809 min), 11 (orange, m/z 714.0730, 10.170 min), and 13 (pink, m/z 814.0666, 11.600 min)).

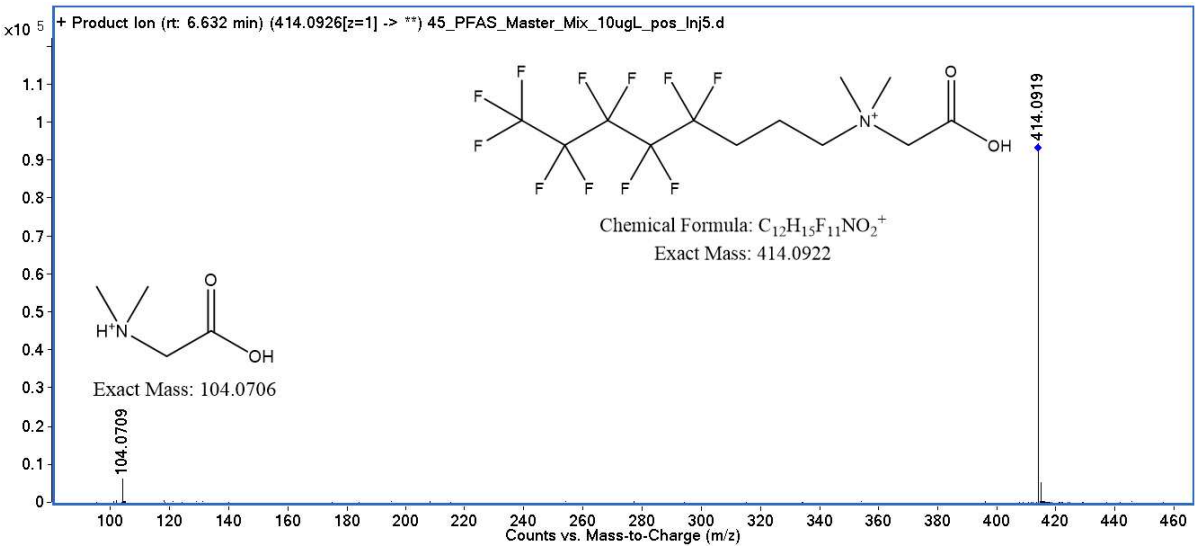

Fig. S35b: MS^2 spectrum (ESI$^+$, 27.4 eV, reference standard) of 5:3 FTB (m/z 414.0922, 6.632 min).

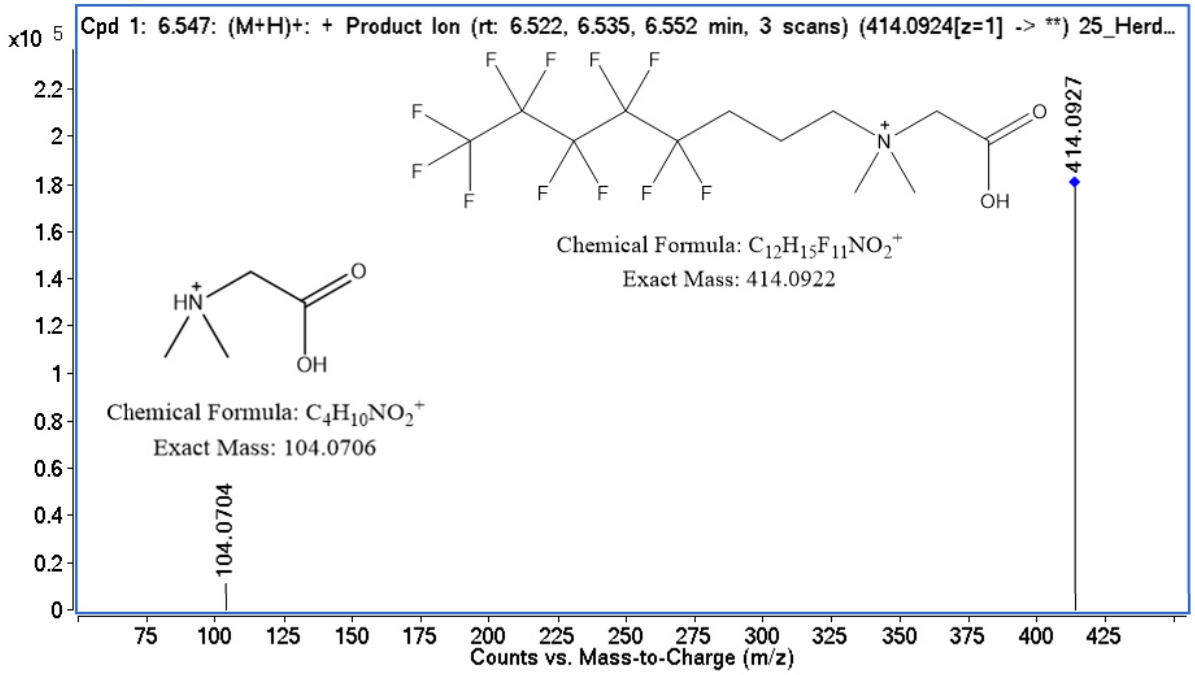

Fig. S35c: MS^2 spectrum (ESI^+, 27.4 eV, soil *S1*, 0 – 0.5 m, first extract, iterative MS^2) of 5:3 FTB (m/z 414.0922, 6.522, 6.535 and 6.552 min).

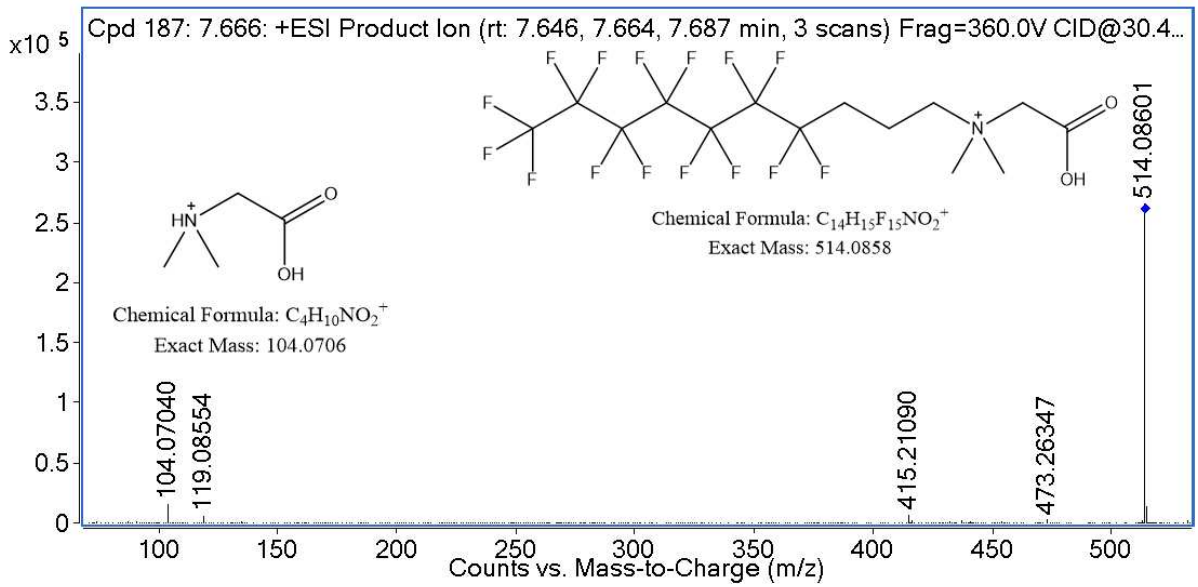

Fig. S35d: MS^2 spectrum (ESI^+, 30.4 eV, soil *S1*, 0 – 0.5 m, first extract, iterative MS^2) of 7:3 FTB (m/z 514.0858, 7.646, 7.664 and 7.687 min).

5. FTSAm-derivatives

n:2 FTSAms (n = 6, 8, 10)

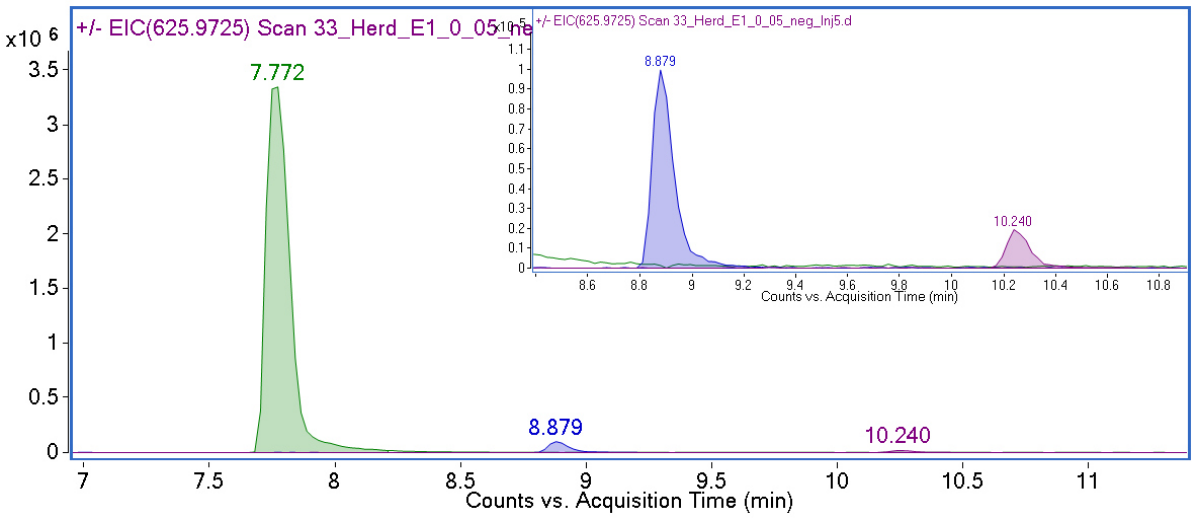

Fig. S36a: Chromatogram (ESI$^-$, soil *S1*, 0 – 0.5 m, first extract) of n:2 FTSAms (n = 6 (green, m/z 425.9839, 7.772 min), 8 (blue, m/z 525.9775, 8.879 min), and 10 (violet, m/z 625.9711, 10.240 min)). Scale-up in top right corner.

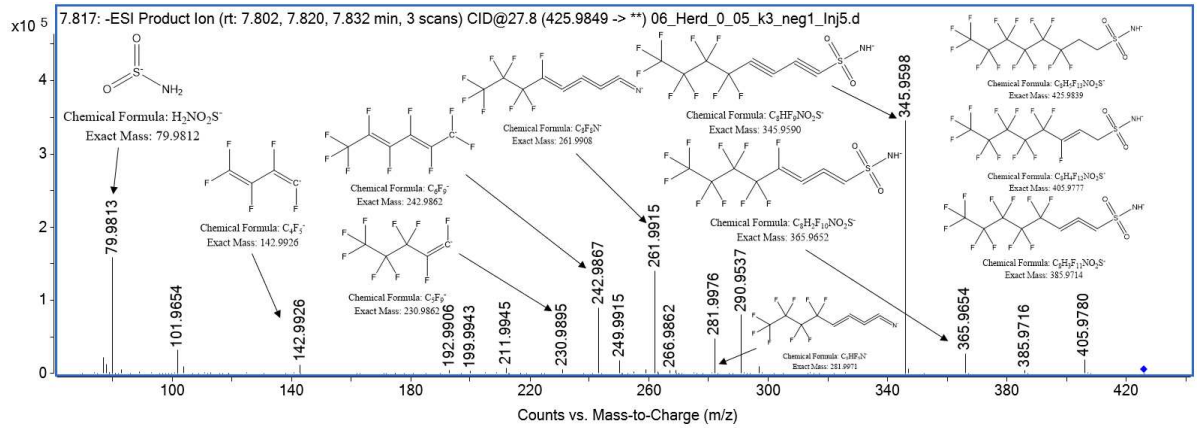

Fig. S36b: MS^2 spectrum (ESI$^-$, 27.8 eV, soil *S1*, 0 – 0.5 m, combined extract, iterative MS^2). of 6:2 FTSAm (m/z 425.9839, 7.802, 7.820, and 7.832 min).

n:2 FTSAm-Pr-Bs (n = 6, 8, 10)

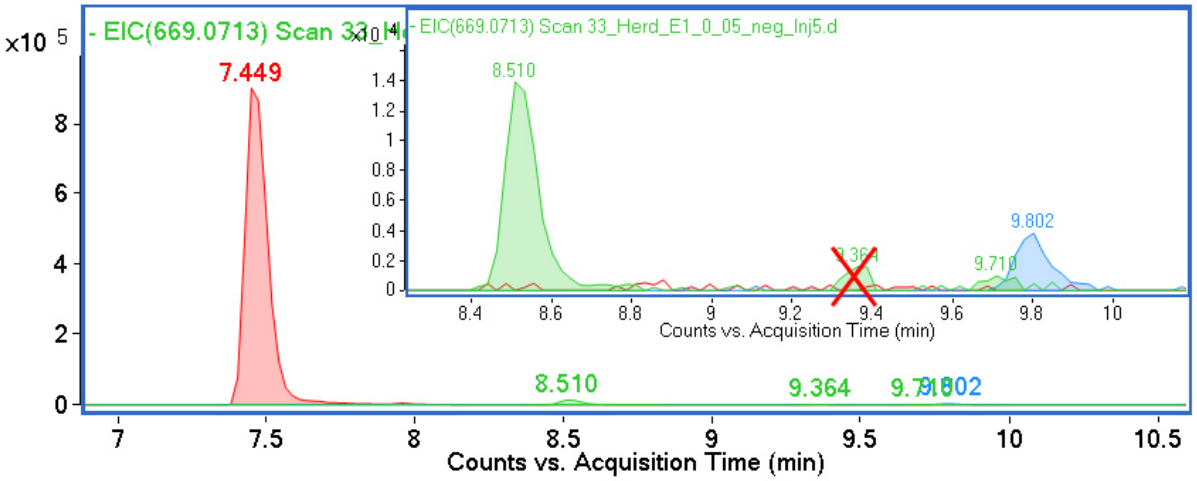

Fig. S37a: Chromatogram (ESI$^-$, soil *S1*, 0 – 0.5 m, first extract) of n:2 FTSAm-Pr-Bs (n = 6 (red, m/z 569.0785, 7.449 min), 8 (green, m/z 669.0721, 8.510 min), and 10 (blue, m/z 769.0657, 9.802 min)).

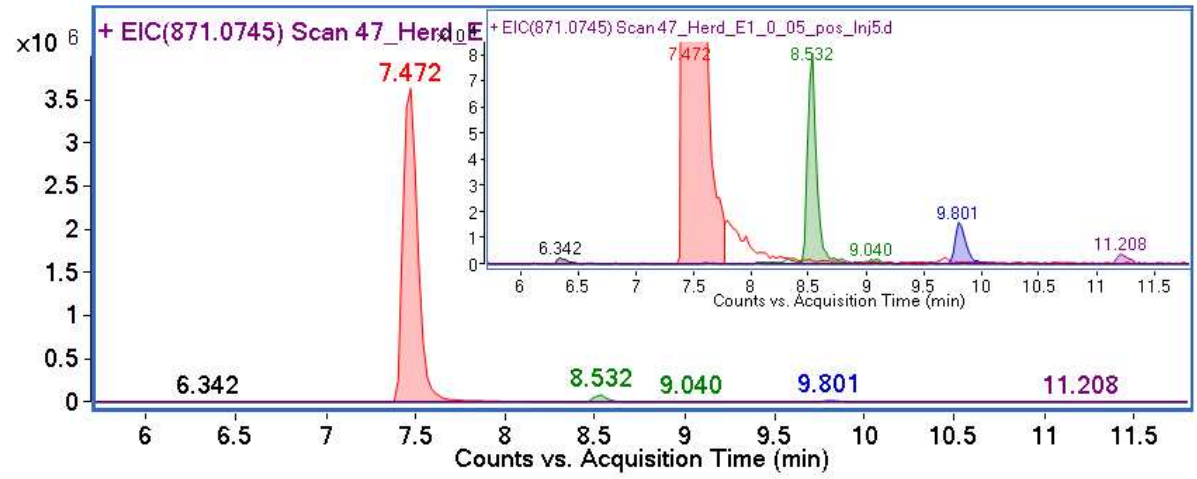

Fig. S37b: Chromatogram (ESI$^+$, soil *S1*, 0 – 0.5 m, first extract) of n:2 FTSAm-Pr-Bs (n = 4 (grey, m/z 471.0995, 6.342 min), 6 (red, m/z 571.0931, 7.472 min), 8 (green, m/z 671.0867, 8.532 min), 10 (blue, m/z 771.0803, 9.801 min), and 12 (violet, m/z 871.0739, 11.208 min)). Scale-up in top right corner.

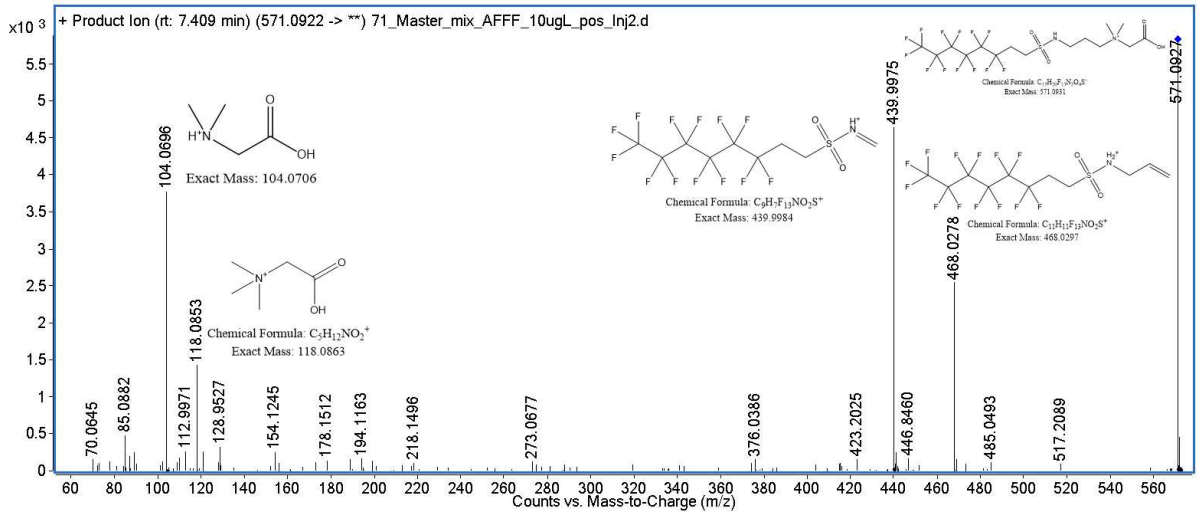

Fig. S37c: MS^2 spectrum (ESI$^+$, 32.1 eV, reference standard) of 6:2 FTSAm-Pr-B (m/z 571.0931, 7.409 min).

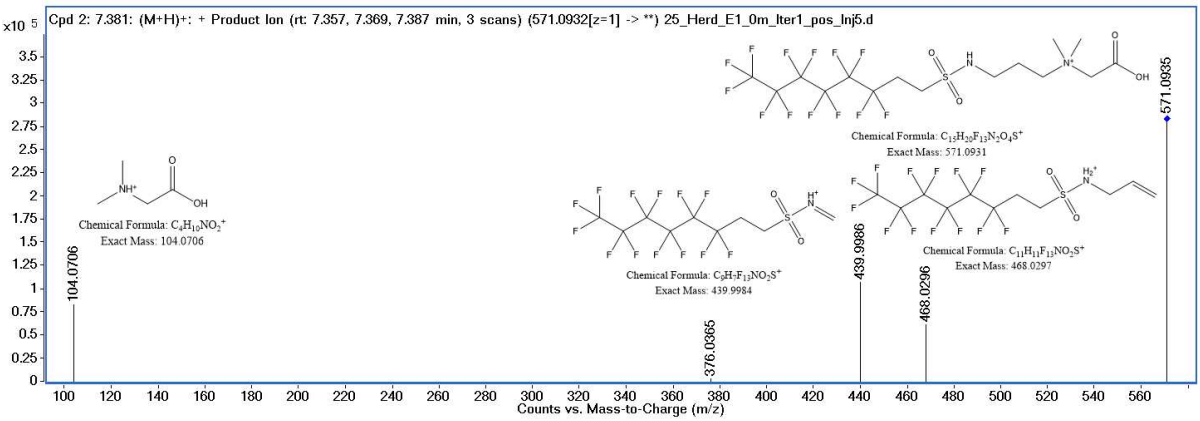

Fig. S37d: MS^2 spectrum (ESI^+, 32.1 eV, soil *S1*, 0 – 0.5 m, first extract, iterative MS^2) of 6:2 FTSAm-Pr-B (m/z 571.0931, 7.357, 7.369 and 7.387 min).

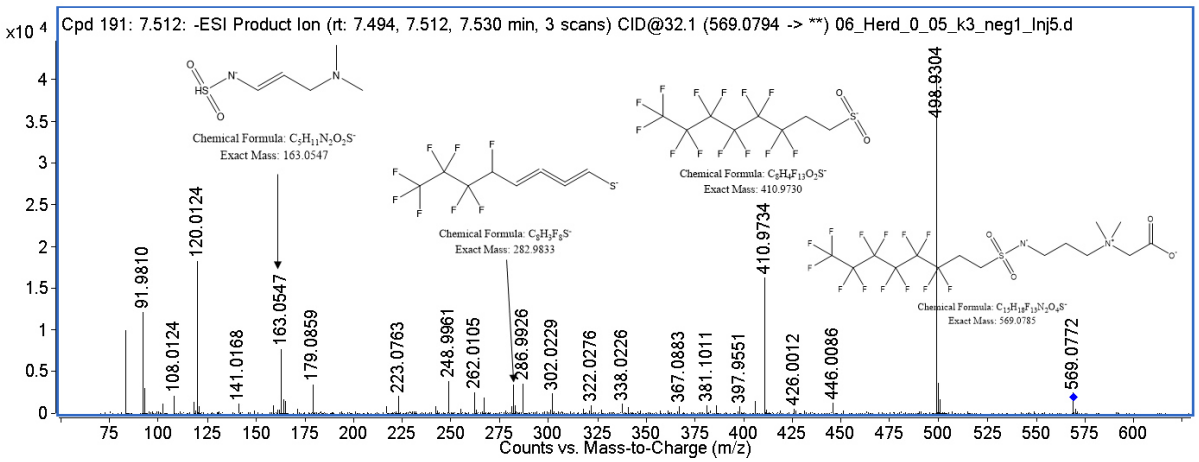

Fig. S37e: MS^2 spectrum (ESI^-, 32.1 eV, soil *S1*, 0 – 0.5 m, combined extract, iterative MS^2) of 6:2 FTSAm-Pr-B (m/z 569.0785, 7.494, 7.512 and 7.530 min).

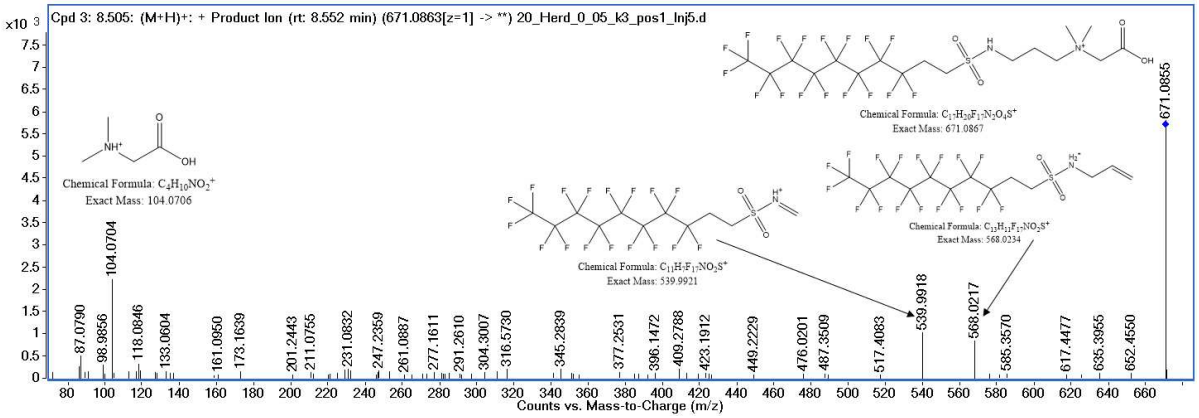

Fig. S37f: MS^2 spectrum (ESI^+, 35.1 eV, soil *S1*, 0 – 0.5 m, combined extract, iterative MS^2) of 8:2 FTSAm-Pr-B (m/z 671.0867, 8.552 min).

n:2 FTSAm-Pr-DiMeNOs (n = 6, 8)

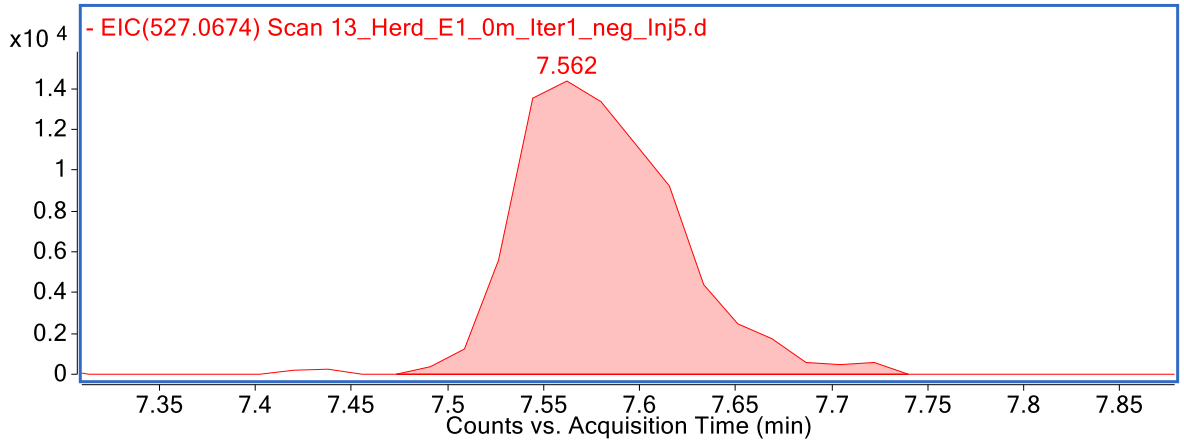

Fig. S38a: Chromatogram (ESI$^-$, soil *S1*, 0 – 0.5 m, first extract) of 6:2 FTSAm-Pr-DiMeNO (red, m/z 527.0680, 7.562 min).

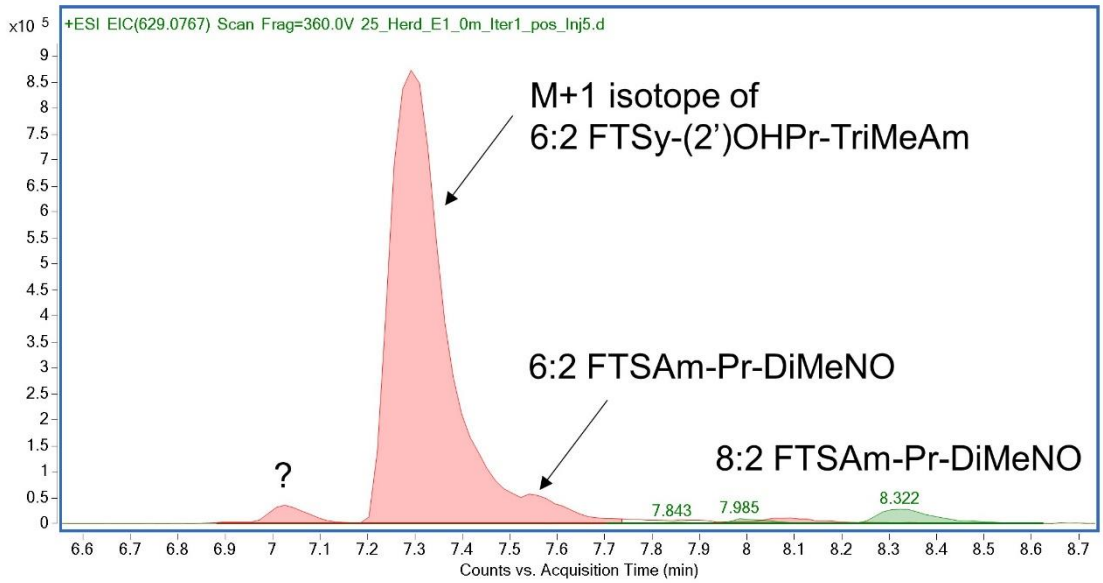

Fig. S38b: Chromatogram (ESI$^+$, soil *S1*, 0 – 0.5 m, first extract) of n:2 FTSAm-Pr-DiMeNOs (n = 6 (red, m/z 529.0825, ≈ 7.57 min) and 8 (green, m/z 629.0761, 8.322 min)).

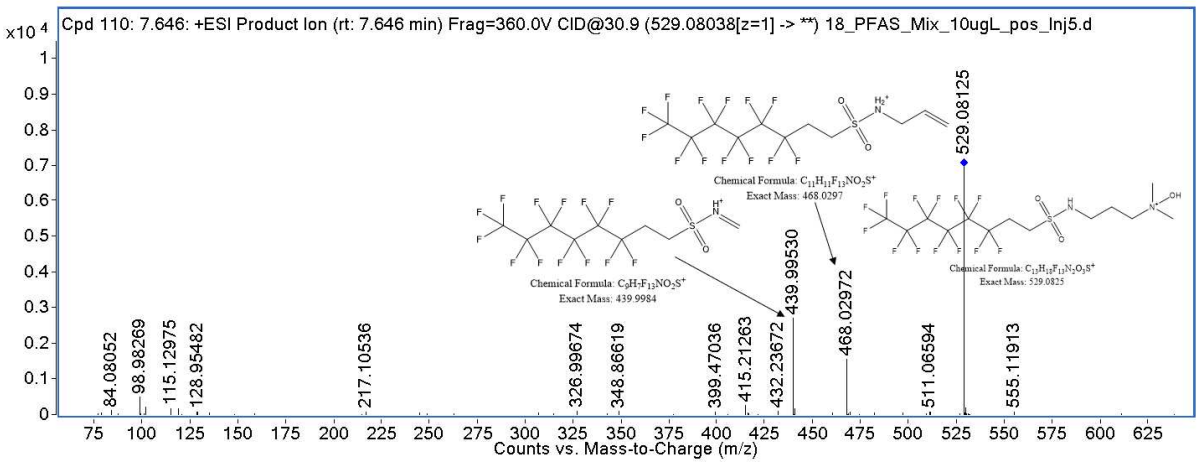

Fig. S38c: MS^2 spectrum (ESI$^+$, 30.9 eV, reference standard) of 6:2 FTSAm-Pr-DiMeNO (m/z 529.0825, 7.646 min). Note: there was no MS^2 for 6:2 FTSAm-Pr-DiMeNO in the soil sample available in ESI+ due to overlapping of the M+1 peak of 6:2 FTSy-(2')OHPr-TriMeAm (compare Fig. S9 (b)) and no MS^2 was available in the negative mode due to low peak intensity.

n:2 FTSAm-Pr-MeAms (n = 6)

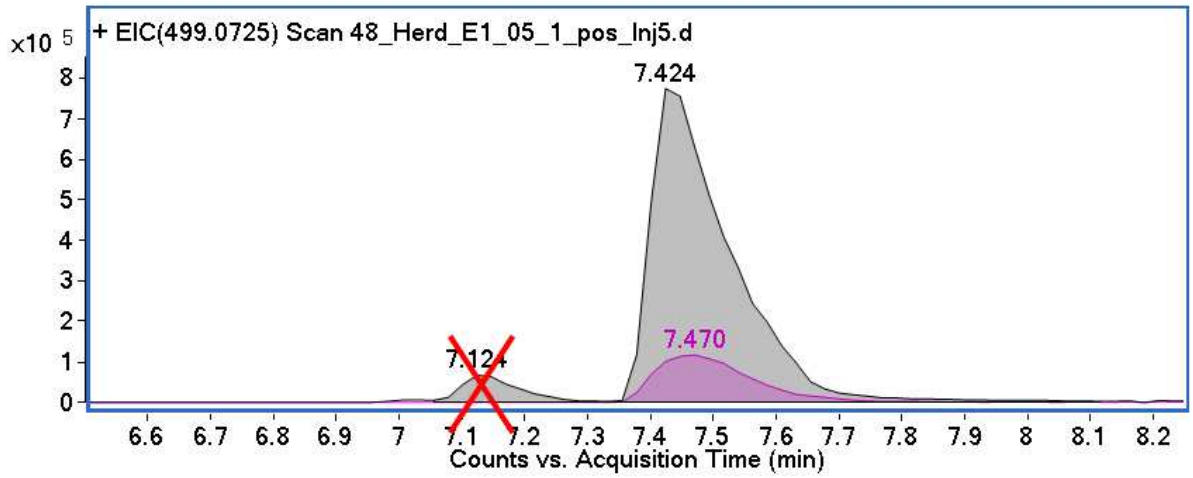

Fig. S39a: Chromatogram (ESI⁻/ESI⁺, soil *S1*, 0.5 – 1 m, first extract) of 6:2 FTSAm-Pr-MeAms in negative (pink, m/z 497.0574, 7.570 min) and positive (grey, m/z 499.0719, 7.424 min) ionization mode. Note: The first peak of 6:2 FTSAm-Pr-MeAm in positive mode is crossed out as it belongs to PFHxSAm-Pr-TriMeAm.

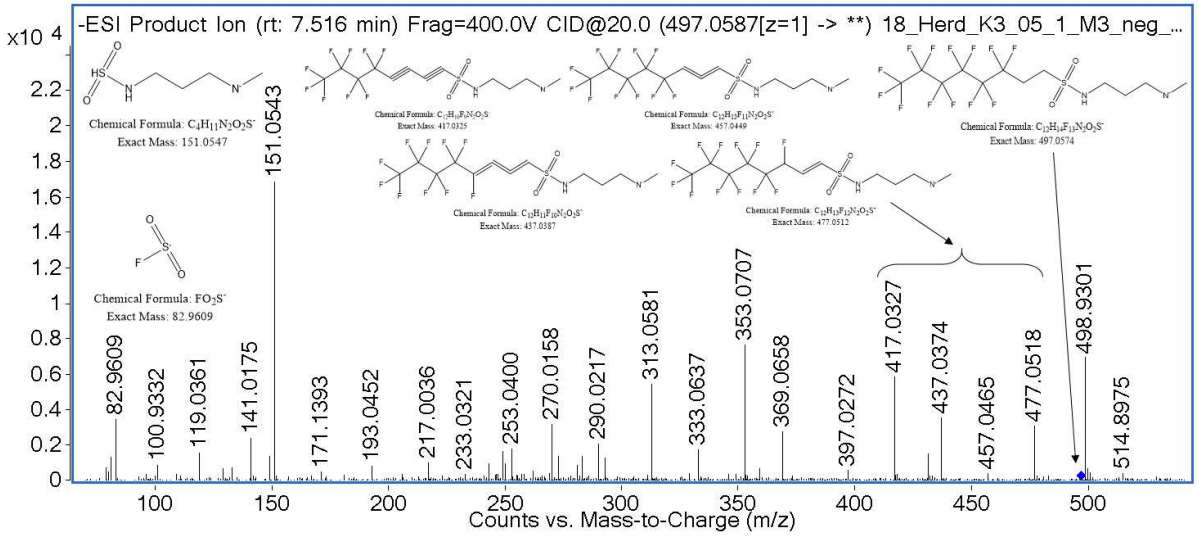

Fig. S39b: MS² spectrum (ESI⁻, 20.0 eV, soil *S1*, 0.5 – 1 m, combined extract, targeted MS²) of 6:2 FTSAm-Pr-MeAm (m/z 497.0574, 7.516 min).

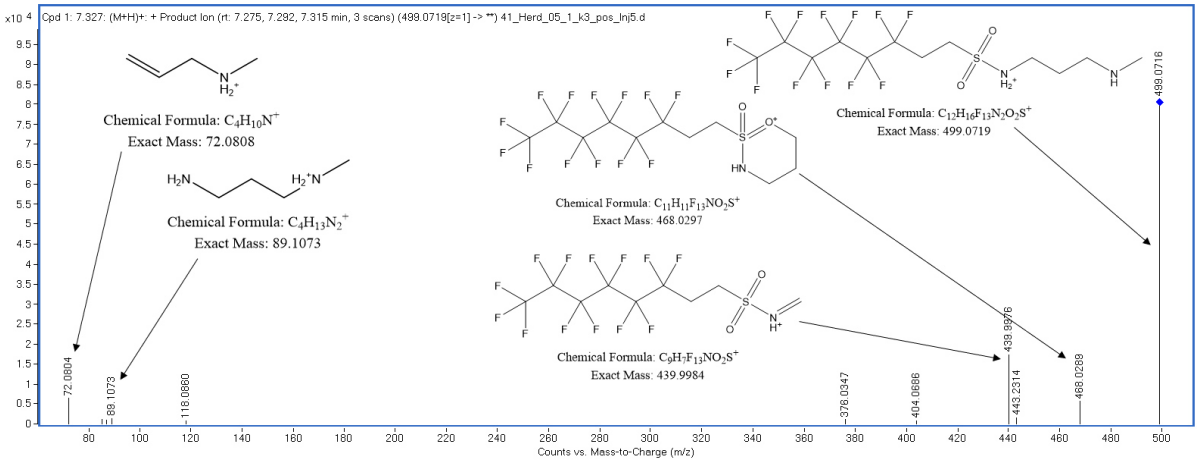

Fig. S39c: MS² spectrum (ESI⁺, 30.0 eV, soil *S1*, 0.5 – 1 m, combined extract) of 6:2 FTSAm-Pr-MeAm (m/z 499.0719, 7.275, 7.292, and 7.315 min).

n:2 FTSAm-Pr-DiMeAms (n = 6, 8)

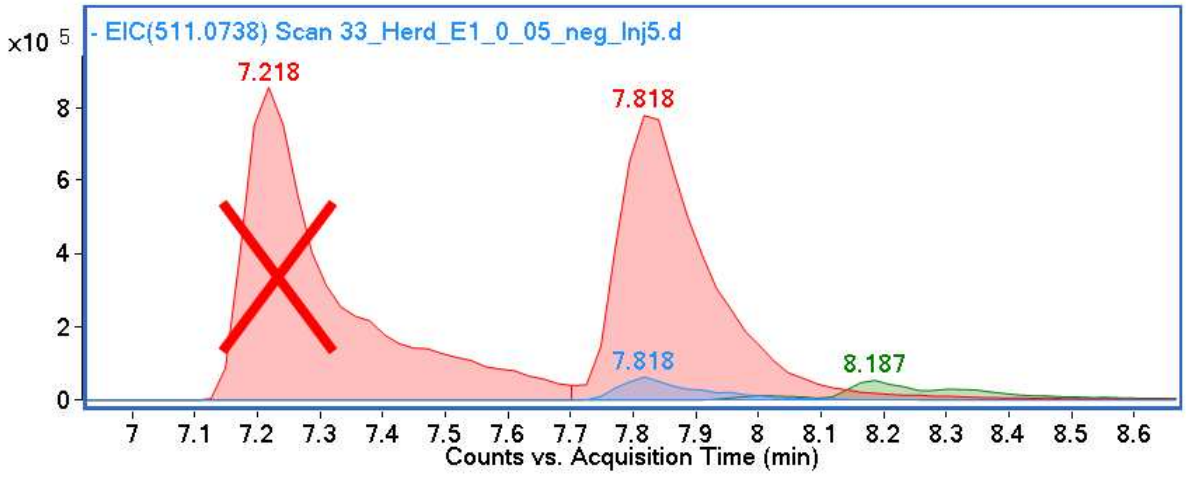

Fig. S40a: Chromatogram (ESI⁻/ESI⁺, soil *S1*, 0 – 0.5 m, first extract) of 6:2 FTSAm-Pr-DiMeAm in negative (blue, m/z 511.0730, 7.818 min) and positive (red, m/z 513.0876, 7.818 min) ionization mode and 8:2 FTSAm-Pr-DiMeAm in positive (green, m/z 613.0812, 8.187 min) ionization mode. Note: First red peak is crossed out as it is the M+1 peak of 6:2 FTSO-(2')OHPr-TriMeAm.

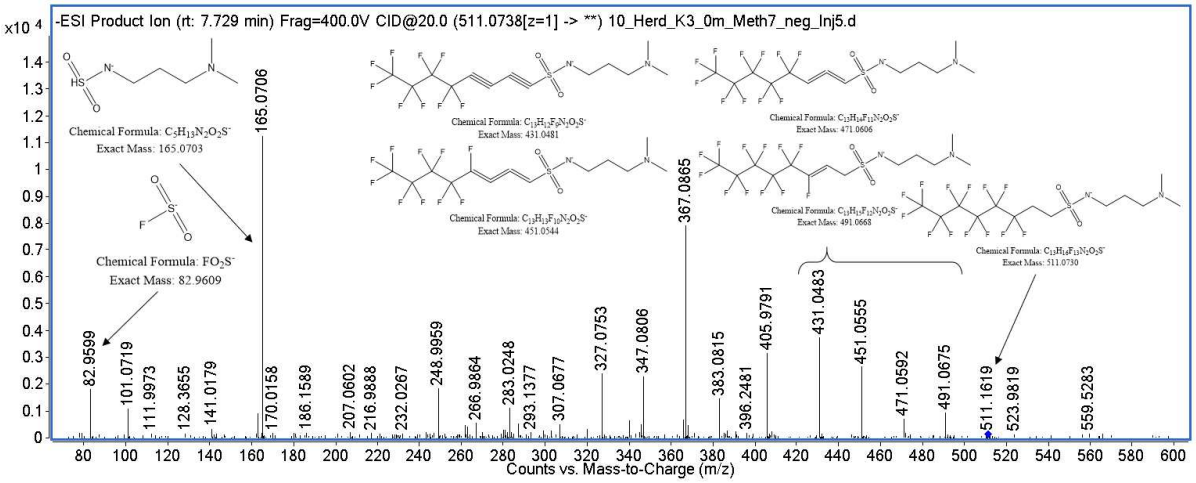

Fig. S40b: MS^2 spectrum (ESI^-, 20.0 eV soil *S1*, 0 – 0.5 m, combined extract, targeted MS^2) of 6:2 FTSAm-Pr-DiMeAm (m/z 511.0730, 7.729 min).

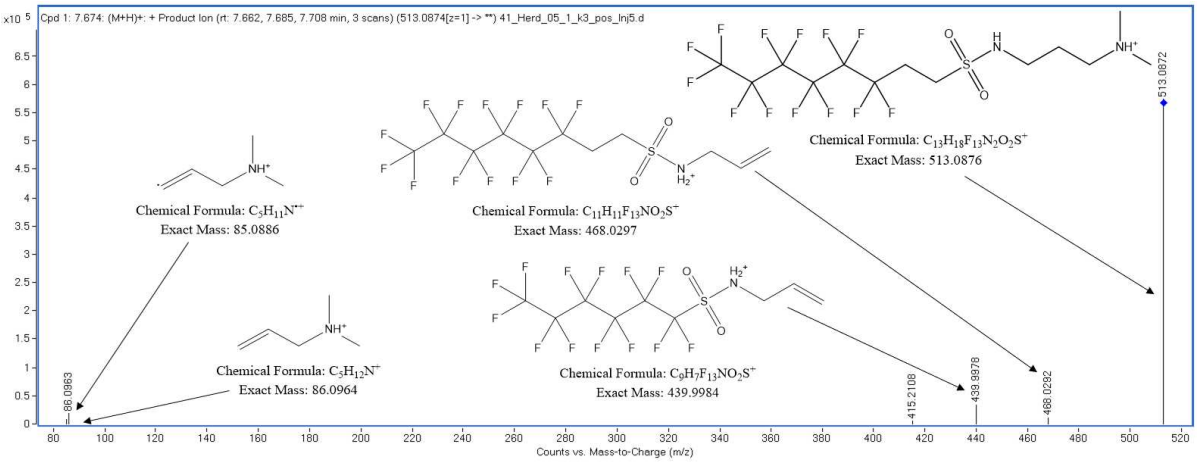

Fig. S40c: MS^2 spectrum (ESI^+, 30.4 eV, soil *S1*, 0.5 – 1 m, combined extract) of 6:2 FTSAm-Pr-DiMeAm (m/z 513.0876, 7.662, 7.685, and 7.708 min).

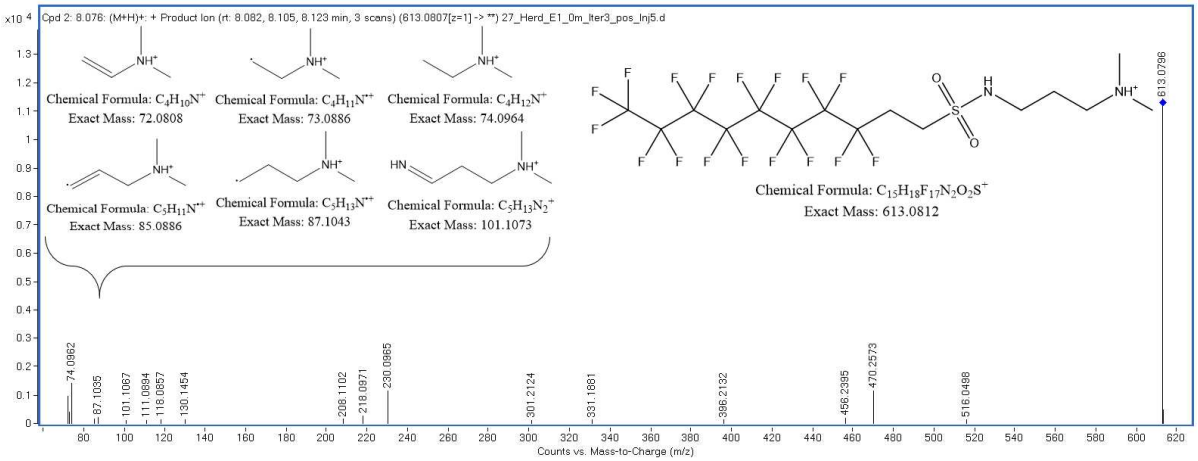

Fig. S40d: MS^2 spectrum (ESI$^+$, 33.4 eV, soil *S1*, 0 – 0.5 m, first extract, iterative MS^2) of 8:2 FTSAm-Pr-DiMeAm (m/z 613.0812, 8.082, 8.105, and 8.123 min).

6. FTSy-derivatives

n:2 FTSy-PrAs (n = 4, 6, 8)

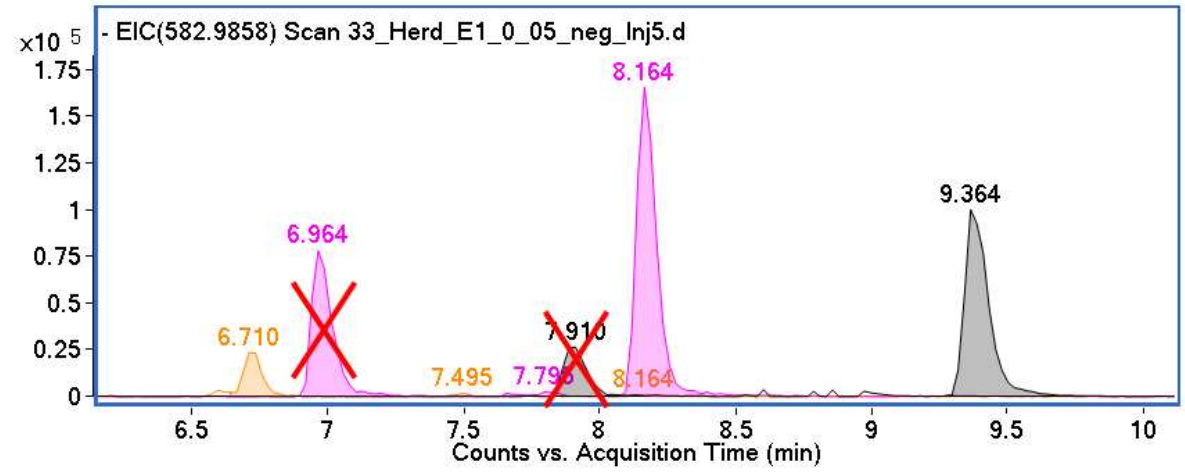

Fig. S41a: Chromatogram (ESI$^-$, soil *S1*, 0 – 0.5 m, first extract) of n:2 FTSy-PrAs (n = 4 (orange, m/z 383.0005, 6.710 min), 6 (pink, m/z 482.9941, 8.164 min), and 8 (grey, m/z 582.9877, 9.364 min)). Note: Two peaks are crossed out as they are in-source adducts of n:2 FTSAs (n = 6 and 8).

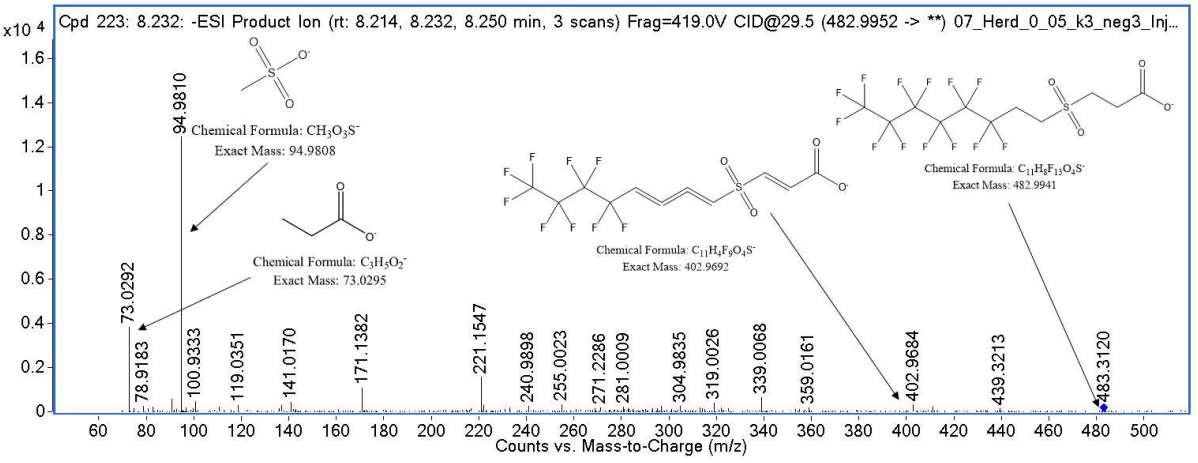

Fig. S41b: MS^2 spectrum (ESI$^-$, soil *S1*, 0 – 0.5 m, combined extract, iterative MS^2) of 6:2 FTSy-PrA (m/z 482.9941, 8.214, 8.232, and 8.250 min).

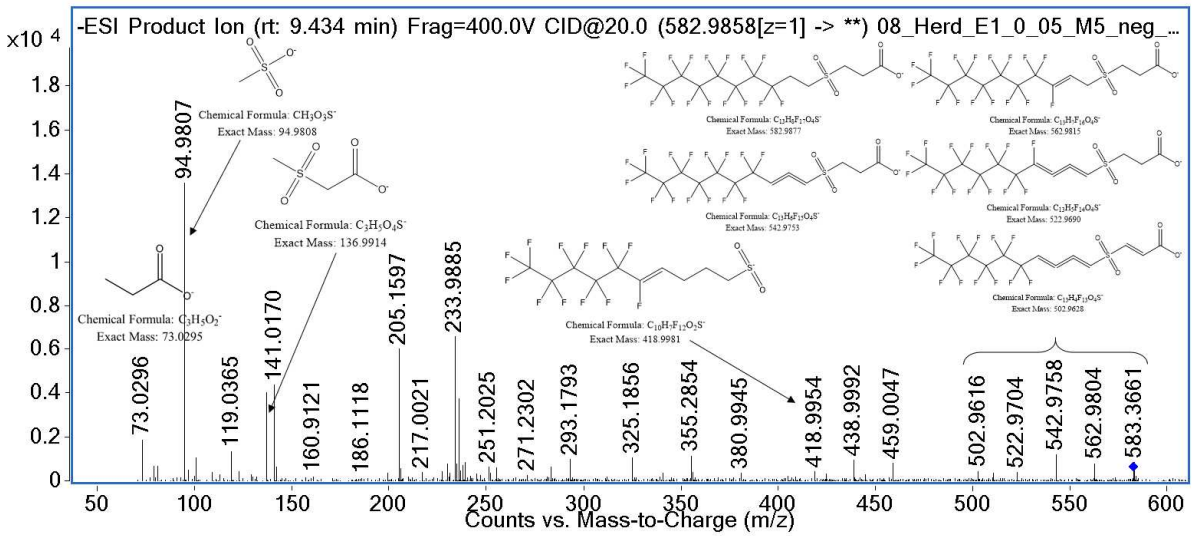

Fig. S41c: MS^2 spectrum (ESI^-, 20.0 eV, soil *S1*, 0 – 0.5 m, first extract, targeted MS^2) of 8:2 FTSy-PrA (m/z 582.9877, 9.434 min).

n:2 FTSy-Pr-Ad-(5',5')DiMeEtSAs (n = 6, 8, 10,12)

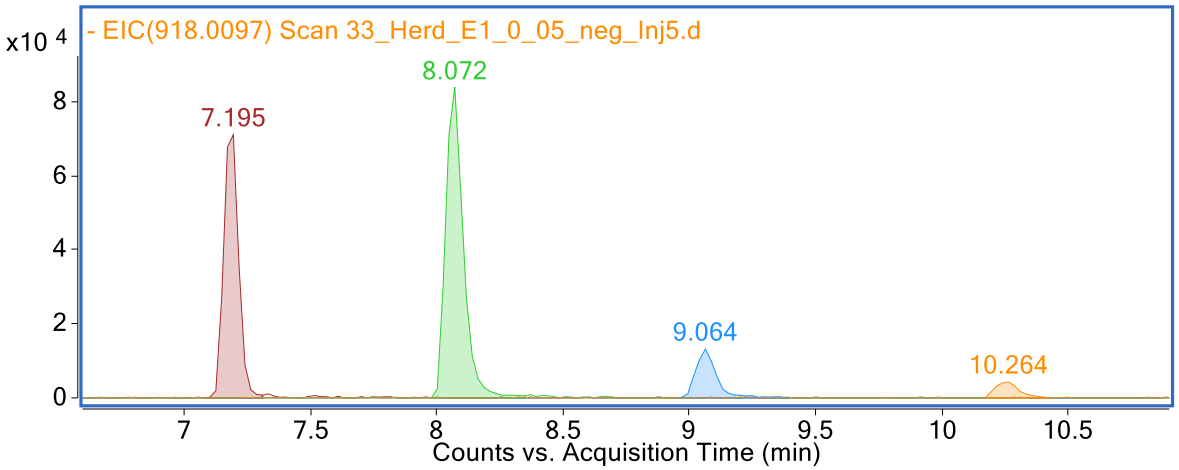

Fig. S42a: Chromatogram (ESI^-, soil *S1*, 0 – 0.5 m, first extract) of n:2 FTSy-Pr-Ad-(5',5')DiMeEtSAs (n = 6 (red, m/z 618.0295, 7.195 min), 8 (green, m/z 718.0231, 8.072 min), 10 (blue, m/z 818.0167, 9.064 min), and 12 (orange, m/z 918.0104, 10.264 min)).

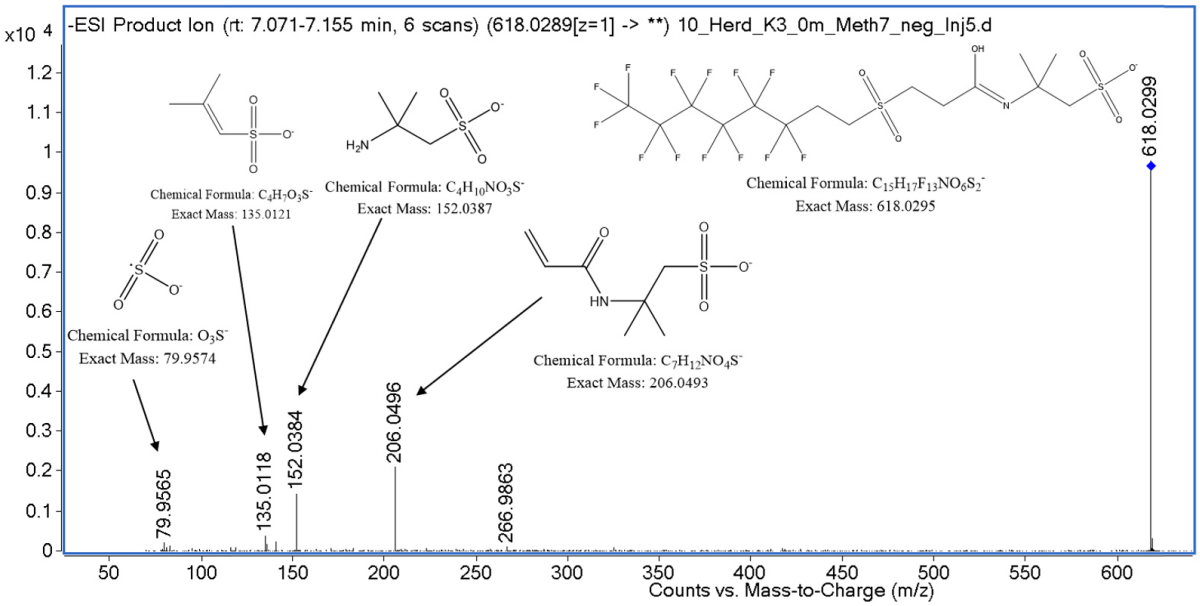

Fig. S42b: MS^2 spectrum (ESI$^-$, different CEs (10 – 40 eV), soil *S1*, 0 – 0.5 m, combined extract, targeted MS^2) of 6:2 FTSy-Pr-Ad-(5',5')DiMeEtSA (m/z 618.0295, 7.071 – 7.155 min).

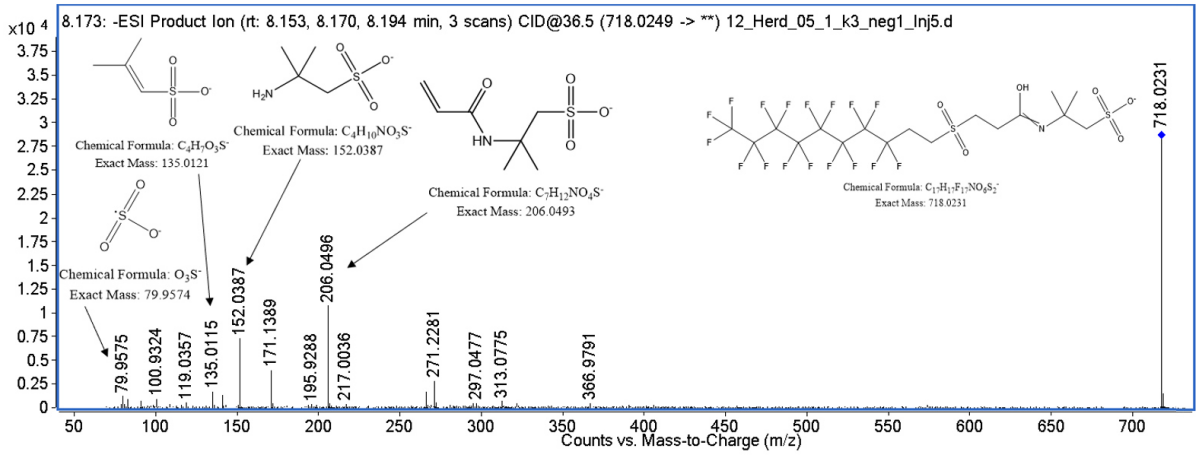

Fig. S42c: MS^2 spectrum (ESI$^-$, 36.5 eV, soil *S1*, 0.5 – 1 m, combined extract, iterative MS^2) of 8:2 FTSy-Pr-Ad-(5',5')DiMeEtSA (m/z 718.0231, 8.153, 8.170, and 8.194 min).

7. FTSO-derivatives

n:2 FTSO-(2')OHPr-TriMeAms (n = 4, 6, 8)

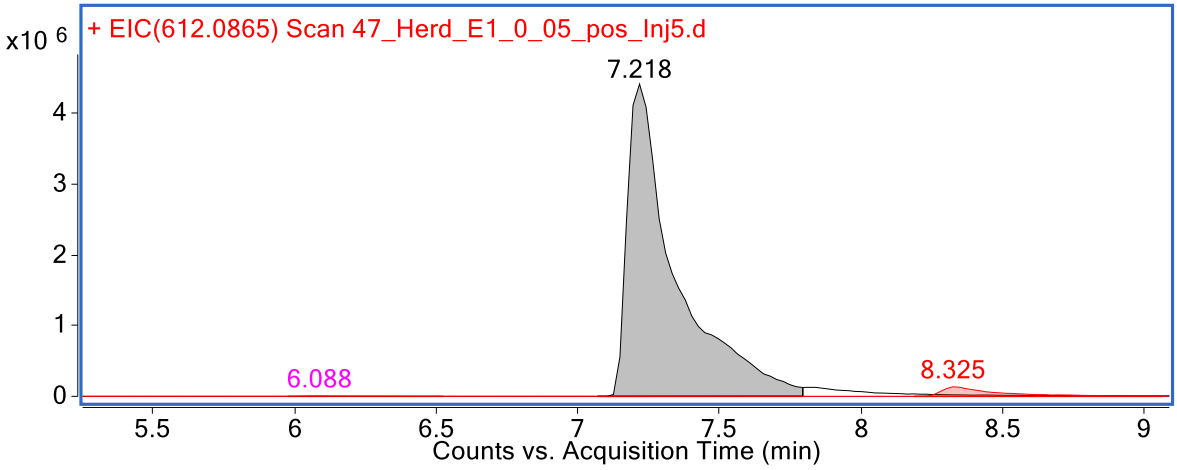

Fig. S43a: Chromatogram (ESI$^+$, soil *S1*, 0 – 0.5 m, first extract) of n:2 FTSO-(2')OHPr-TriMeAms (n = 4 (pink, m/z 412.0987, 6.088 min), 6 (grey, m/z 512.0923, 7.218 min), and 8 (red, m/z 612.0860, 8.325 min)).

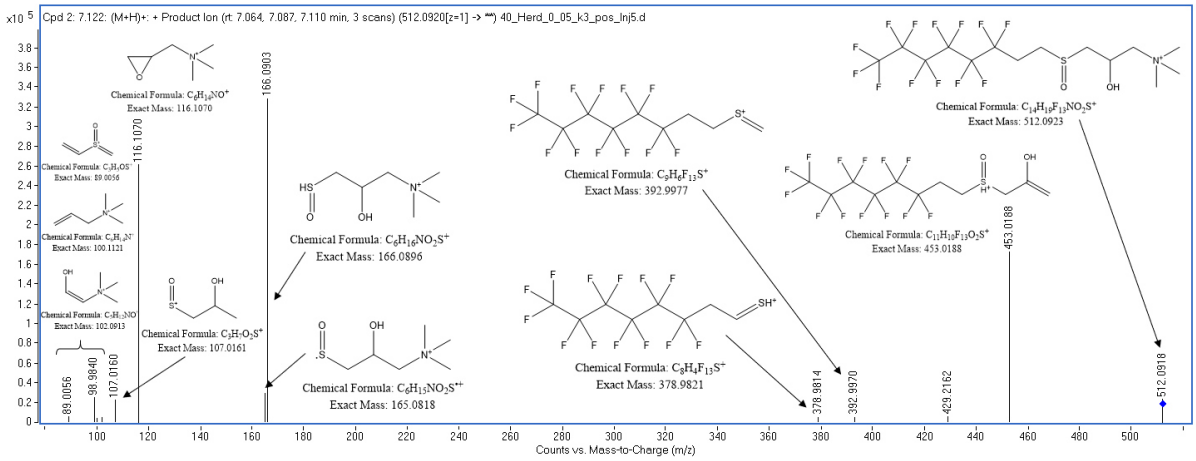

Fig. S43b: MS^2 spectrum (ESI$^+$, 30.4 eV, soil *S1*, 0 – 0.5 m, combined extract) of 6:2 FTSO-(2')OHPr-TriMeAm (m/z 512.0923, 7.064, 7.087, and 7.110 min).

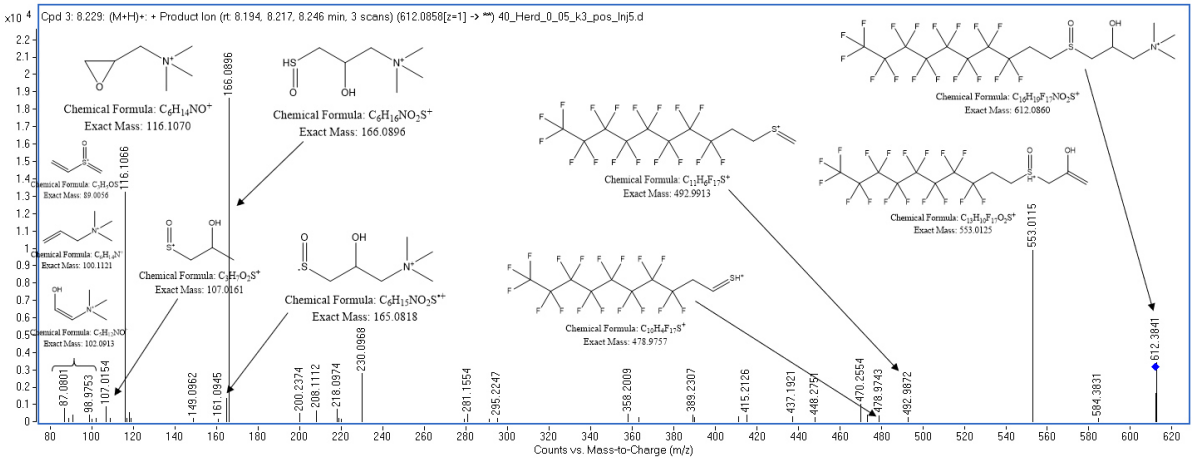

Fig. S43c: MS^2 spectrum (ESI$^+$, 33.4 eV, soil *S1*, 0 – 0.5 m, combined extract) of 8:2 FTSO-(2')OHPr-TriMeAm (m/z 612.0860, 8.194, 8.217, and 8.246 min).

n:2 FTSO-Pr-Ad-(5',5')DiMeEtSAs (n = 6)

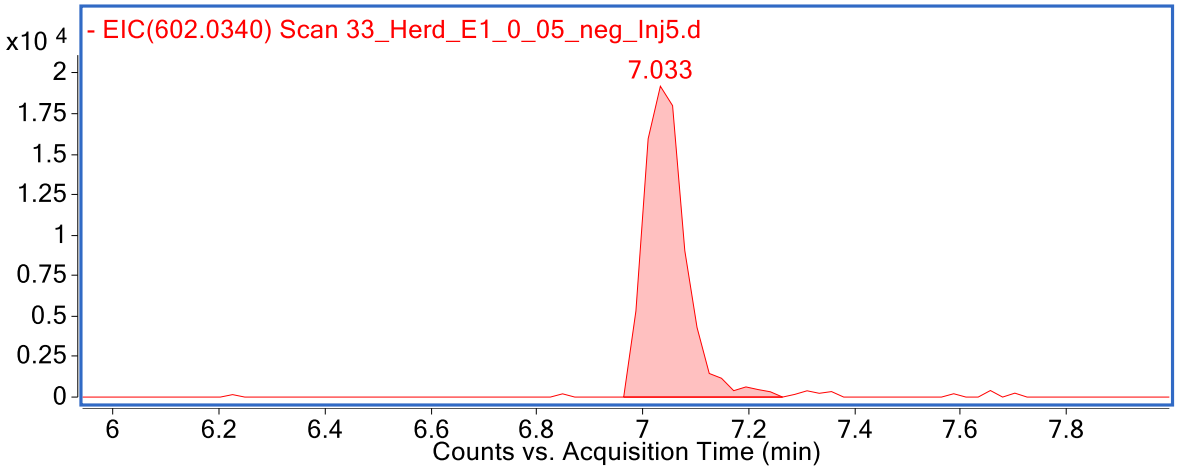

Fig. S44a: Chromatogram (ESI$^-$, soil *S1*, 0 – 0.5 m, first extract) of 6:2 FTSO-Pr-Ad-(5',5')DiMeEtSA (m/z 602.0346, 7.033 min).

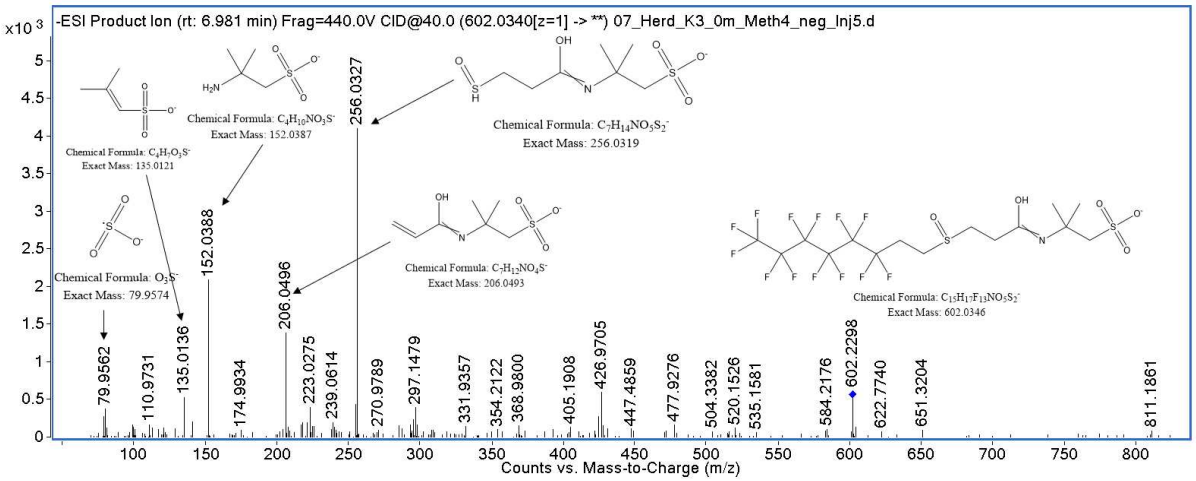

Fig. S44b: MS^2 spectrum (ESI$^-$, 40.0 eV, soil *S1*, 0 – 0.5 m, combined extract, targeted MS^2) of 6:2 FTSO-Pr-Ad-(5',5')DiMeEtSA (m/z 602.0346, 6.981 min).

8. FTTh-derivatives

n:2 FTTh-(2')OHPr-TriMeAms (n = 4, 6, 8, 10)

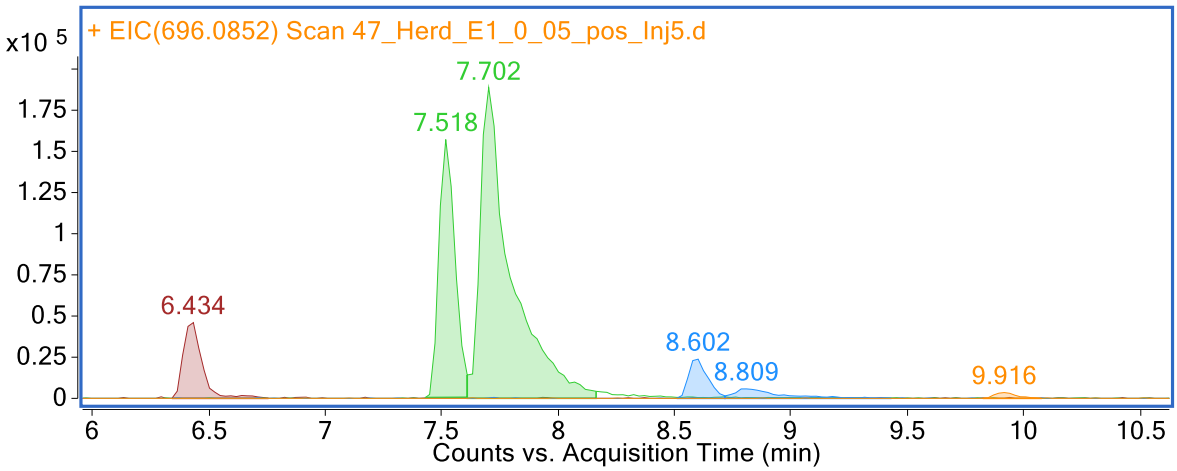

Fig. S45a: Chromatogram (ESI$^+$, soil *S1*, 0 – 0.5 m, first extract) of n:2 FTTh-(2')OHPr-TriMeAms (n = 4 (red, m/z 396.1038, 6.434 min), 6 (green, m/z 496.0974, 7.518 and 7.702 min), 8 (blue, m/z 596.0910, 8.602 and 8.809 min), and 10 (orange, m/z 696.0847, 9.916 min)).

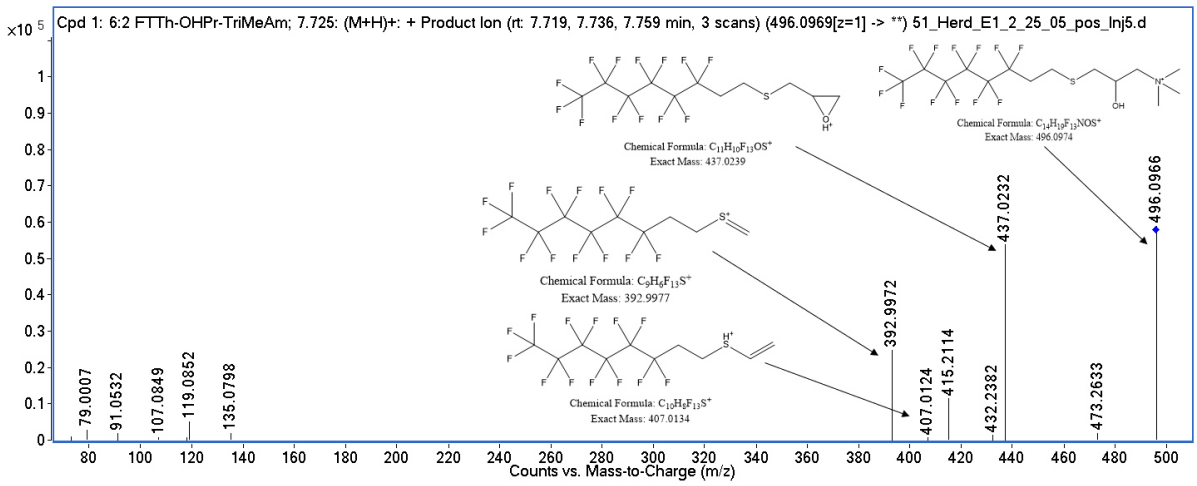

Fig. S45b: MS^2 spectrum (ESI$^+$, 29.9 eV, soil *S1*, 2 – 2.5 m, first extract) of 6:2 FTTh-(2')OHPr-TriMeAm (m/z 496.0974, 7.719, 7.736, and 7.759 min).

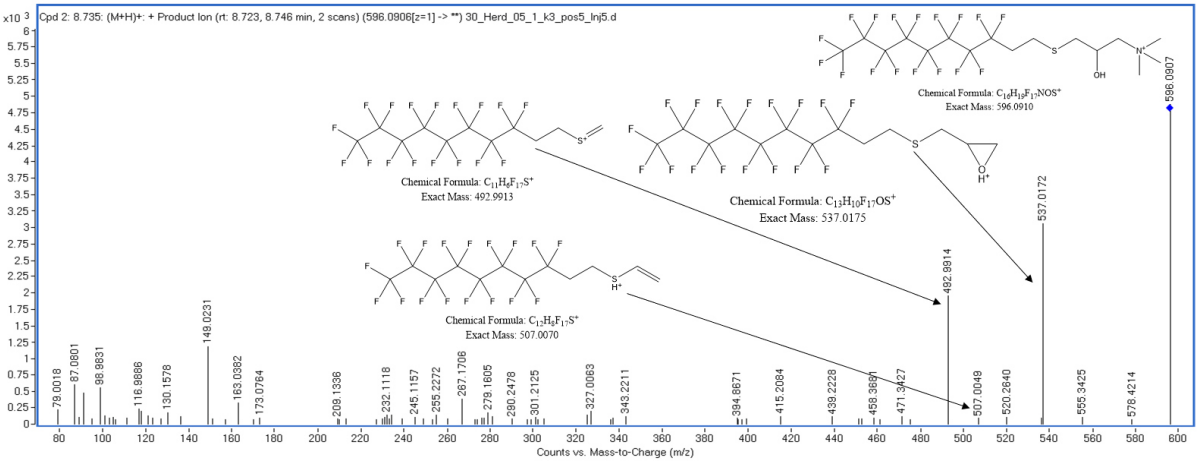

Fig. S45c: MS^2 spectrum (ESI$^+$, 32.9 eV, soil *S1*, 0.5 – 1 m, combined extract, iterative MS^2) of 8:2 FTTh-(2')OHPr-TriMeAm (m/z 596.0910, 8.723 and 8.746 min).

9. FTSA-derivatives

OH-n:2 FTSAs (n = 6, 8)

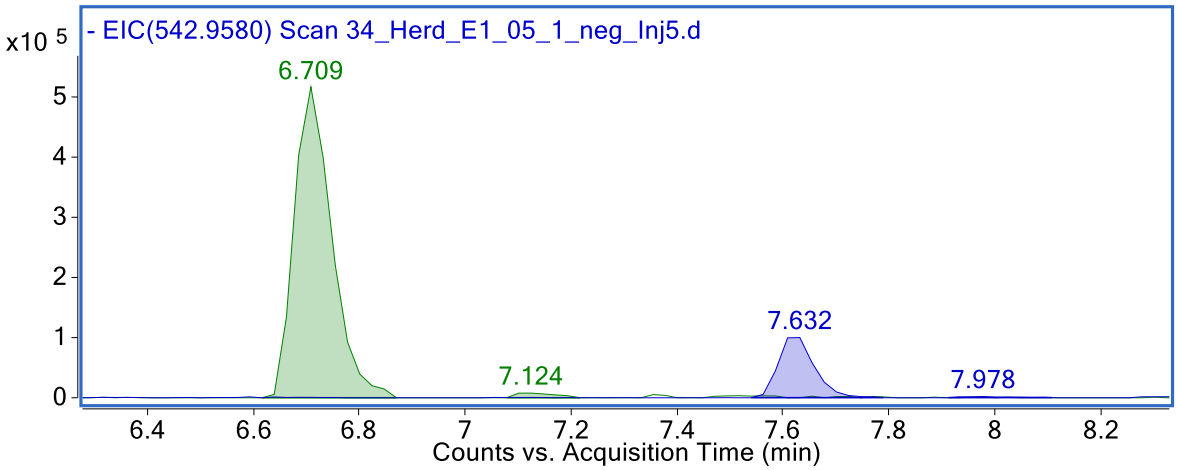

Fig. S46a: Chromatogram (ESI$^-$, soil *S1*, 0.5 – 1 m, first extract) of OH-n:2 FTSAs (n = 6 (green, m/z 442.9628, 6.709 min) and 8 (blue, m/z 542.9564, 7.632 min)).

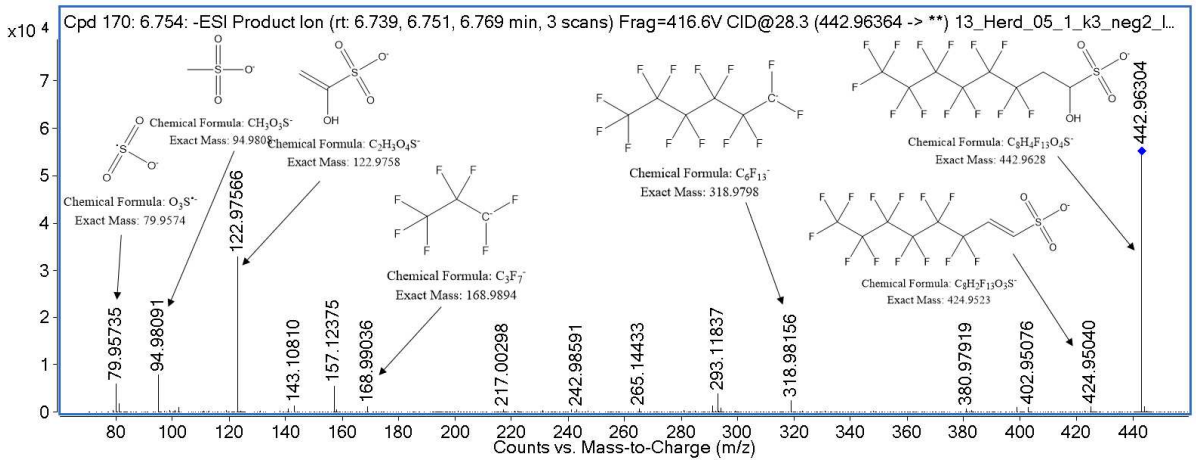

Fig. S46b: MS^2 spectrum mode (ESI$^-$, 28.3 eV, soil *S1*, 0.5 – 1 m, combined extract, iterative MS^2) of OH-6:2 FTSA (m/z 442.9628, 6.739, 6.751, and 6.796 min).

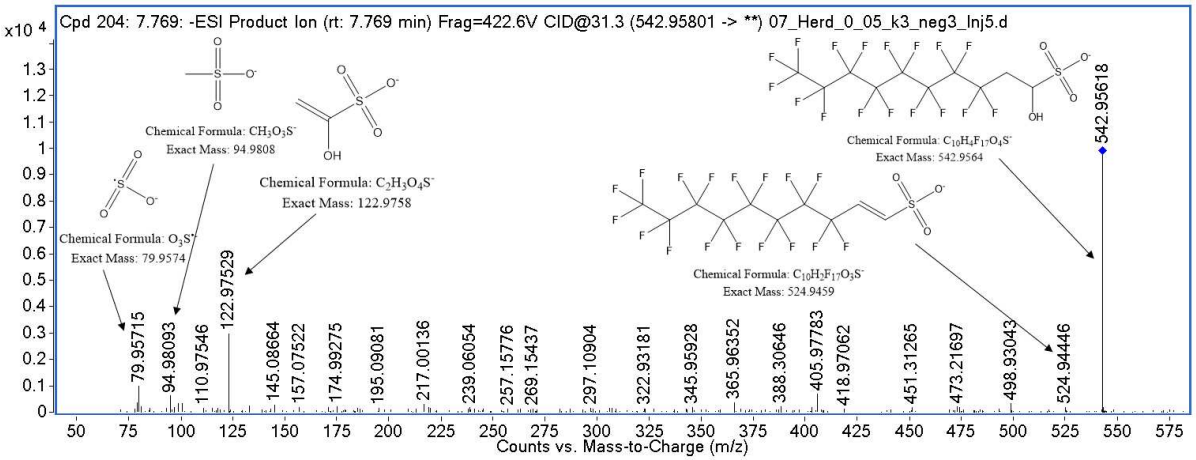

Fig. S46c: MS^2 spectrum (ESI$^-$, 31.3 eV, soil *S1*, 0 – 0.5 m, combined extract, iterative MS^2) of OH-8:2 FTSA (m/z 542.9564, 7.769 min).

Confidence level 4

E-PFSAs (n = 10-17)

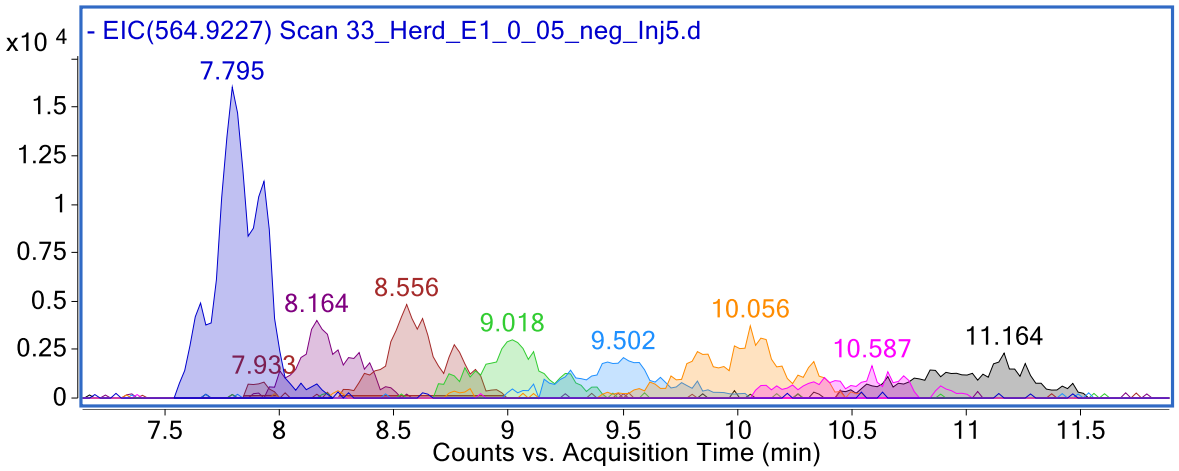

Fig. S47: Chromatogram (ESI$^-$, soil *S1*, 0 – 0.5 m, first extract) of E-PFSAs (n = 10 (dark blue, m/z 564.9219, 7.795 min), 11 (violet, m/z 614.9187, 8.164 min), 12 (dark red, m/z 664.9156, 8.556 min), 13 (green, m/z 714.9124, 9.018 min), 14 (blue, m/z 764.9092, 9.502 min), 15 (orange, m/z 814.9060, 10.056 min), 16 (pink, m/z 864.9028, 10.587 min), and 17 (grey, m/z 914.8996, 11.164 min)).

PFASAm-*N*-Me-*N*-EtAs (or isomers) (n = 8, 13, 15)

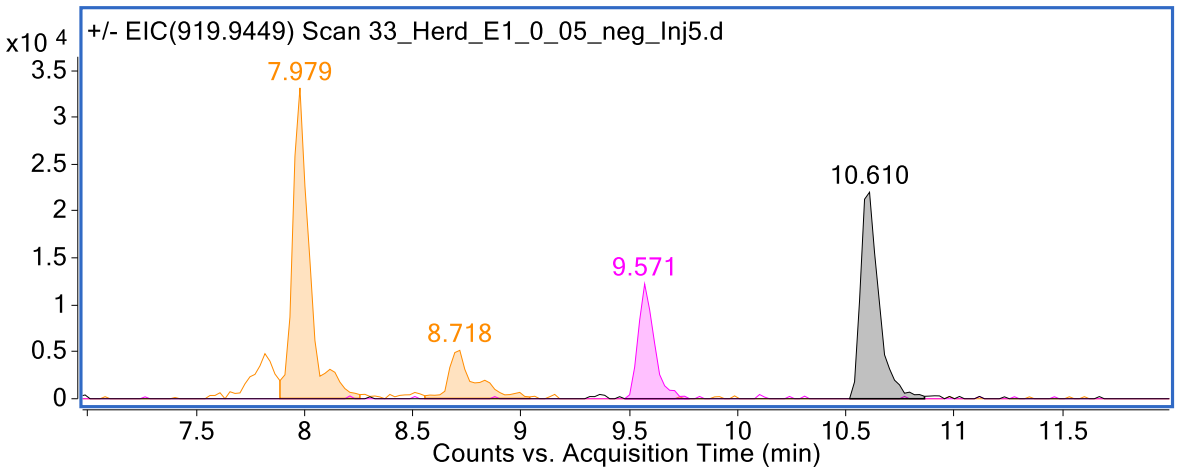

Fig. S48: Chromatogram (ESI$^-$, soil *S1*, 0 – 0.5 m, first extract) of PFASAm-*N*-Me-*N*-EtAs (or isomers) (n = 8 (orange, m/z 569.9673, 7.979 min and/or 8.718 min), 13 (pink, m/z 819.9514, 9.571 min), and 15 (grey, m/z 919.9450, 10.610 min)).

PFASAm-*N*-Et-*N*-EtA and PFASAm-*N*-Me-*N*-PrA (n = 6, 8)

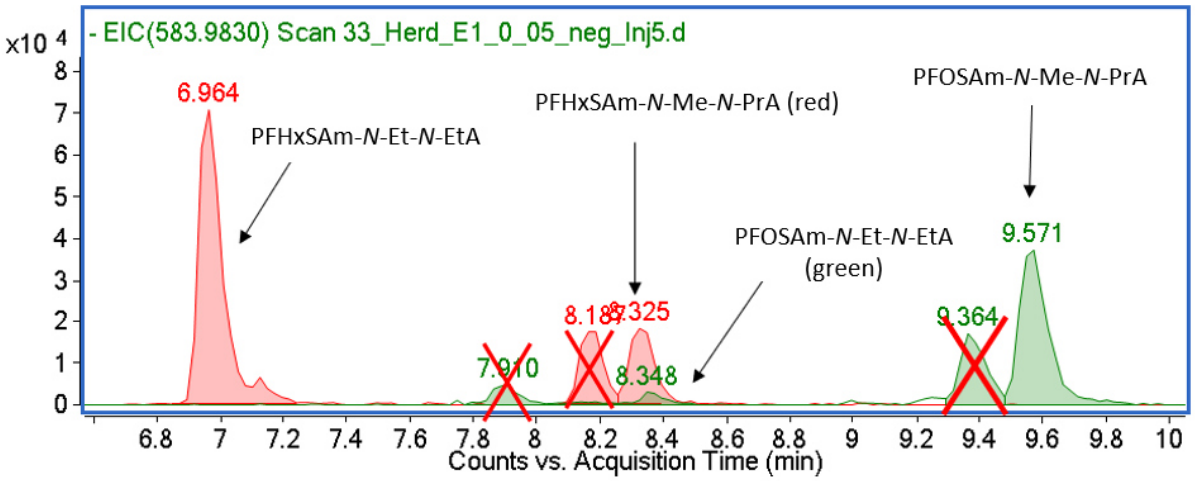

Fig. S49: Chromatogram (ESI$^-$, soil *S1*, 0 – 0.5 m, first extract) of PFASAm-*N*-Et-*N*-EtA (n = 6 (red, m/z 483.9894, 6.964 min) and 8 (green, m/z 583.9830, 8.348 min)) and PFASAm-*N*-Me-*N*-PrA (n = 6 (red, m/z 483.9894, 8.325 min) and 8 (green, m/z 583.9830, 9.571 min)). Note: Three peaks are crossed out as they are the M+1 peaks of n:2 FTSy-PrAs (n = 6 and 8).

n:2 FTSAm-EtOHs (n = 6)

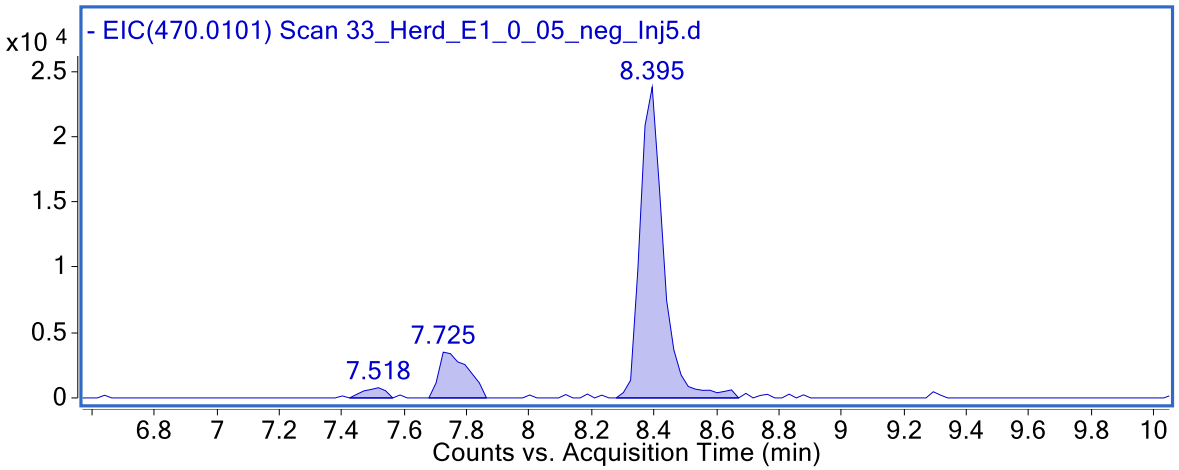

Fig. S50: Chromatogram (ESI$^-$, soil *S1*, 0 – 0.5 m, first extract) of 6:2 FTSAm-EtOH (m/z 470.0096, 8.395 min).

n:2 FTSAm-KAmPes (n = 6)

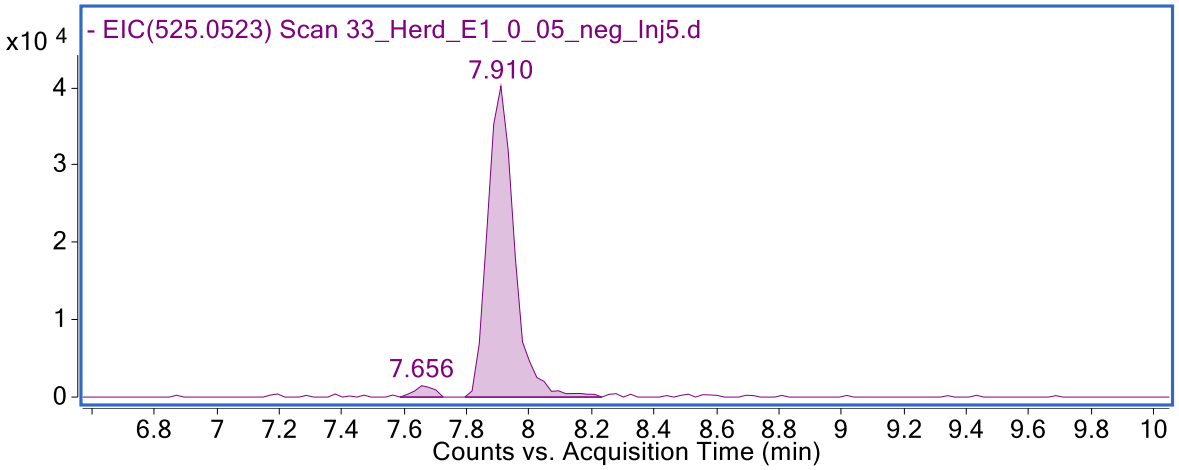

Fig. S51: Chromatogram (ESI$^-$, soil *S1*, 0 – 0.5 m, first extract) of 6:2 FTSAm-KAmPes (m/z 525.0518, 7.910 min).

n:2 FTTh-Pr-Ad-(5',5')DiMeEtSAs (n = 6)

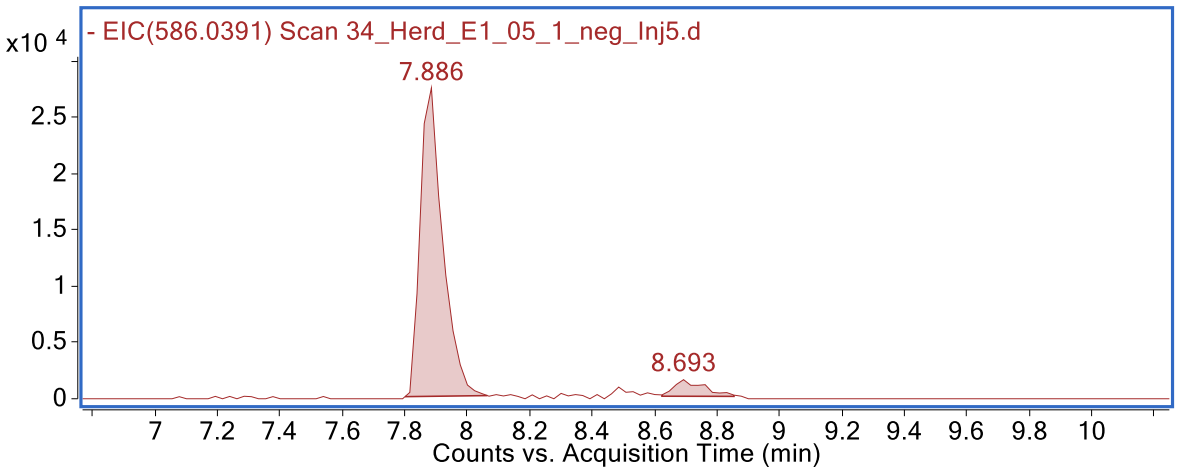

Fig. S52: Chromatogram (ESI$^-$, soil *S1*, 0.5 – 1 m, first extract) of 6:2 FTTh-Pr-Ad-(5',5')DiMeEtSAs (m/z 586.0397, 7.886 min)

U-n:3 FTAds (n = 5, 7)

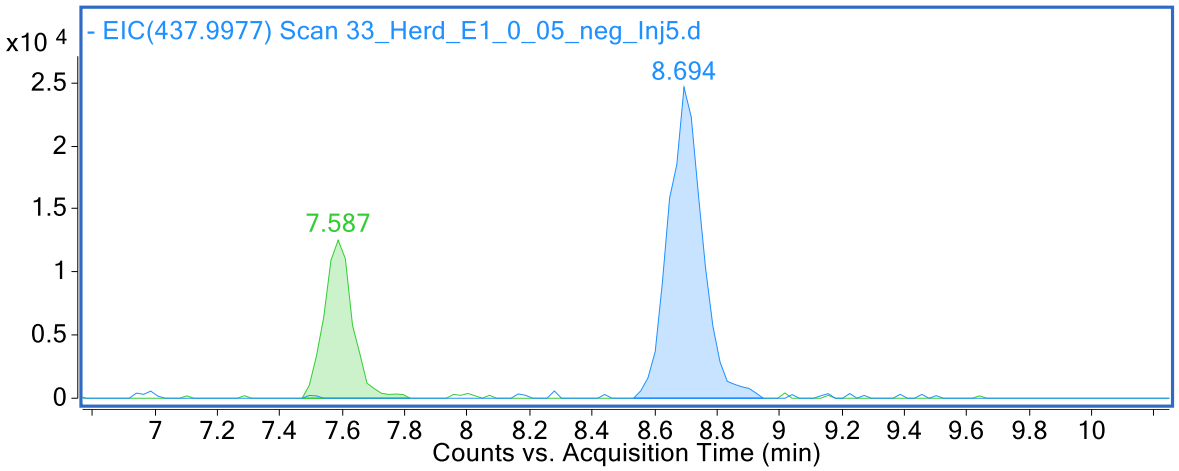

Fig. S53: Chromatogram (ESI$^-$, soil *S1*, 0 – 0.5 m, first extract) of U-n:3 FTAds (n = 5 (green, m/z 338.0040, 7.587 min) and 7 (blue, m/z 437.9981, 8.694 min)).

Confidence level 5

H-E-PFSAs (n = 9, 11)

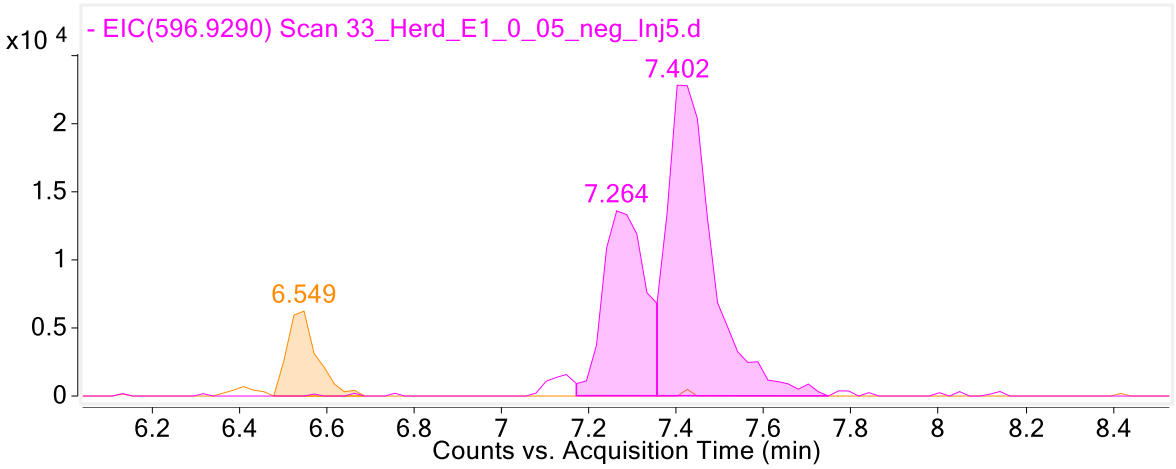

Fig. S54: Chromatogram (ESI$^-$, soil *S1*, 0 – 0.5 m, first extract) of H-E-PFSAs (n = 9 (orange, m/z 496.9346, 6.549 min) and 11 (pink, m/z 596.9282, 7.264 and 7.402 min)).

n/m PFASAm dimers (n/m = 3/3, 3/4, 4/4, 4/5, 5/5, 5/6, 6/6)

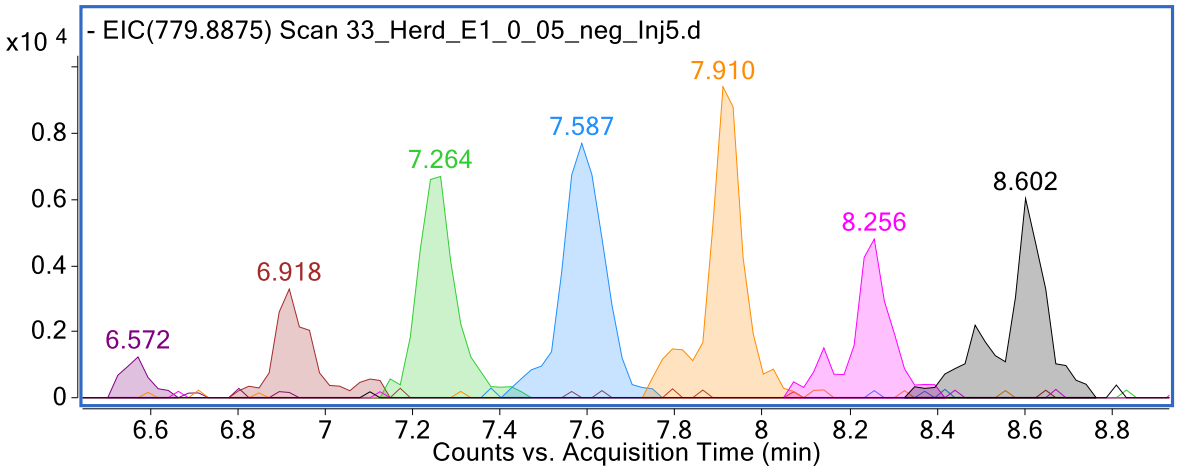

Fig. S55: Chromatogram (ESI$^-$, soil *S1*, 0 – 0.5 m, first extract) of n/m PFASAm dimers (n/m = 3/3 (violet, m/z 479.9051, 6.572 min), 3/4 (red, m/z 529.9019, 6.918 min), 4/4 (green, m/z 579.8987, 7.264 min), 4/5 (blue, m/z 629.8955, 7.587 min), 5/5 (orange, m/z 679.8923, 7.910 min), 5/6 (pink, m/z 729.8891, 8.256 min), and 6/6 (grey, m/z 779.8859, 8.602 min)).

n:2 FTSAm-Ets (n = 6)

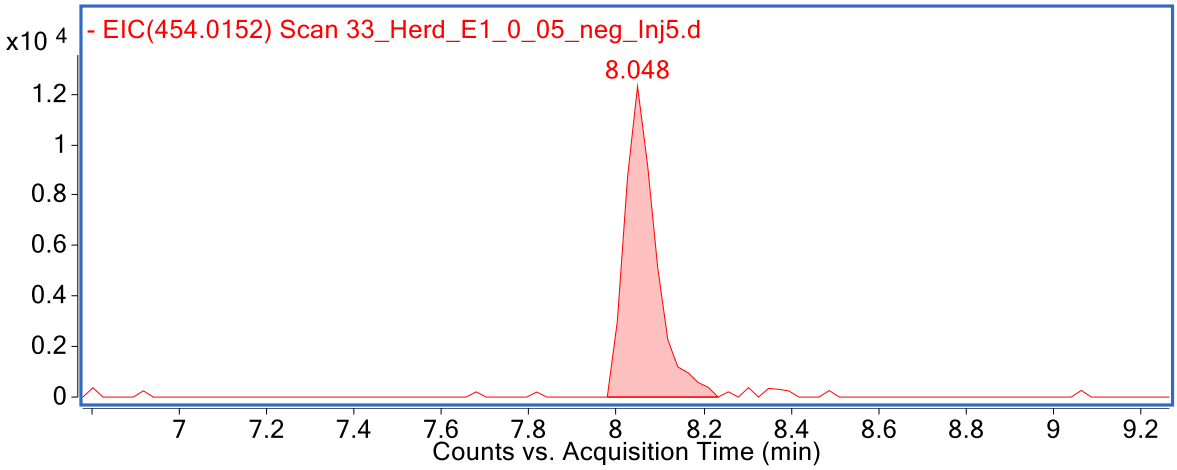

Fig. S56: Chromatogram (ESI$^-$, soil *S1*, 0 – 0.5 m, first extract) of 6:2 FTSAm-Et (m/z 454.0147, 8.048 min).

n:2 FTSAm-EtAls (n = 6)

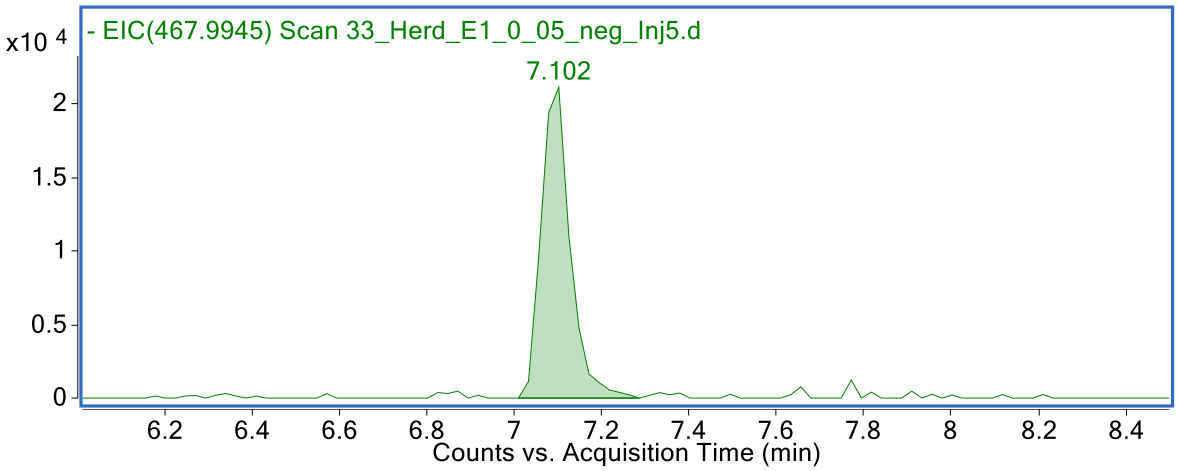

Fig. S57: Chromatogram (ESI$^-$, soil *S1*, 0 – 0.5 m, first extract) of 6:2 FTSAm-EtAl (m/z 467.9940, 7.102 min).

n:2 FTSAm-KAmMePes (n = 6)

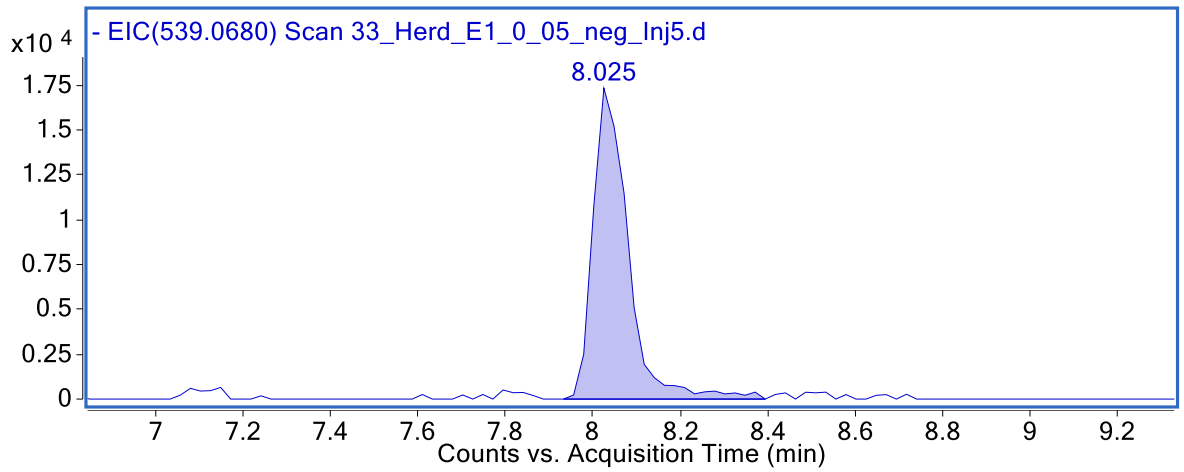

Fig. S58: Chromatogram (ESI$^-$, soil *S1*, 0 – 0.5 m, first extract) of 6:2 FTSAm-KAmMePe (m/z 539.0675, 8.025 min).

References

1. Place B (2021) Suspect List of Possible Per- and Polyfluoroalkyl Substances (PFAS). National Institute of Standards and Technology. https://data.nist.gov/od/id/mds2-2387. Accessed 2023-12-15

2. Charbonnet JA, McDonough CA, Xiao F, Schwichtenberg T, Cao D, Kaserzon S, Thomas KV, Dewapriya P, Place BJ, Schymanski EL, Field JA, Helbling DE, Higgins CP (2022) Communicating Confidence of Per- and Polyfluoroalkyl Substance Identification via High-Resolution Mass Spectrometry. Environ Sci Technol Lett 9 (6):473-481. doi:10.1021/acs.estlett.2c00206

3. Nickerson A, Maizel AC, Kulkarni PR, Adamson DT, Kornuc JJ, Higgins CP (2020) Enhanced Extraction of AFFF-Associated PFASs from Source Zone Soils. Environ Sci Technol 54 (8):4952-4962. doi:10.1021/acs.est.0c00792

4. Rotander A, Karrman A, Toms LM, Kay M, Mueller JF, Gomez Ramos MJ (2015) Novel fluorinated surfactants tentatively identified in firefighters using liquid chromatography quadrupole time-of-flight tandem mass spectrometry and a case-control approach. Environ Sci Technol 49 (4):2434-2442. doi:10.1021/es503653n

Appendix 2

Publication 2

Implementation of Matrix-Matched Semiquantification of PFAS in AFFF-Contaminated Soil

Catharina Capitain[+‖], Melanie Schüßler[+‖], Boris Bugsel[+], Jonathan Zweigle[‡], Christian Vogel[§], Peter Leube[§], Christian Zwiener[+]

[+]Environmental Analytical Chemistry, Department of Geosciences, University of Tübingen, Schnarrenbergstraße 94-96, 72076 Tübingen, Germany

[‡]Department of Plant and Environmental Sciences, University of Copenhagen, Thorvaldsensvej 40, Frederiksberg 1871, Denmark

[§]Federal Institute for Materials Research and Testing, Division 4.4 – Thermochemical Residues Treatment and Resource Recovery, Unter den Eichen 87, 12205 Berlin, Germany

[‖]The authors contributed equally to this work and share first authorship.

Published in: Environmental Science & Technology 59 (14), 7338-7347

DOI: 10.1021/acs.est.4c14255

Environmental Science & Technology

pubs.acs.org/est

Article

Implementation of Matrix-Matched Semiquantification of PFAS in AFFF-Contaminated Soil

Published as part of Environmental Science & Technology special issue "Non-Targeted Analysis of the Environment".

Catharina Capitain,[‖] Melanie Schüßler,[‖] Boris Bugsel, Jonathan Zweigle, Christian Vogel, Peter Leube, and Christian Zwiener*

Cite This: *Environ. Sci. Technol.* 2025, 59, 7338−7347

Read Online

ACCESS | Metrics & More | Article Recommendations | Supporting Information

ABSTRACT: This study presents a novel semiquantification approach for nontarget screening (NTS), combining matrix-matched calibration and ionization class-specific average calibration curves (ACCs) to address the lack of analytical reference standards for most per- and polyfluoroalkyl substances (PFAS). Ionization class-specific ACCs for carboxylic and sulfonic acids, sulfonamides, and cationic PFAS result in high accuracy, with median absolute accuracy quotients below 2.27×. The approach was applied to soil impacted by aqueous film-forming foam (AFFF) contamination. A total of 96 tentatively identified PFAS were semiquantified in addition to 28 quantified compounds based on available standards. Semiquantified concentrations exceeded those of target analytes, demonstrating the critical role of this method in capturing broader PFAS contamination. In this case, validation against extractable organofluorine (EOF) showed a 102% closed mass balance. The innovative approach not only enables comprehensive PFAS contamination assessment in complex matrices but also expands the scope of the NTS for environmental monitoring, remediation, and risk assessment of AFFF-contaminated sites.

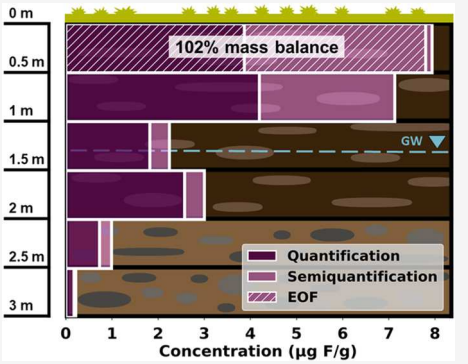

KEYWORDS: *PFAS, AFFF, soil, HRMS, semiquantification*

INTRODUCTION

Per- and polyfluoroalkyl substances (PFAS) have been increasingly detected in soil,[1−5] groundwater,[5−8] drinking water,[9−11] wildlife,[12−14] and human blood,[10,15−17] even in remote regions such as the arctic[18−21] in the past decade. The ubiquitous distribution of PFAS is cause for concern due to their extreme stability in environmental compartments[22−24] and adverse health effects such as liver damage, kidney and testicular cancer, lower birthweight, and thyroid disease.[25]

More than 200 potential applications in industry and consumer products have been identified for PFAS, including as active ingredients in aqueous film-forming foams (AFFF).[26] PFAS employed in AFFF can be of anionic, cationic, or zwitterionic nature and vary in structure and functional groups.[6,8,27−29] Due to the versatile structures of AFFF PFAS, various names for the same substance exist in the literature. In this study, we applied the novel terminology system introduced by Schüßler et al.[30]

AFFF formulations contain about 2−15% of fluorosurfactants.[31] Therefore, during firefighting activities employing AFFF, large amounts of PFAS can enter the environment and, ultimately, groundwater. In 2008, an agricultural area in Reilingen, Germany, was highly contaminated with AFFF PFAS during firefighting operations. An extended characterization of the PFAS contamination pattern in Reilingen by liquid chromatography−high-resolution mass spectrometry (LC-HRMS) was done by Schüßler et al.[30] 124 PFAS from 42 PFAS subclasses could be identified in soil from the Reilingen site after successful data prioritization by the novel MD/C-m/C approach[32] (mass defect per carbon number (MD/C) plotted against mass per carbon number (m/C)) and the recently developed software tool PFΔ*Screen*.[33] Since only 28 of the 124 identified PFAS could be quantified based on analytical standards, semiquantification approaches have to be applied to assess the extent of contamination and to propose suitable remediation measures.

Typically, for semiquantification, a structurally similar substance is selected as a surrogate for the target PFAS for a 1:1 matching procedure. Thereby, the molar response factor

Received: December 18, 2024
Revised: March 1, 2025
Accepted: March 28, 2025
Published: April 3, 2025

https://doi.org/10.1021/acs.est.4c14255
Environ. Sci. Technol. 2025, 59, 7338−7347

(RF) from the surrogate, which is the quotient of a measured chemical signal (e.g., the integrated peak area) and a known concentration, is applied to the suspect PFAS. However, this method requires suitable standards, is time-consuming, and often lacks accuracy, especially when the substances are structurally diverse as in the case of AFFF contamination.

To meet these challenges, Cao et al.[34] developed average calibration curves (ACCs) for cationic and anionic PFAS, respectively. These calibration curves were fitted with log−log and weighted linear regression models and used to semiquantify the suspect PFAS concentrations. In another promising approach, Pu et al.[35] used bootstrap-sampled calibration values from chemical surrogates for semiquantification, demonstrating that the selection of 'expert-selected' surrogates improved predictive accuracy compared to the use of all available surrogates. Another approach is to predict ionization efficiencies in electrospray ionization using a set of molecular predictors and machine learning for semiquantification.[36] An interlaboratory comparison of five quantification approaches for a broad range of analyte structures and properties revealed the best performance for an ionization efficiency prediction approach with a mean prediction error of 15×.[37]

In quantification and semiquantification, it is also important to account for matrix effects (MEs) which is typically done very accurately with the corresponding isotope-labeled standards. However, labeled PFAS standard availability is very limited to a few anionic PFAS. No cationic or zwitterionic labeled PFAS standards were available at the time of this study. Alternatively, the standard addition method can be applied which involves several steps of analyte spikes to an unknown sample and very accurately accounts for ME from the sample matrix during quantification.[38]

Traditional targeted analytical methods focus on a limited set of known PFAS, potentially overlooking numerous unidentified or emerging variants present in the environment. To address this limitation, integrating semiquantitative nontarget screening (NTS) techniques is essential. These approaches enable the detection and estimation of concentrations for a broader spectrum of PFAS, providing a more comprehensive assessment of environmental contamination.[2,39] The objective of this study was therefore to implement a matrix-matched semiquantification approach for AFFF PFAS and their transformation products (TPs), to quantitatively assess the AFFF contamination, and to include a fluorine mass balance based on extractable organofluorine (EOF) measurements. 39 PFAS standards have been subdivided into four subclasses, carboxylic and sulfonic acids, sulfonamides, and cationic/zwitterionic PFAS, and used for matrix-matched class-specific ACCs. Semiquantification was then performed for 96 tentatively identified PFAS in soil samples from the contaminated site. The fluorine mass balance was finally compared to the EOF measurements.

MATERIALS AND METHODS

Chemicals and Reagents. All chemicals were of LC-MS grade. Ammonium acetate (NH_4Ac), methanol (MeOH), and water were purchased from Thermo Fisher Scientific. For detailed information on the 51 authentic PFAS reference standards and the mass-labeled internal standards (IS) that were used for quantification, refer to the Supporting Information (SI, Tables S1 and S2).

Sampling and Processing of Soil Samples. Soil samples from the *Nachtwaidgraben* field site in Reilingen were taken in May 2023, as previously reported.[30] Shortly, at location *S1* four drill cores on a 1 × 1 m^2 (*S1−1, S1−2, S1−3, S1−4*), each reaching up to a depth of 3 m, were acquired (Figure S1). The drill cores were vertically divided into six sections, each measuring 0.5 m. Six composite depth section samples from the four drill cores were then prepared (*S1L1*: 0−0.5, *S1L2*: 0.5−1, *S1L3*: 1−1.5, *S1L4*: 1.5−2, *S1L5*: 2−2.5, *S1L6*: 2.5−3 m). Composite depth section samples were dried (40 °C), ground, and sieved (≤1.6 mm). 5 g soil per composite depth section sample was sequentially extracted three times with MeOH + 0.4 M NH_4Ac as reported elsewhere.[30] The final combined extracts were then used for all further analyses, including EOF measurements. To assess the recovery, the extraction method was tested on standard soil (LUFA SP6S, ∼1.55% organic carbon) spiked with the PFAS standard mixture. MEs were determined using IS spike, and extraction recoveries of compounds with available IS were corrected accordingly. Extraction efficiencies were further compared to sequential extraction with pure MeOH. Extraction blanks consisting of pure extraction solvent were processed the same way as the soil samples to check for background contamination during the extraction process.

Soil Characteristics. Total organic carbon (TOC) and cation exchange capacity (CEC) were determined for all depth sections. For TOC measurements, samples were additionally ground in an oscillating mill (MM400, Retsch, Germany) for 60 s at 20 Hz and analyzed for TOC with a SoliTOC Cube (Elementar, Germany), following DIN 19539.

CEC was determined with a modified NH_4Ac method at pH 8.5 as 5 of 12 soil samples had a pH > 7.4, indicating the presence of calcareous minerals.[40,41] 1.2 g of soil was weighed in a polypropylene (PP) tube, and 20 mL of 1 M NH_4Ac (pH 8.5) extraction solution was added. Samples were then shaken for 1 h, centrifuged for 10 min at 7830 relative centrifugal force (rcf), and the supernatant was filtered (0.2 μm, PES Agilent Captiva syringe filters). Extracts were stored at 4 °C, diluted (1:2, 1:10, and 1:100), and acidified (2% HNO_3) prior to analysis. The extracts were analyzed for Ca^{2+}, Mg^{2+}, Na^+, and K^+ at 393.366, 518.360, 588.995, and 766.491 nm, respectively, by microwave plasma−atomic emission spectroscopy (MP-AES, 4200 MPAES, Agilent Technologies, Australia). CEC was determined according to eq 1, where n is the amount of the respective cation in moles and m is the mass of soil in grams

$$\mathrm{CEC}\left(\frac{\mathrm{mmol_{charge}}}{100\ \mathrm{g_{soil}}}\right) = \frac{2\cdot n_{Ca^{2+}} + 2\cdot n_{Mg^{2+}} + n_{Na^+} + n_{K^+}}{m}\cdot 100 \quad (1)$$

Instrumental Analysis and Data Evaluation. Analysis of soil extracts, extraction blank, MeOH blank, and quality controls (QCs) was performed using a high-performance liquid chromatography (1290 HPLC from Agilent Technologies, Waldbronn, Germany) coupled to a quadrupole time-of-flight mass spectrometer with an electrospray ionization source (6550 QTOF, Agilent Technologies, Santa Clara, HPLC-ESI-QTOF-MS). An Agilent C_{18} column (Poroshell 120 EC-C_{18}, 2.1 × 100 mm, particle size 2.7 μm) was used for separation. Gradient elution with a total runtime of 22 min (chromatographic details in Table S3) with eluent A (95/5 H_2O/MeOH

https://doi.org/10.1021/acs.est.4c14255
Environ. Sci. Technol. 2025, 59, 7338−7347

+ 2 mM NH_4Ac) and eluent B (95/5 MeOH/H_2O + 2 mM NH_4Ac) was employed.

Both ionization modes (ESI−/ESI+) were applied separately. The QTOF was operated in data-dependent MS^2 mode ($ddMS^2$) with an acquisition rate of 3 spectra/s (MS^1 and MS^2). A precursor was selected for MS^2 if a threshold of 1000 counts was exceeded and was excluded for the next 0.5 min after recording 3 MS^2 spectra. The applied collision energy (CE) was determined according to eq 2, where m/z is the mass to charge ratio. This equation was optimized for PFAS standards and demonstrated optimal collision behavior for these compounds

$$\mathrm{CE}\ (m/z) = 3\frac{m/z}{100} + 15\ \mathrm{eV} \tag{2}$$

The 124 identified confidence level 1−3 substances from Schüßler et al.[30] were quantified (confidence level 1) or semiquantified (confidence level 2−3). A more detailed description of the identification of these PFAS and the assignment of the confidence levels can be found elsewhere.[30] The relative standard deviation (RSD) of replicate measurements was better than 5% (n = 5). Samples for quality control (QCs) were analyzed after every eighth sample and confirmed acceptable results with negligible instrument drift (±10%). No contaminants were detected in the extraction or measurement blanks.

Quantification and Semiquantification of PFAS in Topsoil (*S1L1*). The uppermost soil extract of *S1L1* (topsoil) was chosen to set up the quantification and semiquantification model due to the highest peak intensities in this sample. Due to the lack of commercially available mass-labeled internal standards, the basis for both models (quantification and semiquantification) is a standard addition approach in order to account for ME. For quantification (target PFAS, Table S1), standard addition was performed, using seven calibration points in the range of 0.1−10 μg/L in positive and negative ionization mode, respectively. Spiking of the respective volumes of PFAS standard mix into the sample was performed by the autosampler, mixing the respective proportions of PFAS standard mix, dilution solution (MeOH), and soil extract in-needle (total injection volume 10 μL). Diluted samples (1:20, 1:100, 1:200) were also spiked using the same procedure as the undiluted extracts, resulting in up to four calibration curves for each compound.

The limit of quantification (LOQ) was defined as the lowest measured standard for which an S/N ratio >10 was found. The MassHunter Qualitative Analysis 10.0 software was used to detect and integrate suspect peaks with the FindbyFormula algorithm (accuracy of ±10 ppm). The response (area) was calculated from the following ion species: $[M\text{-}H]^-$ for anionic PFAS and $[M + H]^+$, $[M + Na]^+$, $[M + K]^+$, $[M + NH_4]^+$, and $[M + C_2H_7N_2]^+$ (acetonitrile + NH_4) for cationic PFAS with neutral mass [M], as well as all detected isotopes. Neutral losses were not included due to false assignments by the software and to ensure a consistent approach. Consequently, even well-known neutral losses, such as $[M\text{-}CO_2\text{−}H]^-$ for perfluoroalkyl carboxylic acids (PFCAs), were not considered to avoid systematically underestimating tentatively identified PFAS. Linear and branched isomers were integrated and (semi)quantified together. Responses were exported and processed using an in-house developed Python code.

For the semiquantification model of suspect PFAS (Table S4), standard addition was applied as described before, in order to account for ME. Average calibration curves (ACC) were created via log−log transformation of the molar concentrations, and the responses of analytical reference standards were similar to those described by Cao et al.[34] In detail, the intercepts of the calibration curves of each standard (responses from soil sample) were subtracted, and the molar concentration and the responses were logarithmized (log−log transformation). Then, a linear regression of all data points was conducted (calibration curves of perfluorooctanesulfonic acid (PFOS), 6:2 fluorotelomer sulfonamide propyl betaine (FTSAm-Pr-B), and 5:1:2 fluorotelomer betaine (FTB) in the undiluted or less diluted extract matrices were omitted due to a too high concentration of the analyte in the sample itself, which distorts the calibration curves). To improve the accuracy of semiquantification, for each class of functional groups (carboxylic acids, sulfonic acids, sulfonamides, and cationic plus zwitterionic PFAS), a separate ACC was constructed. The four ACCs represent all available standards (Table S5). The ACCs were used to reestimate the concentration levels of the 39 PFAS standards. Absolute accuracy quotients (AAQs) were determined according to eq 3, where $C_{\mathrm{semiquant}}$ is derived from ACCs and C_{quant} is derived by calibration with standard additions of the respective analytical reference standards. Data points with high AAQs (>20) were manually reviewed and considered as outliers since they resulted from systematic errors (19 out of 852 data points).

$$\text{absolute accuracy quotient (AAQ)} = \begin{cases} \dfrac{C_{\mathrm{semiquant}}}{C_{\mathrm{quant}}}, \text{ if } C_{\mathrm{semiquant}} > C_{\mathrm{quant}} \\ \dfrac{C_{\mathrm{quant}}}{C_{\mathrm{semiquant}}}, \text{ if } C_{\mathrm{quant}} > C_{\mathrm{semiquant}} \end{cases} \tag{3}$$

The linear regressions were repeated without outliers to obtain the final four ACCs for the four classes of functional groups. These ACCs were used to perform semiquantification of 96 tentatively identified PFAS (levels 2 and 3 PFAS) which were subdivided also into the 4 ionization classes (Figure S2). If a PFAS contained several functional ionization moieties, it was semiquantified with the ACC with the lowest median AAQ, assuming the lowest error. If necessary, compounds were semiquantified at a 1:200 dilution to ensure that the response was within the calibration range of the applied ACC.

Semiquantification of Other Soil Depths. The matrix-matched ACCs specifically considered the ME of the topsoil extracts. To assess the applicability of these ACCs to soil samples from different depths (*S1L2*−*S1L6*), MEs at different depths were determined using an IS spike (4 μg/L, respectively, Table S2) and calculated according to eq 4, where area IS_{extract} is the peak area of the IS spiked to the soil extract and area $IS_{\mathrm{extract\ topsoil}}$ is the peak area of the IS spiked to the topsoil extract

$$\mathrm{ME}\ (\%) = \left(\frac{\text{area IS}_{\mathrm{extract}}}{\text{area IS}_{\mathrm{extract\ topsoil}}} - 1\right)\cdot 100 \tag{4}$$

Due to instrumental drift of the QTOF between different batches, the peak area was corrected using a factor based on peak area of topsoil from both measurements for each compound. The correction factors were between 0.5 and 5.1, but only 6 out of 124 substances had a factor exceeding 2

https://doi.org/10.1021/acs.est.4c14255
Environ. Sci. Technol. 2025, 59, 7338−7347

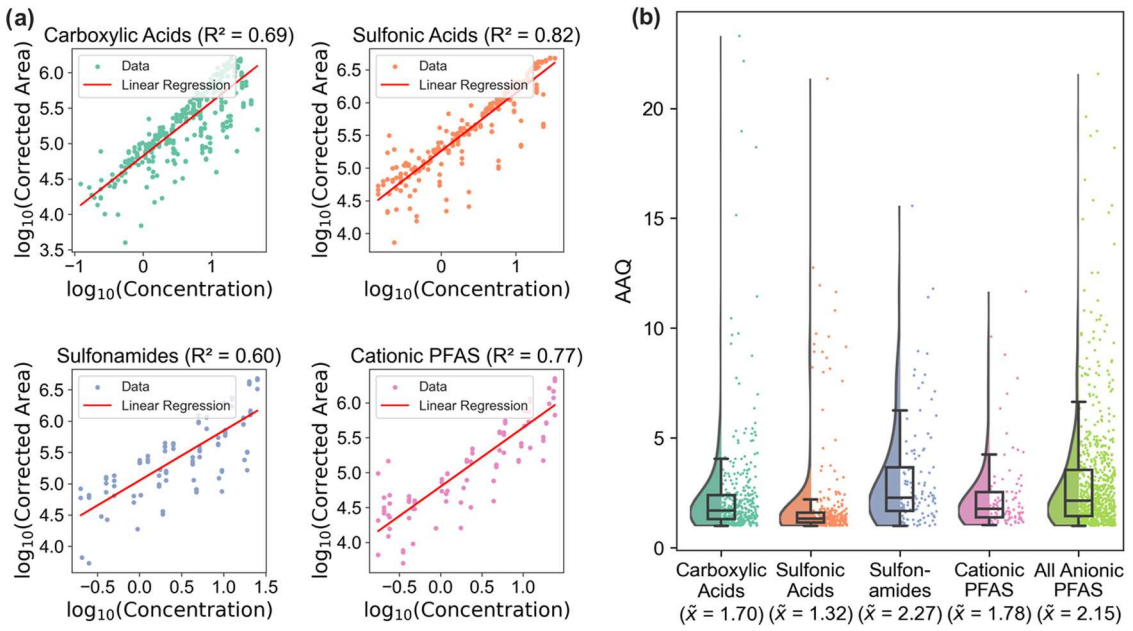

Figure 1. (a) Matrix-matched average calibration curves (ACCs) for four ionization classes based on 39 authentic standards at 7 concentration levels and 4 matrix dilutions (dots represent measured data, lines represent linear regression). (b) Absolute accuracy quotients (AAQ) of the semiquantification of standards for the four ionization classes and all anionic PFAS (box plots with median, 25 and 75 percentile and violin plots).

(mean: 1.1). The calibration curves of individual PFAS standards for quantification, as well as the constructed ACCs for semiquantification, were applied to the different depths, as described above. Concentrations of single PFAS had to be corrected due to peak saturation or concentrations outside the calibration range based on the deviation of the peak area of the undiluted sample compared to that of the diluted sample.

EOF. Extractable organofluorine (EOF) was determined for the top layer of soil (S1L1) by combustion ion chromatography (CIC). 250 μL of extract were injected and combusted in the induction furnace (AQF-2100H, GA-210, Mitsubishi Chemical Analytech, Tokyo, Japan) at 1050 °C under a flow of O_2 (300 mL/min) and Ar (150 mL/min). Combustion gases were absorbed in a freshly prepared 150 μmol/L NH_3 absorption solution with methyl sulfonate (~2 mg/L) as an internal standard in the absorption unit. 100 μL of the absorption solution was then analyzed by ion chromatography (IC; ICS Integrion, Thermo Fisher Scientific, Dreieich, Germany) on a Dionex IonPac AS20 (2 × 250 mm^2) separation column with a KOH gradient program. Fluoride ions were detected by suppressed conductivity using a dynamically regenerated suppressor (Dionex ADRS 600). A nine-point calibration with NH_4F at levels between 44 and 5000 μg F/L (R^2 = 0.9994) was used for quantification. All EOF samples were measured in triplicates. More details are given in the SI (Tables S6−S9).

RESULTS AND DISCUSSION

Method Validation. *Topsoil.* Semiquantification was performed using an ACC approach coupled with the standard addition method to consider ME and therefore improve the quantification accuracy. Distinct ACCs for four ionization classes of PFAS were constructed: cationic and zwitterionic compounds, carboxylic acids, sulfonic acids, and sulfonamides with 5, 21, 12, and 6 analytical reference standards, respectively (Figure 1a and Table S5). The four ACCs were used to reestimate the concentrations of 39 PFAS standards for 4 matrix dilutions at 7 concentration levels, which resulted in 28 data points for each PFAS standard. The AAQ was calculated using the quantified and the semiquantified concentration for each data point, yielding median values for cationic and zwitterionic PFAS, carboxylic acids, sulfonic acids, and sulfonamides of 1.78× (90th percentile = 4.3, n = 5), 1.70× (90th percentile = 4.0, n = 21), 1.32× (90th percentile = 2.5, n = 12), and 2.27× (90th percentile = 6.8, n = 6), respectively (Figure 1b). If all available anionic PFAS standards were used together for one ACC (n = 37), the median AAQ would be 2.15× (90th percentile = 5.7) and the variability would be greater compared to the separate ACCs for the different ionization classes (Figures 1b and S3). This clearly demonstrates that concentrations can be semiquantified more accurately, taking the different ionization classes into consideration. The median AAQ and the standard deviation are higher for sulfonamides, which is a result of the large structural variety of only 6 sulfonamide standards and hence a large range of RFs. Compared to the literature, the AAQs determined in this work are rather low (Table S10), proving the approach of matrix-matched ACCs for specific ionization classes of PFAS viable.[34−37]

All Soil Depths. To assess whether the matrix-matched ACCs for the topsoil are also applicable to other soil depths, the ME of different depths relative to the topsoil were evaluated with IS spikes. In general, most of the mass-labeled IS showed signal enhancement in the lower soil compared to the topsoil, while for short-chain PFCAs (perfluoropentanoic acid (PFPeA), perfluorohexanoic acid (PFHxA)), the signal was suppressed. The MEs of all isotopically labeled PFCAs and perfluoroalkyl sulfonic acids (PFSAs) ranged from −40 to 35% (Figure S4), with the range for individual substances varying between 15 and 40%, except for perfluorononanoic acid (PFNA) and PFOS. The reason for these two compounds deviating significantly in the topsoil is due to signal suppression in the upper soil layers, as PFOS is present in very high concentrations in these layers and coelutes with PFNA, but

https://doi.org/10.1021/acs.est.4c14255
Environ. Sci. Technol. 2025, 59, 7338−7347

also to signal enhancement in deeper soil layers. As mentioned before, substances with excessively high concentrations in the sample, such as PFOS, were therefore excluded from the ACCs. Since all other compounds exhibited MEs in an acceptable range for semiquantification and the fact that ACCs are also based on diluted samples with even lower MEs, the ACCs can be confidently applied to the other depth sections without any adaptation. Minor inaccuracies (<40%) had to be accepted, which, however, fall within the typical error range of semiquantification (Table S10).

PFAS Concentrations in Topsoil. PFAS concentrations were finally semiquantified for the topsoil (topsoil, *S1L1*) with matrix-matched ACCs of the four ionization classes for 96 tentatively identified AFFF PFAS resulting in a sum concentration of 7.86 μg/g (Figures 2, S5, and Table S11). Based on the ACC for cationic PFAS, 36 substances were semiquantified with a sum concentration of 6.83 μg/g. The most abundant cationic AFFFs are 6:2 fluorotelomer sulfoxide propanol trimethylamine (FTSO-(2′)OHPr-TriMeAm, 2.29 μg/g), 6:2 fluorotelomer sulfone propanol trimethylamine (FTSy-(2′)OHPr-TriMeAm, 1.88 μg/g), 7:1:2 FTB (0.88 μg/g), and 9:1:2 FTB (0.64 μg/g). With the sulfonamide-based ACC 6:2 fluorotelomer sulfonamide (FTSAm, 0.57 μg/g) and 9 further AFFF PFAS at a sum concentration of 0.69 μg/g were determined. In the case of anionic PFAS 8 carboxylic acids (sum of 0.14 μg/g) and 42 sulfonic acids (sum of 0.21 μg/g) were semiquantified. The results reveal the dominant abundance of cationic PFAS with 87% semiquantified in the topsoil (Table S11).

Based on matrix-matched standard calibration with authentic standards, 28 PFAS were quantified in the topsoil (Figures 2, S5, and Table S11). The highest concentrations were observed for the AFFF constituents PFOS (1.70 μg/g), 6:2 FTSAm-Pr-B (3.17 μg/g), and 5:1:2 FTB (1.11 μg/g), and the sum concentration is 7.33 μg/g. Also, cationic PFAS dominated with approximately 60%.

This pattern, characterized by many precursors and a high proportion of cationic PFAS, is typical of AFFF-contaminated sites. However, this contaminated soil exhibits a particularly diverse composition of PFAS, as different fire stations were involved, and thus foams from various manufacturers were applied.[5,30,42]

The total sum concentration of quantified and semiquantified PFAS is 15.19 μg/g or on a fluorine basis, 7.96 μg F/g. Comparison to the measured EOF of 7.8 μg F/g reveals a completely closed fluorine mass balance for the topsoil, which is a somehow surprising result considering the limited accuracy of the semiquantified PFAS. Nevertheless, the results show the importance of nontarget screening and semiquantification for site characterization.

Similar high concentrations have been found at other AFFF-contaminated sites, such as in the study by Bigler et al.,[43] which reported concentrations of 31 μg/g, Nickerson et al.,[5] who found up to 3.81 μg/g, at different firefighter training areas, or others.[44]

Since a dominant fraction of the PFAS contamination in the topsoil of 74% was due to cationic PFAS, the importance of addition of ammonia to the extraction solvent was of particular interest. For that, EOF in extracts from extraction with pure MeOH as extraction solvent was compared to those with MeOH + 0.4 M NH_4Ac. The results show that addition of NH_4Ac led to a significantly higher extraction yield of 7.8 μg F/g compared to 4.1 μg F/g with pure MeOH which exhibits

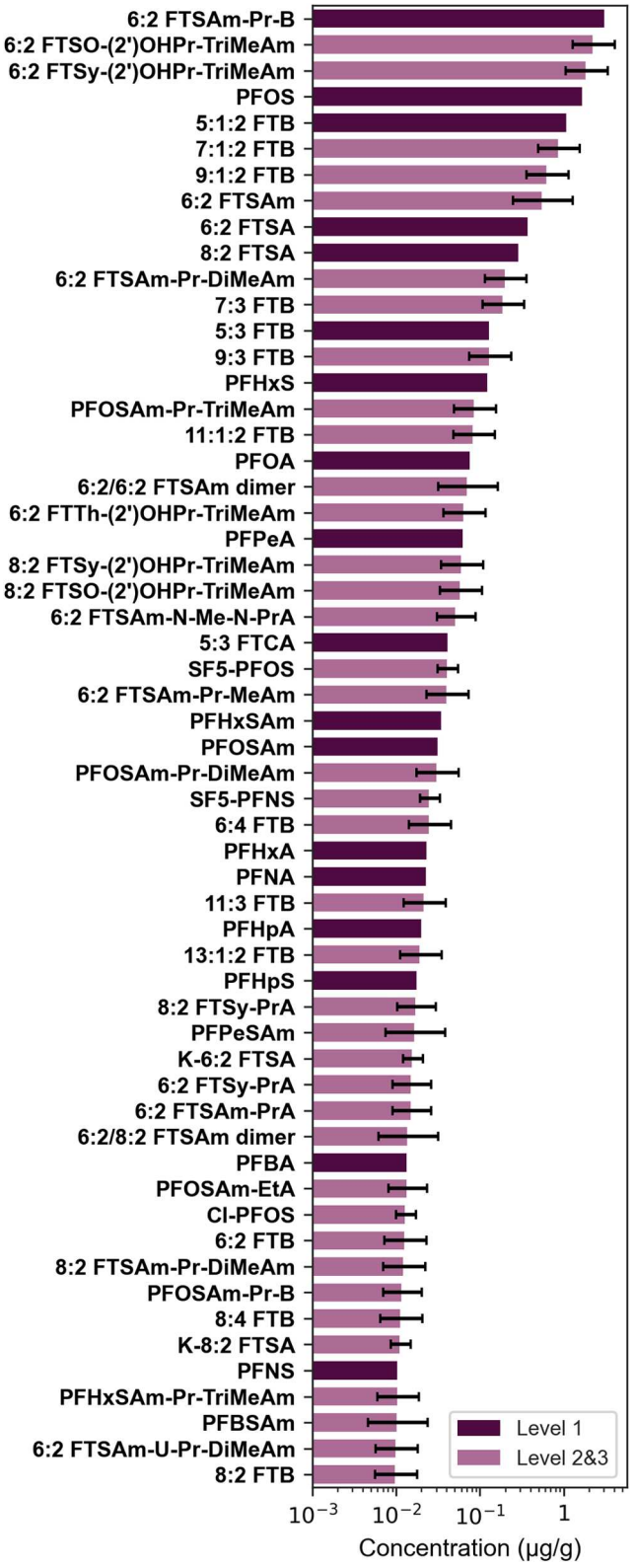

Figure 2. Concentrations of quantified (dark purple) and semiquantified (light purple) PFAS in the extract of topsoil on site *S1L1* in μg/g displayed with a logarithmic scale. Only compounds with concentrations $\geq 10^{-2}$ μg/g are shown (all compounds in Figure S5). Error bars for semiquantified PFAS represent the median AAQ of the corresponding ionization class (compound names and structures in Table S4 and concentrations in Table S11).

https://doi.org/10.1021/acs.est.4c14255
Environ. Sci. Technol. 2025, 59, 7338−7347

47% less organic fluorine (Figure 3 and Table S12). This underlines the importance of ammonia buffer addition for extractions of AFFF-contaminated soils dominated by cationic and zwitterionic PFAS.[45,46]

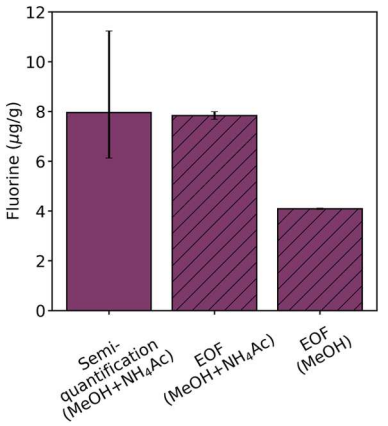

Figure 3. Equivalents of fluorine found by the semiquantification approach (extraction with MeOH + NH_4AC) and by EOF measurements after extractions with MeOH + NH_4Ac and with pure MeOH (error bars represent the median AAQs of the corresponding ionization classes for the semiquantification and the standard deviations for EOF measurements).

To determine the extraction recoveries for the applied extraction method (MeOH + 0.4 mM NH_4Ac), a spike experiment on a standard soil was conducted with a PFAS standard mix (Table S1). Consecutive extraction with MeOH + 0.4 mM NH_4Ac yielded extraction recoveries between 22.5 and 176.8% for cationic and zwitterionic PFAS. In total, only 8 out of 25 compounds showed recoveries between 70 and 130% (Table S13). However, most compounds with available IS were subject to a considerable ME, indicating that the extraction recoveries for other compounds might also be biased. This underlines the significance of MEs in (semi)-quantification methods and the importance of correcting for it, for instance, by a matrix-matched approach.

PFAS Concentrations in Deeper Soil Levels. Generally, the sum of quantified and semiquantified PFAS showed a decreasing concentration trend with depth. Although in the upper two layers 15.19 µg/g (*S1L1*, 0−0.5 m) and 13.34 µg/g (*S1L2*, 0.5−1 m) of PFAS are still found, the sum concentrations in the four bottom layers are only 4.03 µg/g (*S1L3*, 1−1.5 m), 5.02 µg/g (*S1L4*, 1.5−2 m), 1.75 µg/g (*S1L5*, 2−2.5 m), and 0.39 µg/g (*S1L6*, 2.5−3 m) (Figure 4, individual concentrations in Table S11). This means that the majority of the contamination is still present in the top 1 m soil layer (*S1L1* and *S1L2*). This is consistent with findings from other field studies[43,47,48] and may be caused by known retardation mechanisms like adsorption to solids and to the air−water interface. In the top first meter of soil, cationic/zwitterionic PFAS and sulfonamides constitute the largest proportion (Figures 5a and S6). Interestingly, some AFFF constituents (1.68 µg/g 5:2:1 FTB, 0.29 µg/g 5:3 FTB, 0.30 µg/g 6:2 fluorotelomer sulfonamide propyl methylamine (FTSAm-Pr-MeAm), and 0.91 µg/g 6:2 fluorotelomer sulfonamide propyl dimethylamine (FTSAm-Pr-DiMeAm)) and the potential AFFF degradation product 6:2 fluorotelomer sulfonic acid (FTSA, 0.85 µg/g) occur in the second top layer (*S1L2*, 0.5 m) at much higher concentrations than in the topsoil. This behavior may be explained by increased CEC and TOC values in *S1L2* (Figure 4) and therefore increased electrostatic interaction with cationic and zwitterionic PFAS, also observed in other studies.[49,50] However, sorption of zwitter- and cationic PFAS was shown to be complex and not be primarily determined by soil characteristics[51] and can be significantly affected by the presence of further foam constituents in AFFF formulations[52−54] and fluorophilic interactions among the PFAS themselves during the input event and later periods.[55]

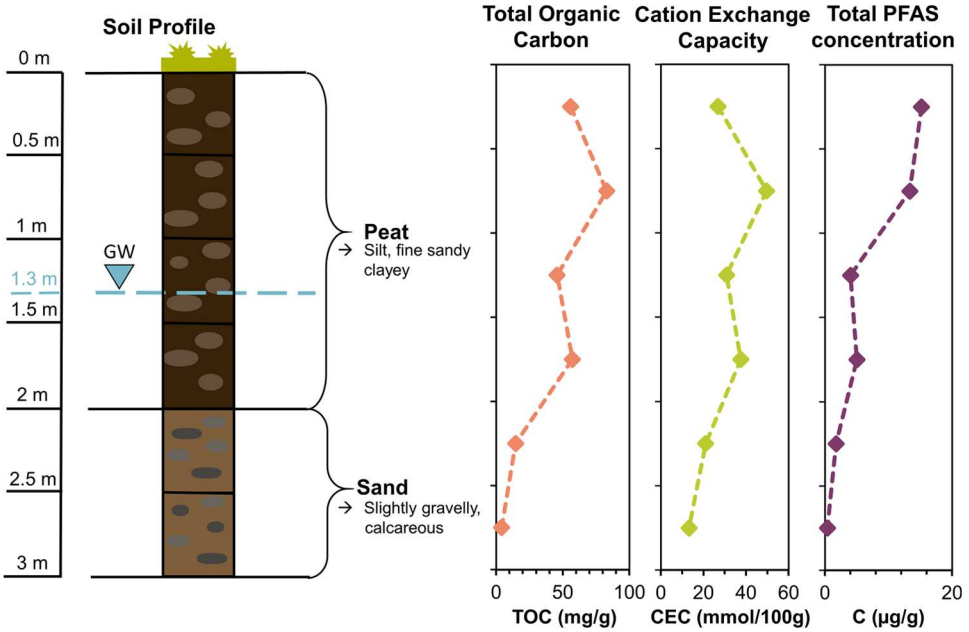

Figure 4. Soil profile for the six layers of *S1*(*L1*−*L6*) with groundwater level (GW), and trends for total organic carbon, cation exchange capacity, and total PFAS concentrations of all quantified and semiquantified PFAS from depths of 0−3 m.

https://doi.org/10.1021/acs.est.4c14255
Environ. Sci. Technol. 2025, 59, 7338−7347

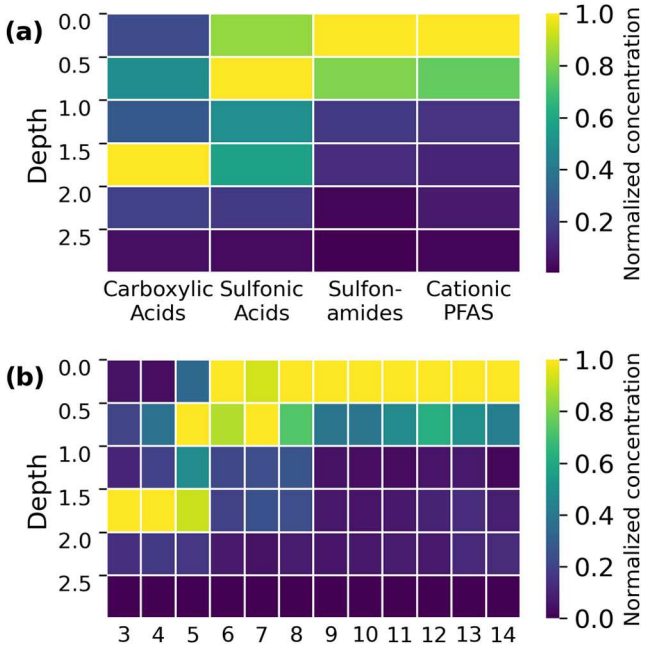

Figure 5. Depth distribution of the sum concentrations segmented by (a) ionization class and (b) chain length, depicted for a normalized scale based on the maximum concentration within an ionization class or chain length, respectively.

The anionic, rather mobile final TPs PFPeA, PFHxA, perfluoroheptanoic acid (PFHpA), and perfluorohexanesulfonic acid (PFHxS) show high concentrations in the saturated zone (Table S14), peaking in the fourth layer (*S1L4*, 1.5–2 m, Figures 5 and S6). This may represent a snapshot of the processes that are composed of in situ transformation of precursors in the two topsoil layers and the retarded transport of the TPs with the seepage water. It is known that sorption of anionic per- and polyfluoroalkyl acids (PFAAs) decreases with decreasing chain length and soil TOC[56] and the more rapid release of PFAAs from AFFF-impacted soils was also described in the literature.[57]

Strengths and Limitations of the Semiquantification Approach. The presented semiquantification approach demonstrates several notable strengths that highlight its effectiveness and reliability. Key features are the classification into specific ionization classes based on the known structures of the compounds and the inclusion of matrix-matched calibration, which both significantly improved the accuracy of the semiquantification.

Limitations of the approach arise from the fact that the structures of the analytes must be known for the classification and calibration and that the calibration must be adapted for each sample matrix. The method is also restricted to well-defined substance classes, and its applicability is dependent on the availability of suitable analytical standards for each ionization class. Substances that fall outside these classes pose challenges for this method due to the lack of matching standards. The accuracy could be improved by refining more groups, provided that suitable reference standards are available.

Given these constraints, predictive methods for ionization efficiency present an opportunity for future development. By integration of such methods, the limitations related to standard availability could be mitigated, expanding the applicability of semiquantification techniques.

Overall, the results emphasize the necessity of applying semiquantification approaches in nontarget screening studies. This approach has proven to be essential for characterizing PFAS contamination more comprehensively, providing a robust basis for remediation and risk assessment efforts.

■ ASSOCIATED CONTENT

Supporting Information

The Supporting Information is available free of charge at https://pubs.acs.org/doi/10.1021/acs.est.4c14255.

Chemicals; sampling site; LC-MS parameters; details to all (semi)quantified PFAS; semiquantification method (standards for individual ACCs, scheme); extractable organofluorine method; method validation (ACC of all anionic PFAS, MEs); concentrations of individual PFAS; extractable organofluorine values; extraction recovery; and depth distribution (PDF)

■ AUTHOR INFORMATION

Corresponding Author

Christian Zwiener − *Environmental Analytical Chemistry, Department of Geosciences, University of Tübingen, 72076 Tübingen, Germany;* orcid.org/0000-0002-6682-5828; Email: christian.zwiener@uni-tuebingen.de

Authors

Catharina Capitain − *Environmental Analytical Chemistry, Department of Geosciences, University of Tübingen, 72076 Tübingen, Germany;* orcid.org/0009-0006-5463-0835

Melanie Schüßler − *Environmental Analytical Chemistry, Department of Geosciences, University of Tübingen, 72076 Tübingen, Germany*

Boris Bugsel − *Environmental Analytical Chemistry, Department of Geosciences, University of Tübingen, 72076 Tübingen, Germany;* orcid.org/0000-0001-9752-9741

Jonathan Zweigle − *Department of Plant and Environmental Sciences, University of Copenhagen, Kobenhavn 1871, Denmark;* orcid.org/0000-0002-7194-1567

Christian Vogel − *Federal Institute for Materials Research and Testing, Division 4.4 − Thermochemical Residues Treatment and Resource Recovery, 12205 Berlin, Germany;* orcid.org/0000-0003-1357-695X

Peter Leube − *Federal Institute for Materials Research and Testing, Division 4.4 − Thermochemical Residues Treatment and Resource Recovery, 12205 Berlin, Germany*

Complete contact information is available at: https://pubs.acs.org/10.1021/acs.est.4c14255

Author Contributions

‖C.C. and M.S. are cofirst authors and they contributed equally to this work.

Funding

The authors acknowledge the Federal Ministry of Education and Research (BMBF) for funding the project PFClean (02WGW1665C), the Deutsche Bundesstiftung Umwelt (DBU) for the scholarship of J.Z., as well as Arcadis Germany GmbH and SAX+KLEE GmbH Bauunternehmung for coordinating and conducting the sampling.

Notes

The authors declare no competing financial interest.

ABBREVIATIONS

AAQ, absolute accuracy quotient; ACC, average calibration curve; AFFF, aqueous film-forming foams; CE, collision energy; CEC, cation exchange capacity; CIC, combustion ion chromatography; $ddMS_2$, data-dependent MS_2 mode; EOF, extractable organofluorine; ESI, electrospray ionization; FTB, fluorotelomer betaine; FTSA, fluorotelomer sulfonic acid; FTSAm, fluorotelomer sulfonamide; FTSAm-Pr-B, fluorotelomer sulfonamide propyl betaine; FTSAm-Pr-DiMeAm, fluorotelomer sulfonamide propyl dimethylamine; FTSAm-Pr-MeAm, fluorotelomer sulfonamide propyl methylamine; FTSO-(2′)OHPr-TriMeAm, fluorotelomer sulfoxide propanol trimethylamine; FTSy-(2′)OHPr-TriMeAm, fluorotelomer sulfone propanol trimethylamine; HPLC, high-performance liquid chromatography; HRMS, high-resolution mass spectrometry; IC, ion chromatography; IS, mass-labeled internal standard; LC, liquid chromatography; LOQ, limit of quantification; m/C, mass per carbon number; M8PFOS, perfluoro-[$^{13}C_8$]octanesulfonic acid; M9PFNA, perfluoro-n-[$^{13}C_9$]nonanoic acid; MD/C, mass defect per carbon number; ME, matrix effect; MeOH, methanol; MP-AES, microwave plasma−atomic emission spectrometer; NH_4Ac, ammonium acetate; NTS, nontarget screening; PFAA, per- and polyfluoroalkyl acid; PFAS, per- and polyfluoroalkyl substances; PFCA, perfluoroalkyl carboxylic acid; PFHpA, perfluoroheptanoic acid; PFHxA, perfluorohexanoic acid; PFHxS, perfluorohexanesulfonic acid; PFNA, perfluorononanoic acid; PFOA, perfluorooctanoic acid; PFOS, perfluorooctanesulfonic acid; PFPeA, perfluoropentanoic acid; PFSA, perfluoroalkyl sulfonic acid; PP, polypropylene; QC, quality control; QTOF, quadrupole time-of-flight; rcf, relative centrifugal forces; RF, response factor; RSD, relative standard deviation; SI, Supporting Information; TOC, total organic carbon; TP, transformation product

REFERENCES

(1) Bugsel, B.; Bauer, R.; Herrmann, F.; Maier, M. E.; Zwiener, C. LC-HRMS screening of per- and polyfluorinated alkyl substances (PFAS) in impregnated paper samples and contaminated soils. *Anal. Bioanal. Chem.* **2022**, *414* (3), 1217−1225.

(2) Zweigle, J.; Bugsel, B.; Röhler, K.; Haluska, A. A.; Zwiener, C. PFAS-Contaminated Soil Site in Germany: Nontarget Screening before and after Direct TOP Assay by Kendrick Mass Defect and FindPFΔS. *Environ. Sci. Technol.* **2023**, *57* (16), 6647−6655.

(3) Nickerson, A.; Maizel, A. C.; Kulkarni, P. R.; Adamson, D. T.; Kornuc, J. J.; Higgins, C. P. Enhanced Extraction of AFFF-Associated PFASs from Source Zone Soils. *Environ. Sci. Technol.* **2020**, *54* (8), 4952−4962.

(4) Röhler, K.; Susset, B.; Grathwohl, P. Production of perfluoroalkyl acids (PFAAs) from precursors in contaminated agricultural soils: Batch and leaching experiments. *Sci. Total Environ.* **2023**, *902*, No. 166555.

(5) Nickerson, A.; Rodowa, A. E.; Adamson, D. T.; Field, J. A.; Kulkarni, P. R.; Kornuc, J. J.; Higgins, C. P. Spatial Trends of Anionic, Zwitterionic, and Cationic PFASs at an AFFF-Impacted Site. *Environ. Sci. Technol.* **2021**, *55* (1), 313−323.

(6) Barzen-Hanson, K. A.; Roberts, S. C.; Choyke, S.; Oetjen, K.; McAlees, A.; Riddell, N.; McCrindle, R.; Ferguson, P. L.; Higgins, C. P.; Field, J. A. Discovery of 40 Classes of Per- and Polyfluoroalkyl Substances in Historical Aqueous Film-Forming Foams (AFFFs) and AFFF-Impacted Groundwater. *Environ. Sci. Technol.* **2017**, *51* (4), 2047−2057.

(7) Xu, B.; Liu, S.; Zhou, J. L.; Zheng, C.; Weifeng, J.; Chen, B.; Zhang, T.; Qiu, W. PFAS and their substitutes in groundwater: Occurrence, transformation and remediation. *J. Hazard. Mater.* **2021**, *412*, No. 125159.

(8) Backe, W. J.; Day, T. C.; Field, J. A. Zwitterionic, cationic, and anionic fluorinated chemicals in aqueous film forming foam formulations and groundwater from U.S. military bases by non-aqueous large-volume injection HPLC-MS/MS. *Environ. Sci. Technol.* **2013**, *47* (10), 5226−5234.

(9) Domingo, J. L.; Nadal, M. Human exposure to per- and polyfluoroalkyl substances (PFAS) through drinking water: A review of the recent scientific literature. *Environ. Res.* **2019**, *177*, No. 108648.

(10) Kotlarz, N.; McCord, J.; Collier, D.; Lea, C. S.; Strynar, M.; Lindstrom, A. B.; Wilkie, A. A.; Islam, J. Y.; Matney, K.; Tarte, P.; Polera, M. E.; Burdette, K.; DeWitt, J.; May, K.; Smart, R. C.; Knappe, D. R. U.; Hoppin, J. A. Measurement of Novel, Drinking Water-Associated PFAS in Blood from Adults and Children in Wilmington, North Carolina. *Environ. Health Perspect.* **2020**, *128* (7), 77005.

(11) Sadia, M.; Nollen, I.; Helmus, R.; Ter Laak, T. L.; Been, F.; Praetorius, A.; van Wezel, A. P. Occurrence, Fate, and Related Health Risks of PFAS in Raw and Produced Drinking Water. *Environ. Sci. Technol.* **2023**, *57* (8), 3062−3074.

(12) Goodrow, S. M.; Ruppel, B.; Lippincott, R. L.; Post, G. B.; Procopio, N. A. Investigation of levels of perfluoroalkyl substances in surface water, sediment and fish tissue in New Jersey, USA. *Sci. Total Environ.* **2020**, *729*, No. 138839.

(13) Witt, C. C.; Gadek, C. R.; Cartron, J. E.; Andersen, M. J.; Campbell, M. L.; Castro-Farias, M.; Gyllenhaal, E. F.; Johnson, A. B.; Malaney, J. L.; Montoya, K. N.; Patterson, A.; Vinciguerra, N. T.; Williamson, J. L.; Cook, J. A.; Dunnum, J. L. Extraordinary levels of per- and polyfluoroalkyl substances (PFAS) in vertebrate animals at a New Mexico desert oasis: Multiple pathways for wildlife and human exposure. *Environ. Res.* **2024**, *249*, No. 118229.

(14) Rupp, J.; Guckert, M.; Berger, U.; Drost, W.; Mader, A.; Nodler, K.; Nurenberg, G.; Schulze, J.; Sohlmann, R.; Reemtsma, T. Comprehensive target analysis and TOP assay of per- and polyfluoroalkyl substances (PFAS) in wild boar livers indicate contamination hot-spots in the environment. *Sci. Total Environ.* **2023**, *871*, No. 162028.

(15) Rotander, A.; Karrman, A.; Toms, L. M.; Kay, M.; Mueller, J. F.; Gomez Ramos, M. J. Novel fluorinated surfactants tentatively identified in firefighters using liquid chromatography quadrupole time-of-flight tandem mass spectrometry and a case-control approach. *Environ. Sci. Technol.* **2015**, *49* (4), 2434−2442.

(16) Olsen, G. W.; Mair, D. C.; Lange, C. C.; Harrington, L. M.; Church, T. R.; Goldberg, C. L.; Herron, R. M.; Hanna, H.; Nobiletti, J. B.; Rios, J. A.; Reagen, W. K.; Ley, C. A. Per- and polyfluoroalkyl substances (PFAS) in American Red Cross adult blood donors, 2000−2015. *Environ. Res.* **2017**, *157*, 87−95.

(17) Fábelová, L.; Beneito, A.; Casas, M.; Colles, A.; Dalsager, L.; Den Hond, E.; Dereumeaux, C.; Ferguson, K.; Gilles, L.; Govarts, E.; Irizar, A.; Lopez Espinosa, M. J.; Montazeri, P.; Morrens, B.; Patayova, H.; Rausova, K.; Richterova, D.; Rodriguez Martin, L.; Santa-Marina, L.; Schettgen, T.; Schoeters, G.; Haug, L. S.; Uhl, M.; Villanger, G. D.; Vrijheid, M.; Zaros, C.; Palkovicova Murinova, L. PFAS levels and exposure determinants in sensitive population groups. *Chemosphere* **2023**, *313*, No. 137530.

(18) Herzke, D.; Nikiforov, V.; Yeung, L. W. Y.; Moe, B.; Routti, H.; Nygard, T.; Gabrielsen, G. W.; Hanssen, L. Targeted PFAS analyses and extractable organofluorine - Enhancing our understanding of the presence of unknown PFAS in Norwegian wildlife. *Environ. Int.* **2023**, *171*, No. 107640.

(19) Roos, A. M.; Gamberg, M.; Muir, D.; Karrman, A.; Carlsson, P.; Cuyler, C.; Lind, Y.; Bossi, R.; Riget, F. Perfluoroalkyl substances in circum-ArcticRangifer: caribou and reindeer. *Environ. Sci. Pollut. Res. Int.* **2022**, *29* (16), 23721−23735.

(20) Garcia-Barrios, J.; Drysdale, M.; Ratelle, M.; Gaudreau, E.; LeBlanc, A.; Gamberg, M.; Laird, B. D. Biomarkers of poly- and perfluoroalkyl substances (PFAS) in Sub-Arctic and Arctic communities in Canada. *Int. J. Hyg. Environ. Health* **2021**, *235*, No. 113754.

https://doi.org/10.1021/acs.est.4c14255
Environ. Sci. Technol. 2025, 59, 7338−7347

(21) Bossi, R.; Dam, M.; Riget, F. F. Perfluorinated alkyl substances (PFAS) in terrestrial environments in Greenland and Faroe Islands. *Chemosphere* **2015**, *129*, 164−169.
(22) Kissa, E. *Fluorinated Surfactants and Repellents*; Marcel Dekker: New York, 2001.
(23) Fang, B.; Chen, H.; Zhou, Y.; Qiao, B.; Baqar, M.; Wang, Y.; Yao, Y.; Sun, H. Fluorotelomer betaines and sulfonic acid in aerobic wetland soil: Stability, biotransformation, and bacterial community response. *J. Hazard. Mater.* **2024**, *477*, No. 135261.
(24) Shahsavari, E.; Rouch, D.; Khudur, L. S.; Thomas, D.; Aburto-Medina, A.; Ball, A. S. Challenges and Current Status of the Biological Treatment of PFAS-Contaminated Soils. *Front. Bioeng. Biotechnol.* **2021**, *8*, No. 602040.
(25) Fenton, S. E.; Ducatman, A.; Boobis, A.; DeWitt, J. C.; Lau, C.; Ng, C.; Smith, J. S.; Roberts, S. M. Per- and Polyfluoroalkyl Substance Toxicity and Human Health Review: Current State of Knowledge and Strategies for Informing Future Research. *Environ. Toxicol. Chem.* **2020**, *40* (3), 606−630.
(26) Glüge, J.; Scheringer, M.; Cousins, I. T.; DeWitt, J. C.; Goldenman, G.; Herzke, D.; Lohmann, R.; Ng, C. A.; Trier, X.; Wang, Z. An overview of the uses of per- and polyfluoroalkyl substances (PFAS). *Environ. Sci.: Processes Impacts* **2020**, *22* (12), 2345−2373.
(27) D'Agostino, L. A.; Mabury, S. A. Identification of novel fluorinated surfactants in aqueous film forming foams and commercial surfactant concentrates. *Environ. Sci. Technol.* **2014**, *48* (1), 121−129.
(28) Liu, M.; Glover, C. M.; Munoz, G.; Duy, S. V.; Sauve, S.; Liu, J. Hunting the missing fluorine in aqueous film-forming foams containing per- and polyfluoroalkyl substances. *J. Hazard. Mater.* **2024**, *464*, No. 133006.
(29) Place, B. J.; Field, J. A. Identification of novel fluorochemicals in aqueous film-forming foams used by the US military. *Environ. Sci. Technol.* **2012**, *46* (13), 7120−7127.
(30) Schüßler, M.; Capitain, C.; Bugsel, B.; Zweigle, J.; Zwiener, C. Non-target screening reveals 124 PFAS at an AFFF-impacted field site in Germany specified by novel systematic terminology *Anal. Bioanal. Chem.* 2024 DOI: 10.1007/s00216-024-05611-3.
(31) Malik, P.; Nandini, D.; Tripathi, B. P. Firefighting aqueous film forming foam composition, properties and toxicity: a review. *Environ. Chem. Lett.* **2024**, *22* (4), 2013−2033.
(32) Kaufmann, A.; Butcher, P.; Maden, K.; Walker, S.; Widmer, M. Simplifying Nontargeted Analysis of PFAS in Complex Food Matrixes. *J. AOAC Int.* **2022**, *105* (5), 1280−1287.
(33) Zweigle, J.; Bugsel, B.; Fabregat-Palau, J.; Zwiener, C. PFΔScreen - an open-source tool for automated PFAS feature prioritization in non-target HRMS data. *Anal. Bioanal. Chem.* **2024**, *416* (2), 349−362.
(34) Cao, D.; Schwichtenberg, T.; Duan, C.; Xue, L.; Muensterman, D.; Field, J. Practical Semiquantification Strategy for Estimating Suspect Per- and Polyfluoroalkyl Substance (PFAS) Concentrations. *J. Am. Soc. Mass Spectrom.* **2023**, *34* (5), 939−947.
(35) Pu, S.; McCord, J. P.; Bangma, J.; Sobus, J. R. Establishing performance metrics for quantitative non-targeted analysis: a demonstration using per- and polyfluoroalkyl substances. *Anal. Bioanal. Chem.* **2024**, *416* (5), 1249−1267.
(36) Lauria, M. Z.; Sepman, H.; Ledbetter, T.; Plassmann, M.; Roos, A. M.; Simon, M.; Benskin, J. P.; Kruve, A. Closing the Organofluorine Mass Balance in Marine Mammals Using Suspect Screening and Machine Learning-Based Quantification. *Environ. Sci. Technol.* **2024**, *58* (5), 2458−2467.
(37) Malm, L.; Liigand, J.; Aalizadeh, R.; Alygizakis, N.; Ng, K.; Fro Kjaer, E. E.; Nanusha, M. Y.; Hansen, M.; Plassmann, M.; Bieber, S.; Letzel, T.; Balest, L.; Abis, P. P.; Mazzetti, M.; Kasprzyk-Hordern, B.; Ceolotto, N.; Kumari, S.; Hann, S.; Kochmann, S.; Steininger-Mairinger, T.; Soulier, C.; Mascolo, G.; Murgolo, S.; Garcia-Vara, M.; Lopez de Alda, M.; Hollender, J.; Arturi, K.; Coppola, G.; Peruzzo, M.; Joerss, H.; van der Neut-Marchand, C.; Pieke, E. N.; Gago-Ferrero, P.; Gil-Solsona, R.; Licul-Kucera, V.; Roscioli, C.; Valsecchi, S.; Luckute, A.; Christensen, J. H.; Tisler, S.; Vughs, D.; Meekel, N.; Talavera Andujar, B.; Aurich, D.; Schymanski, E. L.; Frigerio, G.; Macherius, A.; Kunkel, U.; Bader, T.; Rostkowski, P.; Gundersen, H.; Valdecanas, B.; Davis, W. C.; Schulze, B.; Kaserzon, S.; Pijnappels, M.; Esperanza, M.; Fildier, A.; Vulliet, E.; Wiest, L.; Covaci, A.; Macan Schonleben, A.; Belova, L.; Celma, A.; Bijlsma, L.; Caupos, E.; Mebold, E.; Le Roux, J.; Troia, E.; de Rijke, E.; Helmus, R.; Leroy, G.; Haelewyck, N.; Chrastina, D.; Verwoert, M.; Thomaidis, N. S.; Kruve, A. Quantification Approaches in Non-Target LC/ESI/HRMS Analysis: An Interlaboratory Comparison. *Anal. Chem.* **2024**, *96* (41), 16215−16226.
(38) Hasegawa, K.; Minakata, K.; Suzuki, M.; Suzuki, O. The standard addition method and its validation in forensic toxicology. *Forensic Toxicol.* **2021**, *39* (2), 311−333.
(39) Kruve, A. Semi-quantitative non-target analysis of water with liquid chromatography/high-resolution mass spectrometry: How far are we? *Rapid Commun. Mass Spectrom.* **2019**, *33* (S3), 54−63.
(40) Strobel, C.; Doerrich, M.; Stieff, E. H.; Huisman, J. A.; Cirpka, O. A.; Mellage, A. Organic Matter Matters—The Imaginary Conductivity of Sediments Rich in Solid Organic Carbon. *Geophys. Res. Lett.* **2023**, *50* (23), No. e2023GL104630, DOI: 10.1029/2023GL104630.
(41) Sumner, M. E.; Miller, W. P. Cation Exchange Capacity and Exchange Coefficients. In *Methods of Soil Analysis*; Sparks, D. L.; Page, A. L.; Helmke, P. A.; Loeppert, R. H.; Soltanpour, P. N.; Tabatabai, M. A.; Johnston, C. T.; Sumner, M. E., Eds.; SSSABook Series, Vol. Part 3 Chemical Methods; Soil Science Society of America, 1996; pp 1201−1229.
(42) Yan, P. F.; Dong, S.; Pennell, K. D.; Capiro, N. L. A review of the occurrence and microbial transformation of per- and polyfluoroalkyl substances (PFAS) in aqueous film-forming foam (AFFF)-impacted environments. *Sci. Total Environ.* **2024**, *927*, No. 171883.
(43) Bigler, M. C.; Brusseau, M. L.; Guo, B.; Jones, S. L.; Pritchard, J. C.; Higgins, C. P.; Hatton, J. High-Resolution Depth-Discrete Analysis of PFAS Distribution and Leaching for a Vadose-Zone Source at an AFFF-Impacted Site. *Environ. Sci. Technol.* **2024**, *58* (22), 9863−9874.
(44) Ehsan, M. N.; Riza, M.; Pervez, M. N.; Li, C.-W.; Zorpas, A. A.; Naddeo, V. PFAS contamination in soil and sediment: Contribution of sources and environmental impacts on soil biota. *Case Stud. Chem. Environ. Eng.* **2024**, *9*, No. 100643.
(45) Munoz, G.; Ray, P.; Mejia-Avendano, S.; Duy, S. V.; Do, D. T.; Liu, J.; Sauve, S. Optimization of extraction methods for comprehensive profiling of perfluoroalkyl and polyfluoroalkyl substances in firefighting foam impacted soils. *Anal. Chim. Acta* **2018**, *1034*, 74−84.
(46) Munoz, G.; Taxil-Paloc, A.; Desrosiers, M.; Duy, S. V.; Liu, M.; Houde, M.; Liu, J.; Sauve, S. Zwitterionic, cationic, and anionic PFAS in freshwater sediments from AFFF-impacted and non-impacted sites of Eastern Canada. *J. Hazard. Mater.* **2025**, *484*, No. 136634.
(47) Brusseau, M. L.; Anderson, R. H.; Guo, B. PFAS concentrations in soils: Background levels versus contaminated sites. *Sci. Total Environ.* **2020**, *740*, No. 140017.
(48) Baduel, C.; Mueller, J. F.; Rotander, A.; Corfield, J.; Gomez-Ramos, M.-J. Discovery of novel per- and polyfluoroalkyl substances (PFASs) at a fire fighting training ground and preliminary investigation of their fate and mobility. *Chemosphere* **2017**, *185*, 1030−1038.
(49) Nguyen, T. M. H.; Bräunig, J.; Thompson, K.; Thompson, J.; Kabiri, S.; Navarro, D. A.; Kookana, R. S.; Grimison, C.; Barnes, C. M.; Higgins, C. P.; McLaughlin, M. J.; Mueller, J. F. Influences of Chemical Properties, Soil Properties, and Solution pH on Soil-Water Partitioning Coefficients of Per- and Polyfluoroalkyl Substances (PFASs). *Environ. Sci. Technol.* **2020**, *54* (24), 15883−15892.
(50) Barzen-Hanson, K. A.; Davis, S. E.; Kleber, M.; Field, J. A. Sorption of Fluorotelomer Sulfonates, Fluorotelomer Sulfonamido Betaines, and a Fluorotelomer Sulfonamido Amine in National Foam Aqueous Film-Forming Foam to Soil. *Environ. Sci. Technol.* **2017**, *51* (21), 12394−12404.

(51) Wanzek, T.; Stults, J. F.; Johnson, M. G.; Field, J. A.; Kleber, M. Role of Mineral−Organic Interactions in PFAS Retention by AFFF-Impacted Soil. *Environ. Sci. Technol.* **2023**, *57*, 5231.
(52) Arshadi, M.; Garza-Rubalcava, U.; Guedes, A.; Capiro, N. L.; Pennell, K. D.; Christ, J.; Abriola, L. M. Modeling 1-D aqueous film forming foam transport through the vadose zone under realistic site and release conditions. *Sci. Total Environ.* **2024**, *919*, No. 170566.
(53) Guelfo, J. L.; Higgins, C. P. Subsurface transport potential of perfluoroalkyl acids at aqueous film-forming foam (AFFF)-impacted sites. *Environ. Sci. Technol.* **2013**, *47* (9), 4164−4171.
(54) Pan, G.; Jia, C.; Zhao, D.; You, C.; Chen, H.; Jiang, G. Effect of cationic and anionic surfactants on the sorption and desorption of perfluorooctane sulfonate (PFOS) on natural sediments. *Environ. Pollut.* **2009**, *157* (1), 325−330.
(55) Wanzek, T. A.; Field, J. A.; Kostarelos, K. Repeated Aqueous Film-Forming Foams Applications: Impacts on Polyfluoroalkyl Substances Retention in Saturated Soil. *Environ. Sci. Technol.* **2024**, *58* (3), 1659−1668.
(56) Higgins, C. P.; Luthy, R. G. Sorption of Perfluorinated Surfactants on Sediments. *Environ. Sci. Technol.* **2006**, *40* (23), 7251−7256.
(57) Maizel, A. C.; Shea, S.; Nickerson, A.; Schaefer, C.; Higgins, C. P. Release of Per- and Polyfluoroalkyl Substances from Aqueous Film-Forming Foam Impacted Soils. *Environ. Sci. Technol.* **2021**, *55* (21), 14617−14627.

https://doi.org/10.1021/acs.est.4c14255
Environ. Sci. Technol. 2025, 59, 7338−7347

Supporting Information for

Implementation of matrix-matched semiquantification of PFAS in AFFF contaminated soil

Catharina Capitain[‡,⊥], *Melanie Schüßler*[‡,⊥], *Boris Bugsel*[⊥], *Jonathan Zweigle*[†], *Christian Vogel*[§], *Peter Leube*[§], *Christian Zwiener*[*,⊥]

[⊥]Environmental Analytical Chemistry, Department of Geosciences, University of Tübingen, Schnarrenbergstraße 94-96, 72076 Tübingen, Germany

[†]Department of Plant and Environmental Sciences, University of Copenhagen, Thorvaldsensvej 40, Frederiksberg 1871, Denmark

[§]Federal Institute for Materials Research and Testing, Division 4.4 – Thermochemical Residues Treatment and Resource Recovery, Unter den Eichen 87, 12205 Berlin, Germany

Number of pages: 24

Number of Tables: 14

Number of Figures: 6

Table of content

A. Chemicals

Table S1. Overview of all PFAS reference standards that were included in the PFAS standard mixture and where they were purchased. PFAS originated either from Wellington Laboratories, Guelph, Ontario, Canada (1), Toronto Research Chemicals, North York, Ontario, Canada (2), Dr. Ehrenstorfer, Augsburg, Bavaria, Germany (3) or were custom-synthesized in-house (4).

Acronym	Used standard / purchased chemical	Origin
PFCAs		
PFBA	Perfluorobutanoic acid / perfluoro-n-butanoic acid	(1)
PFPeA	Perfluoropentanoic acid / perfluoro-n-pentanoic acid	(1)
PFHxA	Perfluorohexanoic acid / perfluoro-n-hexanoic acid	(1)
PFHpA	Perfluoroheptanoic acid / perfluoro-n-heptanoic acid	(1)
PFOA	Perfluorooctanoic acid / perfluoro-n-octanoic acid	(1)
PFNA	Perfluorononanic acid / perfluoro-n-nonanic acid	(1)
PFDA	Perfluorodecanoic acid / perfluoro-n-decanoic acid	(1)
PFUnDA	Perfluoroundecanoic acid / perfluoro-n-undecanoic acid	(1)
PFDoDA	Perfluorododecanoic acid / perfluoro-n-dodecanoic acid	(1)
PFTriDA	Perfluorotridecanoic acid / perfluoro-n-tridecanoic acid	(1)
PFTeDA	Perfluorotetradecanoic acid / perfluoro-n-tetradecanoic acid	(1)
PFHxDA	Perfluorohexadecanoic acid / perfluoro-n-hexadecanoic acid	(1)
PFODA	Perfluorooctadecanoic acid / perfluoro-n-octadecanoic acid	(1)
PFSAs		
PFBS	Perfluorobutanesulfonic acid / potassium perfluoro-1-butanesulfonate	(1)
PFPeS	Perfluoropentanesulfonic acid / sodium perfluoro-1-pentanesulfonate	(1)
PFHxS	Perfluorohexanesulfonic acid / sodium perfluoro-1-hexanesulfonate	(1)
PFHpS	Perfluoroheptanesulfonic acid / sodium perfluoro-1-heptanesulfonate	(1)
PFOS	Perfluorooctanesulfonic acid / sodium perfluoro-1-octanesulfonate	(1)
PFNS	Perfluorononanesulfonic acid / sodium perfluoro-1-nonanesulfonate	(1)
PFDS	Perfluorodecanesulfonic acid / sodium perfluoro-1-decanesulfonate	(1)
PFDoDS	Perfluorododecanesulfonic acid / sodium perfluoro-1-dodecanesulfonate	(1)
PFPAs		
PFOPA	Perfluorooctylphosphonic acid	(1)
PFDPA	Perfluorodecylphosphonic acid	(1)
PAPs		
6:2/6:2 diPAP	6:2/6:2 phosphoric acid diester / Bis[2-(perfluorohexyl)ethyl]phosphate	(2)
8:2/8:2 diPAP	6:2/6:2 polyfluoroalkyl phosphoric acid diester / Sodium bis (1H, 1H, 2H, 2H-perfluorodecyl) phosphate	(1)
6:2 PAP	6:2 polyfluoroalkyl phosphoric ester / Mono[2-(perfluorohexyl)ethyl] phosphate	(2)
8:2 PAP	6:2 polyfluoroalkyl phosphoric ester / Sodium 1H, 1H, 2H, 2H-perfluorodecyl phosphate	(1)
PFPiAs		
C6/C6 PFPiA	C6/C6 Perfluoroalkyl phosphinic acid	(2)
PASF-based PFAS		
PFHxSAm	Perfluorohexane sulfonamide	(3)
PFOSAm	Perfluorooctane sulfonamide	(1)
PFOSAm-*N*-Et-*N*-EtA	Perfluorooctane sulfonamide *N*-ethyl *N*-ethanoic acid	(1)
SamPAP	Perfluorooctane sulfonamide ethanol-based phosphate diester /Sodium-2-(N-ethylperfluorooctane-1-sulfonamido) ethyl phosphate	(1)
diSAmPAP	Perfluorooctane sulfonamide ethanol-based phosphate diester/ Sodium bis[2-(N-ethylperfluorooctane-1-sulfonamido) ethyl] phosphate	(1)
FTCAs		
6:2 FTCA	6:2 fluorotelomer carboxylic acid / 2-Perfluorohexyl ethanoic acid (6:2)	(1)

8:2 FTCA	8:2 fluorotelomer carboxylic acid / 2-Perfluorooctyl ethanoic acid (6:2)	(1)
5:3 FTCA	5:3 fluorotelomer carboxylic acid/ 3-Perfluoropentyl propanoic acid	(1)
7:3 FTCA	7:3 fluorotelomer carboxylic acid/ 3-Perfluoroheptyl propanoic acid	(1)
FTUCAs		
6:2 FTUCA	6:2 fluorotelomer unsaturated carboxylic acid/ 2H-Perfluoro-2-octenoic acid (6:2)	(1)
8:2 FTUCA	8:2 fluorotelomer unsaturated carboxylic acid/ 2H-Perfluoro-2-decenoic acid (8:2)	(1)
FTSAs		
6:2 FTSA	6:2 fluorotelomer sulfonic acid / Sodium 1H, 1H,2H,2H-perfluorooctanesulfonate	(1)
8:2 FTSA	8:2 fluorotelomer sulfonic acid / Sodium 1H, 1H,2H,2H-perfluorodecanesulfonate	(1)
FTMAPs		
6:2 FTMAP	6:2 Fluorotelomer mercapto alkyl phosphate	(4)
PFECAs		
HFPO-Da	2,3,3,3-Tetrafluoro-2-(1,1,2,2,3,3,3-heptafluoropropoxy) propanoic acid	(1)
ADONA	Sodium dodecafluoro-3H-4,8-dioxanonanoate	(1)
PFESAs		
9Cl-PF3ONS	Potassium 9-chlorhexadecafluoro-3-oxanonane-1-sulfonate	(1)
11Cl-PF3OUdS	Potassium 11-chloroeicosafluoro-3-oxaundecane-1-sulfonate	(1)
AFFF-substances		
6:2 FTSAm-Pr-DiMeNO	6:2 fluorotelomer sulfonamide propyl methylamineoxide / Capstone product A	(3)
6:2 FTSAm-Pr-B	6:2 fluorotelomer sulfonamide propyl betaine / Capstone product B	(3)
PFHxSAm-Pr-DiMeAm	N-[3(dimethylamino)propyl] perfluoro-1-hexanesulfonamide	(3)
5:3 FTB	5:3 Fluorotelomer Betaine / 2-[4,4,5,5,6,6,7,7,8,8,8-Undecafluorooctyl) dimethylammonio] acetate	(1)
5:1:2 FTB	5:1:2 Fluorotelomer Betaine / 2-[(3,4,4,5,5,6,6,7,7,8,8,8-Dodecafluorooctyl) dimethylammonio] acetate	(1)

Table S2. Internal standards that were used for quantification of the matrix effect in the samples. Internal standards were acquired from Wellington laboratories.

Native PFAS	Mass labeled internal standard
PFPeA	M5PFPeA
PFHxA	M5PFHxA
PFHpA	M4PFHpA
PFOA	M8PFOA
PFNA	M9PFNA
PFDA	M6PFDA
PFUnDA	M7PFUnDA
PFDoDA	MPFDoDA
PFTeDA	M2PFTeDA
PFBS	M3PFBS
PFHxS	M3PFHxS
PFOS	M8PFOS

B. Sampling site

Sampling Site (Soil)	Coordinates
S1-1	49°17'49.2396"N 8°33'40.8816"E
S1-2	49°17'49.2036"N 8°33'40.9284"E
S1-3	49°17'49.1712"N 8°33'40.8816"E
S1-4	49°17'49.2072"N 8°33'40.8312"E

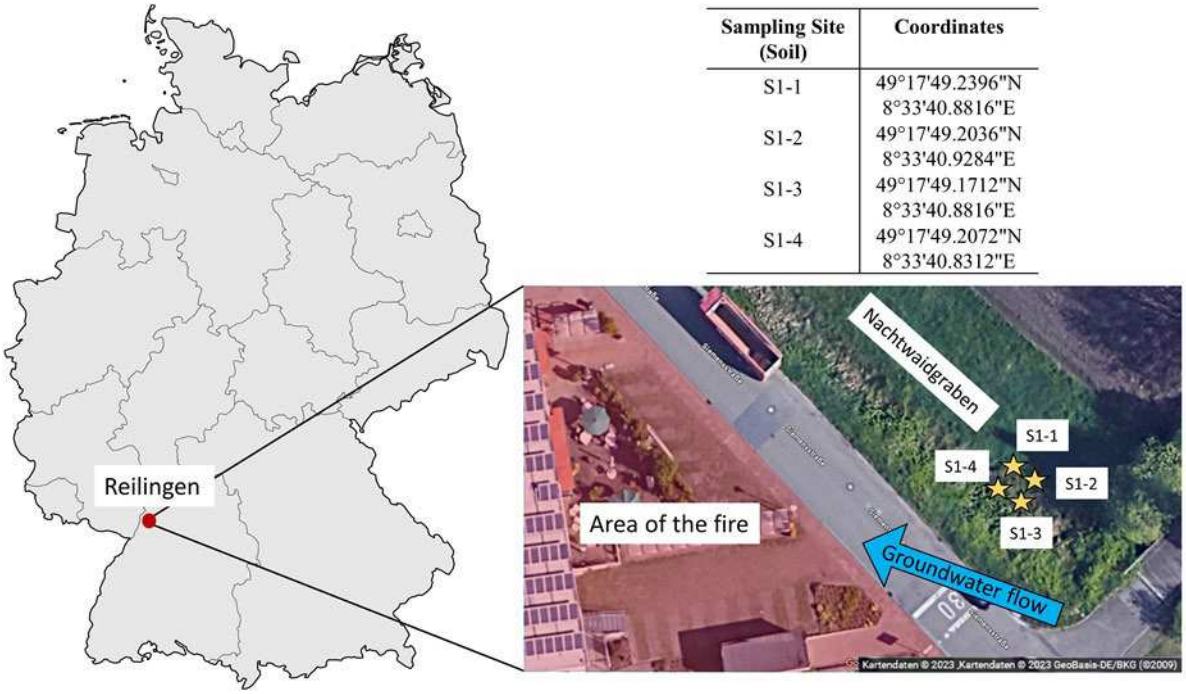

Figure S1. Overview of the sampling site 'Nachtwaidgraben' in Reilingen, Baden Württemberg and coordinates of the respective sampling points. Yellow stars represent the soil sampling points. The screenshot of the field site was taken from Google Maps (15.12.2023). Groundwater flow was determined by Arcadis. Source of map: Wikimedia Commons [1].

C. LC-MS parameters

Table S3. Elution gradient of the applied HPLC-QTOF Method with eluent A (95/5 H_2O/MeOH + 2 mM NH_4Ac) and eluent B (95/5 MeOH/H_2O + 2mM NH_4Ac).

Time (min)	Eluent A (%)	Eluent B (%)
0.0	85	15
2.0	30	70
5.0	10	90
10.0	0	100
15.0	0	100
15.1	85	15
22.0	85	15

D. Details to all (semi)quantified PFAS

Table 4: Acronyms and full names of subclasses/compounds with an example structure, formula, confidence level, ion species and theoretical m/z. Substance classes are organized according to the four ionizing groups of the ACCs.

Subclass	Example structure	Acronym	Neutral formula [M]	Confidence Level	Ion	Theoretical m/z
Ionization class: Carboxylic Acids						
PFCA *Perfluoro carboxylic acid*	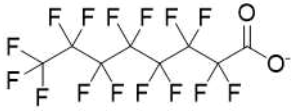	PFBA	C4HF7O2	1	[M-H]-	212.9792
		PFPeA	C5HF9O2	1	[M-H]-	262.9760
		PFHxA	C6HF11O2	1	[M-H]-	312.9728
		PFHpA	C7HF13O2	1	[M-H]-	362.9696
		PFOA	C8HF15O2	1	[M-H]-	412.9664
		PFNA	C9HF17O2	1	[M-H]-	462.9632
		PFDA	C10HF19O2	1	[M-H]-	512.9600
		PFUnDA	C11HF21O2	1	[M-H]-	562.9568
		PFDoDA	C12HF23O2	1	[M-H]-	612.9537
PFASAm-EtA *Perfluoroalkane sulfonamide ethanoic acid*	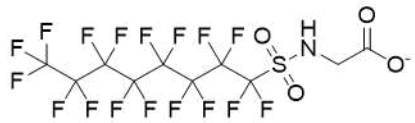	PFHxSAm-EtA	C8H4F13NO4S	2	[M-H]-	455.9581
		PFOSAm-EtA	C10H4F17NO4S	2	[M-H]-	555.9517
PFASAm-Pr-B *Perfluoroalkane sulfonamide propyl betaine*	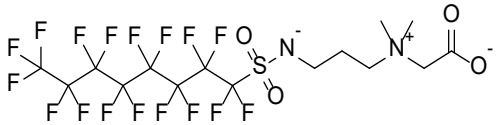	PFBSAm-Pr-B	C11H15F9N2O4S	2	[M+H]+	443.0682
		PFHxSAm-Pr-B	C13H15F13N2O4S	2	[M+H]+	543.0618
					[M-H]-	541.0472
		PFOSAm-Pr-B	C15H15F17N2O4S	2	[M+H]+	643.0554
					[M-H]-	641.0408
n:3 FTCA *n:3 fluorotelomer carboxylic acid*	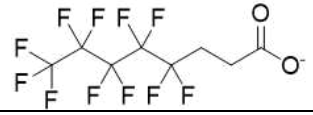	5:3 FTCA	C8H5F11O2	1	[M-H]-	341.0041
		7:3 FTCA	C10H5F15O2	1	[M-H]-	440.9977
n:2 FTSAm-Pr-B *n:2 fluorotelomer sulfonamide propyl betaine*	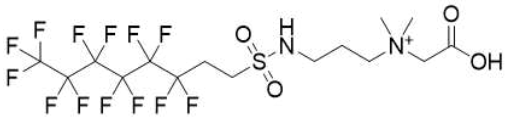	6:2 FTSAm-Pr-B	C15H19F13N2O4S	1	[M+H]+	571.0931
					[M-H]-	569.0785
		8:2 FTSAm-Pr-B	C17H19F17N2O4S	2	[M+H]+	671.0867

n:2 FTSAm-PrA *n:2 fluorotelomer sulfonamide propanoic acid*	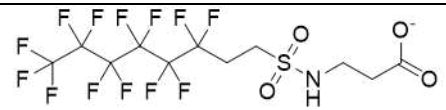	6:2 FTSAm-PrA	C11H10F13NO4S	2	[M-H]-	498.0050
n:2 FTSAm-*N*-Me-*N*-PrA *n:2 fluorotelomer sulfonamide N-methyl N-propanoic acid*	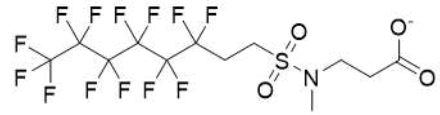	6:2 FTSAm-*N*-Me-*N*-PrA	C12H12F13NO4S	2	[M+H]+	514.0352
					[M-H]-	512.0207
n:2 FTSy-PrA *n:2 fluorotelomer sulfone propanoic acid*	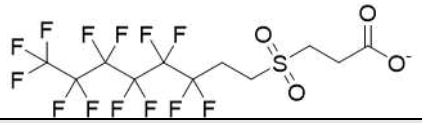	6:2 FTSy-PrA	C11H9F13O4S	2	[M-H]-	482.9941
		8:2 FTSy-PrA	C13H9F17O4S	2	[M-H]-	582.9877
Ionization class: Sulfonic Acids						
PFSA *Perfluoro sulfonic acid*	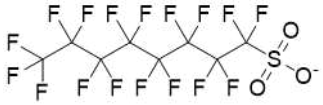	PFPrS	C3HF7O3S	2	[M-H]-	248.9462
		PFBS	C4HF9O3S	1	[M-H]-	298.9430
		PFPeS	C5HF11O3S	1	[M-H]-	348.9398
		PFHxS	C6HF13O3S	1	[M-H]-	398.9366
		PFHpS	C7HF15O3S	1	[M-H]-	448.9334
		PFOS	C8HF17O3S	1	[M-H]-	498.9302
		PFNS	C9HF19O3S	1	[M-H]-	548.9270
U-PFSA *Unsaturated perfluoro sulfonic acid*	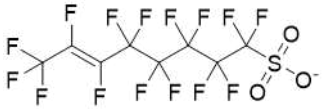	U-PFHxS	C6HF11O3S	2	[M-H]-	360.9398
		U-PFHpS	C7HF13O3S	2	[M-H]-	410.9366
		U-PFOS	C8HF15O3S	2	[M-H]-	460.9334
		U-PFNS	C9HF17O3S	2	[M-H]-	510.9302
		U-PFDS	C10HF19O3S	2	[M-H]-	560.9270
		U-PFUnDS	C11HF21O3S	2	[M-H]-	610.9238
		U-PFDoDS	C12HF23O3S	2	[M-H]-	660.9206
		U-PFTriDS	C13HF25O3S	2	[M-H]-	710.9174
		U-PFTeDS	C14HF27O3S	2	[M-H]-	760.9143
PFASyA *Perfluoro sulfinic acid*	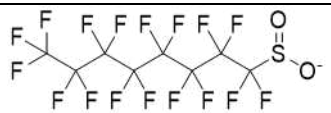	PFOSyA	C8HF17O2S	2	[M-H]-	482.9353
SF_5-PFSA *Pentafluorosulfanyl perfluoro sulfonic acid*	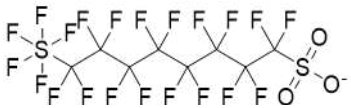	SF_5-PFHpS	C7HF19O3S2	2	[M-H]-	556.8991
		SF_5-PFOS	C8HF21O3S2	2	[M-H]-	606.8959
		SF_5-PFNS	C9HF23O3S2	2	[M-H]-	656.8927
		SF_5-PFDS	C10HF25O3S2	2	[M-H]-	706.8895
		SF_5-U-PFOS	C8HF19O3S2	2	[M-H]-	568.8991

SF_5-U-PFSA *Pentafluorosulfanyl unsaturated perfluoro sulfonic acid*	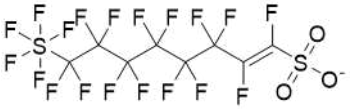	SF_5-U-PFNS	$C_9HF_{21}O_3S_2$	2	[M-H]-	618.8959
Cl-PFSA *Chloro substituted perfluoro sulfonic acid*	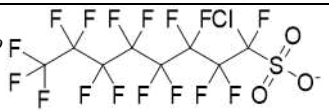	Cl-PFOS	$C_8HClF_{16}O_3S$	2	[M-H]-	514.9007
U-E-PFSA/K-PFSA *Unsaturated ether perfluoro sulfonic acid/Ketone perfluoro sulfonic acid*	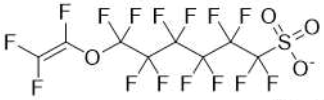	U-E-PFHpS/K-PFHxS	$C_6HF_{11}O_4S$	3	[M-H]-	376.9347
	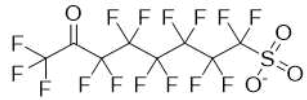	U-E-PFOS/K-PFHpS	$C_7HF_{13}O_4S$	3	[M-H]-	426.9315
		U-E-PFNS/K-PFOS	$C_8HF_{15}O_4S$	3	[M-H]-	476.9283
		U-E-PFTriDS/K-PFDoDS	$C_{12}HF_{23}O_4S$	3	[M-H]-	676.9156
H-PFSA *H-substituted perfluoro sulfonic acid*	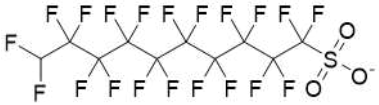	H-PFOS	$C_8H_2F_{16}O_3S$	2	[M-H]-	480.9396
		H-PFDS	$C_{10}H_2F_{20}O_3S$	3	[M-H]-	580.9333
PFASAm-PrSA *Perfluoroalkane sulfonamide propyl sulfonic acid*	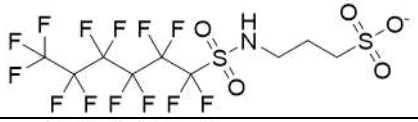	PFHxSAm-PrSA	$C_9H_8F_{13}NO_5S_2$	2	[M-H]-	519.9564
PFASAm-*N*-PrSA-*N*-Pr-DiMeAm *Perfluoroalkane sulfonamide N-propyl sulfonic acid N-propyl dimethylamine*	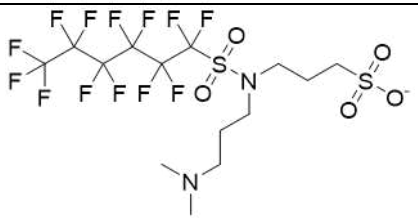	PFHxSAm-*N*-PrSA-*N*-Pr-DiMeAm	$C_{14}H_{19}F_{13}N_2O_5S_2$	3	[M+H]+ [M-H]-	607.0601 605.0455
n:2 FTSA *n:2 fluorotelomer sulfonic acid*	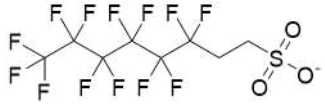	6:2 FTSA	$C_8H_5F_{13}O_3S$	1	[M-H]-	426.9679
		8:2 FTSA	$C_{10}H_5F_{17}O_3S$	1	[M-H]-	526.9615
		10:2 FTSA	$C_{12}H_5F_{21}O_3S$	2	[M-H]-	626.9551
		12:2 FTSA	$C_{14}H_5F_{25}O_3S$	2	[M-H]-	726.9487
		14:2 FTSA	$C_{16}H_5F_{29}O_3S$	2	[M-H]-	826.9424
OH-n:2 FTSA *Hydroxy-n:2 fluorotelomer sulfonic acid*	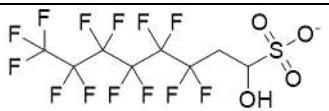	OH-6:2 FTSA	$C_8H_5F_{13}O_4S$	2	[M-H]-	442.9628
		OH-8:2 FTSA	$C_{10}H_5F_{17}O_4S$	2	[M-H]-	542.9564
K-n:2 FTSA *Ketone-n:2 fluorotelomer sulfonic acid*	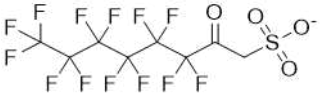	K-6:2 FTSA	$C_8F_{13}H_3SO_4$	2	[M-H]-	440.9472
		K-8:2 FTSA	$C_{10}F_{17}H_3SO_4$	2	[M-H]-	540.9408

U-n:2 FTSA *Unsaturated n:2 fluorotelomer sulfonic acid*	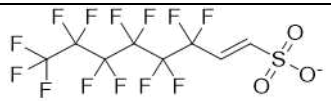	U-6:2 FTSA	C8H3F13O3S	2	[M-H]-	424.9523
		U-8:2 FTSA	C10H3F17O3S	3	[M-H]-	524.9459
n:2 FTSO-Pr-Ad-(5',5')DiMeEtSA *n:2 fluorotelomer sulfoxide propyl amide dimethylethyl sulfonic acid*	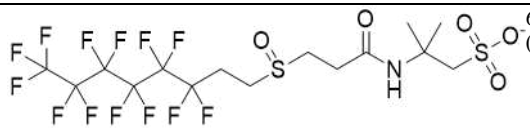	6:2 FTSO-Pr-Ad-(5',5')DiMeEtSA	C15H18F13NO5S2	2	[M-H]-	602.0346
n:2 FTSy-Pr-Ad-(5',5')DiMeEtSA *n:2 fluorotelomer sulfone propyl amide dimethylethyl sulfonic acid*	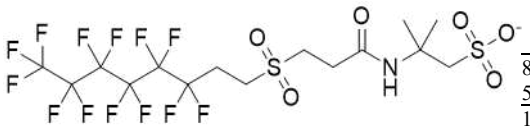	6:2 FTSy-Pr-Ad-(5',5')DiMeEtSA	C15H18F13NO6S2	2	[M-H]-	618.0295
		8:2 FTSy-Pr-Ad-(5', 5')DiMeEtSA	C17H18F17NO6S2	2	[M-H]-	718.0231
		10:2 FTSy-Pr-Ad-(5',5')DiMeEtSA	C19H18F21NO6S2	2	[M-H]-	818.0167
		12:2 FTSy-Pr-Ad-(5',5')DiMeEtSA	C21H18F25NO6S2	2	[M-H]-	918.0104
Ionization class: Sulfonamides						
PFASAm *Perfluoroalkane sulfonamide*	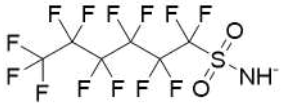	PFBSAm	C4H2F9NO2S	2	[M-H]-	297.9590
		PFPeSAm	C5H2F11NO2S	2	[M-H]-	347.9558
		PFHxSAm	C6H2F13NO2S	1	[M-H]-	397.9526
		PFHpSAm	C7H2F15NO2S	2	[M-H]-	447.9494
		PFOSAm	C8H2F17NO2S	1	[M-H]-	497.9462
PFASAm-Me *Perfluoroalkane sulfonamide methyl*	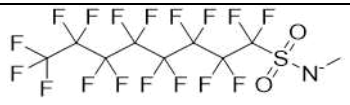	PFBSAm-Me	C5H4F9NO2S	3	[M-H]-	311.9746
		PFOSAm-Me	C9H4F17NO2S	3	[M-H]-	511.9619
n:2 FTSAm *n:2 fluorotelomer sulfonamide*	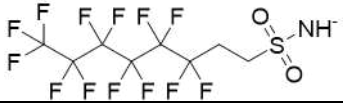	6:2 FTSAm	C8H6F13NO2S	2	[M-H]-	425.9839
		8:2 FTSAm	C10H6F17NO2S	2	[M-H]-	525.9775
		10:2 FTSAm	C12H6F21NO2S	2	[M-H]-	625.9711
n:2/m:2 FTSAm dimer *n:2/m:2 fluorotelomer sulfonamide dimer*	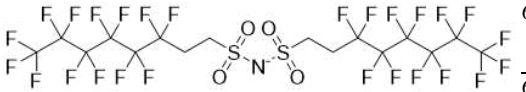	6:2/6:2 FTSAm dimer	C16H9F26NO4S2	2	[M-H]-	835.9485
		6:2/8:2 FTSAm dimer	C18H9F30NO4S2	2	[M-H]-	935.9421

Ionization class: Cationic PFAS						
PFASAm-Pr-DiMeAm *Perfluoroalkane sulfonamide propyl dimethylamine*	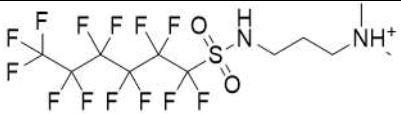	PFHxSAm-Pr-DiMeAm	C11H13F13N2O2S	1	[M+H]+	485.0563
					[M-H]-	483.0417
		PFOSAm-Pr-DiMeAm	C13H13F17N2O2S	2	[M+H]+	585.0499
					[M-H]-	583.0353
PFASAm-Pr-TriMeAm *Perfluoroalkane sulfonamide propyl trimethylamine*	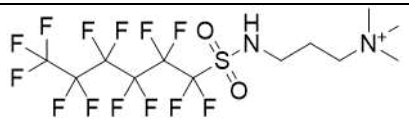	PFHxSAm-Pr-TriMeAm	C12H15F13N2O2S	3	[M+H]+	499.0719
		PFOSAm-Pr-TriMeAm	C14H15F17N2O2S	2	[M+H]+	599.0656
n:1:2 FTB *n:1:2 fluorotelomer betaine*	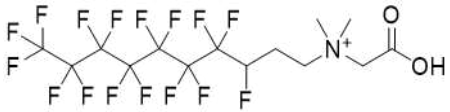	5:1:2 FTB	C12H13F12NO2	1	[M+H]+	432.0827
		7:1:2 FTB	C14H13F16NO2	2	[M+H]+	532.0764
		9:1:2 FTB	C16H13F20NO2	2	[M+H]+	632.0700
		11:1:2 FTB	C18H13F24NO2	2	[M+H]+	732.0636
		13:1:2 FTB	C20H13F28NO2	2	[M+H]+	832.0572
n:1:3 FTB *n:1:3 fluorotelomer betaine*	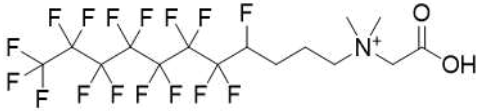	5:1:3 FTB	C13H15F12NO2	3	[M+H]+	446.0984
		7:1:3 FTB	C15H15F16NO2	3	[M+H]+	546.0920
		9:1:3 FTB	C17H15F20NO2	3	[M+H]+	646.0856
n:2 FTB *n:2 fluorotelomer betaine*	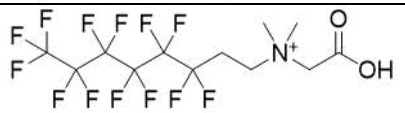	6:2 FTB	C12H12F13NO2	2	[M+H]+	450.0733
		8:2 FTB	C14H12F17NO2	2	[M+H]+	550.0669
		10:2 FTB	C16H12F21NO2	2	[M+H]+	650.0605
n:3 FTB *n:3 fluorotelomer betaine*	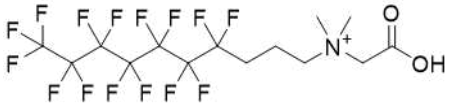	5:3 FTB	C12H14F11NO2	1	[M+H]+	414.0922
		7:3 FTB	C14H14F15NO2	2	[M+H]+	514.0858
		9:3 FTB	C16H14F19NO2	2	[M+H]+	614.0794
		11:3 FTB	C18H14F23NO2	2	[M+H]+	714.0730
		13:3 FTB	C20H14F27NO2	2	[M+H]+	814.0666
n:4 FTB *n:4 fluorotelomer betaine*	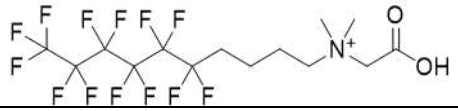	4:4 FTB	C12H16F9NO2	2	[M+H]+	378.1110
		6:4 FTB	C14H16F13NO2	2	[M+H]+	478.1046
		8:4 FTB	C16H16F17NO2	2	[M+H]+	578.0982
		10:4 FTB	C18H16F21NO2	2	[M+H]+	678.0918
n:2 FTSAm-Pr-DiMeAm *n:2 fluorotelomer sulfonamide propyl dimethylamine*	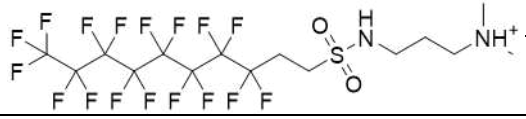	6:2 FTSAm-Pr-DiMeAm	C13H17F13N2O2S	2	[M+H]+	513.0876
					[M-H]-	511.0730
		8:2 FTSAm-Pr-DiMeAm	C15H17F17N2O2S	2	[M+H]+	613.0812

n:2 FTSAm-U-Pr-DiMeAm *n:2 fluorotelomer sulfonamide unsaturated propyl dimethylamine*	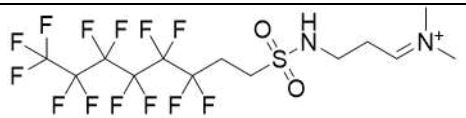	6:2 FTSAm-U-Pr-DiMeAm	$C_{13}H_{15}F_{13}N_2O_2S$	2	[M+H]+ 511.0719
n:2 FTSAm-Pr-DiMeNO *n:2 fluorotelomer sulfonamide propyl dimethylamineoxide*	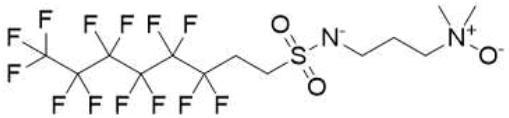	6:2 FTSAm-Pr-DiMeNO	$C_{13}H_{17}F_{13}N_2O_3S$	1	[M+H]+ 529.0825 [M-H]- 527.0680
		8:2 FTSAm-Pr-DiMeNO	$C_{15}H_{17}F_{17}N_2O_3S$	3	[M+H]+ 629.0761
n:2 FTTh-(2')OHPr-TriMeAm *n:2 fluorotelomer thio propanol trimethylamine*	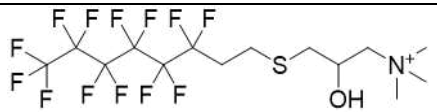	4:2 FTTh-(2')OHPr-TriMeAm	$C_{12}H_{18}F_9NOS$	2	[M+H]+ 396.1038
		6:2 FTTh-(2')OHPr-TriMeAm	$C_{14}H_{18}F_{13}NOS$	2	[M+H]+ 496.0974
		8:2 FTTh-(2')OHPr-TriMeAm	$C_{16}H_{18}F_{17}NOS$	2	[M+H]+ 596.0910
n:2 FTSO-(2')OHPr-TriMeAm *n:2 fluorotelomer sulfoxide propanol trimethylamine*	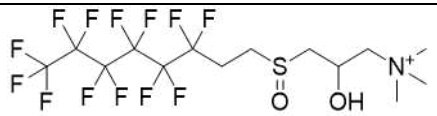	6:2 FTSO-(2')OHPr-TriMeAm	$C_{14}H_{18}F_{13}NO_2S$	2	[M+H]+ 512.0923
		8:2 FTSO-(2')OHPr-TriMeAm	$C_{16}H_{18}F_{17}NO_2S$	2	[M+H]+ 612.0860
n:2 FTSy-(2')OHPr-TriMeAm *n:2 fluorotelomer sulfone propanol trimethylamine*	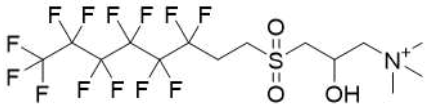	4:2 FTSy-(2')OHPr-TriMeAm	$C_{12}H_{18}F_9NO_3S$	2	[M+H]+ 428.0936
		6:2 FTSy-(2')OHPr-TriMeAm	$C_{14}H_{18}F_{13}NO_3S$	2	[M+H]+ 528.0873
		8:2 FTSy-(2')OHPr-TriMeAm	$C_{16}H_{18}F_{17}NO_3S$	2	[M+H]+ 628.0809

E. Semiquantification method

Table S5. Analytical reference standards of the four average calibration curves for semiquantification.

Carboxylic Acids	Sulfonic Acids	Sulfonamides	Cationic PFAS
PFBA	PFBS	PFHxSAm	PFHxSAm-Pr-DiMeAm
PFPeA	PFPeS	PFOSAm	5:1:2 FTB
PFHxA	PFHxS	PFOSAm-*N*-Et-*N*-EtA	5:3 FTB
PFHpA	PFHpS	PFHxSAm-Pr-DiMeAm	6:2 FTSAm-Pr-B
PFOA	PFOS	6:2 FTSAm-Pr-B	6:2 FTSAm-Pr-DiMeNO
PFNA	PFNS	6:2 FTSAm-Pr-DiMeNO	
PFDA	PFDS		
PFUnDA	PFDoDS		
PFDoDA	6:2 FTSA		
PFTriDA	8:2 FTSA		
PFTeDA	9Cl-PF3ONS		
PFHxDA	11Cl-PF3OUdS		
PFODA			
PFOSAm-*N*-Et-*N*-EtA			
5:3 FTCA			
7:3 FTCA			
U-6:2 FTCA			
U-8:2 FTCA			
6:2 FTSAm-Pr-B			
PFDPA			
ADONA			

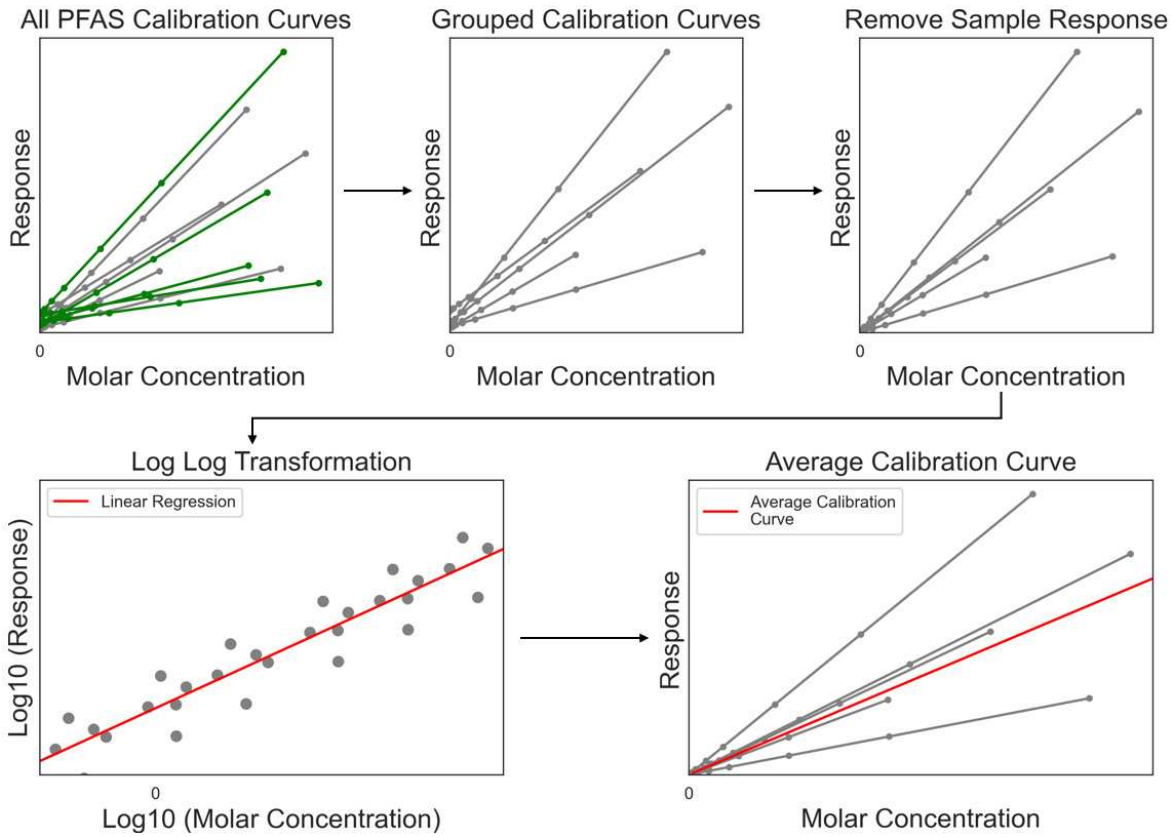

Figure S2. Scheme of semiquantification approach. The green lines represent calibration curves of authentic standards of other ionization classes.

F. EOF method – Combustion ion chromatography settings

Table S6. Combustion parameters.

Combustion component	
Combustion device	AQF-2100H, A1 Enviroscience, Mitsubishi Chemical Analytech Co., Ltd.
Operating temperature	1050 °C
Ar carrier gas flow	150 mL/min
Ar flow of water supply	100 mL/min
O_2 flow	300 mL/min
Absorption solution/internal standard	150 µM NH_3 solution + 2 mg/L $MeSO_3H$
Starting Absorption volume	3.5 mL
Final Absorption volume	~10.5 mL
Sample amount	250 µL
Water supply level	2 (about 0.1 mL/min)

Table S7. Ion chromatography parameters.

Ion chromatography component	
IC-device	ICS Integrion, Thermo Fisher Scientific
Detector	conductivity detector
Guard column	AG20 2x50mm guard column
Analytical column	Dionex IonPac AS20 2x250mm
Eluent	gradient KOH
Flow rate	0.25 mL/min
Run time	22 min
Column temperature	30 °C
Injection volume	100 µL
Suppressor	Dionex ADRS 600 (2mm)

Table S8. Boat program.

Pos [mm]	**Time [s]**	**Pos [mm]**	**Time [s]**	**Pos [mm]**	**Time [s]**	**Pos [mm]**	**Time [s]**	**End Time [s]**	**Cool Time [s]**	**Home Time [s]**	**Ar Time [s]**	**O2 Time [s]**
65	30	100	60	130	60	150	60	460	60	120	10	600

Table S9. IC eluent gradient program for all fluorine detection measurements.

Time (min)	**Eluent concentration (mM)**
0	Start, 1.0
0.1	1.0
0.2	2.0
1.0	2.0
10.0	5.0
10.5	5.0
11.0	80.0
14.0	80.0
14.5	1.0
22.0	stop run

G. Method validation

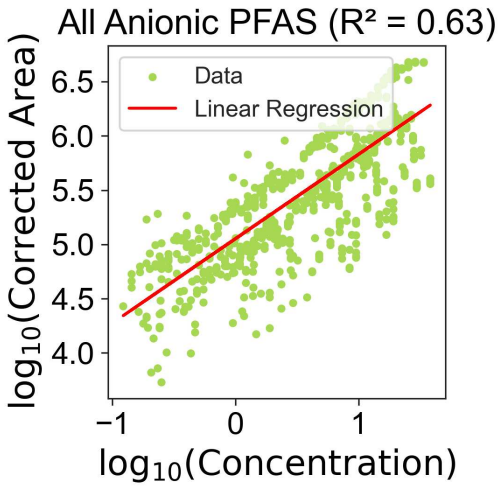

Figure S3. Data points of each standard of all anionic PFAS and average calibration curves displayed on a double logarithmic scale.

Cao, et al. [2] developed the ACC approach and re-estimated 50 different anionic and cationic PFAS, resulting in a median AAQ of 2.89 for the log-log regression approach. Pu, et al. [3] used, among others, bootstrap simulation to estimate population RF percentile values. Estimating all available PFAS standards together, similar to Cao, et al. [2], yielded with a median AAQ of 2.85, which could be decreased to 1.80 by using a suitable subset of the available standards based, chosen based on expert chemical intuition instead of all available surrogates. Lauria, et al. [4] reported mean AAQs of 1.90 when predicting the ionization efficiency of anionic PFAS using machine learning. Malm, et al. [5] evaluated the accuracy and performance variability of five quantification approaches based on surrogate standard quantification and predicted ionization efficiencies, reporting reprocessed mean AAQs ranging from 2.40 to 5.00.

Table S10. AAQs of different approaches compared.

Approach	AAQ	Reference
Average calibration curve (log-log regression)	Median: 2.89	Cao, et al. [2]
Bootstrap-sampled calibration values (“global” chemical surrogates)	Median: 2.85	Pu, et al. [3]
Bootstrap-sampled calibration values (“expert-selected” chemical surrogates)	Median: 1.80	Pu, et al. [3]
Machine learning predict the ionization efficiency	Mean: 1.90	Lauria, et al. [4]
Surrogate standard quantification (3)/Predicted ionization efficiencies (2)	Mean: 2.40-5.00	Malm, et al. [5]

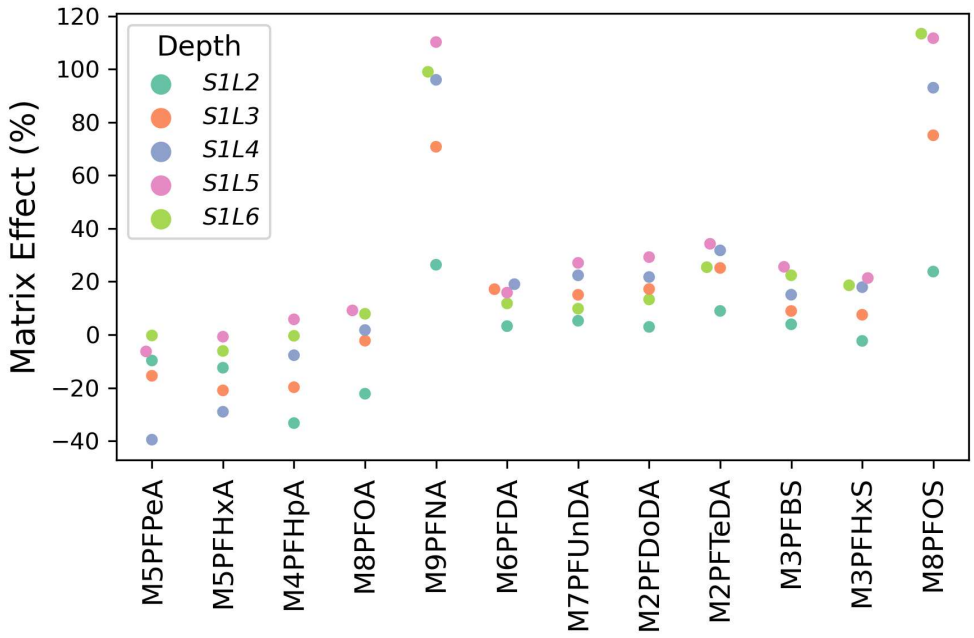

Figure S4. Matrix effects (MEs) of different isotopically labelled PFAS standards relative to the extract of the topsoil.

H. Concentrations of individual PFAS in topsoil

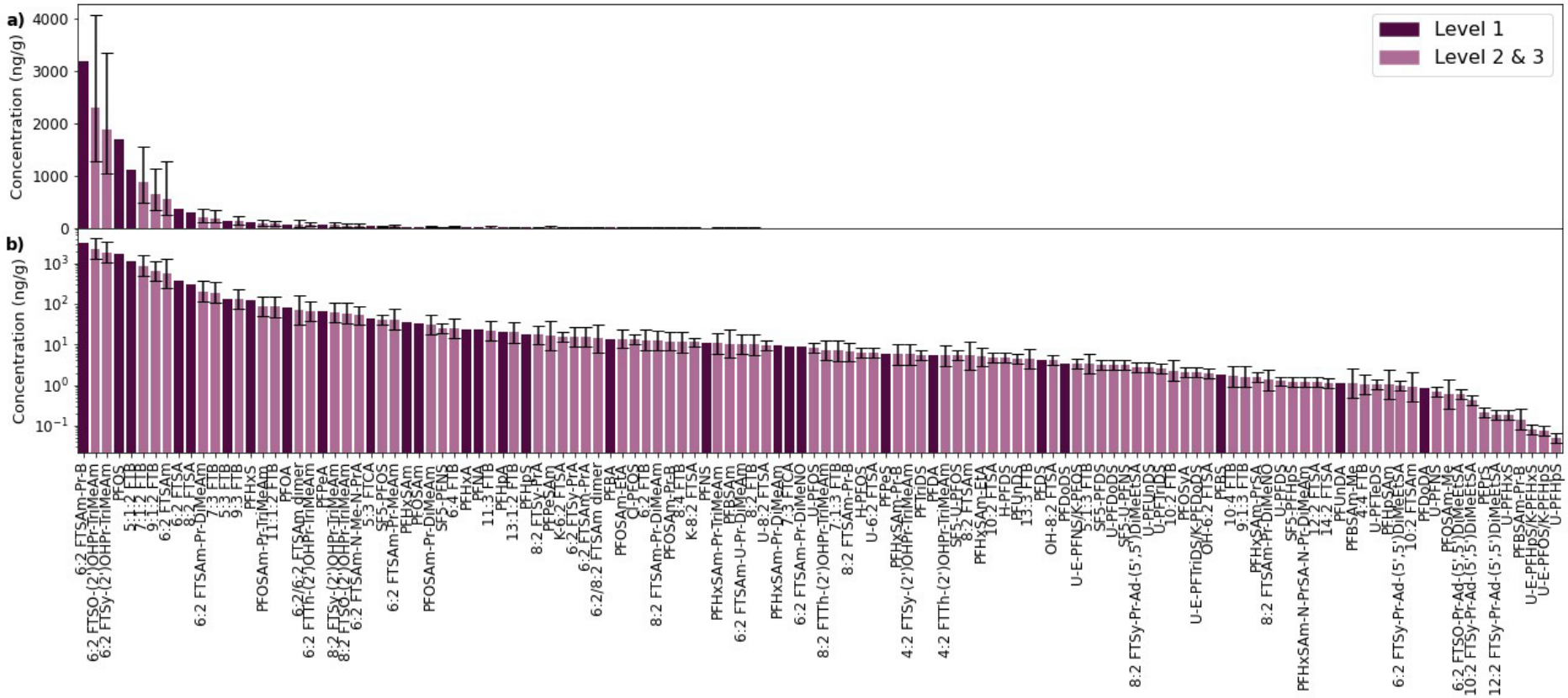

Figure S5. Concentration of quantified (dark purple) and semiquantified (light purple) PFAS in the extract of topsoil on site *S1L1* in µg/g displayed with a) linear scale and b) logarithmic scale. Error bars for semiquantified PFAS represent the median AAQ of the corresponding ionization class (compound names and structures in Table S4, concentrations in Table S12).

I. Concentrations of individual PFAS in all depths

Table S11. (Semi)quantified concentrations (ng/g) of all identified PFAS in different depths. Substances are organized in two groups, depending if they were quantified or semiquantified and ordered according to concentration in topsoil within each group.

	Acronym	C (ng/g) at 0-0.5 m	C (ng/g) at 0.5-1 m	C (ng/g) at 1-1.5 m	C (ng/g) at 1.5-2 m	C (ng/g) at 2-2.5 m	C (ng/g) at 2.5-3 m
Quantified	6:2 FTSAm-Pr-B	3168.96	1689.00	362.36	248.77	186.58	72.83
	PFOS	1696.75	1486.70	776.42	706.88	264.44	53.60
	5:1:2 FTB	1114.49	1678.51	647.76	284.73	129.07	47.05
	6:2 FTSA	380.23	854.85	481.55	647.14	182.19	33.33
	8:2 FTSA	295.75	227.70	42.98	42.38	9.04	3.00
	5:3 FTB	133.55	288.70	103.56	43.68	23.90	7.98
	PFHxS	127.24	337.74	189.15	229.57	55.49	11.26
	PFOA	78.51	157.44	52.85	63.71	12.54	2.85
	PFPeA	64.81	328.99	220.18	1003.56	215.95	51.77
	5:3 FTCA	42.50	40.24	8.67	9.11	0.00	0.00
	PFHxSAm	35.33	40.69	12.89	7.73	0.86	0.23
	PFOSAm	32.46	15.76	3.90	3.63	0.85	0.27
	PFHxA	23.77	158.79	137.19	417.69	81.84	18.04
	PFNA	23.21	16.18	6.50	7.02	0.00	0.00
	PFHpA	20.44	87.23	61.42	122.87	20.39	4.57
	PFHpS	18.12	27.47	8.78	7.94	1.88	0.40
	PFBA	13.84	46.17	23.60	196.87	30.37	2.95
	PFNS	10.69	5.59	1.78	1.83	0.70	0.00
	PFHxSAm-Pr-DiMeAm	9.38	15.56	3.02	3.37	5.24	1.00
	7:3 FTCA	9.09	4.82	1.01	1.22	0.00	0.46
	6:2 FTSAm-Pr-DiMeNO	9.08	14.48	2.39	2.21	0.00	0.00
	PFPeS	5.89	54.72	42.00	79.37	14.18	2.72
	PFDA	5.43	2.57	0.00	0.00	0.00	0.00
	PFDS	4.14	1.94	0.48	0.62	0.26	0.00
	PFDoDS	3.41	1.91	0.50	0.70	0.00	0.00
	PFBS	1.87	15.36	16.18	64.29	10.43	2.34
	PFUnDA	1.08	0.00	0.00	0.00	0.00	0.00
	PFDoDA	0.84	0.00	0.00	0.00	0.00	0.00
Semiquantified	6:2 FTSO-(2')OHPr-TriMeAm	2287.23	1483.84	146.58	171.38	135.02	18.31
	6:2 FTSy-(2')OHPr-TriMeAm	1880.23	820.60	66.81	107.66	14.87	4.05
	7:1:2 FTB	877.92	422.99	57.44	42.16	21.34	7.23
	9:1:2 FTB	641.06	255.54	29.36	41.02	49.67	9.18
	6:2 FTSAm	567.26	361.05	70.35	50.50	6.16	1.35
	6:2 FTSAm-Pr-DiMeAm	203.42	910.59	147.39	94.05	55.37	5.33
	7:3 FTB	190.68	128.42	16.60	10.34	5.63	1.05
	9:3 FTB	132.99	47.18	5.48	7.59	9.90	1.48
	PFOSAm-Pr-TriMeAm	87.71	32.74	4.46	5.85	6.31	0.56
	11:1:2 FTB	85.20	46.22	4.25	7.92	12.54	3.61

6:2/6:2 FTSAm dimer	72.35	56.44	7.00	10.43	2.64	0.28
6:2 FTTh-(2')OHPr-TriMeAm	65.67	102.62	39.64	54.81	109.83	10.52
8:2 FTSy-(2')OHPr-TriMeAm	61.21	15.58	1.41	2.92	0.62	0.13
8:2 FTSO-(2')OHPr-TriMeAm	59.10	35.28	2.64	3.96	4.38	0.92
6:2 FTSAm-*N*-Me-*N*-PrA	52.37	7.44	1.34	1.50	0.25	0.00
SF_5-PFOS	41.40	21.99	3.91	5.08	1.49	0.18
6:2 FTSAm-Pr-MeAm	41.25	302.93	60.27	30.28	7.35	0.70
PFOSAm-Pr-DiMeAm	31.13	89.28	13.46	13.89	14.87	1.58
SF_5-PFNS	25.35	13.75	2.49	3.17	0.82	0.09
6:4 FTB	25.33	28.23	5.15	2.74	1.61	0.43
11:3 FTB	21.90	11.77	1.10	1.97	3.06	0.87
13:1:2 FTB	19.71	14.81	1.49	3.13	5.25	1.08
8:2 FTSy-PrA	17.47	4.73	0.70	1.35	0.00	0.00
PFPeSAm	16.83	59.35	14.09	6.95	0.41	0.07
K-6:2 FTSA	15.87	74.21	23.40	28.41	4.22	0.54
6:2 FTSy-PrA	15.44	18.05	1.33	0.77	0.00	0.00
6:2 FTSAm-PrA	15.32	1.78	0.36	0.38	0.00	0.00
6:2/8:2 FTSAm dimer	13.93	0.68	0.15	0.77	0.08	0.00
PFOSAm-EtA	13.69	2.19	0.35	0.48	0.00	0.00
Cl-PFOS	13.12	10.25	2.28	1.95	0.29	0.00
6:2 FTB	12.91	18.88	4.81	1.91	0.67	0.24
8:2 FTSAm-Pr-DiMeAm	12.44	5.12	0.66	0.58	0.82	0.00
PFOSAm-Pr-B	11.96	5.68	0.57	0.46	0.41	0.00
8:4 FTB	11.53	4.04	0.50	0.65	0.81	0.09
K-8:2 FTSA	11.29	9.38	2.14	1.60	0.00	0.00
PFHxSAm-Pr-TriMeAm	10.56	12.26	1.66	1.33	0.30	0.08
PFBSAm	10.49	69.51	21.14	15.69	0.99	0.14
6:2 FTSAm-U-Pr-DiMeAm	10.13	25.12	8.94	10.18	5.67	0.67
8:2 FTB	10.00	4.37	0.62	0.62	0.26	0.07
U-8:2 FTSA	9.75	7.04	0.00	0.00	0.00	0.00
U-PFOS	8.09	19.85	5.32	4.57	0.78	0.12
8:2 FTTh-(2')OHPr-TriMeAm	7.20	10.72	2.75	4.48	10.45	1.88
7:1:3 FTB	7.06	2.29	0.18	0.24	0.12	0.00
8:2 FTSAm-Pr-B	6.57	1.71	0.22	0.25	0.22	0.16
H-PFOS	6.33	9.62	3.27	3.31	0.68	0.00
U-6:2 FTSA	6.18	23.81	8.91	10.65	1.44	0.00
PFHxSAm-Pr-B	5.74	8.55	1.41	0.96	0.43	0.00
4:2 FTSy-(2')OHPr-TriMeAm	5.68	2.28	0.00	0.00	0.00	0.00
PFTriDS	5.58	3.63	0.75	1.14	0.60	0.00
4:2 FTTh-(2')OHPr-TriMeAm	5.39	18.19	0.00	1.89	0.99	0.23
SF_5-U-PFOS	5.33	2.51	0.40	0.39	0.00	0.00
8:2 FTSAm	5.27	1.15	0.29	0.36	0.05	0.00
PFHxSAm-EtA	5.05	4.70	0.77	1.00	0.25	0.05
10:2 FTSA	4.85	1.82	0.20	0.45	0.00	0.00
H-PFDS	4.80	3.51	1.22	1.00	0.31	0.00

PFUnDS	4.53	1.77	0.49	0.66	0.22	0.00
13:3 FTB	4.46	2.69	0.30	0.62	1.04	0.21
OH-8:2 FTSA	4.11	2.56	0.58	0.52	0.00	0.00
U-E-PFNS/K-PFOS	3.40	4.39	1.14	0.97	0.19	0.04
5:1:3 FTB	3.36	2.85	0.34	0.00	0.00	0.00
SF_5-PFDS	3.17	1.72	0.41	0.48	0.00	0.00
U-PFDoDS	3.14	0.00	0.30	0.39	0.00	0.00
SF_5-U-PFNS	3.08	1.45	0.29	0.34	0.00	0.00
8:2 FTSy-Pr-Ad-(5',5')DiMeEtSA	2.71	10.02	0.62	0.27	0.03	0.00
U-PFUnDS	2.65	1.06	0.20	0.29	0.10	0.00
U-PFTriDS	2.47	0.00	0.00	0.00	0.00	0.00
10:2 FTB	2.26	0.92	0.12	0.00	0.21	0.00
U-E-PFTriDS/K-PFDoDS	2.04	1.06	0.00	0.00	0.00	0.00
PFOSyA	2.04	0.31	0.12	0.24	0.49	0.08
OH-6:2 FTSA	1.99	15.69	5.62	11.77	1.01	0.13
10:4 FTB	1.65	0.74	0.06	0.00	0.26	0.00
9:1:3 FTB	1.61	0.40	0.00	0.09	0.00	0.00
PFHxSAm-PrSA	1.52	5.11	1.09	1.14	0.21	0.00
8:2 FTSAm-Pr-DiMeNO	1.32	0.70	0.16	0.26	0.00	0.00
SF_5-PFHpS	1.23	0.70	0.13	0.15	0.00	0.00
U-PFDS	1.23	0.69	0.00	0.00	0.00	0.00
PFHxSAm-*N*-PrSA-*N*-Pr-DiMeAm	1.21	4.28	0.77	0.57	0.22	0.00
12:2 FTSA	1.17	0.37	0.06	0.12	0.00	0.00
14:2 FTSA	1.09	0.36	0.07	0.11	0.00	0.00
PFBSAm-Me	1.08	3.01	0.35	0.15	0.00	0.00
4:4 FTB	1.03	2.76	0.58	0.35	0.00	0.00
U-PFTeDS	1.03	0.00	0.00	0.00	0.00	0.00
PFHpSAm	1.02	0.60	0.12	0.00	0.00	0.00
6:2 FTSy-Pr-Ad-(5',5')DiMeEtSA	1.00	6.28	0.75	0.64	0.04	0.00
10:2 FTSAm	0.88	0.14	0.08	0.06	0.00	0.00
U-PFNS	0.67	0.55	0.00	0.00	0.00	0.00
PFOSAm-Me	0.59	0.26	0.00	0.04	0.00	0.00
6:2 FTSO-Pr-Ad-(5',5')DiMeEtSA	0.58	0.34	0.03	0.04	0.00	0.00
10:2 FTSy-Pr-Ad-(5',5')DiMeEtSA	0.42	1.25	0.13	0.13	0.00	0.00
PFPrS	0.21	2.25	2.24	23.17	2.54	0.50
U-PFHxS	0.18	2.38	2.06	4.33	0.99	0.00
12:2 FTSy-Pr-Ad-(5',5')DiMeEtSA	0.18	0.20	0.03	0.00	0.00	0.00
U-E-PFHpS/K-PFHxS	0.08	0.91	0.47	0.99	0.13	0.02
U-E-PFOS/K-PFHpS	0.07	0.37	0.14	0.15	0.02	0.00
U-PFHpS	0.05	0.38	0.17	0.19	0.00	0.00
PFBSAm-Pr-B	0.00	0.13	0.05	0.00	0.00	0.00

J. Extractable organofluorine

Table S12. Mean extractable organofluorine ($\overline{\mathbf{EOF}}$) and relative standard deviation (RSD) of combined extracts from sequential extraction with methanol only (MeOH) and methanol with 0.4 M NH_4Ac (MeOH+NH_4Ac) in triplicates for soil (A, B, C) and extraction blank. The limit of quantification (LOQ) was 0.08 µg F/g.

Sample	$\overline{\mathbf{EOF}}$ (µg F/g)	RSD (%)
Extract MeOH A	4.12	0.23
Extract MeOH B	4.14	0.02
Extract MeOH C	4.02	1.67
Extract blank MeOH	0.09	4.87
Extract MeOH+NH_4Ac A	7.53	2.38
Extract MeOH+NH_4Ac B	7.91	2.31
Extract MeOH+NH_4Ac C	8.08	1.11
Extract blank MeOH	0.09	5.43

K. Extraction recovery

Table S13. Mean extraction recovery and RSD determined from spike experiment on standard soil (LUFA SP6S, ~1.55% organic carbon), as well as MEs for compounds with available internal standard. ME was calculated according to equation 4 (n.a. = not applicable). Note that for substances where the ME could be calculated (blue font) the extraction recovery was corrected for ME.

Standard	$\overline{\text{Recovery}}$ (%)	RSD (%)	ME (%)
PFBA	122.50	2.79	-92.36
PFPeA	143.96	5.2	-81.91
PFHxA	138.96	7.59	-21.33
PFHpA	148.89	9.03	-11.66
PFOA	139.63	3.77	-32.19
PFNA	144.26	7.46	-6.6
PFDA	173.05	2.01	-20.59
PFBS	138.02	6.01	-42.72
PFPeS	103.79	6.41	25.08
PFHxS	181.52	3.79	-14.4
PFHpS	135.70	7.05	n.a.
PFOS	144.88	8.13	6.96
PFHxSAm	126.74	13.59	n.a.
PFOSAm	124.77	1.82	n.a.
PFOSAm-*N*-Et-*N*-EtA	84.14	10.34	n.a.
PFHxSAm-Pr-DiMeAm	105.17	10.03	n.a.
5:3 FTCA	61.51	7.1	n.a.
U-6:2 FTCA	70.17	4.15	n.a.
U-8:2 FTCA	92.35	4.02	n.a.
6:2 FTSA	296.74	10.48	n.a.
8:2 FTSA	175.65	1.92	n.a.
5:1:2 FTB	28.53	21.77	n.a.
5:3 FTB	22.54	6.61	n.a.
6:2 FTSAm-Pr-B	47.75	30.24	n.a.
6:2 FTSAm-Pr-DiMeNO	176.86	1.9	n.a.

L. Depth distribution

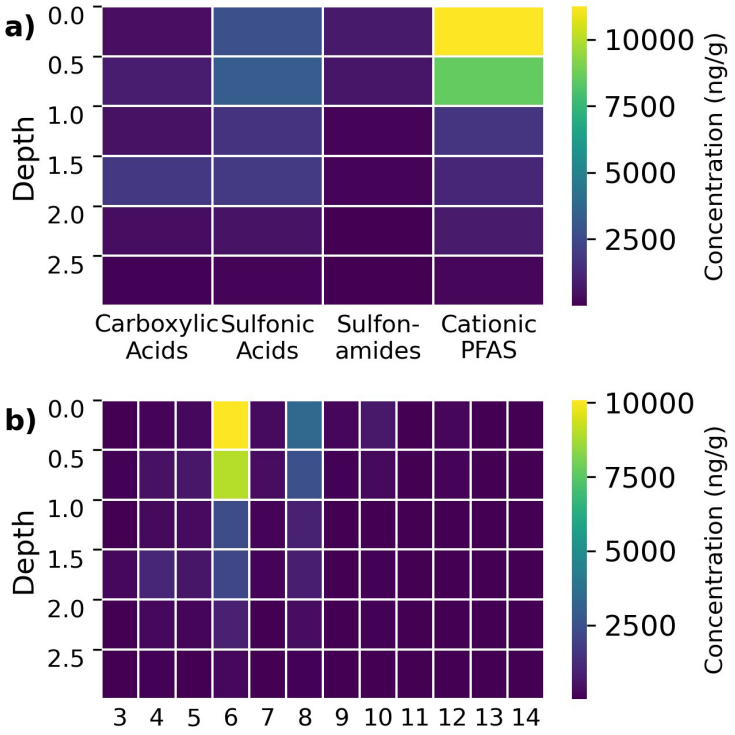

Figure S6. Depth distribution of summed concentrations segmented by a) ionization class and b) chain length.

Table S14. Water content.

Depth (m)	Water content (% w/w)
0-0.5	12.6
0.5-1	33.7
1-1.5	19.9
1.5-2	51.3
2-2.5	32.8
2.5-3	14.1

References

(1) Wikimedia Commons. Karte Deutschland. 2021. https://commons.wikimedia.org/wiki/File:Karte_Deutschland.svg (accessed 02.07.2024).
(2) Cao, D.; Schwichtenberg, T.; Duan, C.; Xue, L.; Muensterman, D.; Field, J. Practical Semiquantification Strategy for Estimating Suspect Per- and Polyfluoroalkyl Substance (PFAS) Concentrations. *J Am Soc Mass Spectrom* **2023**, *34* (5), 939-947. DOI: 10.1021/jasms.3c00019
(3) Pu, S.; McCord, J. P.; Bangma, J.; Sobus, J. R. Establishing performance metrics for quantitative non-targeted analysis: a demonstration using per- and polyfluoroalkyl substances. *Anal Bioanal Chem* **2024**, *416* (5), 1249-1267. DOI: 10.1007/s00216-023-05117-4
(4) Lauria, M. Z.; Sepman, H.; Ledbetter, T.; Plassmann, M.; Roos, A. M.; Simon, M.; Benskin, J. P.; Kruve, A. Closing the Organofluorine Mass Balance in Marine Mammals Using Suspect Screening and Machine Learning-Based Quantification. *Environ Sci Technol* **2024**, *58* (5), 2458-2467. DOI: 10.1021/acs.est.3c07220
(5) Malm, L.; Liigand, J.; Aalizadeh, R.; Alygizakis, N.; Ng, K.; Fro Kjaer, E. E.; Nanusha, M. Y.; Hansen, M.; Plassmann, M.; Bieber, S.; Letzel, T.; Balest, L.; Abis, P. P.; Mazzetti, M.; Kasprzyk-Hordern, B.; Ceolotto, N.; Kumari, S.; Hann, S.; Kochmann, S.; Steininger-Mairinger, T.; Soulier, C.; Mascolo, G.; Murgolo, S.; Garcia-Vara, M.; Lopez de Alda, M.; Hollender, J.; Arturi, K.; Coppola, G.; Peruzzo, M.; Joerss, H.; van der Neut-Marchand, C.; Pieke, E. N.; Gago-Ferrero, P.; Gil-Solsona, R.; Licul-Kucera, V.; Roscioli, C.; Valsecchi, S.; Luckute, A.; Christensen, J. H.; Tisler, S.; Vughs, D.; Meekel, N.; Talavera Andujar, B.; Aurich, D.; Schymanski, E. L.; Frigerio, G.; Macherius, A.; Kunkel, U.; Bader, T.; Rostkowski, P.; Gundersen, H.; Valdecanas, B.; Davis, W. C.; Schulze, B.; Kaserzon, S.; Pijnappels, M.; Esperanza, M.; Fildier, A.; Vulliet, E.; Wiest, L.; Covaci, A.; Macan Schonleben, A.; Belova, L.; Celma, A.; Bijlsma, L.; Caupos, E.; Mebold, E.; Le Roux, J.; Troia, E.; de Rijke, E.; Helmus, R.; Leroy, G.; Haelewyck, N.; Chrastina, D.; Verwoert, M.; Thomaidis, N. S.; Kruve, A. Quantification Approaches in Non-Target LC/ESI/HRMS Analysis: An Interlaboratory Comparison. *Anal Chem* **2024**, *96* (41), 16215-16226. DOI: 10.1021/acs.analchem.4c02902

Appendix 3

Publication 3

Characterization of per- and polyfluoroalkyl substances (PFAS) in AFFF-contaminated soil by photocatalytic oxidation (PhotoTOP)

Catharina Capitain[+], Christian Zwiener[+]

[+]Environmental Analytical Chemistry, Department of Geosciences, University of Tübingen, Schnarrenbergstraße 94-96, 72076 Tübingen, Germany

Published online in: Analytical and Bioanalytical Chemistry (11 November 2025)

DOI: 10.1007/s00216-025-06208-0

Analytical and Bioanalytical Chemistry
https://doi.org/10.1007/s00216-025-06208-0

PAPER IN FOREFRONT

Characterization of per- and polyfluoroalkyl substances (PFAS) in AFFF-contaminated soil by photocatalytic oxidation (PhotoTOP)

Catharina Capitain[1] · **Christian Zwiener**[1]

Received: 6 August 2025 / Revised: 6 October 2025 / Accepted: 22 October 2025

Abstract

Per- and polyfluoroalkyl substances (PFAS) comprise a diverse group of thousands of compounds, for which only a limited number of analytical reference standards are available. This presents significant challenges for the identification and quantification of PFAS in environmental samples. The PhotoTOP assay addresses this issue by photocatalytic oxidation of PFAS precursors into quantifiable perfluoroalkyl carboxylic acids. In this study, the PhotoTOP was applied for the first time to both aqueous film-forming foam (AFFF)–related PFAS standards and AFFF-contaminated soil. Precursors, intermediates, and final oxidation products were identified using target analysis and non-target screening (NTS). Numerous novel PhotoTOP intermediates were detected, such as perfluoroalkyl sulfonamide–based and fluorotelomer sulfonamide–based compounds, dimers, fluorotelomer betaines, and unsaturated perfluoroalkyl sulfonic acids. Mass balance analysis based on semiquantitative NTS (qNTS) data revealed near-complete conversion of PFAS precursors in both standards and contaminated soil. Additionally, transformation kinetics were investigated, providing insight into the behavior and persistence of PFAS precursors during PhotoTOP treatment and their potential fate in the environment.

Keywords AFFF · PFAS · Soil · Photocatalytic oxidation · HRMS · NTS

Introduction

Per- and polyfluoroalkyl substances (PFAS) are a large group of synthetic chemicals known for their exceptional stability, resistance to heat, and water- and oil-repellent properties [1]. Due to these characteristics, PFAS have been widely used in various industrial and consumer products, including non-stick cookware, water-resistant fabrics, and food packaging [2, 3]. However, their environmental persistence [4] and potential health risks have raised significant concerns, as PFAS can accumulate in living organisms and are associated with adverse effects on human health, such as endocrine disruption and carcinogenicity [5–8].

One major source of PFAS contamination is aqueous film-forming foams (AFFFs), which are specific firefighting foams used to suppress fuel-based fires [9, 10]. AFFFs contain PFAS to create a stable film that quickly smothers flames and prevents re-ignition [11]. Despite their effectiveness, AFFF use has led to widespread environmental contamination, especially around military bases, airports, and industrial sites where they have been used extensively [9, 10, 12–14]. As a result, understanding and mitigating PFAS contamination from AFFF is a critical focus of environmental research and regulation.

PFAS encompass a highly diverse group of compounds, with over 4700 distinct PFAS identified [15]. However, only a limited number of analytical reference standards is available for these compounds, making their identification and quantification challenging. Semiquantitative non-target screening (qNTS) is necessary to address this limitation, but it requires the use of high-resolution mass spectrometry (HRMS) and comprehensive data analysis workflows, which are labor-intensive and time-consuming [16, 17].

Another approach to estimate the total PFAS load in environmental samples is the total oxidizable precursor (TOP) assay [18]. The TOP assay is a method used to assess PFAS

Published in the topical collection highlighting *The Challenge PFAS – Analysis, Occurrence, Fate, and Exposure* with guest editors Jonathan Zweigle and Christian Zwiener.

✉ Christian Zwiener
christian.zwiener@uni-tuebingen.de

[1] Environmental Analytical Chemistry, Department of Geosciences, University of Tübingen, Schnarrenbergstraße 94-96, 72076 Tübingen, Germany

Published online: 11 November 2025

precursor compounds that are difficult to detect directly but can be converted into stable, measurable end products through oxidation. In this assay, PFAS precursors are oxidized by strong oxidizing agents into perfluoroalkyl carboxylic acids (PFCAs) and sulfonic acids (PFSAs) that are easier to analyze. By comparing PFAS concentrations before and after oxidation, the amount of initially undetectable precursor compounds can be estimated [18–22]. The TOP assay provides a more comprehensive understanding of PFAS contamination, as it reveals hidden or precursor-based PFAS that might otherwise go undetected in standard analyses.

The PhotoTOP assay is an alternative to the traditional TOP assay, with a key difference in the oxidation process. While the TOP assay relies on strong chemical oxidizing agents to transform PFAS precursor compounds into stable, measurable end products, the PhotoTOP assay uses ultraviolet (UV) light in combination with the catalyst titanium dioxide (TiO_2) to achieve transformation through photochemical oxidation [23]. The main advantage of the PhotoTOP compared to the TOP assay is the absence of high salt concentrations, allowing for direct injection of samples without requiring any cleanup. Additionally, the method results in less shortening of the perfluoroalkyl chain length compared to the TOP assay, leading to more meaningful results. The use of UV light and TiO_2 in the PhotoTOP assay also ensures the continuous generation of oxidants, which ensures complete oxidation of PFAS precursor compounds, and the ability to collect sampling time points during the assay allows for monitoring, improving the accuracy and reliability of the results [24].

The objectives of this study were to conduct the PhotoTOP assay on AFFF standards to identify transformation products (TPs) and pathways, as well as to apply the assay to heavily contaminated soil samples from Reilingen in Southwest Germany. The PhotoTOP assay was applied both directly to the contaminated soil and to soil extract to investigate PFAS extractability and matrix-related effects. The resulting data provide insights into potential TPs and allow for validation of the qNTS data published previously [25], which combined matrix-matched calibration and ionization class-specific average calibration curves. Additionally, this study examines the stability and transformation kinetics of precursors.

Materials and methods

Chemicals and reagents

Methanol (MeOH), ammonium acetate (NH_4Ac), and water were of optima LC-MS grade and were ordered from Thermo Fisher Scientific. Titanium(IV) dioxide (TiO_2 anatase, powder, 99.8% trace metal basis) was purchased from Sigma-Aldrich. A PFAS standard mixture containing 51 authentic reference standards was used for identification. Detailed information on the reference standards can be found in the Electronic Supplementary Material (ESM; Table S1).

Site characteristics, soil sampling, and processing

Soil samples were collected from a site in Reilingen in Southwest Germany, where a significant fire incident occurred at a mattress warehouse in 2008. During this event, firefighting efforts involved multiple local fire departments and extensive use of various AFFF formulations, which drained into a nearby irrigation trench (*Nachtwaidgraben*) and impacted an adjacent agricultural field. Soil samples from the *Nachtwaidgraben* were collected and processed as described by Schüßler et al. (2024) [26]. Briefly, in May 2023, drill core sampling was conducted to a depth of 3 m. For this study, only the uppermost soil section (0–0.5 m depth) was analyzed. This sample represents a composite of four drill cores collected in a 1×1 m grid. The soil sample was dried at 40 °C, ground, and sieved to a remaining fraction of ≤ 1.6 mm. The water content was 12.6 w/w %.

Photocatalytic oxidation

The previously developed PhotoTOP protocol [23] was applied to AFFF PFAS reference standards, to the collected soil sample, and to a methanolic extract derived from the soil sample.

AFFF standards (6:2 fluorotelomer sulfonamide propyl betaine (FTSAm-Pr-B; Capstone B), 6:2 fluorotelomer sulfonamide propyl dimethylamine oxide (FTSAm-Pr-DiMeNO; Capstone A), 5:3 fluorotelomer betaine (FTB), 5:1:2 FTB, perfluorohexane sulfonamide (PFHxSAm), perfluorooctane sulfonamide (PFOSAm), perfluorohexane sulfonamide propyl dimethylamine (PFHxSAm-Pr-DiMeAm)) were pipetted into individual 20-mL Pyrex EPA screw-cap glass vials, reaching a final concentration of 2.3 µg. To each vial, 10 mg of TiO_2 was added.

For soil treatment, 100 mg of soil was weighed into 20-mL Pyrex EPA screw-cap glass vials. Each vial was supplemented with 30 mg TiO_2 and 200 µL of MeOH to facilitate the coating of the TiO_2 particles.

For the PhotoTOP of soil extracts, 15 g of soil was extracted in 15 mL of MeOH. The samples were sonicated in an ultrasonic bath for 1 h, shaken on a rotary shaker for 24 h, and centrifuged at 7197 relative centrifugal forces (rcf) for 20 min. After centrifugation, the supernatant was decanted, and 9 mL of the supernatant (corresponding to the extract from 9 g of soil) was pipetted into a 20-mL EPA screw-cap glass vial and evaporated under a gentle stream of nitrogen. Subsequently, 30 mg of TiO_2 and 200 µL of

MeOH were added to the vial for resuspension and coating of the particles.

All sample setups (standards, soil, and soil extract) were thoroughly mixed, sonicated for 1 min to disperse any particle clumps, and left uncovered overnight to allow complete evaporation of MeOH. The following day, 23 mL of water and a magnetic stir bar were added to each vial, and the mixtures were sonicated for 5 min to ensure thorough dispersion.

The vials were then transferred to a UVA Cube 400 (Hönle UV Technology, equipped with a 1200-W lamp; for details, see Zweigle et al. (2022) [23]) and irradiated for 5 h (standards) or 46 h (soil and soil extract samples), respectively. Samples were collected at regular intervals: for standard samples, 100 µL was taken and diluted with 900 µL of MeOH. For soil and soil extract samples, 400 µL was taken and combined with 400 µL of MeOH. These were then centrifuged for 30 min at 20,817 rcf, and 500 µL of the supernatant was transferred into HPLC vials for subsequent analysis.

During the 46-h irradiation process, intervals of irradiation were interrupted for up to several days, and samples were stored at room temperature. After each interruption, the vials were sonicated for 5 min and sampled before resuming irradiation.

Instrumental analysis

Target PFAS (confidence level 1, Table S1) were quantified with high-performance liquid chromatography (1290 II HPLC from Agilent Technologies, Waldbronn, Germany) coupled to a 6490 triple quadrupole mass spectrometer (Agilent Technologies, Santa Clara, USA; HPLC-QqQ-MS). The separation was conducted on a Waters Acquity BEH C_{18} column (2.1 mm × 100 mm, 1.7 µm particle size) at a flow rate of 0.4 mL/min and maintained at a column temperature of 60 °C. The injection volume was 5 µL for all samples. An 8-min gradient elution was utilized with eluent A consisting of 95% H_2O and 5% MeOH with 2 mM NH_4Ac, and eluent B composed of 95% MeOH and 5% H_2O also with 2 mM NH_4Ac, starting with 60% eluent B and increased linearly to 100% B over 3.5 min, where it was held constant until 6.0 min. At 6.1 min, the gradient returned to the initial condition of 40% B and was maintained until 8.0 min for re-equilibration before the next injection. Electrospray ionization was operated in negative and positive mode, and every analyte was measured with two mass transitions, except for perfluorobutanoic acid (PFBA) and perfluorooctane sulfonamide (PFOSAm), for which only one product ion was available. In addition to duplicate sample injections, the analysis included a blank, a seven-point calibration curve of the PFAS standard mixture (0.05–10 µg/L, $R^2 > 0.99$), and quality controls (QCs; PFAS standard mixture, ± 10%) every tenth injection to ensure data accuracy. Details on the limit of detection can be found in Table S2.

For suspect and non-target screening of PFAS identified by Schüßler et al. (2024) [26] (at confidence levels 2 and 3), high-performance liquid chromatography (1290 HPLC from Agilent Technologies, Waldbronn, Germany) coupled to a quadrupole time-of-flight mass spectrometer with an electrospray ionization source (6550 QTOF, Agilent Technologies, Santa Clara, USA; HPLC-ESI-QTOF-MS) was applied. The separation was conducted on an Agilent Poroshell 120 EC-C_{18} column (2.1 mm × 100 mm, 2.7 µm particle size) at a flow rate of 0.3 mL/min and maintained at a column temperature of 40 °C. A sample injection volume of 10 µL was used. A 23-min gradient elution was utilized with identical solvents as for target analysis. The gradient program started with 15% eluent B and gradually increased to 100% over 10 min, then held at 100% B for 5 min. Following each run, an 8-min post-run equilibration returned conditions to 15% B to prepare for subsequent injections. For mass spectrometric detection, ionization was conducted separately in both positive and negative electrospray ionization (ESI+/ESI−) modes to enable the detection of anionic, cationic, and zwitterionic analytes. Data acquisition was performed using the QTOF mass spectrometer in a scan or data-dependent MS/MS (ddMS^2) mode. A threshold of 1000 counts was set to trigger MS^2 acquisition, and each precursor m/z was excluded for 0.5 min after collecting three MS^2 spectra. Both MS^1 and MS^2 spectra acquisition rates were set at 3 spectra per second, with a narrow isolation window of 1.3 m/z. Collision energy for MS^2 was m/z-dependent and calculated using the formula: CE (m/z) = 3 (m/z)/100 + 15 eV, employing collision-induced dissociation. This equation was optimized for PFAS and was found to provide good collision behavior for these compounds. In addition to duplicate sample injections, the analysis included a blank and QCs (± 10%) every fifteenth injection to ensure data accuracy.

Information on the detected PFAS classes and compounds, including acronyms, full names, molecular formulas, mass-to-charge ratios *m/z*, ionization polarity, confidence levels, and the oxidized matrices in which each compound was identified, can be found in Table S3 and S4. For improved readability, all PFAS are referred to by their acronyms in the following sections.

Data analysis

Concentrations were calculated using Agilent MassHunter Quantitative Analysis 10.0 software based on a seven-point calibration curve. The mass balance was calculated by comparing the summed molar concentrations before and after oxidation, or from qNTS data and after oxidation, assuming 1 mol of precursor yields 1 mol of TP (except for dimers).

To assess the kinetics and stability of the different PFAS during the PhotoTOP, the transformation and formation curves were fitted using four different models, depending on the curve shape: logistic formation (Eq. 1), exponential decay (Eq. 2), a combination of logistic formation and exponential decay (Eq. 3), and a two-step exponential formation and decay model (Eq. 4) with concentration $C(t)$, initial concentration C_{start}, maximum concentration C_{max}, time when the formation rate is at its maximum t_{max}, formation rate k_f, and decay rate k_d:

$$C(t) = C_{start} + \frac{C_{max} - C_{start}}{1 + e^{-k_f \cdot (t - t_{max})}} \quad (1)$$

$$C(t) = C_{start} \cdot e^{-k_d \cdot t} \quad (2)$$

$$C(t) = C_{start} \cdot \frac{C_{max}}{1 + e^{-k_f \cdot (t - t_{max})}} \cdot e^{-k_d \cdot t} \quad (3)$$

$$C(t) = C_{start} \cdot e^{-k_d \cdot t} + C_{max} \cdot (1 - e^{-k_f \cdot t}) \quad (4)$$

The RMSE (root mean square error) was used to evaluate the goodness of fit between the observed and predicted data. It was first calculated as the square root of the mean squared difference between observed and predicted values. The normalized RMSE was then obtained by dividing the RMSE by the maximum observed value, with lower values indicating better agreement: values below 10% were considered good, 10–20% acceptable, and above 20% suboptimal.

To investigate the influence of perfluorinated chain length on transformation kinetics, Spearman correlations were calculated between chain length and the formation or decay rates within individual PFAS classes. Only PFAS classes with at least two homologs were included in the analysis. Spearman's ρ was computed using Python's scipy.stats.spearmanr function.

Results and discussion

Oxidative conversion of AFFF standards

To evaluate the suitability and performance of the PhotoTOP assay for AFFF oxidation, the transformation of seven known precursors was examined. Therefore, four fluorotelomer PFAS (6:2 FTSAm-Pr-B, 6:2 FTSAm-Pr-DiMeNO, 5:3 FTB, 5:1:2 FTB) and three perfluoroalkane sulfonamide–based PFAS (PFHxSAm, PFOSAm, and PFHxSAm-Pr-DiMeAm) were irradiated, and samples were taken and analyzed.

All precursors and intermediates were transformed within the first hour. Final TPs increased with a time delay, reaching their maximum concentration after no more than 2 h, and remained stable until the end (5 h). After 5 h of oxidation, the mass balance for all substances ranged between 85 and 121% with the exception of 6:2 FTSAm-Pr-DiMeNO, for which the initial concentration was underestimated due to sorption and hence the mass balance was overestimated (Fig. 1, Table S5).

The three perfluoroalkane sulfonamide–based PFAS formed PFCAs, with the length of the perfluorinated carbon chain (n) reduced by 1. Minor fractions of shorter-chain PFCAs were also formed: 11% of the TPs of PFHxSAm and 2% of the TPs of PFOSAm and PFHxSAm-Pr-DiMeAm, respectively (Table S5). However, for PFHxSAm, these probably result largely from impurities in the standard, which already contained the short-chain precursors PFBSAm and PFPeSAm. PFHxSAm-Pr-DiMeAm contained PFHxSAm and 6:2 FTSA prior to irradiation, whereby PFHxSAm might also be a previously formed TP whose concentration further increased during irradiation and was then finally completely transformed.

The four fluorotelomer PFAS formed PFCAs with chain lengths of n (19–43%), n-1 (41–68%), and n-2 (9–16%). 6:2 FTSAm-Pr-B and 6:2 FTSAm-Pr-DiMeNO also formed the intermediates 6:2 FTCA and U-6:2 FTCA. Additionally, 6:2 FTSAm-Pr-DiMeNO contained 6:2 FTSA and 6:2/6:2 FTSAm dimer prior to irradiation, either as impurities or as previously formed transformation products.

The mass balance reached a minimum at 0.5 h for 6:2 FTSAm-Pr-B, both FTBs, and both PFASAms, indicating

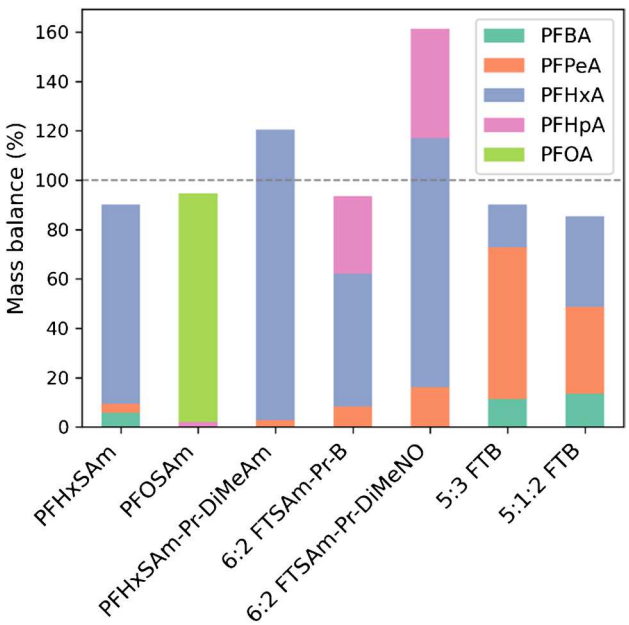

Fig. 1 Molar contributions (%) of TPs to mass balance after PhotoTOP of AFFF standards

the presence of potential unknown intermediates. However, with NTS, no further TPs could be identified in this study.

Martin et al. (2019) [27] analyzed selected PFAS standards using the TOP assay, including PFHxSAm, PFOSAm, PFOSAm-Pr-DiMeAm, and 6:2 FTSAm-Pr-B, as in this study. They identified the same TPs for PFHxSAm, PFOSAm, and PFOSAm-Pr-DiMeAm, but observed more pronounced chain shortening for 6:2 FTSAm-Pr-B. Their main TPs were PFBA and PFPeA, whereas the PhotoTOP treatment primarily produced PFHxA and PFHpA, potentially as a result of milder conditions and the absence of sulfate radicals [23].

Oxidative conversion of contaminated soil

The PhotoTOP was applied to both soil and soil extract for 46 h. The advantage of direct soil oxidation is that it eliminates the need for extraction, thereby avoiding potential analyte losses; however, it also results in a significantly higher matrix load, which can interfere with the oxidation efficiency. In contrast, oxidation of the soil extract allows for the application of larger soil equivalents due to the reduced matrix load. As a result, the soil equivalent in the extract-based approach is approximately 90 times higher compared to the direct soil treatment.

After 46 h of soil oxidation, the summed PFAS concentration, including TPs, stable compounds, and remaining precursors, was 27.6 nmol/g, whereas extract oxidation yielded only 9.5 nmol/g (Fig. 2a, Table S6). This clearly indicates that the extraction process was insufficient to recover the full PFAS burden from the soil. The recently published qNTS approach [25], which referred to the same soil sample, reported a sum of (semi)quantified concentrations of 29.6 nmol/g (Fig. 2b), with 6:2 FTSAm-Pr-B, 6:2 FTSO-(2′)OHPr-TriMeAm, 6:2 FTSy-(2′)OHPr-TriMeAm, PFOS, various FTBs, 6:2 FTSAm, 6:2 and 8:2 FTSA, 6:2 FTSAm-Pr-DiMeAm, and PFHxS, accounting for 90% of the total contamination (Table S7). Only 32.1% of the (semi) quantified PFAS could be recovered through extract oxidation. This poor recovery is due to the different extraction method used in this study, as the qNTS approach employed three sequential extractions with MeOH + 0.4 M ammonium acetate (NH_4Ac), which is particularly more effective for cationic and zwitterionic substances that are the major contributors to the total PFAS load in this soil. In contrast, 93.2% of the (semi)quantified PFAS could be captured by the direct PhotoTOP assay. This high recovery highlights the effectiveness of the direct oxidation method in capturing a broad range of PFAS of the prevailing contamination, including the fraction missed by extraction.

The molar distribution of perfluorinated carbon chain lengths for all PFAS in the qNTS study [25] was dominated by chains of six (58%) and eight (16%) perfluorinated

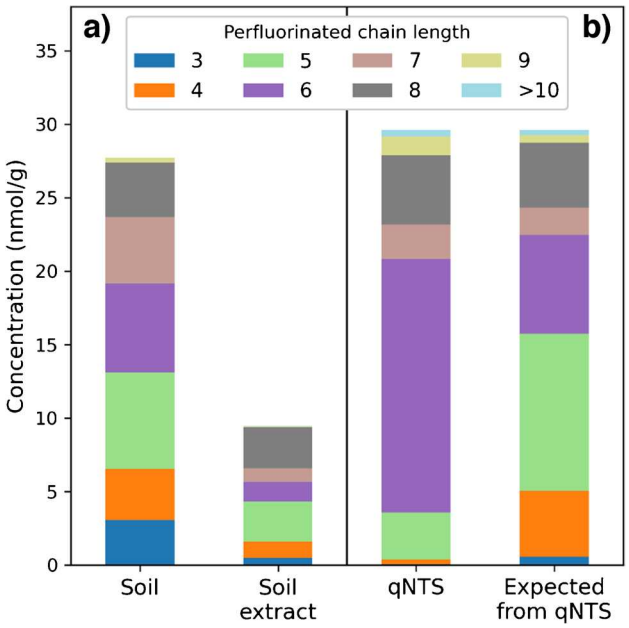

Fig. 2 Molar concentrations (nmol/g) of **a**) TPs, stable compounds, and remaining precursors after PhotoTOP with 46-h oxidation of soil and soil extract and of **b**) all PFAS detected by target and qNTS [25], along with expected concentrations based on the observed PhotoTOP transformation patterns

carbons (Fig. 2b). After PhotoTOP treatment, this distribution of TPs, stable compounds, and remaining precursors became blurred due to chain shortening during the oxidation process, particularly for fluorotelomer PFAS (Fig. 2a), which is consistent with results from AFFF standard oxidation. Applying the observed PhotoTOP transformation pattern from standard oxidation, namely, a perfluorinated chain shortening of n-1 for ECF precursors, and a distribution of 30% n, 55% n-1, and 15% n-2 for fluorotelomer precursors, to the qNTS results (Fig. 2b) shows agreement with the outcomes of the PhotoTOP treatment (Fig. 2a). Specifically, the molar distribution of perfluorinated carbon chain lengths obtained from direct soil oxidation versus those expected from qNTS was 13% vs. 15% ($n = 4$), 24% vs. 36% ($n = 5$), 22% vs. 23% ($n = 6$), 16% vs. 6% ($n = 7$), and 13% vs. 15% ($n = 8$), respectively.

Transformation kinetics of precursors during photocatalytic oxidation

During 46 h of direct soil and soil extract oxidation, precursors transformed, intermediates were formed and subsequently transformed, and PFCAs emerged as main TPs (Figs. 3 and 4).

In the case of direct soil oxidation (Fig. 3), the concentration of some PFCAs, particularly those with perfluorinated chains < 6, was still increasing at the end of the 46-h

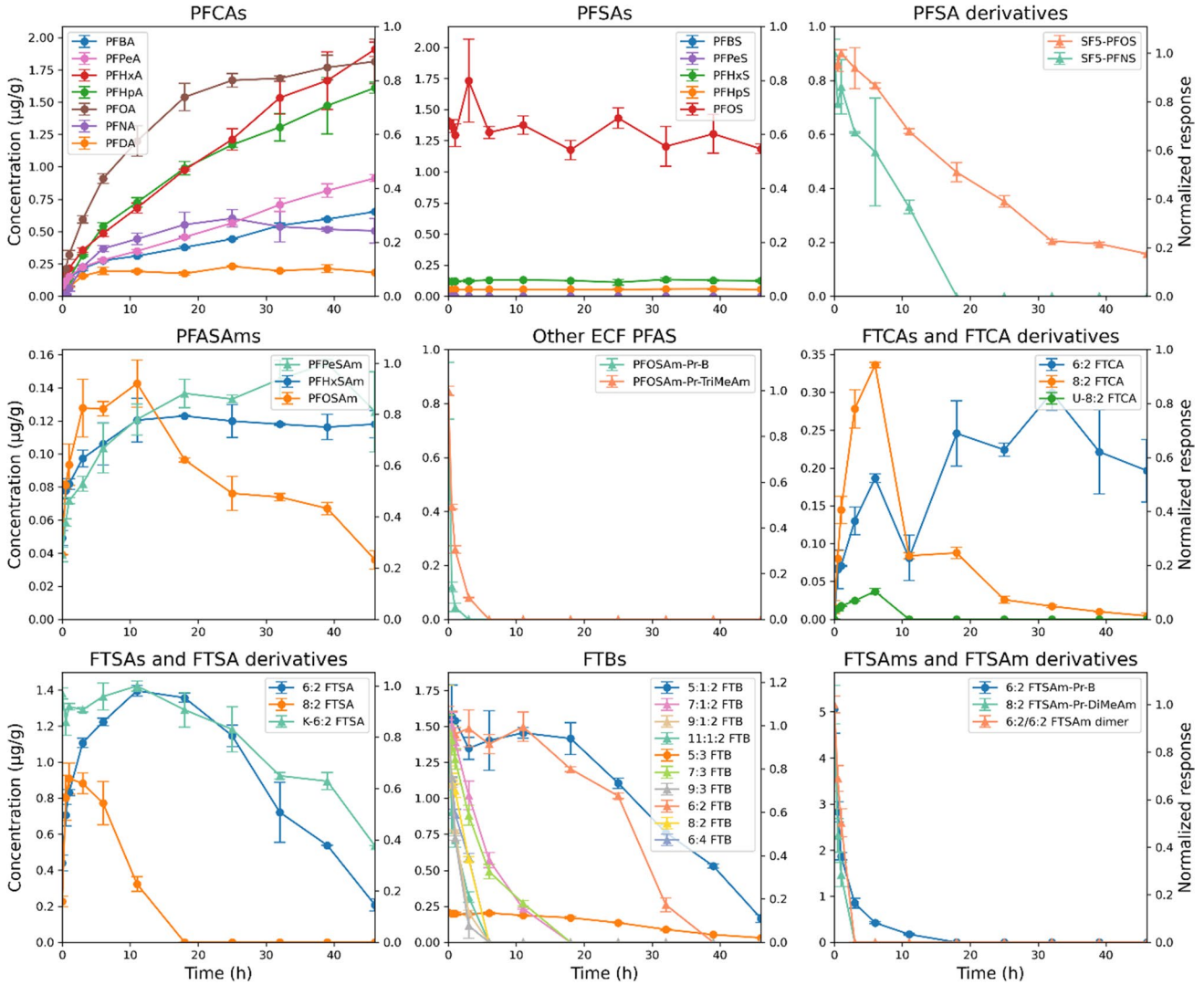

Fig. 3 PhotoTOP of contaminated soil containing 124 PFAS. Time trends are shown for precursors, intermediates, and final TPs. Concentrations of level 1 PFAS are plotted on the left axis (µg/g, circles), while normalized responses of level 2 and 3 PFAS are plotted on the right axis (triangles). Error bars represent the standard deviation of duplicate measurements ($n = 2$)

irradiation period. Additionally, intermediates such as PFASAms, FTCAs, and FTSAs had not yet fully transformed, indicating that photocatalytic oxidation was incomplete. Consequently, the measured total PFAS concentration of 27.6 nmol/g is likely a slight underestimation. Precursors such as SF_5-PFSAs, PFOSAm-Pr-B, PFOSAm-Pr-TriMeAm, FTBs, 6:2 FTSAm-Pr-B, 8:2 FTSAm-Pr-DiMeAm, and 6:2/6:2 FTSAm dimer were transformed, with some compounds (e.g., SF_5-PFOS, 5:1:2 FTB, and 5:3 FTB) being only partially but predominantly converted. To the best of our knowledge, this study is the first to demonstrate the transformation of SF_5-PFSAs. Zweigle et al. (2023) [28] reported that SF_5-PFSAs were stable in the TOP assay.

As seen from the mass balance, oxidation of soil, rather than soil extract, captures almost all (semi)quantified PFAS. However, the soil oxidation process requires a longer reaction time compared to soil extract oxidation (Figs. 3 and 4), and the higher soil equivalent used in the extract-based approach results in a higher response during measurement and therefore a greater number of detectable PFAS: 42 in the case of direct soil oxidation versus 91 for the extract-based approach (Table S4). In contrast to soil oxidation, by the end of soil extract oxidation (Fig. 4), PFCA concentrations had stabilized and precursors as well as intermediates were nearly completely transformed, indicating that photocatalytic oxidation was likely complete. Due to faster transformation, higher signal responses, and a greater number of detectable PFAS, soil extract oxidation was used to investigate the behavior and fate of different PFAS classes during the PhotoTOP assay. For this purpose, substances were classified

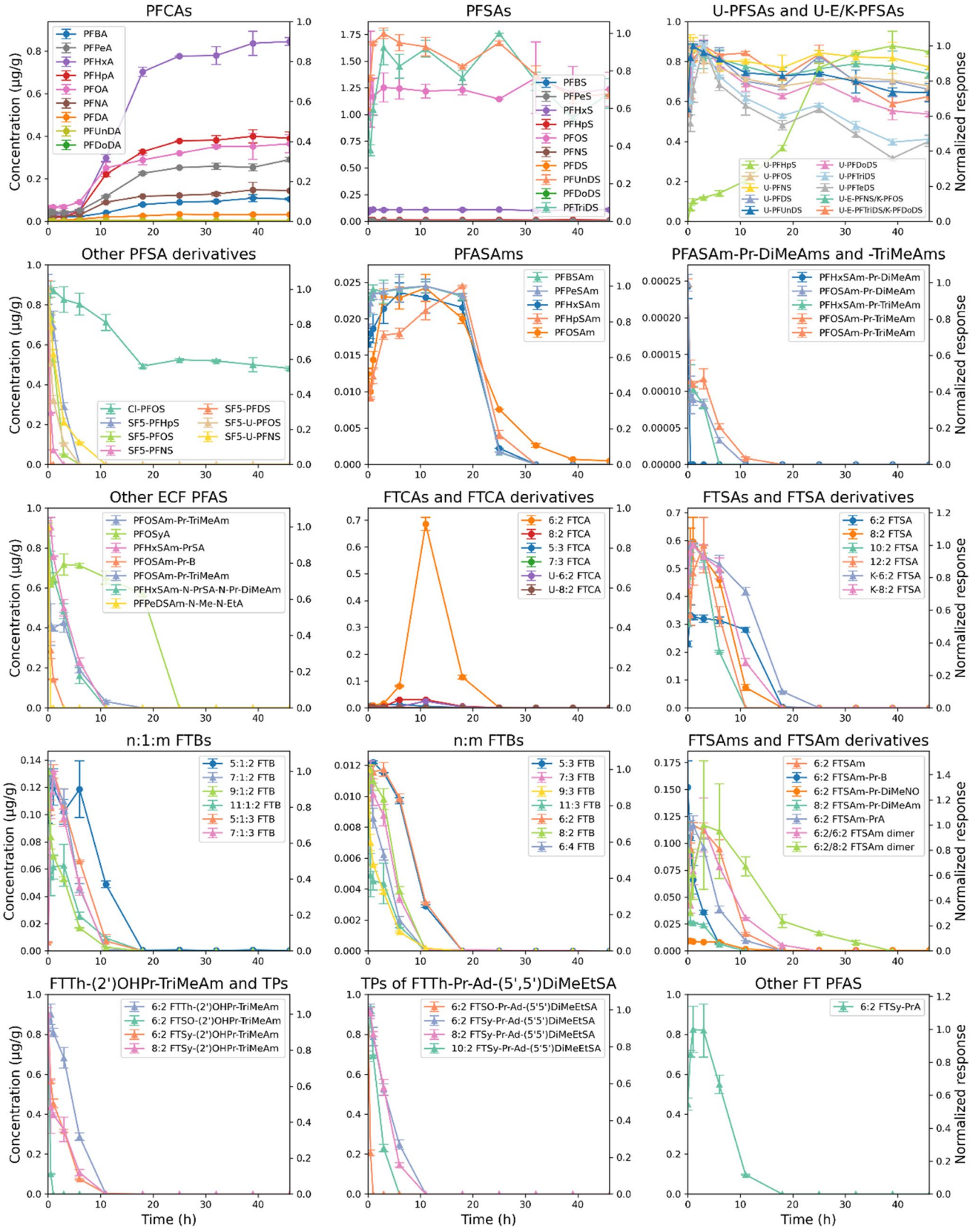

Fig. 4 PhotoTOP of extract from contaminated soil containing 124 PFAS. Time trends are shown for precursors, intermediates, and final TPs. Concentrations of level 1 PFAS are plotted on the left axis (µg/g, circles), while normalized responses of level 2 and 3 PFAS are plotted on the right axis (triangles). Error bars represent the standard deviation of duplicate measurements ($n=2$)

as precursors, intermediates, terminal TPs, or stable compounds, based on whether they were formed, showed a rise followed by a decline, underwent transformation only, or remained unchanged (Table S8). However, this classification has some limitations, as some precursors may also act as intermediates, and vice versa. For instance, certain compounds (e.g., Cl-PFOS, K-n:2 FTSA, n:2, n:3, n:1:2 FTB, and n:2 FTSy-Pr-Ad-(5′5′)DiMeEtSA) exhibited a slight initial increase in concentration during the PhotoTOP process. This could be attributed to strong sorption to surfaces such as the glass vial and the soil, followed by desorption during irradiation, possibly triggered by rising temperature and stirring, or to formation as intermediates during the experiment. Moreover, most intermediates were already present prior to irradiation, suggesting they may have formed in the environment through other processes such as biotic and abiotic transformation [29–32]. We have to remember that the contamination already occurred 15 years ago. Consequently, it is likely that many substances are transformed and formed simultaneously during the assay.

Precursors include a variety of perfluorinated PFAS produced by electrochemical fluorination (ECF), such as Cl-PFSA, SF_5-PFSA, SF_5-U-PFSA, PFASAm-PrSA, PFASAm-Pr-B, PFASAm-*N*-PrSA-*N*-Pr-DiMeAm, and PFASAm-*N*-Me-*N*-EtA, as well as fluorotelomer-based PFAS such as K-n:2 FTSA, n:1:2, n:2, n:3, and n:4 FTB, n:2 FTSAm-Pr-B, n:2 FTSAm-Pr-DiMeNO, n:2 FTSAm-Pr-DiMeAm, n:2 FTTh-(2′)OHPr-TriMeAm, n:2 FTSO-(2′)OHPr-TriMeAm, FTSy-(2′)OHPr-TriMeAm, n:2 FTSO-Pr-Ad-(5′5′)DiMeEtSA, and FTSy-Pr-Ad-(5′5′)DiMeEtSA. Intermediates comprise ECF-derived compounds including U-PFSA, PFASAm, PFASyA, PFASAm-Pr-DiMeAm, and PFASAm-Pr-TriMeAm, as well as fluorotelomer-derived compounds such as n:2 and n:3 FTCA, U-n:2 FTCA, n:2 FTSA, n:1:3 FTB, n:2 FTSAm, n:2 FTSAm-PrA, n:2/m:2 FTSAm dimer, and n:2 FTSy-PrA. The fate of U-E-PFSA/K-PFSA remains unclear, as it could not be definitively categorized as stable, intermediate, or precursor based on the observed data. PFCAs with perfluorinated chain lengths $n = 3$–11 were formed as terminal TPs, with PFHxA being the predominant TP. In contrast, PFSAs ($n = 4$–13) remained stable throughout the PhotoTOP process, with PFOS reaching the highest concentration. This is the first study to apply PhotoTOP to AFFF-contaminated soil, revealing a wide range of previously uncharacterized precursors and intermediates.

In comparison to the PhotoTOP assay results from previous studies, such as the one by Zweigle et al. (2022) [23], the transformation into PFCAs as main terminal products was comparable. The study also highlighted that the initial PFCA formation was suppressed in the extract with a higher matrix load, as can be clearly seen in this study. However, the extent of transformation and formation delay due to the matrix was less pronounced in Zweigle et al. (2022) [23], likely because the matrix was less concentrated (factor ≈ 8) and the PFAS contamination pattern was simpler (only 8:2 FTSA), which may have affected the overall transformation dynamics.

Martin et al. (2019) [27] also compared the oxidative conversion yields of selected precursors into PFCAs in the TOP assay using both matrix-free (ultra-pure) water and matrix-specific (groundwater) samples. An investigation using 10:2 FTSA as a model compound revealed no significant influence of the groundwater matrix on oxidative conversion. This is likely because the groundwater matrix is less complex than that of soil, consumes fewer hydroxyl radicals, and therefore has a reduced influence on the oxidation process. Both studies also used FTSAs as model compounds, which are characterized by a relatively high susceptibility to oxidative transformation [23, 27].

Al Amin et al. (2023) [21] applied a modified TOP assay to several AFFF formulations and a PFAS-contaminated soil extract. As in this study, the sum of PFCAs increased by several orders of magnitude in both the AFFF samples and the soil extract. Al Amin et al. (2023) [21] used 6:2 and 8:2 FTSAs as oxidation indicators to monitor the progress of oxidation and transformation. However, in this study, these compounds were already transformed after 18 h, whereas other compounds such as PFASAm took much longer to transform and would therefore serve as more reliable indicators. Al Amin et al. (2023) [21] also reported the presence of various perfluorooctane sulfonamide–based PFAS that reached a steady state through the TOP assay, likely because they were simultaneously formed and transformed.

Martin et al. (2019) [27] analyzed AFFF-impacted groundwater samples from an active firefighting training site and reported that a significant portion of the increase in individual PFCAs could be attributed to precursors such as 6:2 FTSAm-Pr-B, FTSAs, PFOSAm-Pr-DiMeAm, and PFHxSAm. Similarly, in this study, 6:2 FTSAm-Pr-B and PFHxSAm were among the compounds with the highest concentrations prior to oxidation.

As noted by Wang et al. (2025) [22], the mass balance after the TOP assay may not be fully closed compared to extractable organofluorine (EOF) results, due to nonoxidizable unknown PFAS, incomplete conversion of unknown PFAS precursors, and the presence of ultra-short-chain PFAS following oxidative conversion. This also applies to the PhotoTOP assay. Therefore, combining oxidative conversion with NTS or EOF analysis, as in this study, is recommended. Additionally, including trifluoroacetic acid (TFA) and HF in the analysis could provide further valuable insights.

To evaluate the kinetics and stability of the different PFAS during the PhotoTOP, the transformation and formation curves were fitted using four different models: logistic formation, exponential decay, a combination of logistic

formation and exponential decay, and a two-step exponential formation and decay model. These simplified models were used to describe the overall reaction as a sum of various processes, like transformation of precursors, formation and further transformation of intermediates, and formation of final transformation products. Included are also sorption and desorption on surfaces and TiO_2 particles, which may delay reactive processes. The models primarily represent the bottleneck reactions that limit the overall reaction rates, but they do not capture all processes involved in detail. Interactions between different PFAS compounds influence the reactions due to competition and transformation among them. As a result, time shifts of the course of reactions can occur, and the models may not always perfectly reflect the system dynamics. The fitted parameters and curves are shown in Table S9 and Figures S1 and S2. The normalized RMSE is below 21%, with a median of 4%, indicating a rather good model fit.

By comparing formation and decay rates, the stability of different PFAS compounds during the PhotoTOP assay can be assessed. Higher decay rates indicate faster transformation processes, which may result from lower chemical stability or stronger sorption affinity to TiO_2 particles, where OH radicals are generated. The newly identified intermediates, U-PFSAs, exhibit very low decay rates ($> 0.7\ h^{-1}$), suggesting high stability under PhotoTOP conditions. PFHxSAm, the perfluorinated analogue of 6:2 FTSAm, shows a higher decay rate than 6:2 FTSAm ($0.49\ h^{-1}$ vs. $0.17\ h^{-1}$), indicating it undergoes less simultaneous formation, likely due to a higher abundance of fluorotelomer-based precursors compared to perfluorinated ones. This is supported by the higher formation rate of 6:2 FTSAm ($2.08\ h^{-1}$) compared to PFHxSAm ($0.51\ h^{-1}$). A comparison between PFASAm-Pr-DiMeAm and PFASAm-Pr-TriMeAm, with perfluorinated chain lengths of $n = 6$ and $n = 8$, shows that PFASAm-Pr-DiMeAm has decay rates approximately seven times higher than PFASAm-Pr-TriMeAm for $n = 6$, and about three times higher for $n = 8$. This indicates that PFASAm-Pr-DiMeAm transforms faster than its trimethylated analogue, likely due to the presence of a free electron pair which can be oxidized. Furthermore, the decay rates of 6:2 FTSO-(2′)OHPr-TriMeAm ($2.19\ h^{-1}$ for soil and $4.42\ h^{-1}$ for soil extract) and 6:2 FTSO-Pr-Ad-(5′5′)DiMeEtSA ($3.16\ h^{-1}$ for soil extract) are significantly higher than those of 6:2 FTSy-(2′)OHPr-TriMeAm ($0.26\ h^{-1}$ for soil and $0.43\ h^{-1}$ for soil extract) and 6:2 FTSy-Pr-Ad-(5′5′)DiMeEtSA ($0.23\ h^{-1}$ for soil extract), which in turn are higher than the decay rate of 6:2 FTTh-(2′)OHPr-TriMeAm ($0.16\ h^{-1}$ for soil and $0.18\ h^{-1}$ for soil extract). This trend highlights the strong effect of easily oxidizable chemical structure moieties on the overall transformation behavior during the PhotoTOP assay. While the stability observed in the PhotoTOP assay can provide insights into environmental stability, it may not directly reflect real-world behavior, as other processes and environmental conditions can significantly affect PFAS transformation. For example, n:2 FTTh-(2′)OHPr-TriMeAm serves as the precursor for n:2 FTSO-(2′)OHPr-TriMeAm, which is subsequently transformed into n:2 FTSy-(2′)OHPr-TriMeAm. qNTS revealed higher concentrations of 6:2 FTSO-(2′)OHPr-TriMeAm and 6:2 FTSy-(2′)OHPr-TriMeAm compared to their precursor [25]. Therefore, under environmental conditions, the decay of n:2 FTSO-(2′)OHPr-TriMeAm and n:2 FTSy-(2′)OHPr-TriMeAm cannot exceed that of n:2 FTTh-(2′)OHPr-TriMeAm.

Fang et al. (2024) [33] demonstrated in biotransformation experiments in aerobic sludge that 6:2 FTSAm-Pr-B is significantly more stable than 6:2 FTSAm-Pr-DiMeAm and more stable than 6:2 FTSAm-Pr-DiMeNO, which is consistent with the observed stability of their perfluorinated analogues in aerobic soil [34]. In contrast, the results presented here show the opposite trend: 6:2 FTSAm-Pr-B transforms faster than 6:2 FTSAm-Pr-DiMeNO, and PFOSAm-Pr-B transforms faster than PFOSAm-Pr-DiMeAm. Although FTBs have previously been reported to be highly resistant to microbial degradation [35], in this study, under OH radical-mediated conditions, they transformed at rates comparable to those of other precursors.

Zweigle et al. (2023) [28] reported that Cl-PFOS, SF_5-PFSAs, SF_5-U-PFSAs, U-PFSAs, and U-E-PFSAs were stable in the TOP assay, whereas, in the PhotoTOP assay, these substances were observed to transform, albeit very slowly. Notably, U-PFSAs, especially U-PFHpS, were even formed as intermediates. This discrepancy may be due to the fact that the TOP assay does not allow for time-resolved monitoring, and therefore transformation processes may not have reached completion.

Spearman correlations between perfluorinated chain length and formation/decay rates indicate a strong positive correlation for soil oxidation, but both strong positive and strong negative correlations for soil extract oxidation (Figure S3). The strong correlation observed in soil oxidation likely reflects that longer homologues have a higher sorption affinity for TiO_2 particles, leading to faster transformation compared to shorter homologues. In contrast, the strong positive and strong negative correlations in soil extract oxidation may result from strong initial sorption of PFAS to the glass vials. In this case, PFAS must first desorb from the glass before they can sorb to the TiO_2 particles, disrupting the expected correlation pattern.

This correlation in the PhotoTOP contradicts the observed microbial stability. As Dong et al. (2024) [31] suggested, a longer perfluorinated carbon chain may lead to increased microbial stability. This further highlights that PhotoTOP results may not directly reflect real-world environmental

behavior. Nevertheless, it provides valuable insight into which substances are highly stable and which intermediates and TPs can be expected.

Conclusion

Precursors represent a complex source of persistent perfluoroalkyl acids (PFAAs) in the environment, with many transformation pathways still insufficiently understood. The PhotoTOP approach offers a valuable tool for addressing these knowledge gaps by enabling long-term prediction of TPs and providing insights into precursor fate. Key advantages of the PhotoTOP are its ability to largely preserve the original chain length distribution, resulting in a relatively narrow chain length distribution of the TPs as a mix of n, n-1, and n-2, offering additional information about precursor chain lengths, and the temporal monitoring of PFAS transformation. When combined with NTS, it facilitates comprehensive monitoring of transformation kinetics from precursors through intermediates to final products. Moreover, PhotoTOP serves as a complementary method for validating qNTS. Its application to both soil and soil extracts presents distinct benefits: direct oxidation of soil circumvents limitations due to incomplete extraction, while extract oxidation yields higher PFAS concentrations in measured samples and enhanced analytical sensitivity due to reduced matrix loads. Altogether, the PhotoTOP represents a robust and versatile tool for improving our understanding and assessment of PFAS contamination and transformation in environmental matrices.

Supplementary Information The online version contains supplementary material available at https://doi.org/10.1007/s00216-025-06208-0.

Author contribution CC: conceptualization, writing of the original draft. CZ: supervision of the study, supporting data interpretation, reviewing and revising the manuscript.

Funding Open Access funding enabled and organized by Projekt DEAL. The authors acknowledge the Federal Ministry of Research, Technology and Space (BMFTR) for funding the project PFClean (02WGW1665C).

Data availability Data will be made available on request.

Declarations

Competing interests Christian Zwiener is guest editor of ABC but was not involved in the peer review of this paper. All authors declare no competing interests.

References

1. Kissa E. Fluorinated surfactants and repellents. New York: Marcel Dekker; 2001.
2. Glüge J, Scheringer M, Cousins IT, DeWitt JC, Goldenman G, Herzke D, et al. An overview of the uses of per- and polyfluoroalkyl substances (PFAS). Environ Sci Process Impacts. 2020;22(12):2345–73. https://doi.org/10.1039/d0em00291g.
3. Evich MG, Davis MJB, McCord JP, Acrey B, Awkerman JA, Knappe DRU, et al. Per- and polyfluoroalkyl substances in the environment. Science. 2022;375(6580):eabg9065. https://doi.org/10.1126/science.abg9065.
4. Cousins IT, DeWitt JC, Gluge J, Goldenman G, Herzke D, Lohmann R, et al. The high persistence of PFAS is sufficient for their management as a chemical class. Environ Sci Process Impacts. 2020;22(12):2307–12. https://doi.org/10.1039/d0em00355g.
5. Dewapriya P, Nilsson S, GhorbaniGorji S, O'Brien JW, Braunig J, Gomez Ramos MJ, et al. Novel per- and polyfluoroalkyl substances discovered in cattle exposed to AFFF-impacted groundwater. Environ Sci Technol. 2023;57(36):13635–45. https://doi.org/10.1021/acs.est.3c03852.
6. East AG, Narizzano AM, Holden LA, Bazar MA, Bohannon ME, Pervitsky D, et al. Comparative toxicity of seven aqueous film-forming foam to in vitro systems and *Mus*. Environ Toxicol Chem. 2023;42(11):2364–74. https://doi.org/10.1002/etc.5714.
7. Habib Z, Song M, Ikram S, Zahra Z. Overview of per- and polyfluoroalkyl substances (PFAS), their applications, sources, and potential impacts on human health. Pollutants. 2024;4(1):136–52. https://doi.org/10.3390/pollutants4010009.
8. Pickard HM, Haque F, Sunderland EM. Bioaccumulation of perfluoroalkyl sulfonamides (FASA). Environ Sci Technol Lett. 2024;11(4):350–6. https://doi.org/10.1021/acs.estlett.4c00143.
9. Backe WJ, Day TC, Field JA. Zwitterionic, cationic, and anionic fluorinated chemicals in aqueous film forming foam formulations and groundwater from U.S. military bases by nonaqueous large-volume injection HPLC-MS/MS. Environ Sci Technol. 2013;47(10):5226–34. https://doi.org/10.1021/es3034999.
10. Barzen-Hanson KA, Roberts SC, Choyke S, Oetjen K, McAlees A, Riddell N, et al. Discovery of 40 classes of per- and polyfluoroalkyl substances in historical aqueous film-forming foams (AFFFs) and AFFF-impacted groundwater. Environ Sci Technol. 2017;51(4):2047–57. https://doi.org/10.1021/acs.est.6b05843.
11. Weiner B, Yeung LWY, Marchington EB, D'Agostino LA, Mabury SA. Organic fluorine content in aqueous film forming foams (AFFFs) and biodegradation of the foam component 6: 2 fluorotelomermercaptoalkylamido sulfonate (6: 2 FTSAS). Environ Chem. 2013;10(6):486–93. https://doi.org/10.1071/En13128.
12. Houtz EF, Higgins CP, Field JA, Sedlak DL. Persistence of perfluoroalkyl acid precursors in AFFF-impacted groundwater and soil. Environ Sci Technol. 2013;47(15):8187–95. https://doi.org/10.1021/es4018877.
13. Dauchy X, Boiteux V, Bach C, Rosin C, Munoz JF. Per- and polyfluoroalkyl substances in firefighting foam concentrates and water samples collected near sites impacted by the use of these foams. Chemosphere. 2017;183:53–61. https://doi.org/10.1016/j.chemosphere.2017.05.056.
14. Bigler MC, Brusseau ML, Guo B, Jones SL, Pritchard JC, Higgins CP, et al. High-resolution depth-discrete analysis of PFAS distribution and leaching for a vadose-zone source at an

AFFF-impacted site. Environ Sci Technol. 2024;58(22):9863–74. https://doi.org/10.1021/acs.est.4c01615.
15. OECD. Summary report on the new comprehensive global database of Per- and Polyfluoroalkyl Substances (PFASs). OECD Series on Risk Management of Chemicals. Paris: OECD Publishing; 2018. https://doi.org/10.1787/1a14ad6c-en.
16. Bugsel B, Zweigle J, Zwiener C. Nontarget screening strategies for PFAS prioritization and identification by high resolution mass spectrometry: a review. Trends Environ Anal Chem. 2023;40:e00216. https://doi.org/10.1016/j.teac.2023.e00216.
17. Malm L, Liigand J, Aalizadeh R, Alygizakis N, Ng K, FroKjaer EE, et al. Quantification approaches in non-target LC/ESI/HRMS analysis: an interlaboratory comparison. Anal Chem. 2024;96(41):16215–26. https://doi.org/10.1021/acs.analchem.4c02902.
18. Houtz EF, Sedlak DL. Oxidative conversion as a means of detecting precursors to perfluoroalkyl acids in urban runoff. Environ Sci Technol. 2012;46(17):9342–9. https://doi.org/10.1021/es302274g.
19. Janda J, Nodler K, Scheurer M, Happel O, Nurenberg G, Zwiener C, et al. Closing the gap - inclusion of ultrashort-chain perfluoroalkyl carboxylic acids in the total oxidizable precursor (TOP) assay protocol. Environ Sci Process Impacts. 2019;21(11):1926–35. https://doi.org/10.1039/c9em00169g.
20. Göckener B, Lange FT, Lesmeister L, Gökçe E, Dahme HU, Bandow N, et al. Digging deep—implementation, standardisation and interpretation of a total oxidisable precursor (TOP) assay within the regulatory context of per- and polyfluoroalkyl substances (PFASs) in soil. Environ Sci Eur. 2022;34(1):52. https://doi.org/10.1186/s12302-022-00631-1.
21. Al Amin M, Luo Y, Shi F, Yu L, Liu Y, Nolan A, et al. A modified TOP assay to detect per- and polyfluoroalkyl substances in aqueous film-forming foams (AFFF) and soil. Front Chem. 2023;11:1141182. https://doi.org/10.3389/fchem.2023.1141182.
22. Wang Q, van Hees P, Karlsson P, Jiao E, Filipovic M, Lam PKS, et al. What we learn from using mass balance approach and oxidative conversion - a case study on PFAS contaminated soil samples. Environ Pollut. 2025;376:126420. https://doi.org/10.1016/j.envpol.2025.126420.
23. Zweigle J, Bugsel B, Capitain C, Zwiener C. PhotoTOP: PFAS precursor characterization by UV/TiO(2) photocatalysis. Environ Sci Technol. 2022;56(22):15728–36. https://doi.org/10.1021/acs.est.2c05652.
24. Zweigle J, Capitain C, Simon F, Roesch P, Bugsel B, Zwiener C. Non-extractable PFAS in functional textiles - characterization by complementary methods: oxidation, hydrolysis, and fluorine sum parameters. Environ Sci Process Impacts. 2023;25(8):1298–310. https://doi.org/10.1039/d3em00131h.
25. Capitain C, Schüßler M, Bugsel B, Zweigle J, Vogel C, Leube P, et al. Implementation of matrix-matched semiquantification of PFAS in AFFF-contaminated soil. Environ Sci Technol. 2025;59(14):7338–47. https://doi.org/10.1021/acs.est.4c14255.
26. Schüßler M, Capitain C, Bugsel B, Zweigle J, Zwiener C. Nontarget screening reveals 124 PFAS at an AFFF-impacted field site in Germany specified by novel systematic terminology. Anal Bioanal Chem. 2024. https://doi.org/10.1007/s00216-024-05611-3.
27. Martin D, Munoz G, Mejia-Avendaño S, Duy SV, Yao Y, Volchek K, et al. Zwitterionic, cationic, and anionic perfluoroalkyl and polyfluoroalkyl substances integrated into total oxidizable precursor assay of contaminated groundwater. Talanta. 2019;195:533–42.
28. Zweigle J, Bugsel B, Röhler K, Haluska AA, Zwiener C. PFAS-contaminated soil site in Germany: nontarget screening before and after direct TOP assay by Kendrick mass defect and FindPFΔS. Environ Sci Technol. 2023;57(16):6647–55. https://doi.org/10.1021/acs.est.2c07969.
29. Choi YJ, Helbling DE, Liu J, Olivares CI, Higgins CP. Microbial biotransformation of aqueous film-forming foam derived polyfluoroalkyl substances. Sci Total Environ. 2022;824:153711. https://doi.org/10.1016/j.scitotenv.2022.153711.
30. Cook EK, Olivares CI, Antell EH, Yi S, Nickerson A, Choi YJ, et al. Biological and chemical transformation of the six-carbon polyfluoroalkyl substance N-dimethyl ammonio propyl perfluorohexane sulfonamide (AmPr-FHxSA). Environ Sci Technol. 2022;56(22):15478–88. https://doi.org/10.1021/acs.est.2c00261.
31. Dong S, Yan PF, Manz KE, Abriola LM, Pennell KD, Capiro NL. Fate and transformation of 15 classes of per- and polyfluoroalkyl substances in aqueous film-forming foam (AFFF)-amended soil microcosms. Environ Sci Technol. 2024;58(51):22777–89. https://doi.org/10.1021/acs.est.4c08665.
32. Fang B, Chen H, Zhao M, Qiao B, Zhou Y, Wang Y, et al. Biotic and abiotic transformations of aqueous film-forming foam (AFFF)-derived emerging polyfluoroalkyl substances in aerobic soil slurry. Water Res. 2025;276:123284. https://doi.org/10.1016/j.watres.2025.123284.
33. Fang B, Zhang Y, Chen H, Qiao B, Yu H, Zhao M, et al. Stability and biotransformation of 6:2 fluorotelomer sulfonic acid, sulfonamide amine oxide, and sulfonamide alkylbetaine in aerobic sludge. Environ Sci Technol. 2024;58(5):2446–57. https://doi.org/10.1021/acs.est.3c05506.
34. Liu M, Munoz G, Vo Duy S, Sauve S, Liu J. Stability of nitrogen-containing polyfluoroalkyl substances in aerobic soils. Environ Sci Technol. 2021;55(8):4698–708. https://doi.org/10.1021/acs.est.0c05811.
35. Fang B, Chen H, Zhou Y, Qiao B, Baqar M, Wang Y, et al. Fluorotelomer betaines and sulfonic acid in aerobic wetland soil: stability, biotransformation, and bacterial community response. J Hazard Mater. 2024;477:135261. https://doi.org/10.1016/j.jhazmat.2024.135261.

Catharina Capitain is a PhD student in the research group of Christian Zwiener at the University of Tübingen. Her research focuses on quantitative non-target screening approaches for per- and polyfluoroalkyl substances (PFAS), particularly those related to aqueous film-forming foams (AFFFs). She investigates the occurrence, transformation, and fate of PFAS at AFFF-contaminated field sites, including photocatalytic oxidation and biodegradation processes.

Christian Zwiener is Head of the Group of Environmental Analytical Chemistry in the Department of Geosciences at the Eberhard Karls Universität Tübingen. His research focuses on the analysis, occurrence, and fate of organic micropollutants in the environment and in water treatment with an emphasis on non-target screening strategies for per- and polyfluorinated alkyl substances (PFAS) and their fate in remediation and environmental processes.

Analytical and Bioanalytical Chemistry

Electronic Supplementary Material

Characterization of per and polyfluoroalkyl substances (PFAS) in AFFF contaminated soil by photocatalytic oxidation (PhotoTOP)

Catharina Capitain[1], Christian Zwiener[1]

1 Environmental Analytical Chemistry, Department of Geosciences, University of Tübingen, Schnarrenbergstraße 94-96, 72076 Tübingen, Germany

Table of content

ESM A Chemicals

Table S1: Overview about all PFAS reference standards that were included in the PFAS standard mixture and where they were purchased. PFAS originated either from Wellington Laboratories, Guelph, Ontario, Canada (1), Toronto Research Chemicals, North York, Ontario, Canada (2), Dr. Ehrenstorfer, Augsburg, Bavaria, Germany (3) or were custom-synthesized in-house (4).

Acronym	Used standard / purchased chemical	Origin
PFCAs		
PFBA	Perfluorobutanoic acid / perfluoro-n-butanoic acid	(1)
PFPeA	Perfluoropentanoic acid / perfluoro-n-pentanoic acid	(1)
PFHxA	Perfluorohexanoic acid / perfluoro-n-hexanoic acid	(1)
PFHpA	Perfluoroheptanoic acid / perfluoro-n-heptanoic acid	(1)
PFOA	Perfluorooctanoic acid / perfluoro-n-octanoic acid	(1)
PFNA	Perfluorononanic acid / perfluoro-n-nonanic acid	(1)
PFDA	Perfluorodecanoic acid / perfluoro-n-decanoic acid	(1)
PFUnDA	Perfluoroundecanoic acid / perfluoro-n-undecanoic acid	(1)
PFDoDA	Perfluorododecanoic acid / perfluoro-n-dodecanoic acid	(1)
PFTriDA	Perfluorotridecanoic acid / perfluoro-n-tridecanoic acid	(1)
PFTeDA	Perfluorotetradecanoic acid / perfluoro-n-tetradecanoic acid	(1)
PFHxDA	Perfluorohexadecanoic acid / perfluoro-n-hexadecanoic acid	(1)
PFODA	Perfluorooctadecanoic acid / perfluoro-n-octadecanoic acid	(1)
PFSAs		
PFBS	Perfluorobutanesulfonic acid / potassium perfluoro-1-butanesulfonate	(1)
PFPeS	Perfluoropentanesulfonic acid / sodium perfluoro-1-pentanesulfonate	(1)
PFHxS	Perfluorohexanesulfonic acid / sodium perfluoro-1-hexanesulfonate	(1)
PFHpS	Perfluoroheptanesulfonic acid / sodium perfluoro-1-heptanesulfonate	(1)
PFOS	Perfluorooctanesulfonic acid / sodium perfluoro-1-octanesulfonate	(1)
PFNS	Perfluorononanesulfonic acid / sodium perfluoro-1-nonanesulfonate	(1)
PFDS	Perfluorodecanesulfonic acid / sodium perfluoro-1-decanesulfonate	(1)
PFDoDS	Perfluorododecanesulfonic acid / sodium perfluoro-1-dodecanesulfonate	(1)
PFPAs		
PFOPA	Perfluorooctylphosphonic acid	(1)
PFDPA	Perfluorodecylphosphonic acid	(1)
PAPs		
6:2/6:2 diPAP	6:2/6:2 phosphoric acid diester / Bis[2-(perfluorohexyl)ethyl] phosphate	(2)
8:2/8:2 diPAP	6:2/6:2 polyfluoroalkyl phosphoric acid diester / Sodium bis (1H, 1H, 2H, 2H-perfluorodecyl) phosphate	(1)
6:2 PAP	6:2 polyfluoroalkyl phosphoric ester / Mono[2-(perfluorohexyl)ethyl] phosphate	(2)

8:2 PAP	6:2 polyfluoroalkyl phosphoric ester / Sodium 1H, 1H, 2H, 2H-perfluorodecyl phosphate	(1)
PFPiAs		
C6/C6 PFPiA	C6/C6 Perfluoroalkyl phosphinic acid	(2)
PASF-based PFAS		
PFHxSAm	Perfluorohexane sulfonamide	(3)
PFOSAm	Perfluorooctane sulfonamide	(1)
PFOSAm-*N*-Et-*N*-EtA	Perfluorooctane sulfonamide *N*-ethyl *N*-ethanoic acid	(1)
SamPAP	Perfluorooctane sulfonamide ethanol-based phosphate diester /Sodium-2-(N-ethylperfluorooctane-1-sulfonamido) ethyl phosphate	(1)
diSAmPAP	Perfluorooctane sulfonamide ethanol-based phosphate diester/ Sodium bis[2-(N-ethylperfluorooctane-1-sulfonamido) ethyl] phosphate	(1)
FTCAs		
6:2 FTCA	6:2 fluorotelomer carboxylic acid / 2-Perfluorohexyl ethanoic acid (6:2)	(1)
8:2 FTCA	8:2 fluorotelomer carboxylic acid / 2-Perfluorooctyl ethanoic acid (6:2)	(1)
5:3 FTCA	5:3 fluorotelomer carboxylic acid/ 3-Perfluoropentyl propanoic acid	(1)
7:3 FTCA	7:3 fluorotelomer carboxylic acid/ 3-Perfluoroheptyl propanoic acid	(1)
U-FTCAs		
U-6:2 FTCA	6:2 fluorotelomer unsaturated carboxylic acid/ 2H-Perfluoro-2-octenoic acid (6:2)	(1)
U-8:2 FTCA	8:2 fluorotelomer unsaturated carboxylic acid/ 2H-Perfluoro-2-decenoic acid (8:2)	(1)
FTSAs		
6:2 FTSA	6:2 fluorotelomer sulfonic acid / Sodium 1H, 1H,2H,2H-perfluorooctanesulfonate	(1)
8:2 FTSA	8:2 fluorotelomer sulfonic acid / Sodium 1H, 1H,2H,2H-perfluorodecanesulfonate	(1)
FTMAPs		
6:2 FTMAP	6:2 Fluorotelomer mercapto alkyl phosphate	(4)
PFECAs		
HFPO-Da	2,3,3,3-Tetrafluoro-2-(1,1,2,2,3,3,3-heptafluoropropoxy) propanoic acid	(1)
ADONA	Sodium dodecafluoro-3H-4,8-dioxanonanoate	(1)
PFESAs		
9Cl-PF3ONS	Potassium 9-chlorhexadecafluoro-3-oxanonane-1-sulfonate	(1)
11Cl-PF3OUdS	Potassium 11-chloroeicosafluoro-3-oxaundecane-1-sulfonate	(1)
AFFF-substances		
6:2 FTSAm-Pr-DiMeNO	6:2 fluorotelomer sulfonamide propyl methylamineoxide / Capstone product A	(3)
6:2 FTSAm-Pr-B	6:2 fluorotelomer sulfonamide propyl betaine / Capstone product B	(3)
PFHxSAm-Pr-DiMeAm	N-[3(dimethylamino)propyl] perfluoro-1-hexanesulfonamide	(3)

5:3 FTB	5:3 Fluorotelomer betaine / 2-[4,4,5,5,6,6,7,7,8,8,8-Undecafluorooctyl) dimethylammonio] acetate	(1)
5:1:2 FTB	5:1:2 Fluorotelomer etaine / 2-[(3,4,4,5,5,6,6,7,7,8,8,8-Dodecafluorooctyl) dimethylammonio] acetate	(1)

ESM B Limit of detection

Table S2: Limits of detection (LOD) for PFAS detected in soil and soil extracts.

Name	LOD for standard oxidation (nM)	LOD in soil (pmol/g)	LOD in soil extract (pmol/g)
PFBA	0.23	108.0	1.2
PFPeA	0.38	174.9	1.9
PFHxA	0.16	73.5	0.8
PFHpA	0.28	126.7	1.4
PFOA	0.12	55.7	0.6
PFNA	0.11	49.7	0.6
PFDA	0.10	44.8	0.5
PFUnDA	0.09	40.9	0.5
PFDoDA	0.08	37.5	0.4
PFBS	0.17	76.9	0.9
PFPeS	0.14	65.9	0.7
PFHxS	0.13	57.7	0.6
PFHpS	0.11	51.2	0.6
PFOS	0.10	46.1	0.5
PFNS	0.09	41.9	0.5
PFDS	0.08	38.4	0.4
PFDoDS	0.07	32.9	0.4
PFHxSAm	0.13	57.8	0.6
PFOSAm	0.10	46.2	0.5
PFHxSAm-Pr-DiMeAm	0.10	47.4	0.5
6:2 FTCA	0.27	122.0	1.4
8:2 FTCA	0.10	48.2	0.5
5:3 FTCA	0.15	67.4	0.7
U-6:2 FTCA	0.14	64.4	0.7
U-8:2 FTCA	0.11	50.3	0.6
6:2 FTSA	0.12	53.9	0.6
8:2 FTSA	0.19	87.3	1.0
5:1:2 FTB	0.12	53.2	0.6
5:3 FTB	0.12	55.5	0.6
6:2 FTSAm-Pr-B	0.18	80.5	0.9
6:2 FTSAm-Pr-DiMeNO	0.09	43.5	0.5

ESM C Information on all identified classes/compounds

Table S3: All detected classes with acronyms and full names.

Acronym	Class
Cl-PFSA	Chloro substituted perfluoro sulfonic acid
K-n:2 FTSA	Ketone-n:2 fluorotelomer sulfonic acid
n:1:2 FTB	n:1:2 fluorotelomer betaine
n:1:3 FTB	n:1:3 fluorotelomer betaine
n:2 FTB	n:2 fluorotelomer betaine
n:2 FTCA	n:2 fluorotelomer carboxylic acid
n:2 FTSA	n:2 fluorotelomer sulfonic acid
n:2 FTSAm	n:2 fluorotelomer sulfonamide
n:2 FTSAm-PrA	n:2 fluorotelomer sulfonamide propanoic acid
n:2 FTSAm-Pr-B	n:2 fluorotelomer sulfonamide propyl betaine
n:2 FTSAm-Pr-DiMeAm	n:2 fluorotelomer sulfonamide propyl dimethylamine
n:2 FTSAm-Pr-DiMeNO	n:2 fluorotelomer sulfonamide propyl dimethylamineoxide
n:2 FTSO-(2')OHPr-TriMeAm	n:2 fluorotelomer sulfoxide (2')-propanol trimethylamine
n:2 FTSO-Pr-Ad-(5',5')DiMeEtSA	n:2 fluorotelomer sulfoxide propyl amide (5'5')-dimethylethyl sulfonic acid
n:2 FTSy-(2')OHPr-TriMeAm	n:2 fluorotelomer sulfone (2')-propanol trimethylamine
n:2 FTSy-PrA	n:2 fluorotelomer sulfone propanoic acid
n:2 FTSy-Pr-Ad-(5',5')DiMeEtSA	n:2 fluorotelomer sulfone propyl amide (5'5')-dimethylethyl sulfonic acid
n:2 FTTh-(2')OHPr-TriMeAm	n:2 fluorotelomer thio (2')-propanol trimethylamine
n:2/m:2 FTSAm dimer	n:2/m:2 fluorotelomer sulfonamide dimer
n:3 FTB	n:3 fluorotelomer betaine
n:3 FTCA	n:3 fluorotelomer carboxylic acid
n:4 FTB	n:4 fluorotelomer betaine
PFASAm	Perfluoroalkane sulfonamide
PFASAm-*N*-Me-*N*-EtA	Perfluoroalkane sulfonamide *N*-methyl *N*-ethanoic acid
PFASAm-*N*-PrSA-*N*-Pr-DiMeAm	Perfluoroalkane sulfonamide *N*-propyl sulfonic acid *N*-propyl dimethylamine
PFASAm-Pr-B	Perfluoroalkane sulfonamide propyl betaine
PFASAm-Pr-DiMeAm	Perfluoroalkane sulfonamide propyl dimethylamine
PFASAm-PrSA	Perfluoroalkane sulfonamide propyl sulfonic acid
PFASAm-Pr-TriMeAm	Perfluoroalkane sulfonamide propyl trimethylamine
PFASyA	Perfluoro sulfinic acid
PFCA	Perfluoro carboxylic acid
PFSA	Perfluoro sulfonic acid
SF_5-PFSA	Pentafluorosulfanyl perfluoro sulfonic acid
SF_5-U-PFSA	Pentafluorosulfanyl unsaturated perfluoro sulfonic acid

U-E-PFSA/K-PFSA	Unsaturated ether perfluoro sulfonic acid/Ketone perfluoro sulfonic acid
U-n:2 FTSA	Unsaturated n:2 fluorotelomer sulfonic acid
U-PFSA	Unsaturated perfluoro sulfonic acid

Table S4: All detected compounds with formula, mass to charge ratio *m/z*, polarity, confidence level, and the oxidized matrix in which each compound was identified.

Name	Formula	m/z	Polarity	Confidence level	Oxidized matrix
10:2 FTSA	C12 H5 F21 O3 S	626.9542	Negative	Level 2&3	Soil extract
10:2 FTSy-Pr-Ad-(5'5')DiMeEtSA	C19 H18 F21 N O6 S2	818.0145	Negative	Level 2&3	Soil extract
11:1:2 FTB	C18 H13 F24 N O2	732.0617	Positive	Level 2&3	Soil and soil extract
11:3 FTB	C18 H14 F23 N O2	714.0722	Positive	Level 2&3	Soil extract
12:2 FTSA	C14 H5 F25 O3 S	726.9482	Negative	Level 2&3	Soil extract
5:1:2 FTB	C12 H13 F12 N O2	432.0825	Positive	Level 1	Soil and soil extract
5:1:3 FTB	C13 H15 F12 N O2	446.0981	Positive	Level 2&3	Soil extract
5:3 FTB	C12 H14 F11 N O2	414.0916	Positive	Level 1	Soil and soil extract
5:3 FTCA	C8 H5 F11 O2	341.0029	Negative	Level 1	Soil extract
6:2 FTB	C12 H12 F13 N O2	450.0726	Positive	Level 2&3	Soil and soil extract
6:2 FTCA	C8 H3 F13 O2	376.9847	Negative	Level 1	Soil and soil extract
6:2 FTSA	C8 H5 F13 O3 S	426.9676	Negative	Level 1	Soil and soil extract
6:2 FTSAm	C8 H6 F13 N O2 S	425.9837	Negative	Level 2&3	Soil extract
6:2 FTSAm-PrA	C11 H10 F13 N O4 S	498.0038	Negative	Level 2&3	Soil extract
6:2 FTSAm-Pr-B	C15 H19 F13 N2 O4 S	571.0929	Positive	Level 1	Soil and soil extract
6:2 FTSAm-Pr-DiMeNO	C13 H17 F13 N2 O3 S	529.0837	Positive	Level 1	Soil extract
6:2 FTSO-(2')OHPr-TriMeAm	C14 H18 F13 N O2 S	512.0921	Positive	Level 2&3	Soil and soil extract
6:2 FTSO-Pr-Ad-(5'5')DiMeEtSA	C15 H18 F13 N O5 S2	602.0325	Negative	Level 2&3	Soil extract
6:2 FTSy-(2')OHPr-TriMeAm	C14 H18 F13 N O3 S	528.087	Positive	Level 2&3	Soil and soil extract
6:2 FTSy-PrA	C11 H9 F13 O4 S	482.9926	Negative	Level 2&3	Soil extract
6:2 FTSy-Pr-Ad-(5'5')DiMeEtSA	C15 H18 F13 N O6 S2	618.028	Negative	Level 2&3	Soil extract
6:2 FTTh-(2')OHPr-TriMeAm	C14 H18 F13 N O S	496.0955	Positive	Level 2&3	Soil and soil extract
6:2/6:2 FTSAm dimer	C16 H9 F26 N O4 S2	835.9468	Negative	Level 2&3	Soil and soil extract
6:2/8:2 FTSAm dimer	C18 H9 F30 N O4 S2	935.9405	Negative	Level 2&3	Soil extract

6:4 FTB	C14 H16 F13 N O2	478.1039	Positive	Level 2&3	Soil and soil extract
7:1:2 FTB	C14 H13 F16 N O2	532.076	Positive	Level 2&3	Soil and soil extract
7:1:3 FTB	C15 H15 F16 N O2	546.0917	Positive	Level 2&3	Soil extract
7:3 FTB	C14 H14 F15 N O2	514.0854	Positive	Level 2&3	Soil and soil extract
7:3 FTCA	C10 H5 F15 O2	440.9958	Negative	Level 1	Soil extract
8:2 FTB	C14 H12 F17 N O2	550.0662	Positive	Level 2&3	Soil and soil extract
8:2 FTCA	C10 H3 F17 O2	476.9783	Negative	Level 1	Soil and soil extract
8:2 FTSA	C10 H5 F17 O3 S	526.9608	Negative	Level 1	Soil and soil extract
8:2 FTSAm-Pr-DiMeAm	C15 H17 F17 N2 O2 S	613.0825	Positive	Level 2&3	Soil and soil extract
8:2 FTSy-(2')OHPr-TriMeAm	C16 H18 F17 N O3 S	628.08	Positive	Level 2&3	Soil and soil extract
8:2 FTSy-Pr-Ad-(5'5')DiMeEtSA	C17 H18 F17 N O6 S2	718.0217	Negative	Level 2&3	Soil extract
9:1:2 FTB	C16 H13 F20 N O2	632.0693	Positive	Level 2&3	Soil and soil extract
9:3 FTB	C16 H14 F19 N O2	614.0785	Positive	Level 2&3	Soil and soil extract
Cl-PFOS	C8 H Cl F16 O3 S	514.9016	Negative	Level 2&3	Soil extract
K-6:2 FTSA	C8 H3 F13 O4 S	440.9464	Negative	Level 2&3	Soil and soil extract
K-8:2 FTSA	C10 H3 F17 O4 S	540.9401	Negative	Level 2&3	Soil extract
PFBA	C4 H F7 O2	212.9791	Negative	Level 1	Soil and soil extract
PFBS	C4 H F9 O3 S	298.9427	Negative	Level 1	Soil and soil extract
PFBSAm	C4 H2 F9 N O2 S	297.9589	Negative	Level 2&3	Soil extract
PFDA	C10 H F19 O2	512.9601	Negative	Level 1	Soil and soil extract
PFDoDA	C12 H F23 O2	612.9551	Negative	Level 1	Soil extract
PFDoDS	C12 H F25 O3 S	698.9158	Negative	Level 1	Soil extract
PFDS	C10 H F21 O3 S	598.9226	Negative	Level 1	Soil extract
PFHpA	C7 H F13 O2	362.9713	Negative	Level 1	Soil and soil extract
PFHpS	C7 H F15 O3 S	448.9329	Negative	Level 1	Soil and soil extract
PFHpSAm	C7 H2 F15 N O2 S	447.9486	Negative	Level 2&3	Soil extract
PFHxA	C6 H F11 O2	312.9738	Negative	Level 1	Soil and soil extract
PFHxS	C6 H F13 O3 S	398.9362	Negative	Level 1	Soil and soil extract
PFHxSAm	C6 H2 F13 N O2 S	397.952	Negative	Level 1	Soil and soil extract

PFHxSAm-N-PrSA-N-Pr-DiMeAm	C14 H19 F13 N2 O5 S2	607.0592	Positive	Level 2&3	Soil extract
PFHxSAm-Pr-DiMeAm	C11 H13 F13 N2 O2 S	485.0559	Positive	Level 1	Soil extract
PFHxSAm-PrSA	C9 H8 F13 N O5 S2	519.955	Negative	Level 2&3	Soil extract
PFHxSAm-Pr-TriMeAm	C12 H15 F13 N2 O2 S	499.0711	Positive	Level 2&3	Soil extract
PFNA	C9 H F17 O2	462.9626	Negative	Level 1	Soil and soil extract
PFNS	C9 H F19 O3 S	548.9265	Negative	Level 1	Soil extract
PFOA	C8 H F15 O2	412.9659	Negative	Level 1	Soil and soil extract
PFOS	C8 H F17 O3 S	498.9299	Negative	Level 1	Soil and soil extract
PFOSAm	C8 H2 F17 N O2 S	497.9451	Negative	Level 1	Soil and soil extract
PFOSAm-Pr-B	C15 H15 F17 N2 O4 S	643.0551	Positive	Level 2&3	Soil and soil extract
PFOSAm-Pr-DiMeAm	C13 H13 F17 N2 O2 S	583.0332	Negative	Level 2&3	Soil extract
PFOSAm-Pr-TriMeAm	C14 H15 F17 N2 O2 S	599.0648	Positive	Level 2&3	Soil and soil extract
PFOSyA	C8 H F17 O2 S	482.9342	Negative	Level 2&3	Soil extract
PFPeA	C5 H F9 O2	262.9772	Negative	Level 1	Soil and soil extract
PFPeDSAm-N-Me-N-EtA	C18 H6 F31 N O4 S	919.9454	Negative	Level 2&3	Soil extract
PFPeS	C5 H F11 O3 S	348.9394	Negative	Level 1	Soil and soil extract
PFPeSAm	C5 H2 F11 N O2 S	347.9556	Negative	Level 2&3	Soil and soil extract
PFTriDS	C13 H F27 O3 S	748.9127	Negative	Level 2&3	Soil extract
PFUnDA	C11 H F21 O2	562.9562	Negative	Level 1	Soil extract
PFUnDS	C11 H F23 O3 S	648.9194	Negative	Level 2&3	Soil extract
SF_5-PFDS	C10 H F25 O3 S2	706.888	Negative	Level 2&3	Soil extract
SF_5-PFHpS	C7 H F19 O3 S2	556.8978	Negative	Level 2&3	Soil extract
SF_5-PFNS	C9 H F23 O3 S2	656.8902	Negative	Level 2&3	Soil and soil extract
SF_5-PFOS	C8 H F21 O3 S2	606.8943	Negative	Level 2&3	Soil and soil extract
SF_5-U-PFNS	C9 H F21 O3 S2	618.8944	Negative	Level 2&3	Soil extract
SF_5-U-PFOS	C8 H F19 O3 S2	568.8982	Negative	Level 2&3	Soil extract
U-6:2 FTCA	C8 H2 F12 O2	356.9791	Negative	Level 1	Soil extract
U-8:2 FTCA	C10 H2 F16 O2	456.9749	Negative	Level 1	Soil and soil extract
U-E-PFNS/K-PFOS	C8 H F15 O4 S	476.9273	Negative	Level 2&3	Soil extract
U-E-PFTriDS/K-PFDoDS	C12 H F23 O4 S	676.9138	Negative	Level 2&3	Soil extract
U-PFDoDS	C12 H F23 O3 S	660.9193	Negative	Level 2&3	Soil extract
U-PFDS	C10 H F19 O3 S	560.9263	Negative	Level 2&3	Soil extract

U-PFHpS	C7 H F13 O3 S	410.936	Negative	Level 2&3	Soil extract
U-PFNS	C9 H F17 O3 S	510.9294	Negative	Level 2&3	Soil extract
U-PFOS	C8 H F15 O3 S	460.9327	Negative	Level 2&3	Soil extract
U-PFTeDS	C14 H F27 O3 S	760.9139	Negative	Level 2&3	Soil extract
U-PFTriDS	C13 H F25 O3 S	710.9163	Negative	Level 2&3	Soil extract
U-PFUnDS	C11 H F21 O3 S	610.9242	Negative	Level 2&3	Soil extract

ESM D Results of AFFF standard oxidation

Table S5: Initial concentration of individual precursors, their terminal transformation products after the PhotoTOP, and mass balance (MB). Values marked as n.d. indicate that the compound was not detected.

Precursor	Initial concentration of precursor (nM)	Transformation products (nM)					MB (%)
		PFBA	PFPeA	PFHxA	PFHpA	PFOA	
PFHxSAm	26.0	1.541	1.0	21.7	n.d.	n.d.	90.1
PFOSAm	16.1	n.d.	n.d.	n.d.	0.3	14.9	94.7
PFHxSAm-Pr-DiMeAm	13.8	n.d.	0.4	16.3	n.d.	n.d.	120.5
6:2 FTSAm-Pr-B	15.5	n.d.	1.3	8.4	4.8	n.d.	93.4
6:2 FTSAm-Pr-DiMeNO	11.5	n.d.	1.9	11.6	5.1	n.d.	161.2
5:3 FTB	18.3	2.1	11.2	3.1	n.d.	n.d.	90.0
5:1:2 FTB	17.7	2.4	6.3	6.5	n.d.	n.d.	85.3

ESM E Results after direct soil and soil extract oxidation

Table S6: Molar concentrations (pmol/g) of precursors and transformation products (TPs) after PhotoTOP with 46 h oxidation of soil (C_{soil}) and soil extract ($C_{soil\ extract}$).

Name	Perfluorinated chain	C_{soil} (pmol/g)	$C_{soil\ extract}$ (pmol/g)
PFBA	3	30701	494
PFPeA	4	3474	1105
PFHxA	5	6098	2702
PFHpA	6	4439	1076
PFOA	7	4394	884
PFNA	8	1093	313
PFDA	9	359	63
PFUnDA	10	n.d.	5
PFDoDA	11	n.d.	1
PFBS	4	n.d.	7
PFPeS	5	n.d.	13
PFHxS	6	314	271
PFHpS	7	123	25.9
PFOS	8	2373	2478
PFNS	9	n.d.	8
PFDS	10	n.d.	2
PFDoDS	12	n.d.	1
PFHxSAm	6	297	n.d.
PFOSAm	8	72	1
6:2 FTCA	6	521	n.d.
6:2 FTSA	6	487	n.d.
5:1:2 FTB	5	386	1
5:3 FTB	5	77	n.d.
6:2 FTSAm-Pr-DiMeNO	6	n.d.	1

ESM F Results from qNTS study

Table S7: PFAS accounting for 90% of the total contamination identified in the qNTS approach [1].

Name	Concentration (µg/g)
6:2 FTSAm-Pr-B	3.17
6:2 FTSO-(2')OHPr-TriMeAm	2.29
6:2 FTSy-(2')OHPr-TriMeAm	1.88
PFOS	1.70
5:1:2 FTB	1.11
7:1:2 FTB	0.88
9:1:2 FTB	0.64
6:2 FTSAm	0.57
6:2 FTSA	0.38
8:2 FTSA	0.30
6:2 FTSAm-Pr-DiMeAm	0.20
7:3 FTB	0.19
5:3 FTB	0.13
9:3 FTB	0.13
PFHxS	0.13

ESM G Fate of PFAS classes in PhotoTOP

Table S8: Fate of PFAS classes in PhotoTOP. Note that the classification has limitations as some intermediates may also be precursors, or vice versa.

Class	Type
Cl-PFSA	Precursor
K-n:2 FTSA	Precursor
n:1:2 FTB	Precursor
n:2 FTB	Precursor
n:2 FTSAm-Pr-B	Precursor
n:2 FTSAm-Pr-DiMeAm	Precursor
n:2 FTSAm-Pr-DiMeNO	Precursor
n:2 FTSO-(2')OHPr-TriMeAm	Precursor
n:2 FTSO-Pr-Ad-(5',5')DiMeEtSA	Precursor
n:2 FTSy-(2')OHPr-TriMeAm	Precursor
n:2 FTSy-Pr-Ad-(5',5')DiMeEtSA	Precursor
n:2 FTTh-(2')OHPr-TriMeAm	Precursor
n:3 FTB	Precursor
n:4 FTB	Precursor
PFASAm-*N*-Me-*N*-EtA	Precursor
PFASAm-*N*-PrSA-*N*-Pr-DiMeAm	Precursor
PFASAm-Pr-B	Precursor
PFASAm-PrSA	Precursor
SF_5-PFSA	Precursor
SF_5-U-PFSA	Precursor
n:1:3 FTB	Intermediate
n:2 FTCA	Intermediate
n:2 FTSA	Intermediate
n:2 FTSAm	Intermediate
n:2 FTSAm-PrA	Intermediate
n:2 FTSy-PrA	Intermediate
n:2/m:2 FTSAm dimer	Intermediate
n:3 FTCA	Intermediate
PFASAm	Intermediate
PFASAm-Pr-DiMeAm	Intermediate
PFASAm-Pr-TriMeAm	Intermediate
PFASyA	Intermediate
U-n:2 FTSA	Intermediate
U-PFSA	Intermediate
PFCA	TP
U-E-PFSA/K-PFSA	Unclear
PFSA	Stable

ESM H Kinetics

Table S9: Fitting results with name of individual PFAS, oxidized matrix, applied model, initial concentration C_{start}, maximum concentration C_{max}, time when the formation rate is at its maximum t_{max}, formation rate k_f, decay rate k_d, and normalized root mean square error (RMSE). *C_{start} and C_{max} are expressed in µg/g for level 1 PFAS or as normalized response for level 2 and 3 PFAS.

Name	Oxidized matrix	Fitted model	C_{start} (*)	C_{max} (*)	t_{max} (h)	k_f (h^{-1})	k_d (h^{-1})	Normalized RMSE (%)
PFBA	Soil extract	Logistic formation	0.01	0.10	14.50	0.21		3.42
PFBA	Soil	Logistic formation	0.00	0.69	15.24	0.08		5.08
PFPeA	Soil extract	Logistic formation	0.03	0.27	13.04	0.31		3.28
PFPeA	Soil	Logistic formation	0.00	1.01	20.78	0.08		3.86
PFHxA	Soil extract	Logistic formation	0.01	0.81	12.79	0.36		2.33
PFHxA	Soil	Logistic formation	0.00	1.92	18.59	0.11		4.37
PFHpA	Soil extract	Logistic formation	0.00	0.38	10.72	0.33		3.20
PFHpA	Soil	Logistic formation	0.00	1.50	13.37	0.14		6.32
PFOA	Soil extract	Logistic formation	0.03	0.34	9.40	0.27		5.00
PFOA	Soil	Logistic formation	0.00	1.72	6.73	0.25		5.22
PFNA	Soil extract	Logistic formation	0.01	0.14	9.93	0.26		5.23
PFNA	Soil	Logistic formation	0.00	0.53	4.33	0.54		6.64
PFDA	Soil extract	Logistic formation	0.00	0.03	9.48	0.21		3.46
PFDA	Soil	Logistic formation	0.01	0.20	1.77	1.06		6.10
PFUnDA	Soil extract	Logistic formation	0.00	0.00	2.40	0.64		13.48
PFDoDA	Soil extract	Logistic formation	0.00	0.00	32.25	2.49		21.15
Cl-PFOS	Soil extract	Two-step exponential decay	0.83	0.56		0.63	0.14	4.74
SF5-PFHpS	Soil extract	Exponential decay	1.05				0.39	4.18
SF5-PFOS	Soil extract	Exponential decay	1.06				0.64	4.30
SF5-PFOS	Soil	Exponential decay	1.01				0.04	3.88
SF5-PFNS	Soil extract	Exponential decay	1.00				2.45	0.11
SF5-PFNS	Soil	Exponential decay	0.95				0.11	6.99

SF5-U-PFOS	Soil extract	Exponential decay	0.98				0.96	2.26
SF5-U-PFNS	Soil extract	Exponential decay	0.99				0.44	1.84
U-PFHpS	Soil extract	Logistic formation with exponential decay	1.61	1.33	23.20	0.15	0.02	4.50
U-PFOS	Soil extract	Two-step exponential decay	0.68	0.80		1.63	0.57	2.45
U-PFNS	Soil extract	Two-step exponential decay	0.79	0.92		1.13	0.70	2.76
U-PFDS	Soil extract	Two-step exponential decay	0.68	0.81		1.20	0.41	5.16
U-PFUnDS	Soil extract	Two-step exponential decay	0.65	0.80		1.20	0.34	3.93
U-PFDoDS	Soil extract	Two-step exponential decay	0.63	0.68		1.05	0.17	4.42
U-PFTriDS	Soil extract	Two-step exponential decay	0.66	0.47		0.78	0.08	5.64
U-PFTeDS	Soil extract	Two-step exponential decay	0.66	0.41		0.51	0.07	9.19
PFBSAm	Soil extract	Logistic formation with exponential decay	1015.47	1019.52	20.86	0.67	0.66	2.93
PFPeSAm	Soil extract	Logistic formation with exponential decay	625.84	625.08	20.57	0.63	0.62	3.90
PFPeSAm	Soil	Logistic formation with exponential decay	3.95	0.23	1.90	0.26	0.00	5.64
PFHxSAm	Soil extract	Logistic formation with exponential decay	23.43	20.33	19.81	0.51	0.49	4.53
PFHxSAm	Soil	Logistic formation with exponential decay	0.55	0.21	0.00	0.57	0.00	4.65
PFHpSAm	Soil extract	Logistic formation with exponential decay	85.30	69.67	19.83	0.48	0.42	6.35
PFOSAm	Soil extract	Logistic formation with	0.41	0.41	9.71	0.26	0.12	9.11

		exponential decay						
PFOSAm	Soil	Logistic formation with exponential decay	0.85	0.19	0.65	1.18	0.03	7.47
PFOSyA	Soil extract	Logistic formation with exponential decay	Overshooting		19.95	1.44	1.45	7.33
PFHxSAm-PrSA	Soil extract	Exponential decay	1.05				0.23	3.79
PFOSAm-Pr-B	Soil extract	Exponential decay	1.00				2.12	1.36
PFOSAm-Pr-B	Soil	Exponential decay	1.00				3.78	0.94
PFHxSAm-Pr-DiMeAm	Soil extract	Logistic formation with exponential decay	0.03	0.03	10.99	0.07	4.75	2.87
PFOSAm-Pr-DiMeAm	Soil extract	Logistic formation with exponential decay	0.77	2.38	11.58	0.00	1.00	11.23
PFHxSAm-Pr-TriMeAm	Soil extract	Logistic formation with exponential decay	4.21	0.42	11.62	0.00	0.67	9.10
PFOSAm-Pr-TriMeAm	Soil extract	Logistic formation with exponential decay	0.87	1.75	11.26	0.00	0.25	11.26
PFOSAm-Pr-TriMeAm	Soil	Logistic formation with exponential decay	1.20	1.64	11.17	0.00	1.23	2.52
PFHxSAm-N-PrSA-N-Pr-DiMeAm	Soil extract	Exponential decay	0.98				0.26	3.41
6:2 FTCA	Soil extract	Logistic formation with exponential decay	25.16	25.03	12.39	0.96	0.48	0.27
6:2 FTCA	Soil	Logistic formation with exponential decay	1.90	0.71	23.95	0.12	0.04	14.69
8:2 FTCA	Soil extract	Logistic formation with exponential decay	2.93	0.17	7.08	0.91	0.25	2.80
8:2 FTCA	Soil	Logistic formation with exponential decay	0.84	1.30	3.10	0.94	0.19	8.46

5:3 FTCA	Soil extract	Logistic formation with exponential decay	0.49	0.16	4.51	0.53	0.24	1.96
7:3 FTCA	Soil extract	Logistic formation with exponential decay	20.92	20.92	10.80	1.18	1.24	14.53
U-6:2 FTCA	Soil extract	Logistic formation with exponential decay	6.37	6.36	12.68	0.90	0.52	0.73
U-8:2 FTCA	Soil extract	Logistic formation with exponential decay	0.56	0.07	6.73	0.80	0.32	6.17
U-8:2 FTCA	Soil	Logistic formation with exponential decay	4.97	4.82	5.89	1.35	0.98	8.83
6:2 FTSA	Soil extract	Logistic formation with exponential decay	71.35	73.17	12.56	0.78	0.76	7.17
6:2 FTSA	Soil	Logistic formation with exponential decay	1.05	3.97	7.98	0.21	0.05	7.85
8:2 FTSA	Soil extract	Logistic formation with exponential decay	2.31	5.23	5.70	0.55	0.45	6.74
8:2 FTSA	Soil	Logistic formation with exponential decay	1.62	0.81	0.40	3.23	0.13	8.66
10:2 FTSA	Soil extract	Logistic formation with exponential decay	8.19	0.35	0.98	1.49	0.36	2.17
12:2 FTSA	Soil extract	Logistic formation with exponential decay	Overshooting		5.96	3.99	3.92	9.17
K-6:2 FTSA	Soil extract	Logistic formation with exponential decay	23.36	22.88	13.58	0.47	0.47	4.00
K-6:2 FTSA	Soil	Logistic formation with exponential decay	1.08	4.38	18.99	0.08	0.05	4.18
K-8:2 FTSA	Soil extract	Logistic formation with	1.87	7.25	6.10	0.44	0.34	4.89

		exponential decay						
5:1:2 FTB	Soil extract	Logistic formation with exponential decay	Overshooting		10.85	2.38	2.38	6.19
5:1:2 FTB	Soil	Logistic formation with exponential decay	12.78	13.43	33.42	0.14	0.14	4.24
7:1:2 FTB	Soil extract	Logistic formation with exponential decay	0.65	8.26	2.41	0.67	0.45	2.59
7:1:2 FTB	Soil	Logistic formation with exponential decay	1.91	1.07	0.00	0.30	0.25	1.71
9:1:2 FTB	Soil extract	Logistic formation with exponential decay	2.08	0.85	11.28	0.00	0.35	6.21
9:1:2 FTB	Soil	Logistic formation with exponential decay	222.56	221.54	4.41	2.45	3.10	0.25
11:1:2 FTB	Soil extract	Logistic formation with exponential decay	1.12	1.33	11.35	0.00	0.24	11.88
11:1:2 FTB	Soil	Logistic formation with exponential decay	0.66	2.90	11.50	0.00	0.68	3.78
5:3 FTB	Soil extract	Logistic formation with exponential decay	0.69	0.28	6.35	0.44	0.37	2.91
5:3 FTB	Soil	Logistic formation with exponential decay	2.22	2.05	27.57	0.11	0.11	1.58
7:3 FTB	Soil extract	Logistic formation with exponential decay	6.96	7.16	5.25	0.75	0.78	2.47
7:3 FTB	Soil	Exponential decay	1.01				0.18	1.88
9:3 FTB	Soil extract	Logistic formation with exponential decay	0.69	2.57	11.27	0.00	0.46	6.33
9:3 FTB	Soil	Logistic formation with	1.80	1.11	0.00	1.51	1.20	0.92

		exponential decay						
11:3 FTB	Soil extract	Logistic formation with exponential decay	0.71	2.24	11.61	0.00	0.46	11.20
5:1:3 FTB	Soil extract	Logistic formation with exponential decay	1.79	0.72	0.40	7.47	0.18	5.19
7:1:3 FTB	Soil extract	Logistic formation with exponential decay	1.00	1.30	0.42	10.00	0.22	4.35
6:2 FTB	Soil extract	Logistic formation with exponential decay	2.31	4.61	5.36	0.45	0.33	2.38
6:2 FTB	Soil	Logistic formation with exponential decay	302.66	296.57	28.89	0.39	0.40	3.30
8:2 FTB	Soil extract	Logistic formation with exponential decay	1.27	2.55	1.25	0.87	0.39	3.54
8:2 FTB	Soil	Exponential decay	0.99				0.38	4.12
6:4 FTB	Soil extract	Exponential decay	1.02				0.27	3.53
6:4 FTB	Soil	Exponential decay	0.96				0.40	4.59
6:2 FTSAm	Soil extract	Logistic formation with exponential decay	6.82	0.25	0.55	2.08	0.17	8.09
6:2 FTSAm-Pr-B	Soil extract	Exponential decay	0.15				0.64	3.84
6:2 FTSAm-Pr-B	Soil	Exponential decay	4.90				0.92	4.57
6:2 FTSAm-Pr-DiMeNO	Soil extract	Exponential decay	0.01				0.10	11.55
8:2 FTSAm-Pr-DiMeAm	Soil extract	Exponential decay	0.99				2.29	7.78
8:2 FTSAm-Pr-DiMeAm	Soil	Exponential decay	0.99				1.41	1.85
6:2 FTSAm-PrA	Soil extract	Logistic formation with exponential decay	1.46	0.96	0.20	3.86	0.22	4.29
6:2/6:2 FTSAm dimer	Soil extract	Logistic formation with exponential decay	6.91	0.55	2.86	0.64	0.25	10.77

6:2/6:2 FTSAm dimer	Soil	Logistic formation with exponential decay	1612.78	1612.77	2.22	6.67	7.37	0.47
6:2/8:2 FTSAm dimer	Soil extract	Logistic formation with exponential decay	1.84	1.46	3.10	0.45	0.13	12.71
6:2 FTTh-(2')OHPr-TriMeAm	Soil extract	Exponential decay	1.04				0.18	7.66
6:2 FTTh-(2')OHPr-TriMeAm	Soil	Exponential decay	0.98				0.16	3.43
6:2 FTSO-(2')OHPr-TriMeAm	Soil extract	Exponential decay	1.00				4.42	0.37
6:2 FTSO-(2')OHPr-TriMeAm	Soil	Exponential decay	0.99				2.19	3.08
6:2 FTSy-(2')OHPr-TriMeAm	Soil extract	Exponential decay	0.90				0.43	5.82
6:2 FTSy-(2')OHPr-TriMeAm	Soil	Exponential decay	0.98				0.26	1.23
8:2 FTSy-(2')OHPr-TriMeAm	Soil extract	Exponential decay	0.83				0.44	9.16
8:2 FTSy-(2')OHPr-TriMeAm	Soil	Exponential decay	1.06				0.38	6.40
6:2 FTSO-Pr-Ad-(5'5')DiMeEtSA	Soil extract	Exponential decay	1.00				3.16	1.39
6:2 FTSy-Pr-Ad-(5'5')DiMeEtSA	Soil extract	Exponential decay	1.06				0.23	4.00
8:2 FTSy-Pr-Ad-(5'5')DiMeEtSA	Soil extract	Exponential decay	1.07				0.25	4.70
10:2 FTSy-Pr-Ad-(5'5')DiMeEtSA	Soil extract	Exponential decay	0.95				0.36	9.95
6:2 FTSy-PrA	Soil extract	Logistic formation with exponential decay	1.53	1.32	0.65	1.42	0.21	4.51

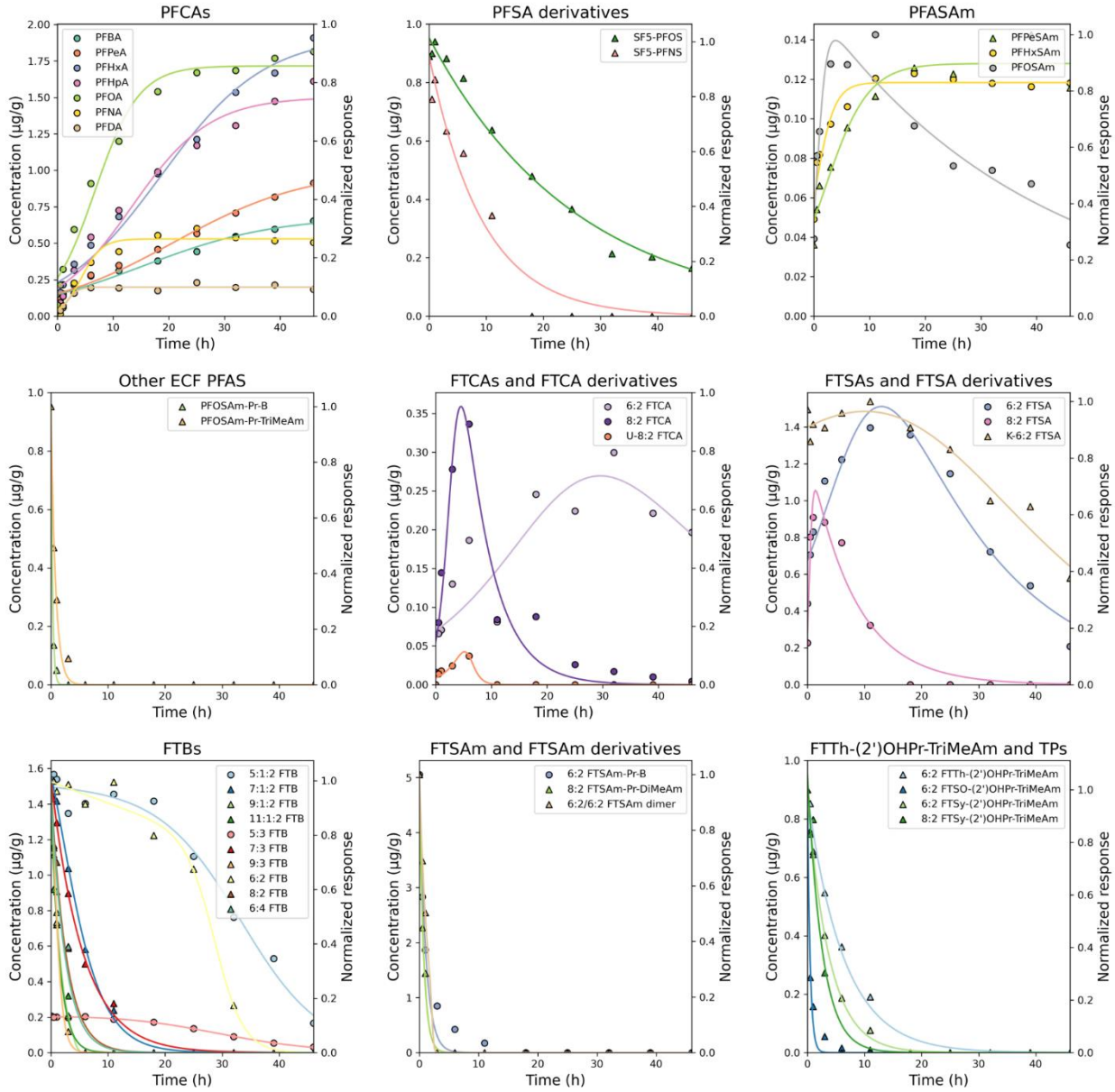

Figure S1: Fitted formation and degradation curves showing the concentration (µg/g) of level 1 PFAS (left axis, circles) and the normalized response of level 2 and 3 PFAS (right axis, triangles) during 46 h of direct soil irradiation.

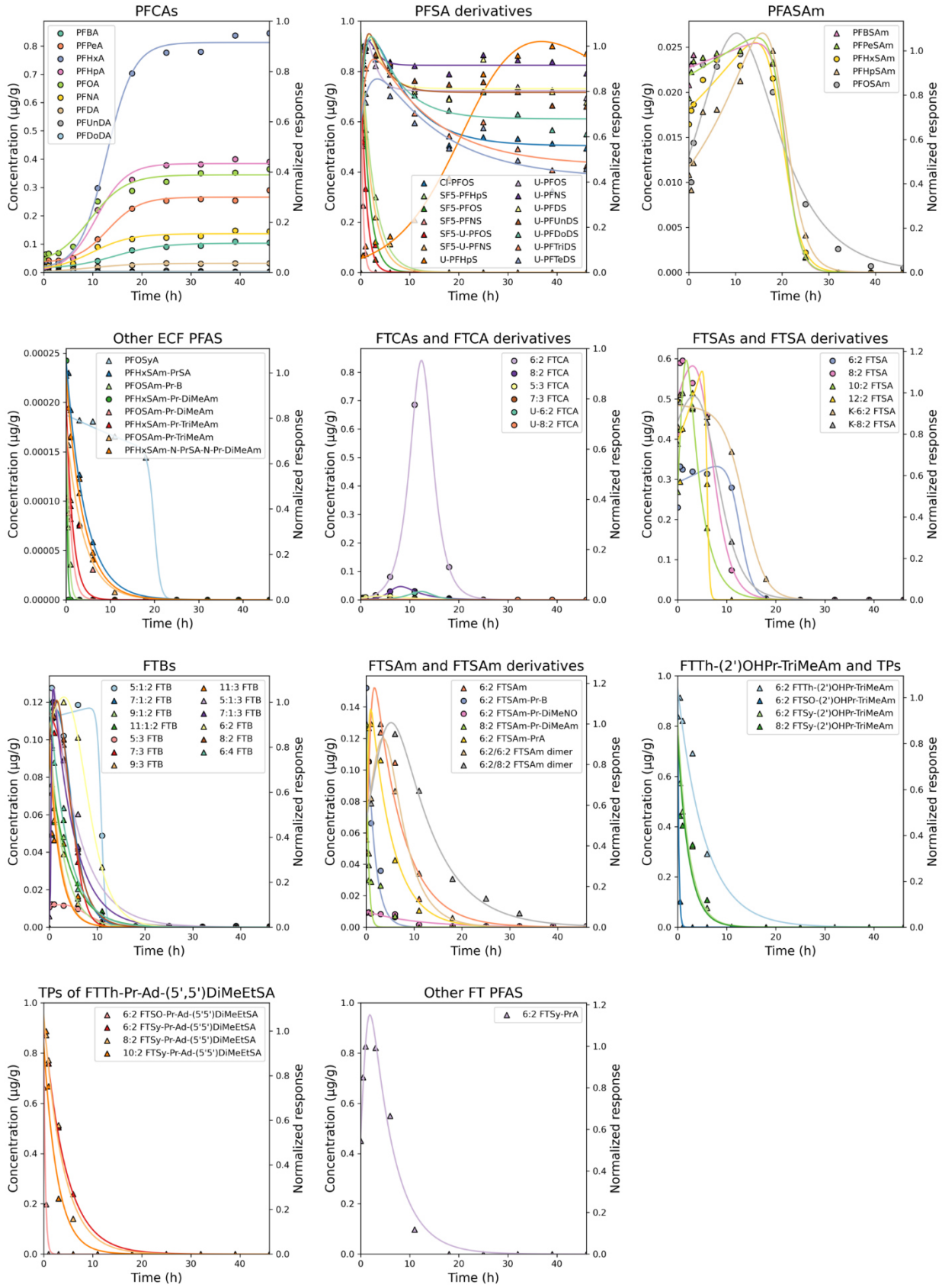

Figure S2: Fitted formation and degradation curves showing the concentration (µg/g) of level 1 PFAS (left axis, circles) and the normalized response of level 2 and 3 PFAS (right axis, triangles) during 46 h of soil extract irradiation.

ESM I Spearman correlations

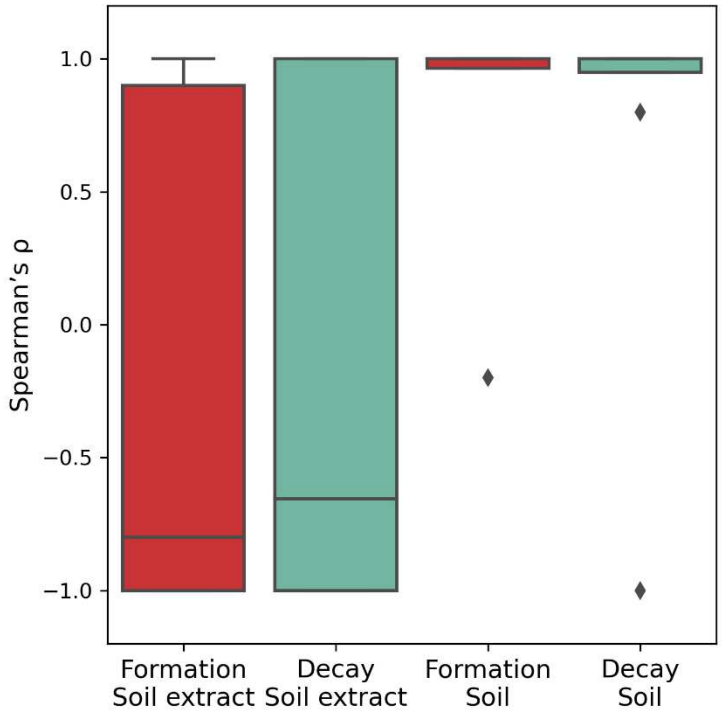

Figure S3: Boxplot of Spearman correlations between perfluorinated chain length and transformation or formation rates within individual PFAS classes.

References

1. Capitain C, Schüßler M, Bugsel B, Zweigle J, Vogel C, Leube P, Zwiener C (2025) Implementation of Matrix-Matched Semiquantification of PFAS in AFFF-Contaminated Soil. Environ Sci Technol 59 (14):7338-7347. doi:10.1021/acs.est.4c14255